

Top of the Line Corrosion in CO₂/H₂S Environments

A dissertation presented to
the faculty of
the Russ College of Engineering and Technology of Ohio University

In partial fulfillment
of the requirements for the degree
Doctor of Philosophy

Najmiddin Yaakob

May 2015

© 2015 Najmiddin Yaakob. All Rights Reserved.

This dissertation titled
Top of the Line Corrosion Behavior in CO₂/H₂S Environments

by
NAJMIDDIN YAAKOB

has been approved for
the Department of Chemical and Biomolecular Engineering
and the Russ College of Engineering and Technology by

Srdjan Nesic
Professor of Chemical and Biomolecular Engineering

Dennis Irwin
Dean, Russ College of Engineering and Technology

ABSTRACT

YAAKOB, NAJMIDDIN, Ph.D., May 2015, Chemical Engineering

Top of the Line Corrosion Behavior in CO₂/H₂S Environments

Director of Dissertation: Srdjan Nestic

Top of the line (TLC) corrosion in sour (H₂S) environments has not been well understood until now, since most reported TLC research has focused on sweet (CO₂) conditions, with various models developed to predict corrosion rates and related phenomena in sweet systems. This has led to many unanswered questions relating to TLC mechanisms in CO₂/H₂S environments. In most sour environments, the nature of the FeS corrosion product layer is dependent on the concentration of H₂S present in the mixed H₂S/CO₂ environment. Therefore, the intent of this research is to determine the TLC behavior in marginally (less than 1 mbar/1000 ppm of H₂S) and highly sour environments (more than 10 mbar/10000 ppm H₂S), since both described conditions would lead to different TLC mechanisms.

Experiments were conducted in custom designed autoclaves. Weight loss method for corrosion rate measurement, corrosion product analysis by SEM/EDX, optical profilometry, and condensed water analysis were used to investigate the TLC mechanisms. In marginally sour TLC between 0.015 mbar (15 ppm) to 0.03 mbar (30 ppm H₂S), a non-homogenous FeS layer formed on the steel surface in shorter experiments (lasting a few days), with some areas being covered and others not. This localized corrosion which was not sustained, since pits were not seen in longer experiments lasting 28 days. Increases in H₂S concentration between 0.08 mbar (80 ppm)

to 0.15 mbar (150 ppm) did not lead to initiation of localized corrosion. The steel surface was uniformly covered by an FeS layer due to the greater scaling tendency that overcame the undermining by corrosion. Low general corrosion rate were found. Increase in water condensation rate lead to higher TLC rate due to saturation limits with respect to aqueous species required for formation of both FeCO_3 and FeS, phases that can confer a degree of protection against corrosion.

In highly sour TLC, the main parameter which controls TLC behavior is the characteristics of the FeS layer formed on the steel surface. The formation of more coherent FeS layers was observed at higher steel temperature and conferred greater protectiveness regardless of the water condensation rate which is the main controlling factor in sweet TLC. Water condensation rate acts as a secondary effect that lowers the steel temperature. Finally, the TLC corrosion mechanisms in $\text{CO}_2/\text{H}_2\text{S}$ environments (marginally and highly sour) were proposed through a descriptive model approach.

DEDICATION

To

My parents, Jainabee LS Md Kassim and Yaakob Lazim

My mother-in-law, Noormi Ahmad

My beloved wife, Faridah Manaf, my children, Najwa Humaira, Nasrul Hakim

and all other family members

For their constant support and love

ACKNOWLEDGMENTS

Even though the following dissertation is an individual work, I would not have completed it without the help, support, and guidance from a lot of people. Firstly I would like to express my gratitude and indebtedness to my academic advisor, Prof. Srdjan Nesic, for his excellent supervision, guidance, and advice throughout my PhD program. Frankly, I am impressed by and admire his knowledge, energy, and teaching skill, which have contributed a lot in the success of my PhD journey.

I would like to extend my appreciation to Prof. Dina Lopez, Prof. Jeffrey J. Rack, Prof. Kevin Crist, and Dr. Monica Burdick for serving on my PhD committee and providing valuable feedback on my dissertation.

I would like to acknowledge my former group leader and current faculty member of the Chemical Engineering Department, Dr. Marc Singer, for his valuable assistance and advice, especially in TLC experiments. Without his support, I would not have reached this far. A special thank you goes to Dr. Fernando Farelas, the current TLC project leader, on his commitment and help in ensuring the experiments were successfully executed.

Another appreciation goes to Dr. David Young for his kindness, care, effort, and advice, especially in chemistry and in improving my dissertation. I would also like to thank Mr. Cody Shafer, Mr. Phil Bullington, Mr. Alexis Barxias, Mr. Daniel Cain, Mr. Steve Upton, Mrs. Becky Gill, and Mr. Albert Shubert who untiringly attended to any experimental problem and ensured the experiments could be successfully completed. Thank you to Dr. Bruce Brown for his advice and help related to H₂S experiments.

I also would like to acknowledge Ministry of Education Malaysia and Universiti Teknologi MARA, Malaysia for the full scholarships given to me during the duration of my PhD program.

Above all, I am greatly indebted to my family members, especially my parents, mother-in-law, beloved wife, and children for their prayer, support and understanding. Special appreciation goes to my beloved wife, Faridah Manaf, and my parents, Jainabee Kassim and Yaakob Lazim, who sacrificed a lot and were always there when I needed them.

Last but not least, I would like to thank all my friends and colleagues in ICMT who helped me in many ways and make me feel at home whenever working in the lab.

TABLE OF CONTENTS

	Page
Abstract.....	3
Dedication.....	5
Acknowledgments.....	6
List of Tables	11
List of Figures	12
Chapter 1: Introduction	19
Chapter 2: Background and Literature Review	24
2.1 Background of CO ₂ and H ₂ S Corrosion.....	24
2.1.1 Corrosion Product Layer in CO ₂ Environment.....	27
2.1.2 Corrosion Product Layer in H ₂ S Environment	28
2.2 Overview of Top-of-the-Line Corrosion	32
2.3 Top- of-the-Line Corrosion Behavior in Sweet Environment	34
2.3.1 Sweet TLC Field Experience	34
2.3.2 Sweet TLC Mechanism.....	36
2.4 Research Specific to Sour Top-of-the-line Corrosion	38
2.4.1 Sour TLC Field Experience	38
2.4.2 Influence of Water Condensation Rate and Temperature on Sour TLC.....	42
2.4.3 Influence of Hydrogen Sulfide Concentration on TLC	45
2.4.4 Top-of-the-Line Corrosion in Marginally Sour Environments.....	47
2.5 Research Gaps Associated with Sour Top-of-the-Line Corrosion	50
Chapter 3: Research Objectives and Hypotheses.....	52
3.1 Research Objectives.....	52
3.2 Hypotheses.....	52
3.2.1 TLC Behavior in Marginally Sour Environments	52
3.2.2 TLC Behavior in Highly Sour Environments	53
Chapter 4: Methodology and Experimental Design.....	55
4.1 TLC in Marginally Sour Environments	55
4.1.1 Equipment.....	55

4.1.2	Material Tested	57
4.1.3	Test Matrices.....	57
4.1.4	Experimental and Analytical Procedures.....	59
4.2	TLC in Highly Sour Environments.....	62
4.2.1	Equipment.....	62
4.2.2	Material Tested	64
4.2.3	Test Matrices.....	65
4.2.4	Experimental and Analytical Procedures.....	66
Chapter 5: Results and Discussions		68
5.1	TLC in Marginally Sour Environments	68
5.1.1.	Results and Discussion for 40°C and 60°C Gas Temperatures.....	68
5.1.2.	Effect of Exposure Time.....	113
5.2	TLC in Highly Sour Environments.....	120
5.2.1	Effect of Gas/Steel Temperature and Water Condensation Rate.....	120
5.2.2	Effect of H ₂ S Partial Pressure.....	131
Chapter 6: Descriptive Model of TLC Corrosion Mechanisms.....		143
6.1	TLC Corrosion Mechanism in Sweet Environments	143
6.2	TLC Corrosion Mechanisms in Marginally Sour Environments.....	144
6.2.1	Basis of Localized Corrosion Mechanism in Marginally Sour Environments 144	
6.2.2	Descriptive Model for TLC in Marginally Sour Environments.....	146
6.2.3	Descriptive Model for the Effect of Exposure Time on Localized Corrosion in Marginally Sour TLC.....	152
6.3	TLC Corrosion Mechanism in Highly Sour Environments	155
6.4	Overall Schematic of TLC Behavior in CO ₂ /H ₂ S Environments	158
6.5	Summary of TLC Descriptive Model in CO ₂ /H ₂ S Environments	162
Chapter 7: Conclusions and Recommendations		164
7.1	Conclusions.....	164
7.1.1	TLC Behavior in Marginally Sour Environments	164
7.1.2	TLC Behavior in Highly Sour Environments[53]	165
7.1.3	TLC Descriptive Model in CO ₂ /H ₂ S Environments	165
7.2	Recommendations for Future Research	166

References.....	168
Appendix A: Weight Loss Corrosion Rate Calculation Method	177
Appendix B: Reaction Rate Calculation Method (Scaling Formation and Corrosion Rate)	178
Appendix C: Hypothesis Testing Using P-Value Method.....	179
Appendix D: Permission to Reproduce Figures from NACE International	180

LIST OF TABLES

	Page
Table 1: Chemical composition of weight loss steel samples - API 5L X65 (balance Fe).	57
Table 2: Test matrix part A; marginally sour TLC	58
Table 3: Test matrix part B; marginally sour TLC	58
Table 4: Test matrix part C; marginally sour TLC	58
Table 5: Test matrix for the effect of temperature/water condensation rate; highly sour TLC	65
Table 6: Test matrix for the effect of H ₂ S partial pressure; highly sour TLC	66
Table 7: Summary of TLC key factors in marginally sour environments	162
Table 8: Summary of TLC key factors in highly sour environments	163

LIST OF FIGURES

	Page
Figure 1: Corrosion product stability with regards to temperature and H ₂ S activity (Reproduced from [25] – © NACE International 2002).....	30
Figure 2: Similarity of the Fe atom geometry between the <i>bcc</i> iron lattice and mackinawite (Brown-Fe). Images, generated with CrystalMaker, courtesy of David Young (ICMT).	32
Figure 3: Key elements in TLC.	33
Figure 4: Schematic diagram of the location along the pipeline affected by TLC (Reproduced from [36] – © NACE International 1999).....	34
Figure 5: Cross section of the affected area (Reproduced from [36] – © NACE International 1999).....	35
Figure 6: Corrosion on upper part of the pipeline (Reproduced from [37]– © NACE International 1963).....	39
Figure 7: Cross sectional diagram of the failure (Reproduced from [38]– © NACE International 1987).....	40
Figure 8: MFL analysis result for sweet TLC (Reproduced from [42]– © NACE International 2009).....	41
Figure 9: MFL analysis result for sour TLC (Reproduced from [42]– © NACE International 2009).....	42
Figure 10: Influence of condensation rate on TLC (Reproduced from [11]– © NACE International 2012).....	44
Figure 11: Influence of gas temperature rate on TLC (Reproduced from [11]– © NACE International 2012).....	45
Figure 12: Influence of H ₂ S concentration on TLC (Reproduced from [12]– © NACE International 2008).....	46
Figure 13: Influence of H ₂ S concentration on TLC with the presence of 1000 ppm acetic acid (Reproduced from [45]– © NACE International 2010).....	47
Figure 14: SEM analysis of corrosion product layers showing formation of both FeCO ₃ and FeS (Reproduced from [14]– © NACE International 2012).....	50

Figure 15: Glass cell experimental set up for marginally sour TLC experiments. Images courtesy of Cody Shafer, ICMT.....	56
Figure 16: X65 sample coupon for marginally sour TLC experiments.....	61
Figure 17: Overall experimental setup for marginally sour TLC experiments. Image courtesy of Cody Shafer, ICMT.....	61
Figure 18: Holder for TLC samples; highly sour TLC experiments	63
Figure 19: 20L UNS N10276 autoclave; highly sour TLC experiments	63
Figure 20: Weight loss sample coupon for TLC in highly sour environments.....	64
Figure 21: Comparison of corrosion rate from weight loss measurement and pit penetration rate-Part A (gas temperature = 40°C)	70
Figure 22: Comparison of corrosion rate from weight loss measurement and pit penetration rate-Part B (gas temperature = 60°C)	72
Figure 23: Comparison of reaction rate (CR and SFR) and scaling tendency (ST)-Part A (gas temperature 40°C)	74
Figure 24: Comparison of reaction rate (CR and SFR) and scaling tendency (ST)-Part B (gas temperature 60°C)	75
Figure 25: Mass balance between total Fe loss from corrosion, Fe in corrosion product layer and Fe in condensed water-Part A (gas temperature 40°C).....	77
Figure 26: Mass balance between total Fe loss from corrosion, Fe in corrosion product layer and Fe in condensed water-Part B (gas temperature 60°C).....	78
Figure 27: Comparison of Fe ²⁺ concentration in condensed water-Part A (gas temperature 40°C)	79
Figure 28: Comparison of Fe ²⁺ concentration in condensed water-Part B (gas temperature 60°C)	80
Figure 29: Comparison of measured and calculated condensed water pH-Part A (gas temperature 40°C).....	82
Figure 30: Comparison of measured and calculated condensed water pH-Part B (gas temperature 60°C)	83
Figure 31: Comparisons of saturation of FeS-Part A (gas temperature 40°C).....	85

Figure 32: Comparisons of saturation of FeS-Part B (gas temperature 60°C).....	86
Figure 33: Comparisons of saturation of FeCO ₃ -Part A (gas temperature 40°C).....	87
Figure 34: Comparisons of saturation of FeCO ₃ -Part B (gas temperature 60°C).....	88
Figure 35: SEM/EDX analysis with corrosion product layer (0 mbar H ₂ S, T _{gas} = 40°C)	89
Figure 36: SEM/EDX analysis with corrosion product layer (0.015 mbar H ₂ S, T _{gas} = 40°C).....	90
Figure 37: SEM/EDX analysis with corrosion product layer (0.03 mbar H ₂ S, T _{gas} = 40°C).....	90
Figure 38: SEM/EDX analysis with corrosion product layer (0.08 mbar H ₂ S, T _{gas} = 40°C).....	91
Figure 39: SEM/EDX analysis with corrosion product layer (0.15 mbar H ₂ S, T _{gas} = 40°C).....	91
Figure 40: SEM/EDX analysis with corrosion product layer (0 mbar H ₂ S, T _{gas} = 60°C)	92
Figure 41: SEM/EDX analysis with corrosion product layer (0.015 mbar H ₂ S, T _{gas} = 60°C).....	93
Figure 42: SEM/EDX analysis with corrosion product layer (0.03 mbar H ₂ S, T _{gas} = 60°C).....	93
Figure 43: SEM/EDX analysis with corrosion product layer (0.08 mbar H ₂ S, T _{gas} = 60°C).....	94
Figure 44: SEM/EDX analysis with corrosion product layer (0.15 mbar H ₂ S, T _{gas} = 60°C).....	94
Figure 45: Cross-section analysis with corrosion product layer (0 mbar H ₂ S, T _{gas} = 40°C).....	95
Figure 46: Cross-section analysis with corrosion product layer (0.015 mbar H ₂ S, T _{gas} = 40°C).....	96
Figure 47: Cross section analysis with corrosion product layer (0.03 mbar H ₂ S, T _{gas} = 40°C).....	96
Figure 48: Cross section analysis with corrosion product layer (0.08 mbar H ₂ S, T _{gas} = 40°C).....	97

Figure 49: Cross section analysis with corrosion product layer (0.15 mbar H ₂ S, T _{gas} = 40°C)	98
Figure 50: Cross-section analysis with corrosion product layer (0 mbar H ₂ S, T _{gas} = 60°C)	99
Figure 51: Cross-section analysis with corrosion product layer (0.015 mbar H ₂ S, T _{gas} = 60°C)	100
Figure 52: Cross-section analysis with corrosion product layer (0.03 mbar H ₂ S, T _{gas} = 60°C)	101
Figure 53: Cross-section analysis with corrosion product layer (0.08 mbar H ₂ S, T _{gas} = 60°C)	102
Figure 54: Cross-section analysis with corrosion product layer (0.15 mbar H ₂ S, T _{gas} = 60°C)	102
Figure 55: SEM surface analysis after removal of corrosion product layer (0, 0.015, 0.03, 0.08, and 0.15 mbar H ₂ S. T _{gas} = 40°C)	103
Figure 56: SEM analysis on steel surface after removal of corrosion product layer (0, 0.015, 0.03, 0.08, and 0.15 mbar H ₂ S, T _{gas} = 60°C).....	104
Figure 57: Surface profilometry analysis after removal of corrosion product layer (0 mbar H ₂ S, T _{gas} = 40°C)	106
Figure 58: Surface profilometry analysis after removal of corrosion product layer (0.015 mbar H ₂ S, T _{gas} = 40°C)	106
Figure 59: Surface profilometry analysis after removal of corrosion product layer (0.03 mbar H ₂ S, T _{gas} = 40°C)	107
Figure 60: Surface profilometry analysis after removal of corrosion product layer (0.08 mbar H ₂ S, T _{gas} = 40°C)	107
Figure 61: Surface profilometry analysis after removal of corrosion product layer (0.15 mbar H ₂ S, T _{gas} = 40°C)	108
Figure 62: Surface profilometry analysis after removal of corrosion product layer (0 mbar H ₂ S, T _{gas} = 60°C)	109
Figure 63: Surface profilometry analysis after removal of corrosion product layer (0.015 mbar H ₂ S, T _{gas} = 60°C)	109

Figure 64: Surface profilometry analysis after removal of corrosion product layer (0.03 mbar H ₂ S, T _{gas} = 60°C)	110
Figure 65: Surface profilometry analysis after removal of corrosion product layer (0.08 mbar H ₂ S, T _{gas} = 60°C)	110
Figure 66: Surface profilometry analysis after removal of corrosion product layer (0.15 mbar H ₂ S, T _{gas} = 60°C)	111
Figure 67: Comparison of corrosion rate from weight loss measurement and pit penetration rate at 3, 7, and 28 days.....	114
Figure 68: SEM/EDX analysis with corrosion product layer (0.03 mbar H ₂ S, T _{gas} = 40°C, 0-3 days).....	115
Figure 69: SEM/EDX analysis with corrosion product layer (0.03 mbar H ₂ S, T _{gas} = 40°C, 0-7 days).....	115
Figure 70: SEM/EDX analysis with corrosion product layer (0.03 mbar H ₂ S, T _{gas} = 40°C, 0-28 days).....	116
Figure 71: Comparison of SEM images without corrosion product layer at 0-7 and 0-28 days (0.03 mbar H ₂ S, T _{gas} = 40°C).....	116
Figure 72: Surface profilometry analysis after removal of corrosion product layer (0.03 mbar H ₂ S, T _{gas} = 40°C, 0-7 days).....	117
Figure 73: Surface profilometry analysis after removal of corrosion product layer (0.03 mbar H ₂ S, T _{gas} = 40°C, 0-28 days).....	118
Figure 74: Cross-section images at 0-3, 0-7, and 0-28 days, 0.03 mbar H ₂ S, T _{gas} = 40°C	119
Figure 75: Top of the line general corrosion rate: effect of steel temperature	122
Figure 76: Top of line general corrosion rate: effect of water condensation rate	122
Figure 77: SEM images and XRD patterns of FeS polymorphs at studied conditions...	126
Figure 78: SEM cross-section images at studied steel temperatures and water condensation rates	128
Figure 79: Comparison of FeS layer thickness on highly sour TLC rate	130
Figure 80: Effect of H ₂ S partial pressure on sour top of line corrosion rate (T _{gas} =40°C, pCO ₂ =10 bar, WCR = 0.01 ml/m ² .s)	134

Figure 81: Effect of H ₂ S partial pressure on sour top of line corrosion rate (T _{gas} =40°C, pCO ₂ =10 bar, WCR = 0.04-0.05 ml/m ² /s).....	134
Figure 82: Influence of H ₂ S partial pressure on sour top of line reaction rate (T _{gas} =40°C, pCO ₂ =10 bar, WCR = 0.01 ml/m ² /s)	135
Figure 83: Influence of H ₂ S partial pressure on sour top of line reaction rate (T _{gas} =40°C, pCO ₂ =10 bar, WCR = 0.04 ml/m ² /s).....	135
Figure 84: Influence of H ₂ S partial pressure and steel temperatures on sour TLC rate (T _{gas} =40°C, pCO ₂ =10 bar, WCR = 0.01-0.05 ml/m ² .s)	136
Figure 85: SEM and XRD Image comparison for different H ₂ S partial pressure (T _{gas} =40°C, pCO ₂ =10bars, WCR = 0.01-0.05 ml/m ² .s).....	138
Figure 86:Cross-section analysis comparison for H ₂ S partial pressure (T _{gas} =40°C, pCO ₂ =10 bars, WCR = 0.01-0.05 ml/m ² .s)	141
Figure 87: SEM images of the breakdown of the FeS layer due to undermining corrosion at 0.015 and 0.03 mbar H ₂ S, T _{gas} = 40°C)	147
Figure 88: SEM cross-section images of the breakdown of the FeS layer due to undermining corrosion at 0.015 and 0.03 mbar H ₂ S, T _{gas} = 40°C).....	148
Figure 89: SEM images of multiple layers of FeS by precipitation at 0.08 and 0.15 mbar H ₂ S, T _{gas} = 40°C)	150
Figure 90: Cross-section SEM images of multiple layer of FeS by precipitation at 0.08 and 0.15 mbar H ₂ S, T _{gas} = 40°C)	151
Figure 91: SEM images of FeS failure at 0.03 mbar H ₂ S, T _{gas} = 40°C, 3 days duration	152
Figure 92: Cross-section SEM images for FeS failure at 0.03 mbar H ₂ S, T _{gas} = 40°C, 3 days duration.....	153
Figure 93: SEM images of FeS failure at 0.03 mbar H ₂ S, T _{gas} = 40°C, 7 days duration	153
Figure 94: Top view and cross-section images of initial FeS layer by SEM at 0.03 mbar H ₂ S, T _{gas} = 40°C, 28 days duration.....	154
Figure 95: Cross section images of first and second FeS layer by SEM at T _{steel} more than 30°C, pH ₂ S = 2 bar, pCO ₂ = 10 bar, 21 days duration.....	156
Figure 96: Cross section images of first and second FeS layer by SEM at T _{steel} less than 30°C, pH ₂ S = 2 bar, pCO ₂ = 10 bar, 21 days duration.....	157

Figure 97: Localized corrosion schematic of TLC mechanism in sweet environments .	158
Figure 98: Localized corrosion schematic of TLC mechanism in marginally sour environments.....	159
Figure 99: Localized corrosion schematic of TLC mechanism in marginally sour environments; effect of exposure time.....	160
Figure 100: Schematics for TLC mechanism in highly sour environments	161

CHAPTER 1: INTRODUCTION

Pipeline transmission is the most commonly used method for oil and gas transportation due to the need to transport large volumes and since oil and gas reservoirs can be in remote offshore or onshore locations. This transportation method has been used for almost a century, acting as an economical and reliable method to transfer oil and natural gas, facilitating its further processing and fulfilling market demands. Transmission pipelines are typically tens or hundreds of kilometers in length (although some are thousands of kilometers long), and are made primarily of carbon steel. One of the challenges in the oil and gas industry is to maintain the integrity of pipelines, with a view to their having a lifespan of at least 30 to 50 years. The biggest threat to pipeline integrity that oil and gas companies face is corrosion. In the United States, it has been estimated that corrosion costs have increased up to \$1372 billion per year [1].

The internal corrosion of pipelines occurs during the transportation of fluids, usually in multiphase form and containing gaseous or liquid hydrocarbons, water or brine, acidic gases such as carbon dioxide (CO_2) and hydrogen sulfide (H_2S), organic acids, and often entrained solids (sand). The presence of these acidic gases and water has the potential to accelerate corrosion in pipelines which are normally made of carbon steel. Thus, the most common method to mitigate internal pipeline corrosion is by injecting corrosion inhibitors, which are typically a surface active chemical that dissolved in oil or water [2]. However, since corrosion inhibitors are virtually non-volatile liquids, this corrosion mitigation technique works best at the bottom of the pipeline.

In the present study, the scope of work is focused on gas lines and corrosion environments where the pipeline contains condensable liquids (water, organic acids, hydrocarbons), usually known as *wet gas*. The resultant corrosion phenomenon is termed top-of-the-line corrosion (TLC) as the attack mainly occurs on the upper inner surfaces of the pipeline where the corrosion inhibitor cannot reach. Water vapor inside the pipeline condenses when a significant temperature difference exists between the external environment and the gas inside the pipeline. This is particularly prevalent at locations where thermal insulation of the pipeline is poor or has failed. Corrosive species such as acidic gases (CO_2 and/or H_2S) can then dissolve into the condensed water, while organic acids (acetic acid, formic acid, etc.) may co-condense. Consequently, this condensed water is acidic and accelerates the corrosion process on the upper (top) surface of the pipeline and, in the long-term, leads to pipeline failure [3][4]. Such corrosion is difficult to mitigate using inhibitor injection. In stratified flow, non-volatile inhibitor would be unable to reach the top surface of the pipeline. This leads to protection around the 6 o'clock position (bottom of line), but pipeline failure due to pitting and localized corrosion around the 12 o'clock (top) position.

In the field, corrosion phenomena are commonly classified into two main categories: *sweet* and *sour* corrosion. Sweet corrosion refers to the corrosion that occurs in the presence of CO_2 , while sour environments are associated with the additional presence of H_2S . As the majority of the research conducted on corrosion in pipelines is very much centered on sweet systems and a limited amount of work has been published in (H_2S) environments, there are many unanswered questions relating to corrosion in H_2S

environments. This is particularly true for sour TLC, which is the focus of the present dissertation. Since more work has focused on sweet (CO_2) TLC, its governing parameters are well explained, namely: water condensation rate, gas temperature, gas flow rate, CO_2 partial pressure, and the presence of organic acids such as acetic acid [5][6]. Sour (H_2S) TLC is not nearly as well understood.

Various models have been developed to predict sweet corrosion based on the formation of protective iron carbonate (FeCO_3) layers. Water condensation rate (WCR) has been identified as the main parameter in controlling the sweet TLC rate related to the formation of protective FeCO_3 layers. At low water condensation rates, FeCO_3 supersaturation can be reached, thus formation of a protective FeCO_3 layer occurs. However, at higher condensation rates iron supersaturation is not reached, thus, the formation of FeCO_3 does not occur and the corrosion rate remains high [5]–[9]. As such, the critical water condensation rate has been identified to be between 0.15 and 0.25 $\text{ml/m}^2/\text{s}$ [5].

Unlike for sweet TLC, researchers are still having difficulties in agreeing on the main mechanism and parameters controlling the corrosion rate in sour TLC. Since most of the sweet TLC models are based on the formation of an FeCO_3 layer, the presence of even a small amount of H_2S (ppm range) in the gas phase would affect the protectiveness and corrosion rate prediction, since iron sulfide (FeS) would be the dominant corrosion product layer instead of FeCO_3 . Thus, the validity of sweet TLC prediction models is questionable, since the formed FeS layer is considerably different than that of FeCO_3 .

[10]. The nature of the FeS corrosion product layer is dependent on the concentration of H₂S present in the mixed H₂S/CO₂ environment.

At higher H₂S concentration (approximately more than 0.01 bar/10000 ppm), typically when FeS is the only component of the corrosion product layer, the environment is considered to be sour [11]–[13]. The presence of traces of H₂S in CO₂ (approximately less than 1 mbar/1000 ppm) can be considered as a marginally sour environment where both FeS and FeCO₃ could form on the steel surface[14]–[16]. Different TLC mechanisms are found due to the differences in the corrosion product layer – solely FeS found at high H₂S partial pressure *versus* FeS mixed with FeCO₃ found otherwise. Further observations regarding highly and marginally sour TLC are discussed in Chapter 2. Until now, there has been a lack of understanding of TLC mechanisms in both highly sour and marginally sour environments. The concentration of H₂S is of key importance in determining the characteristics of the sour corrosion regime, as it is expected that there is a threshold in H₂S concentration where there is a transition between sweet and sour TLC mechanisms since the corrosion behavior is markedly different in each case [14].

In the present study, the main objective is to identify and compare the corrosion mechanisms underlying TLC in marginally and highly sour environments. Comparisons can then be made with well-established sweet TLC mechanisms.

This dissertation is structured as follows: Chapter 2 provides background information and a literature review for top of the line corrosion in sweet and sour environments. The review includes the TLC field experience and reported mechanisms for both sweet and sour environments. Chapter 3 defines research objectives and

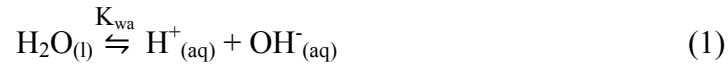
hypotheses for TLC in marginally sour and highly sour environments. Chapter 4 provides the methodology and description for each experimental setup and is followed by a discussion of the results for the experiments done in marginally sour environments. In the same chapter, the results are divided into two parts, which correspond to gas temperatures of 40°C and 60°C, respectively. This is then followed by a discussion of results for highly sour TLC in Chapters 5, which describes the effect of temperature, water condensation rate, and H₂S partial pressure. In Chapter 6, a descriptive model for observed TLC mechanisms in marginally and highly sour environments is proposed. Finally, Chapter 7 presents a summary of important points of this research, and points to a way forward.

Parts of this work have been reported in the internal confidential reports of the Ohio University TLC Joint Industry (TLC-JIP) Advisory Board meetings, over the period 2011 – 2014. Excerpts from the work have been, or will be, published at NACE (National Association of Corrosion Engineers) International conferences.

CHAPTER 2: BACKGROUND AND LITERATURE REVIEW

2.1 Background of CO₂ and H₂S Corrosion

Generally, in a corrosion analysis, water chemistry is one of the most important components in understanding the corrosion mechanism. The basic principles of water chemistry in CO₂/H₂S environments are presented below, which include both chemical and electrochemical reactions [17]. Water will dissociate to form H⁺ ion and OH⁻ ion as shown in reaction (1). The equilibrium expression and constant K_{wa} for the reaction is defined as in equation (2) and (3), respectively[18].



$$K_{wa} = C_{\text{H}^+} C_{\text{OH}^-} \quad (2)$$

$$K_{wa} = 10^{-(29.3868 - 0.0737549T_k + 7.47881 \times 10^{-5}T_k^2)} \quad (3)$$

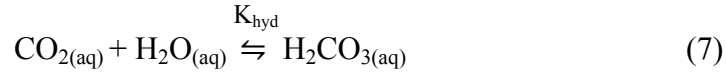
Where: T_k: Temperature (K)

However, this happens to a very small extent and pure water does not lead to significant corrosion of mild steel. CO₂ present in the gas phase will dissolve in water to form aqueous carbon dioxide, which is then followed by hydration of aqueous CO₂ to form carbonic acid as represented by reaction (4) and (7), respectively. The hydration of CO₂ to form carbonic acid is considered to be the slowest process. The expression and constant K_{sol} and K_{hyd} are shown in equation (5),(6) and (8)[19], [20].



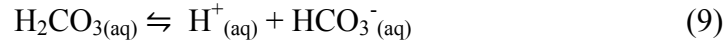
$$K_{sol} = \frac{C_{\text{CO}_2}}{p_{\text{CO}_2}} \quad (5)$$

$$K_{sol} = \frac{14.5}{1.00258} 10^{-(2.27+5.65 \times 10^{-3} T_f - 8.06 \times 10^{-6} T_f^2 + 0.075I)} \quad (6)$$



$$K_{hyd} = 2.58 \times 10^{-3} \quad (8)$$

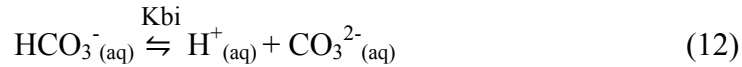
Furthermore, carbonic acid will undergo two dissociation steps to produce bicarbonate ion and carbonate ion as represented by reaction (9) and (12). The expression and constant K_{ca} and K_{bi} are shown in equation (10), (11), (13) and (14)[19].



$$K_{ca} = \frac{C_{HCO_3^-} C_{H^+}}{C_{H_2CO_3}} \quad (10)$$

$$K_{ca} =$$

$$387.6 \times 10^{-(6.41 - 1.594 \times 10^{-3} T_f + 3.52 \times 10^{-6} T_f^2 - 3.07 \times 10^{-5} p - 0.4772I^{0.5} + 0.11807I)} \quad (11)$$



$$K_{bi} = \frac{C_{CO_3^{2-}} C_{H^+}}{C_{HCO_3^-}} \quad (13)$$

$$K_{bi} = 10^{-(10.61 - 4.97 \times 10^{-3} T_f + 1.331 \times 10^{-5} T_f^2 - 2.624 \times 10^{-5} p - 1.66I^{0.5} + 0.34661I)} \quad (14)$$

Where: T_f : Temperature in Fahrenheit

I: Ionic strength (mol/L)

p: partial pressure (bar)

In sour environments, H_2S is three times more soluble in water as compared to CO_2 gas, at the same conditions (partial pressure, temperature, etc.). Given that H_2S is a weak acid, pK_a 7.05, it has the potential to reduce solution pH in a fashion similar to H_2CO_3 (the hydration product of aqueous CO_2), which has a pK_a 6.35. The dissociation

of H₂S gas in water and its equilibrium expression and constant $K_{\text{solH}_2\text{S}}$ are shown from equation (15)-(17). H₂S will dissolve in water to form aqueous H₂S. It will then undergo dissociation to form bisulfide and sulfide ions with the equilibrium expression and constant K_{hs} and K_{bs} are shown from equation (18)-(23)[18], [21].

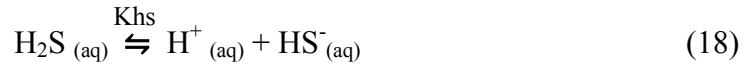
- H₂S dissolution



$$K_{\text{solH}_2\text{S}} = \frac{C_{\text{H}_2\text{S}}}{p_{\text{H}_2\text{S}}} \quad (16)$$

$$K_{\text{solH}_2\text{S}} = 10^{-634.27+0.2709T_k-0.00011132T_k^2-\frac{16719}{T_k}-261.9\text{Log}_{10}T_k} \quad (17)$$

- H₂S dissociation



$$K_{\text{hs}} = \frac{C_{\text{HS}^-} \cdot C_{\text{H}^+}}{C_{\text{H}_2\text{S}}} \quad (19)$$

$$K_{\text{hs}} = 10^{782.43945+0.36126T_k-0.00016722T_k^2-\frac{20565.7315}{T_k}-142.7417222\text{Log}_{10}T_k} \quad (20)$$

- HS⁻ dissociation



$$K_{\text{bs}} = \frac{C_{\text{S}^{2-}} \cdot C_{\text{H}^+}}{C_{\text{HS}^-}} \quad (22)$$

$$K_{\text{bs}} = 10^{(-23.93+0.030446T_k-2.4831 \times 10^{-5}T_k^2)} \quad (23)$$

Where: T_k : Temperature in Kelvin

In corrosion processes in aqueous solution, there are two main reactions that involve transfer of electrons in a conductive media and transfer of ions through a solution (electrolyte). The anodic reaction is the oxidative dissolution of iron into the solution, as represented by reaction (24). The cathodic reaction is most commonly the reduction of

hydrogen ion, as given by reaction (25). These are the two main half-reactions that constitute the corrosion process.



Furthermore, the value of pH is one of the most important factors in the corrosion process. The value of pH is highly dependent on environmental conditions as well as the anodic and cathodic processes. In condensed water, the pH, which corresponds to the concentration of H^{+} , can be determined by calculating each species' concentration using the equilibrium expressions and constants which were previously shown. These include all cations and anions in equilibrium, and the electroneutrality equation as described by equation 26. Since the water chemistry is only focused on condensed water, there are no other species, such as from brine, as there would be in the bottom of the line solution.

$$[\text{H}^{+}] + 2[\text{Fe}^{2+}] = [\text{OH}^{-}] + [\text{HCO}_3^{-}] + 2[\text{CO}_3^{2-}] + [\text{HS}^{-}] + 2[\text{S}^{2-}] \quad (26)$$

2.1.1 Corrosion Product Layer in CO_2 Environment

In sweet (CO_2) environments, FeCO_3 will form as the corrosion product layer, as shown by reaction (27). The supersaturation of FeCO_3 (S_{FeCO_3}) can be calculated by using equation (28), which is based on the well-established equilibrium constant K_{spFeCO_3} , also known as the solubility product of FeCO_3 .



$$S_{\text{FeCO}_3} = \frac{C_{\text{Fe}^{2+}} \times C_{\text{CO}_3^{2-}}}{K_{\text{spFeCO}_3}} \quad (28)$$

The equation to calculate the value of $K_{sp,FeCO_3}$ was reported by Greenberg and Silva as shown in equation (29) [22][23].

$$\begin{aligned} \text{Log}_{K_{sp,FeCO_3}} = & -59.3498 - 0.041377 \times T_K - \frac{2.1968}{T_K} + 24.5724 \times \log(T_K) + \\ & 2.518 \times I^{0.5} - 0.657 \times I \end{aligned} \quad (29)$$

With: $K_{sp,FeCO_3}$: Solubility constant of iron carbonate (mol^2/l^2)

T_K : Temperature (K)

I : Ionic strength (mol/l)

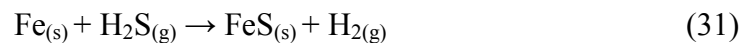
2.1.2 Corrosion Product Layer in H_2S Environment

The corrosion product layer associated with sour corrosion (H_2S) is of FeS type. The formation of FeS has been widely reported to be by either precipitation or direct chemical reaction between iron and H_2S , as represented by reaction (30) and (31) [24],[25]. In a mixed CO_2/H_2S environment, iron sulfide would be the dominant corrosion product layer constituent to much faster kinetics of formation. This would explain the reduction of corrosion rate whenever H_2S is present, as iron sulfide is rapidly formed to confer a degree of protection to the steel surface.

- FeS formation by precipitation



- FeS formation by direct chemical reaction



Based on reaction (30), the supersaturation of FeS (S_{FeS}) (for the fastest forming type of iron sulfide called mackinawite) can be calculated using equation (32), which is

based on the known solubility constant of mackinawite, K_{spFeS} . The temperature dependency of mackinawite's solubility was found by Benning, *et al.*, [26] as shown in equation (33).

$$S_{FeS} = \frac{C_{Fe^{2+}} \times C_{HS^-}}{K_{spFeS} \times C_{H^+}} \quad (32)$$

$$\text{Log}K_{spFeS} = \frac{2848.779}{T_k} - 6.347 + \text{log}K_{H_2S} \quad (33)$$

where: $K_{sp(FeS)}$: solubility limit of mackinawite (mol/l)

T_k : Temperature (K)

K_{H_2S} : Dissociation constant of H_2S (mol/l)

Unlike with $FeCO_3$, the formed FeS layer has the potential to include various iron sulfide polymorphs, such as amorphous iron sulfide (FeS), cubic iron sulfide (FeS), mackinawite (FeS), troilite/pyrrhotite ($FeS/Fe_{1-x}S$), pyrite (FeS_2), Smythite ($Fe_{3+x}S_4$) and greigite (Fe_3S_4), which makes it more complicated when compared to a sweet environment where typically only $FeCO_3$ is formed. Mackinawite is usually considered to be an initial corrosion product due to its fast kinetics. However, it is not stable and will transform to other types of iron sulfides such as troilite, pyrrhotite, greigite, and pyrite, depending on environmental conditions. At higher temperature and H_2S partial pressure, more stable FeS phases such as pyrite and pyrrhotite will form [27][28][29]. The stability of the corrosion product layer with regards to temperature and H_2S activity are summarized by Smith and Pacheco [25], as shown in Figure 1.

Recent work done by Ning, *et al.*, [30] constructed a simplified Pourbaix diagrams for H_2S-H_2O-Fe system which identified the key FeS polymorph which are relevant to

corrosion of mild steel in oil and gas system namely mackinawite, gregite, pyrrhotite and pyrite. The occurrences of the FeS polymorphs were experimentally proven by the author where mackinawite formed at 25°C while gregite and pyrite were detected at 60°C.

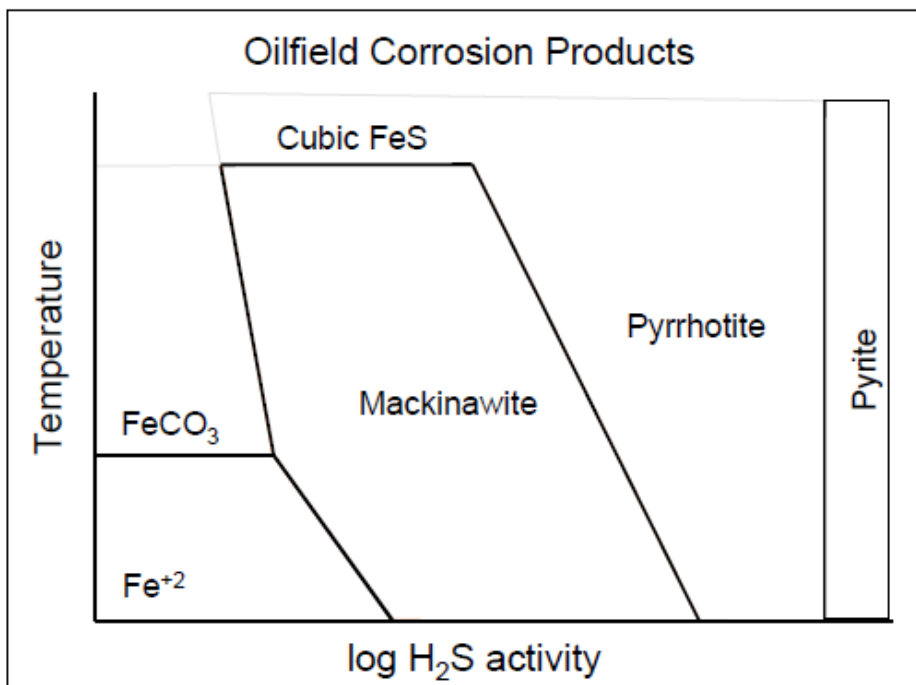


Figure 1: Corrosion product stability with regards to temperature and H₂S activity (Reproduced from [25] – © NACE International 2002)

Work done by Sun, *et al.*, proposed a mechanistic model of H₂S corrosion of mild steel. It was remarked that dissolved Fe²⁺ concentration in pure H₂S corrosion has no significant effect on corrosion rate and iron sulfide scale retention rate [31][32]. This supported the findings from Shoesmith, *et al.*, that an iron sulfide protective film will form in an undersaturated bulk solution at a pH between 5.0 and 5.5 and even lower [24]. A physicochemical model was developed by Sun, *et al.*, describing the mechanism of iron sulfide formation via a direct, solid state corrosion reaction, as shown in equation 31,

which does not include precipitation [31][32]. Based on the proposed model, it follows that a thin mackinawite layer instantaneously forms due to the direct chemical reaction between H_2S and Fe. The formation rate of a mackinawite layer is very rapid compared to that of iron carbonate. This has been hypothesized to be the result of similar geometry between the Fe atoms within the individual mackinawite layers and those for the [100], [010], and [001] planes of *bcc* iron, as shown in Figure 2. This structural similarity means that no rearrangement of Fe atoms needs to occur during the initial formation of mackinawite, a scenario known as topotaxy [33][34]. This provides an optimal surface (α -Fe) for mackinawite to initially nucleate and subsequently grow, given appropriate plane orientation.

Recently, work done by Zheng,[35] explained the formation of double layer structure of FeS formed in H_2S corrosion. The very thin inner FeS layer is formed by direct chemical reaction between H_2S and Fe while the outer layer is formed by precipitation on the corrosion steel surface. The author also concluded that the protectiveness of the outer FeS layer which depends on the surface water chemistry is from the balance between precipitation rate of FeS and the undermining corrosion.

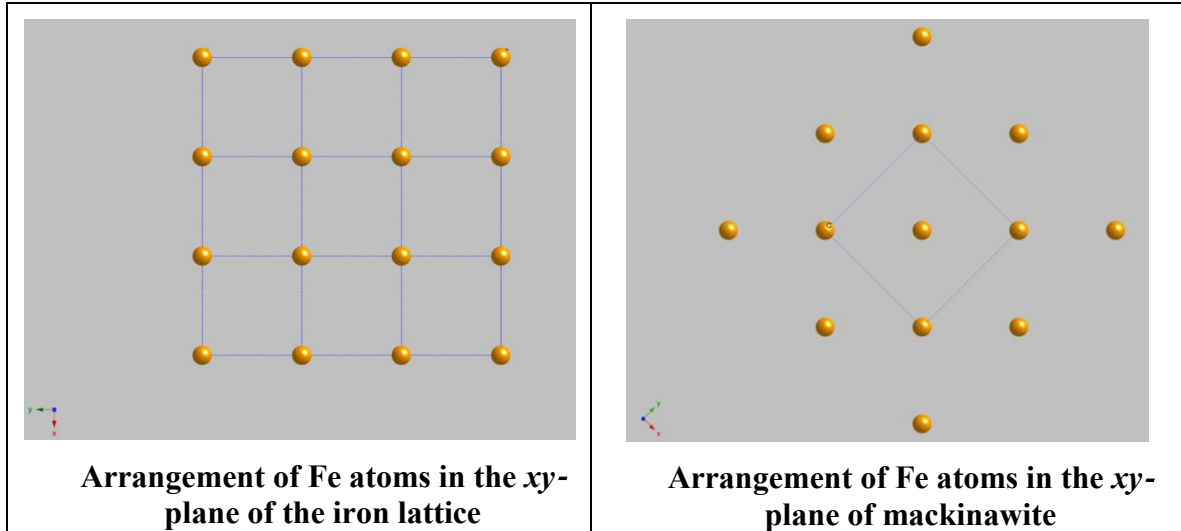


Figure 2: Similarity of the Fe atom geometry between the *bcc* iron lattice and mackinawite (Brown-Fe). Images, generated with CrystalMaker, courtesy of David Young (ICMT).

2.2 Overview of Top-of-the-Line Corrosion

Internal pipeline corrosion can be categorized into three locations of occurrence, bottom, sidewall, and top-of-the-line. As reported by Gunaltun, *et al.*, corrosion at the bottom of the pipeline is normally uniform and can be controlled using corrosion inhibitors[36]. Corrosion at the sidewalls, where the condensed water slides from the top to the bottom of the pipeline, is typically uniform. However, the effectiveness of inhibitors is poor as it is uncertain that they can reach the corroding steel surface. Lastly, corrosion at the top of the pipeline is difficult to control with the use of inhibitors, since they cannot reach the top surface being virtually non-volatile. Thus, the corrosion proceeds unabated and is mainly controlled by the spontaneous formation of protective corrosion product layers such as FeCO_3 and FeS . Nevertheless, localized corrosion could occur if the steel surface is not uniformly covered by the protective corrosion product layer [36].

In general, the key elements in TLC are as depicted in Figure 3, associated with condensation, which occurs due to temperature differences between the gas temperature inside the pipeline and the external temperature. Due to gravitational forces, the condensed water will slide down and accumulate at the bottom of the pipeline. Dissolution of acid gases such as CO_2 and H_2S into condensed water droplets accelerates the corrosion process. The worst aspect of TLC is that the continuous injection of corrosion inhibitor will not protect the top surface of the pipeline, as it is typically insufficiently volatile to reach the surface.

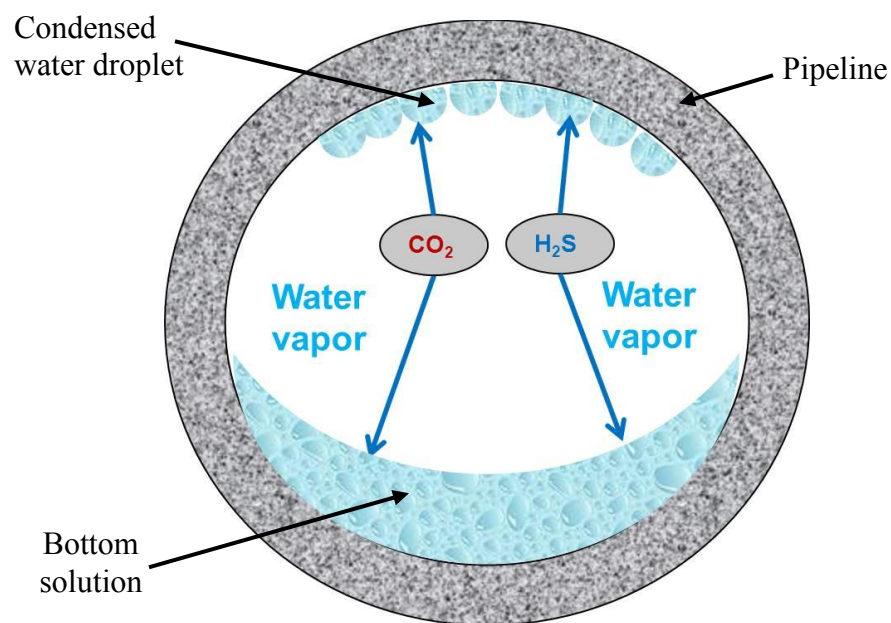


Figure 3: Key elements in TLC.

2.3 Top- of-the-Line Corrosion Behavior in Sweet Environment

2.3.1 Sweet TLC Field Experience

In sweet (CO_2 dominated) TLC, Gunaltun [36], was the first who described in detail a TLC case that occurred in Indonesia. Investigations determined that the corrosion happened at a pipeline location that corresponded to an unburied section exposed to the Mahakam river water in the flowlines of the Tunu field. The three locations which were discovered by In Line Inspection (ILI) tools, as shown in Figure 4, were exposed to excessive cooling, which led to higher water condensation rates. The “dogleg” and upheaval buckling located above the soil level suffered the worst TLC, as shown in the cross section diagram (Figure 5).

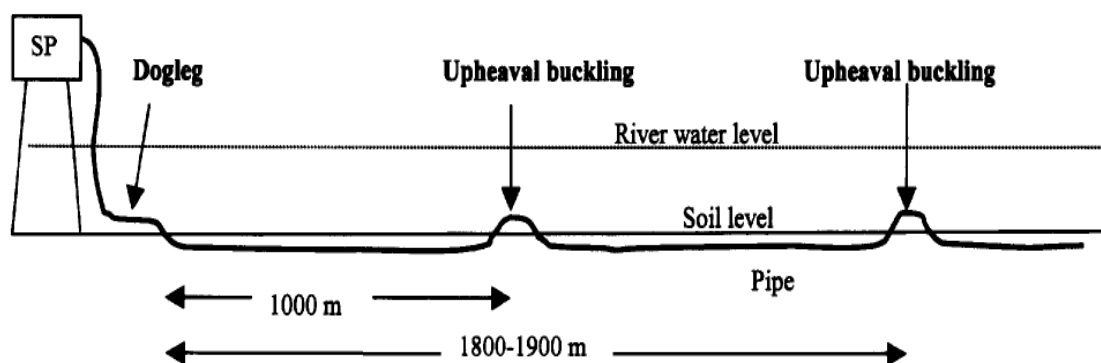


Figure 4: Schematic diagram of the location along the pipeline affected by TLC (Reproduced from [36] – © NACE International 1999)

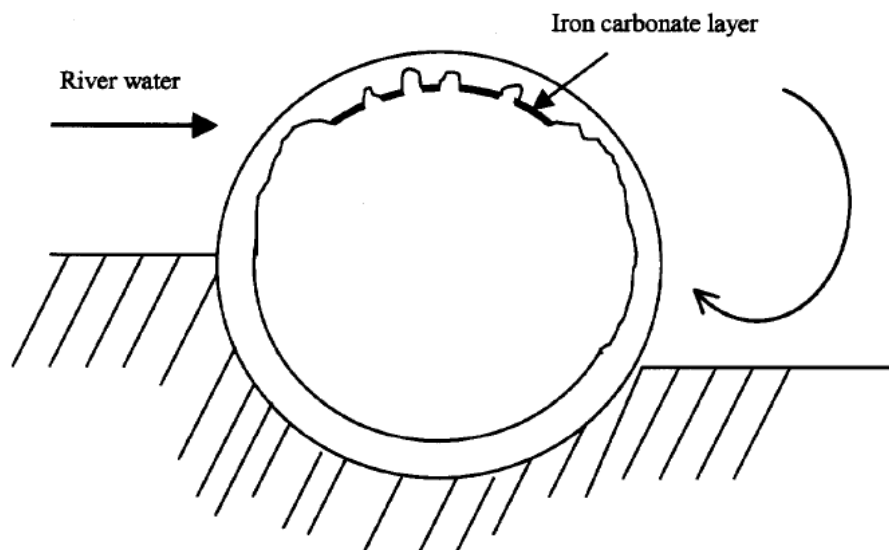


Figure 5: Cross section of the affected area (Reproduced from [36] – © NACE International 1999)

Since water condensation rates were discovered to be the main factor in sweet TLC, the same author completed an analysis of the critical water condensation rate (CWCR) [5]. The value of CWCR was calculated as between 0.15 and 0.25 (ml/m²/s) and used as an engineering rule-of-thumb in order to manage TLC. This value of CWCR is not expected to be valid in all conditions. However, it can still be used as a guideline for TLC if WCR is below the CWCR. The authors also summarized the conditions which accelerate TLC, specifically in wet gas pipelines based on previously reported cases [37]–[39]. TLC cases often occurred with stratified flow in a wet single or multiphase gas pipeline with a large temperature gradient between the inside and outside of the pipeline, which resulted in elevated WCR. This temperature gradient is usually caused by high fluid temperature and external cooling of pipeline either by rivers, sea water or cold air. Locations of the pipeline such as doglegs and unburied protrusions resulting from

upheaval buckling exposed to river or seawater (Figure 4) also contribute to localized excessive cooling of pipeline surfaces. In addition, lack of insulation or compromised insulation, especially at the field joints and where there was broken concrete, was also identified as being the key factors in TLC. The presence of 500 to 3000 ppm acetic acid (HAc) in the produced water would also significantly contribute in TLC rate, since volatile HAc would co-condense with water and further reduce the pH of condensed water and accelerate the corrosion process.

2.3.2 Sweet TLC Mechanism

Sweet TLC mechanisms were briefly described in the previous chapter. For the past 20 years, research in this area has been intensely conducted and the main mechanism and model were developed. In one of the first attempts, Olsen, *et al*, [6] conducted a systematic experimental study to determine the main controlling parameters in sweet TLC. The nature of the corrosion product layer, which is FeCO_3 , is the main controlling parameter in lowering the TLC rate in sweet environments. At low water condensation rates, the TLC rate is governed by the formation of a protective FeCO_3 layer. The precipitation of FeCO_3 could only be achieved if the saturation level is above one, as described below in more detail. The saturation level is mainly dependent on iron dissolution from the corrosion process increasing the concentration of Fe^{2+} in the condensed water, and the rate of water condensation, which dilutes it. At higher water condensation rates, supersaturation of FeCO_3 cannot be achieved since the concentration of Fe^{2+} is reduced by the renewal of freshly condensed water. Therefore, under this

condition, the steel is unprotected by a corrosion product layer, which leads to higher TLC rates.

Research done by Nyborg, *et al*, [10] also supported the sweet TLC mechanism previously described, where the sweet TLC model in wet gas pipelines is proportional to the water condensation rate, supersaturation with respect to the FeCO₃ layer, and its solubility. Their empirical model is shown in equation 34 below. It is only valid at low acetic acid content (<0.001 Mol/L) and low partial pressures of CO₂ (<3 bars). The authors stated that the effect of water condensation rates on TLC rate is more significant than the effect of CO₂ partial pressure.

$$CR = 0.004 \times WCR \times [Fe^{2+}] \times (12.5 - 0.09 \times T) \quad (34)$$

Where CR: Corrosion rate (mm/yr)

WCR: Water condensation rate (g/m²/s)

[Fe²⁺]: Concentration of ferrous ion (ppm_w)

T: Temperature (°C)

The model is also not valid when H₂S is present in the system, since FeS will form rather than FeCO₃ due to its fast kinetics of formation. Further explanations of TLC behavior in the presence of H₂S are given in detail in the present dissertation.

Another sweet TLC model has been described by Singer [40], which was the first attempt to predict the localized corrosion mechanism in TLC scenarios. According to the author, at low water condensation rates the formation of FeCO₃ would reduce the TLC rate. However, in longer term exposure, the local presence of new droplets of freshly condensed water of low pH (3.5-4.0) on the steel surface would re-dissolve the existing

FeCO₃ layer. This is due to the fact that FeCO₃ is not persistent at lower pH since its pH for saturation is higher, at approximately pH 5.5–6.0. Thus, dissolution of the FeCO₃ layer would expose the bare steel surface to the acidic, freshly condensed water and lead to localized corrosion.

2.4 Research Specific to Sour Top-of-the-line Corrosion

2.4.1 Sour TLC Field Experience

As mentioned above, top of the line corrosion was first identified in the 1960s. Therefore, it has been more than 40 years since top of the line corrosion, mainly in sour gas environments, was first reported. The problem of top of the line corrosion in a sour environment is now a growing concern for the oil and gas industry, both onshore and offshore. The first sour gas top of the line corrosion failure was reported at the sour gas field of Lacq in France [37]. The TLC case was reported in a 6” buried pipeline which carried a mixture of 70% methane, 15% H₂S, and 9% CO₂. In addition, a hydrate inhibitor, such as glycol or methanol, was introduced at concentrations of up to 1000 ppm. The failure was determined to be due to sharp edged pits that combined to become a large corroded area on the upper part of the pipeline, as shown in Figure 6. Various methods were suggested in order to mitigate the corrosion, such as elimination of condensed water from gathering lines, coating the inner surface of the pipeline, and the usage of volatile corrosion inhibitor. However, of all the suggested methods, changing the flow pattern from stratified to annular by increasing the gas flow rate was chosen and worked well, since annular flow provided better protection for the top surface.

The second case related to sour TLC failure was reported at the Crossfield gathering system, located approximately 32 km northwest of Calgary, Canada. The 6” pipeline was transporting wet gas which contained 0.3% H₂S and 5.9% CO₂. Due to the low gas velocity that resulted in stratified flow in a few portions of the pipeline, vapor phase corrosion or TLC was detected. The corrosion was also due to the lack of a protecting layer/scale on the internal surface of the steel pipeline. Based on data analysis, a significant loss of wall thickness was observed between the 7 and 5 o’clock positions of the pipeline, as shown in Figure 7, as compared to nominal wall thickness at the bottom of the pipeline [38].



Figure 6: Corrosion on upper part of the pipeline (Reproduced from [37]– © NACE International 1963)

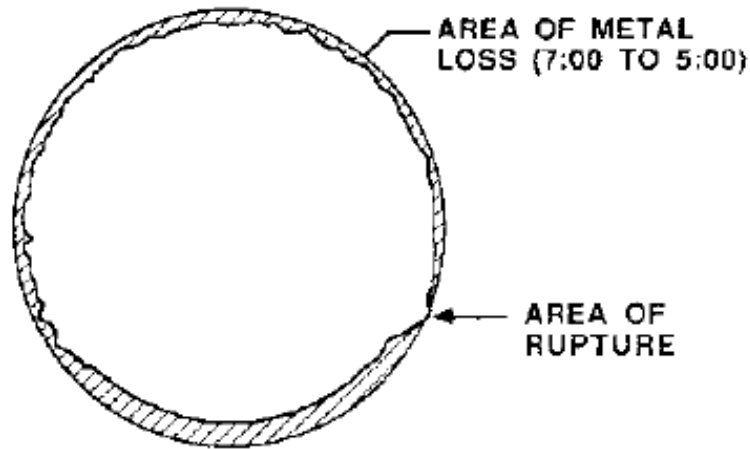


Figure 7: Cross sectional diagram of the failure (Reproduced from [38]– © NACE International 1987)

Magnetic flux leakage (MFL) is one of the most common TLC inspection methods systems used in the field and is utilized in large diameter carbon steel sour wet gas pipelines to identify TLC. In MFL, the pipeline is magnetized and the corrosion or pitting which occurs is indicated by a distorted magnetic field signal which is used to determine extent of metal loss at the wall. Sample metal loss plots are shown in Figure 8 and Figure 9 [41]. In sweet TLC, the MFL result (Figure 8) showed a high TLC rate for the first 1.5 km of the pipeline, measured from the pipeline inlet. This resulted from the high initial water condensation rate at the inlet due to the large temperature gradient between the gas inside the pipeline and the external environment, which hinders formation of a FeCO_3 layer. This result agreed with the sweet TLC model that was explained in the previous chapter.

However, the situation for the sour CO₂/H₂S system shown in Figure 9, the MFL analysis showed different corrosion behavior as compared to that for the CO₂ environment shown in Figure 8. In this pipeline, the wet gas contained 15% CO₂ and 50 ppm H₂S, at a gas temperature of 40°C. The analysis showed no top of the line corrosion was detected at the pipeline inlet (first 10 km) where a high water condensation rate occurred. This finding contradicts the result found in sweet environments, since in this case the TLC rate did not have a similar correlation with water condensation rate [42]. Therefore, it was demonstrated that the sweet TLC model could not be applied to sour environments since the corrosion mechanism is different.

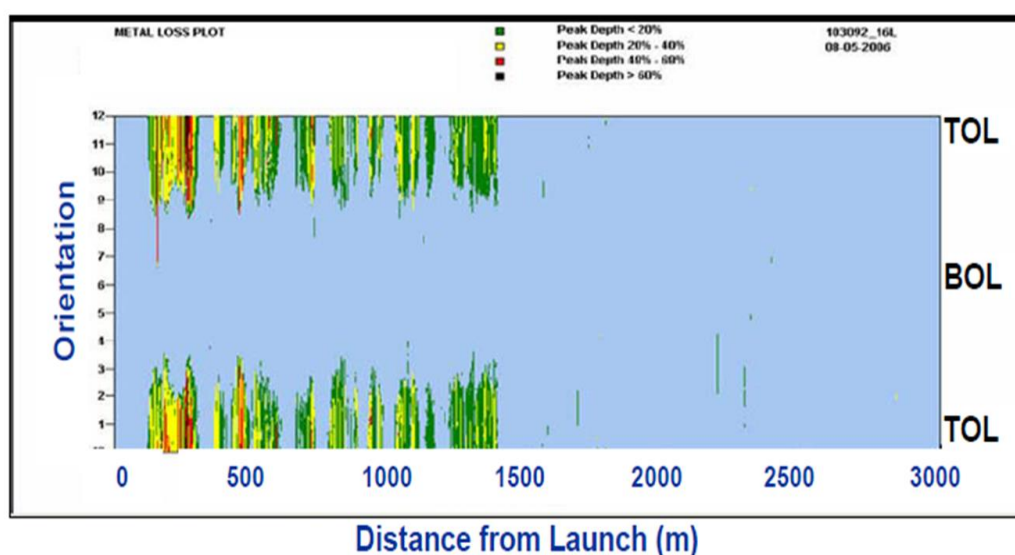


Figure 8: MFL analysis result for sweet TLC (Reproduced from [42]– © NACE International 2009)

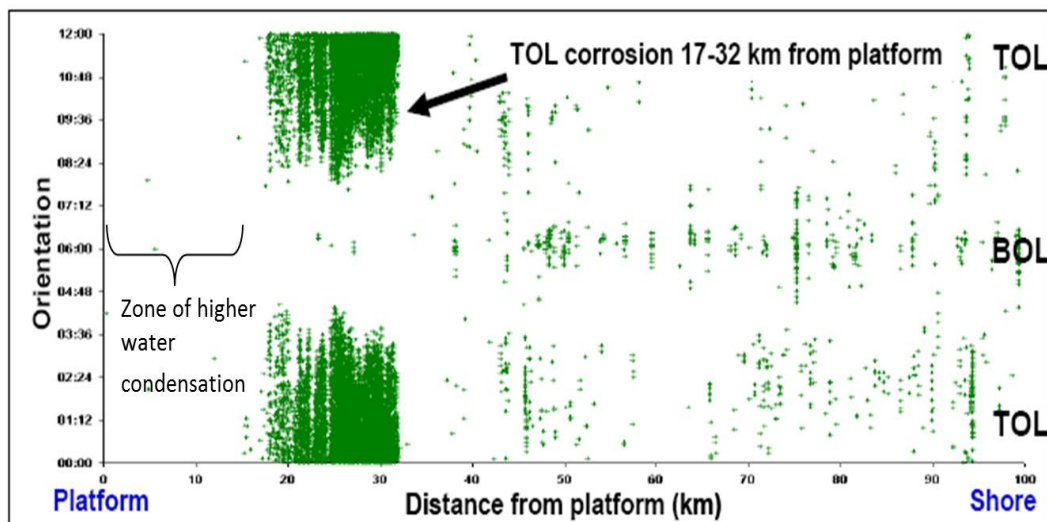


Figure 9: MFL analysis result for sour TLC (Reproduced from [42]– © NACE International 2009)

2.4.2 Influence of Water Condensation Rate and Temperature on Sour TLC

As mentioned in the previous chapter, in sweet TLC the water condensation rate was determined to be one of the main parameters governing the corrosion rate. However, in sour gas, as reported by Pugh, *et al.*, the TLC rate demonstrated a different dependence on water condensation as compared to a sweet system. In the work done at low and high water condensation rates, at 25°C and 55°C, respectively, the top of the line corrosion rate was determined to be higher at low condensation rates as compared to that for a high condensation rate. Since condensation rate and gas temperature are interdependent, full immersion corrosion tests (matching TLC environments) were performed to distinguish the parametric effect between temperature and condensation rate [42]. It was shown that the corrosion rate at the low temperature (25°C) was higher than that for the higher temperature (55°C). Temperature also seemed to be the controlling parameter that governs the type of iron sulfide layer formed, such as whether it contains mackinawite

and/or pyrrhotite. Other reported key variables, affecting both corrosion rate and iron sulfide type, were reported to be H₂S partial pressure, experimental duration, and pH. Other research has been conducted to investigate the formation of iron sulfide polymorphs in particular parametric ranges [25][43][44].

The corrosion rate that was obtained in the full immersion test was higher than that for the condensation rate test, which indicates that condensation rate is a secondary parameter in sour TLC. However, the correlation between temperature and sour TLC rate needs to be verified to take into account the various types of FeS phase formed and the physical properties of the FeS layer (dense or porous) in relation to how the metal becomes protected from corrosion.

Extensive sour TLC experiments were conducted by Singer, *et al.*, [11] to simulate as closely as possible the specific conditions of a gas field of interest located in the Arabian Gulf. The experiments were conducted in a large scale flow loop and autoclave. The H₂S partial pressure tested were between 0.1 and 4.0 bars, with gas temperatures from 40 to 55°C, which created various water condensation rates and steel temperatures. It was shown that there was no clear effect of water condensation rate on TLC, as shown in Figure 10. Comparisons with the findings reported by Pugh, *et al.*, confirmed that higher TLC rates were obtained at lower temperature and *vice versa*, as shown in Figure 11.

Nevertheless, broader ranges of water condensation rate and temperature need to be tested in order to make further correlations relating to sour TLC. Thus, further investigation is required for verification purposes at higher total pressures and

concentrations of H_2S . Based on experimental observations, a systematic approach in order to study and verify the effect of temperature and water condensation rate in sour TLC was done by the author of this dissertation.

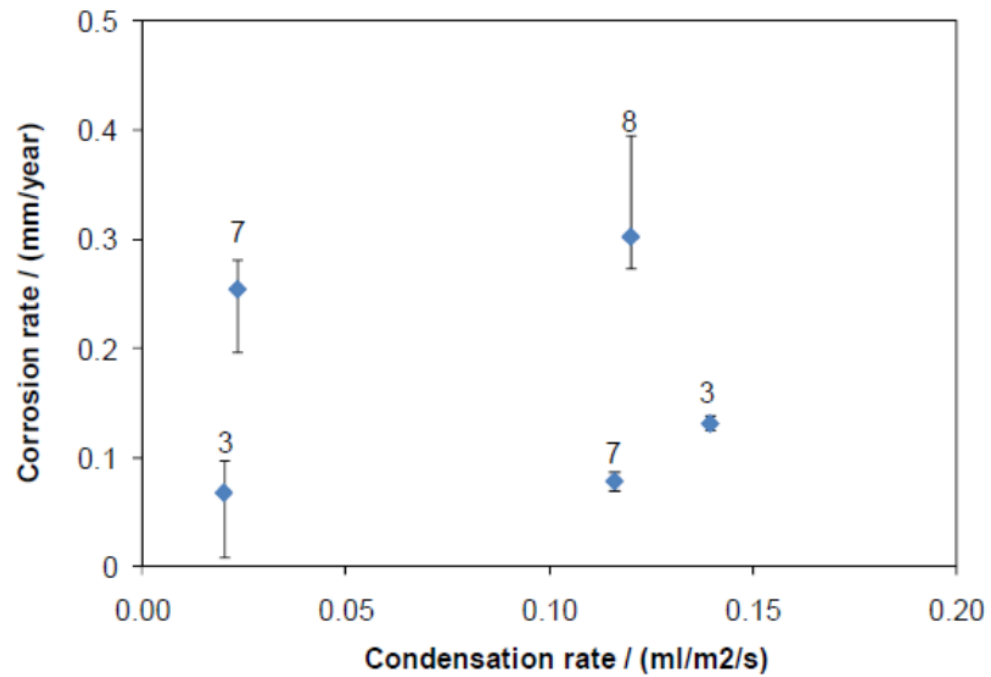


Figure 10: Influence of condensation rate on TLC (Reproduced from [11]– © NACE International 2012)

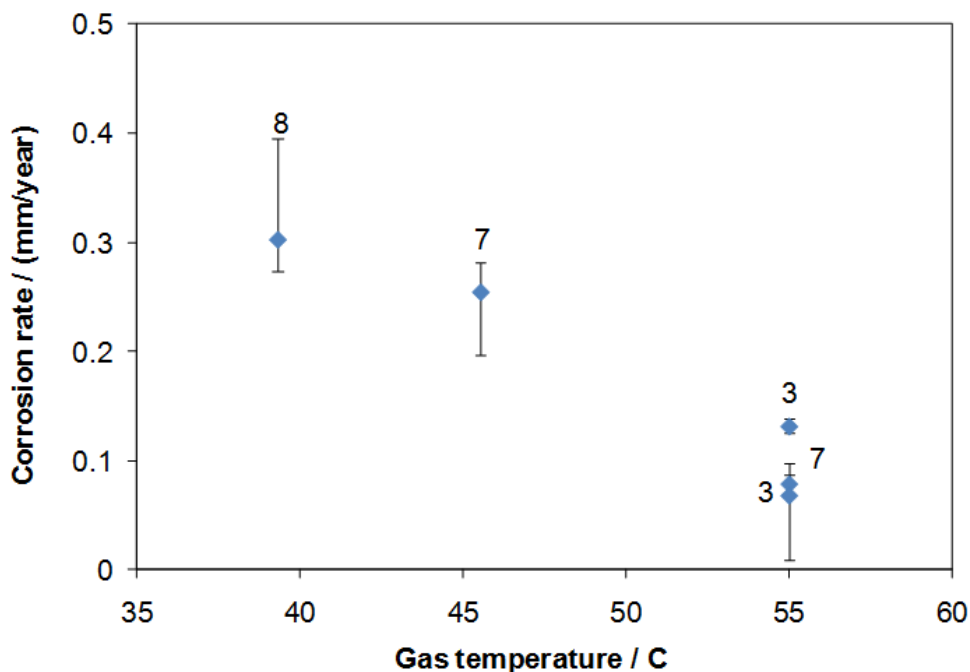


Figure 11: Influence of gas temperature rate on TLC (Reproduced from [11]– © NACE International 2012)

2.4.3 Influence of Hydrogen Sulfide Concentration on TLC

Camacho, *et al.*, performed a series of tests in a flow loop to investigate the influence of traces of H₂S present with CO₂ on TLC [12]. The concentration of H₂S in the system was between 0 and 0.13 bars, with 3 bars of total pressure. Based on their findings, the authors concluded that an increase in H₂S concentration in a CO₂ environment retards the general top of the line corrosion rate through formation of an iron sulfide layer, as shown in Figure 12 . It was also found that, regardless of partial pressure of CO₂, the corrosion product layer will be dominated with an FeS layer whenever H₂S is present, even at a low concentration.

Another series of sour TLC experiments were done by Singer, *et.al.*, [45] where the effect of partial pressure of H₂S in the presence of acetic acid (HAc) was studied. It

was found that the presence of acetic acid increased the TLC rate, as shown in Figure 13. The presence of acetic acid affected the protectiveness of the FeS layer, which led to localized corrosion. However, the effect of acetic acid on sour TLC mechanisms is outside the scope of this dissertation. In order to understand the sour TLC mechanism, the main parameters that control sour TLC, such as the effect of H₂S concentration, water condensation rates, and temperature, have to be studied first.

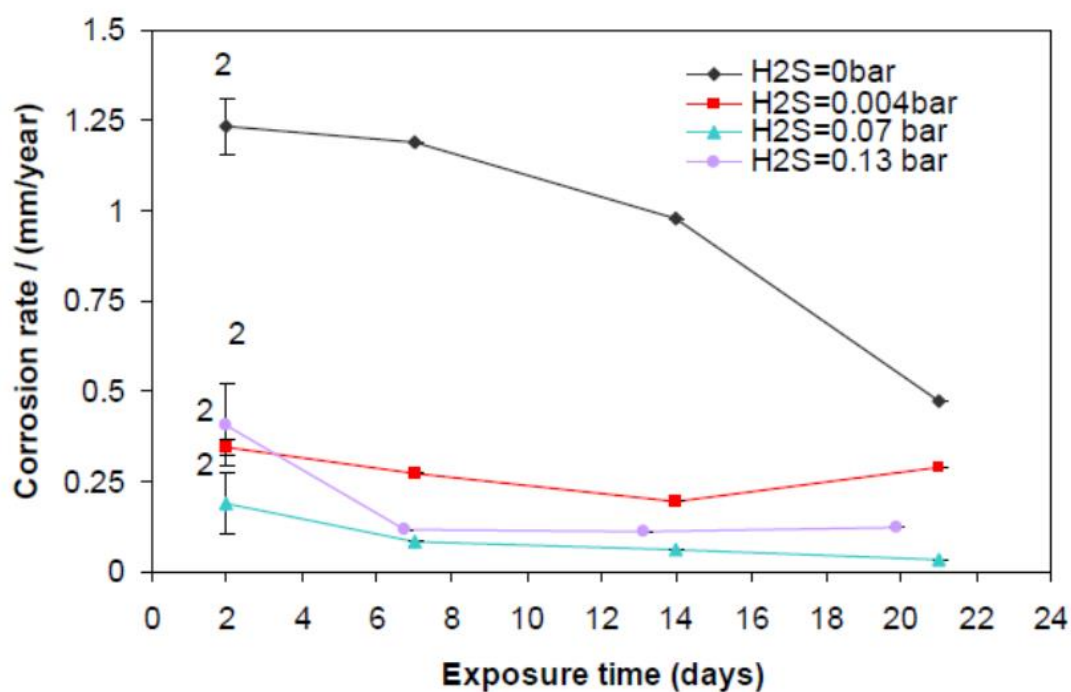


Figure 12: Influence of H₂S concentration on TLC (Reproduced from [12]– © NACE International 2008)

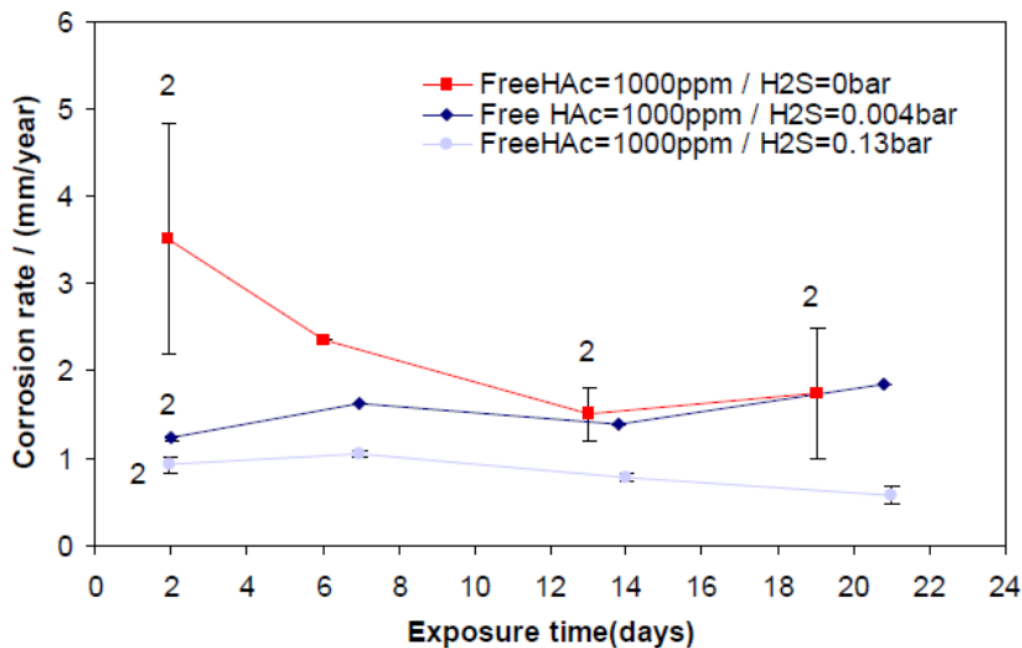


Figure 13: Influence of H₂S concentration on TLC with the presence of 1000 ppm acetic acid (Reproduced from [45]– © NACE International 2010)

2.4.4 Top-of-the-Line Corrosion in Marginally Sour Environments

It is well known and has been previously explained that the TLC mechanism between sweet and sour environments is different. Therefore, it is important to know the threshold of the H₂S level at which the TLC mechanism switches from sweet to sour. Work done by Dunlop, *et al.*, [46] and Smith [47] reported a CO₂/H₂S ratio of 500 as a reference point for the transition between sweet and sour corrosion. If the ratio is higher than 500, it is presumed that iron carbonate (FeCO₃) should prevail, and if it is lower than 500, iron sulfide should form. However, this ratio is very sensitive to thermodynamic data used by these researchers, such as FeS heat of formation and FeCO₃ Gibbs free energy values. This rule of thumb is not recommended as an engineering tool to predict corrosion in the field, but it can act as a guideline to investigate the transition point between sweet and sour environments.

Until now, there has been no known mechanism to identify whether the system is marginally sour or not. The question which needs to be answered is, “What constitutes marginally sour environments?” There are a few methods which can be suggested in order to elucidate this problem. The first one is by identification of the corrosion product layer. As mentioned previously, in sweet environments, iron carbonate (FeCO_3) or iron carbide (Fe_3C) should be seen as the corrosion product. In fully sour environments, only iron sulfide has been proven to form due its faster kinetics of formation. Thus, in marginally sour conditions, it is expected that both FeS and FeCO_3 could be seen on the steel surface. The second method was suggested by Dunlop, *et al.*, and was discussed in the previous paragraph, which is using the ratio of partial pressure of CO_2 and H_2S ($\text{pCO}_2/\text{pH}_2\text{S}$). However, this method (ratio) could not be extrapolated to other conditions as it is very sensitive to temperature. Another possible method involves use of Pourbaix diagrams to predict the equilibrium phase for resultant corrosion products given particular parameters, such as partial pressure of CO_2 or H_2S , pH, and temperature. The last method which could accurately represent the system is calculating the ratio of total aqueous concentration of carbonate species to total sulfide species. However, no correlation of the ratio with experimental data is available. Investigating the correct method to define a marginally sour environment is not an objective of this work. However, data reported herein may provide additional information that leads to a better understanding of how to define marginally sour environments.

Up to the present date, there have been few publications that have dealt with slightly sour environments, especially in TLC. Brown, *et al.*, [48] reported localized

corrosion as high as 30 mm/y in 10 milibar (mbar) H₂S (1500 ppm) in steel samples exposed to bottom of the line conditions. A few researchers in ICMT, Navabzadeh, [49] and Wei Yan [50] also observed localized corrosion as high as 8 mm/yr and 11 mm/yr in marginally sour environments with between 0.03 mbar (30 ppm) and 0.09 mbar (90 ppm) of H₂S.

In TLC work done by R. Nyborg, *et al.*, [15] in slightly sour environments 2 mbar (200 ppm) H₂S, 10 bar CO₂, 500 ppm HAc and 25°C, the authors reported the formation of a porous FeS layer (50 - 100 μm) with poor corrosion protection. Close to the steel surface a protective FeCO₃ layer formed. The authors claimed sulfide depletion close to the metal surface resulting in the formation of FeCO₃. The TLC behaves similarly to what was observed in a sweet environment, where a high TLC rate was associated with a high water condensation rate. Furthermore, the calculated TLC rate in this work with the presence of small amounts of H₂S was higher as compared to that predicted in the sweet TLC model without H₂S. Other research performed by Li, *et al.*, [14] in slightly sour TLC (1000 ppm H₂S, 7 bars CO₂, T_{steel} = 40°C) showed that both FeS and FeCO₃ could form together on the steel surface, as shown in Figure 14. The author reported similar findings compared to sweet environments, where higher water condensation rates led to higher TLC rates. Higher water condensation rates reduced the supersaturation of FeCO₃, leading to a less protective corrosion product. Thus, it is important to understand formation of corrosion product layers in TLC.

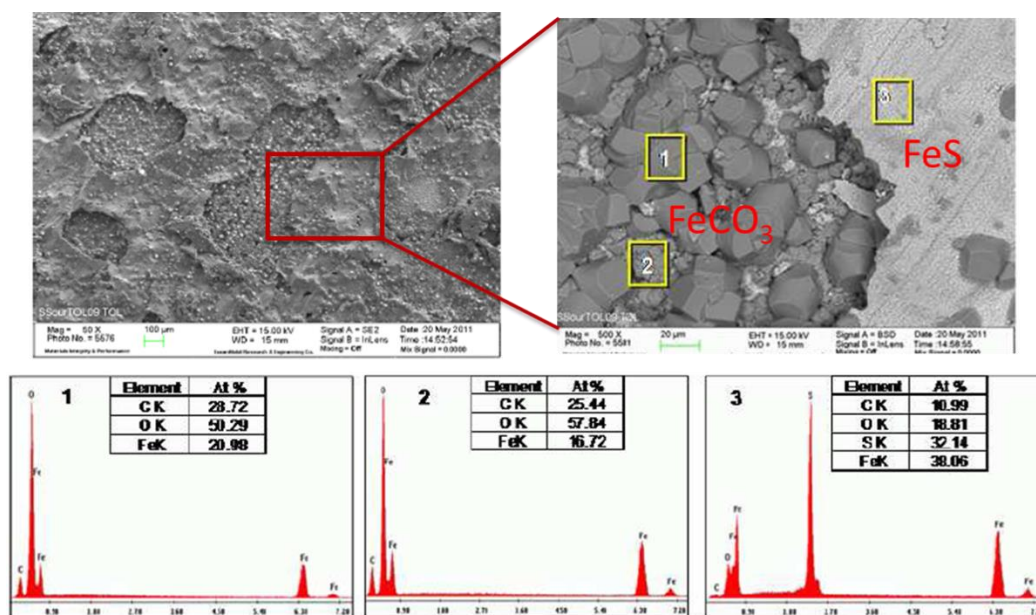


Figure 14: SEM analysis of corrosion product layers showing formation of both FeCO₃ and FeS (Reproduced from [14]– © NACE International 2012)

2.5 Research Gaps Associated with Sour Top-of-the-Line Corrosion

Most of the work done in sour gas environments was mainly to investigate the corrosion mechanism and the parameters that significantly affect the corrosion behavior. However, most of the work performed thus far has focused on the bottom of the line corrosion under full water immersion. Limited research has focused on sour gas TLC. Another factor which makes sour gas TLC less well understood is that most of the previous work has focused on sweet (CO₂) TLC, the lessons from which cannot be directly applied to H₂S environments. Even in marginally sour TLC, small amounts of H₂S in a sweet environment will affect the corrosion rate and mechanisms. The oil and gas industry has used sweet corrosion prediction methods in predicting sour TLC, thus leading to inaccuracy [42].

Therefore, in this work, the main focus is to investigate TLC behavior in the presence of H₂S to obtain a better understanding of the corrosion mechanism and the factors which affect the sour TLC rate. Detailed objectives and explanations related to this work are discussed in the next chapter.

CHAPTER 3: RESEARCH OBJECTIVES AND HYPOTHESES

3.1 Research Objectives

Based on the literature review, the TLC mechanism in the presence of H₂S is still unclear. Thus, the main objective of this work is to study corrosion mechanisms in CO₂/H₂S environments relating to TLC by developing an understanding of the protective corrosion product layer formation processes at various gas/steel temperatures, water condensation rates, and H₂S concentrations. This will permit construction of a descriptive model for corrosion behavior in CO₂/H₂S top-of-the-line corrosion. The experimental work is divided into two parts. In the first part, the TLC mechanisms are studied and discussed at marginal H₂S concentrations. In the second part, TLC mechanisms are investigated at high H₂S partial pressure, an environment that is also called highly sour or H₂S dominant.

3.2 Hypotheses

3.2.1 *TLC Behavior in Marginally Sour Environments*

In marginally sour TLC, the steel surface could be covered with a very thin mixed FeS/FeCO₃ layer which does not confer great protectiveness from corrosion which leads to undermining and compromises the protection by the thin corrosion product layer. Local failure of this layer may lead to partial coverage of the steel. If this happens, the portions of the steel surface which are bare would be exposed to both H₂CO₃ and aqueous H₂S, leading to localized corrosion. The increase in the H₂S concentration would increase the protectiveness of the FeS layer by increasing its supersaturation near the steel and

accelerating the rate of precipitation, thus providing better coverage of the steel surface, which would lead to a lower TLC rate and absence of localized corrosion. Thus, the research strategy in relation to this hypothesis was as follows:

1. Investigate the effect of the temperature (gas and steel) and water condensation rate in marginally sour TLC, all of which affect the formation of the protective corrosion product layer.
2. Uncover the reasons for occurrence and mechanism of pitting corrosion in marginally sour TLC.
3. Develop a descriptive model of marginally sour TLC behavior which includes a localized corrosion mechanism.

3.2.2 TLC Behavior in Highly Sour Environments

In highly sour environments, the formation of FeS controls sour TLC through the formation of more stable and protective corrosion product layers which include stable polymorphs, particularly at high temperature. Water condensation rate (WCR) is a secondary factor, acting indirectly when a higher WCR would lower the steel temperature, what results in less protective corrosion product layers and increased TLC rate. The research strategies to test the hypothesis are as follows:

1. Investigate the effect of gas/steel temperature on highly sour TLC.
2. Study the effect of water condensation rate on highly sour TLC.
3. Study TLC behavior at increasing H₂S partial pressure while controlling the temperature of the steel.

4. Develop a descriptive model of highly sour TLC which covers the effects of gas/steel temperatures, H_2S partial pressure, and water condensation rate.

CHAPTER 4: METHODOLOGY AND EXPERIMENTAL DESIGN

This chapter is sub-divided into two parts, each dealing with methodologies and experimental design for TLC studies, first in marginally sour and then in highly sour environments. Experimental equipment, test matrices, and procedures for each condition are described.

4.1 TLC in Marginally Sour Environments

As discussed in the previous chapters, there is a need to separately investigate TLC in marginally and highly sour environments as both have different mechanisms. Thus, in this part of the research, experiments were designed to primarily investigate TLC behavior in the presence of gas phase concentrations of H₂S of up to 0.15 mbar/ 150 ppm. Experimental design is explained further in the following sub-sections.

4.1.1 *Equipment*

A 2 L glass cell setup was used to conduct experiments at atmospheric pressure, as shown in Figure 15. Two X65 carbon steel coupons were flush mounted on the lid of the glass cell. Cooling coils were placed around the sample holders and water circulated therein in order to cool the steel and facilitate condensation on the coupon surface. A hot plate was used to heat the solution in order to achieve the desired gas temperature. One coupon was used for weight loss corrosion rate determination and the other for cross-section analysis. Condensed water was collected in the collection cup for determination of ferrous ion concentration, condensation rate, and pH measurement. The pH of the

condensed water and the bottom solution were measured *in situ*. Sample preparation and post analysis methods are discussed further in the next section.

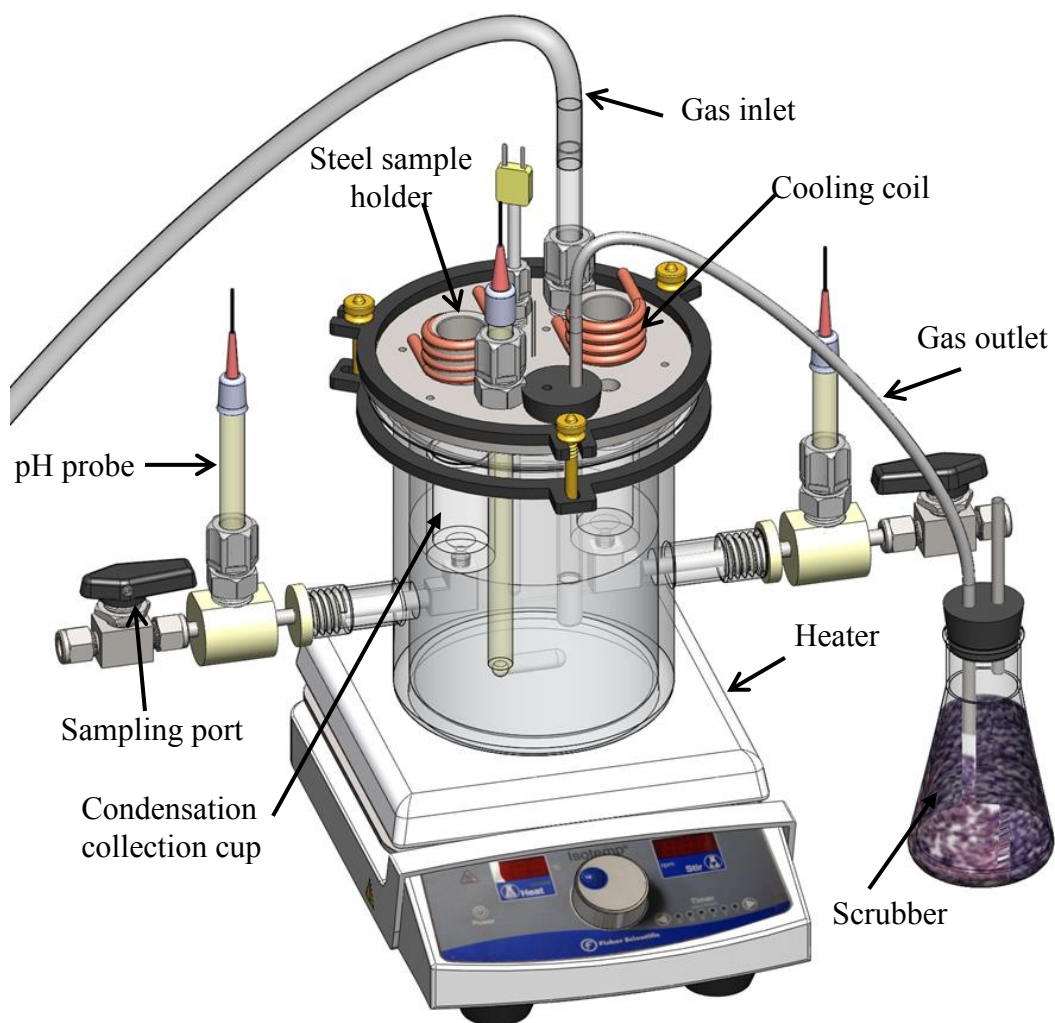


Figure 15: Glass cell experimental set up for marginally sour TLC experiments. Images courtesy of Cody Shafer, ICMT

4.1.2 Material Tested

The material tested in this experimental is a quenched & tempered API 5L X65 carbon steel with the chemical composition shown in Table 1. Samples consisting of round coupons (3.2 cm diameter and 1.2 cm thickness) were coated on the sides and bottom with Teflon paint to avoid any galvanic effect due to contact with the sample holder, leaving an exposed area of 8 cm², as shown in Figure 16.

Table 1: Chemical composition of weight loss steel samples - API 5L X65 (balance Fe).

Material name	Al	As	B	C	Ca	Co	Cr	Cu
X65	0.032%	0.008%	0.001%	0.13%	0.002%	0.007%	0.14%	0.131%
	Mn	Mo	Nb	Ni	P	Pb	S	Sb
	1.16%	0.16%	0.017%	0.36%	0.009%	<0.001%	0.009%	0.009%
	Si	Sn	Ta	Ti	V	Zr		
	0.26%	0.007%	<0.001%	<0.001%	0.047%	<0.001%		

4.1.3 Test Matrices

Two test matrices with differing temperatures, Part A (Table 2) and Part B (Table 3), are outlined below. Experiments were of 7 days duration with H₂S partial pressures of 0, 0.015, 0.030, 0.080, and 0.150 mbar. Part A has a gas temperature of 40°C; for Part B this value is 60°C. An additional test matrix, Part C (Table 4), describes experiments used to explore the effect of experiment duration on observed TLC phenomena; test time was 3, 7, and 21 days with a gas temperature of 40°C, and 0.03 mbar H₂S.

Table 2: Test matrix part A; marginally sour TLC

Investigating	TLC in mixed CO ₂ /H ₂ S environment				
Total pressure (bar)	1				
pCO ₂ (bar)	0.93				
Gas temperature (°C)	40				
Steel temperature (°C)	28 ± 1	28.0 ± 0.3	27.4 ± 0.8	25 ± 1	28 ± 1
Condensation rate (mL/m ² /s)	0.38 ± 0.1	0.26 ± 0.05	0.28 ± 0.06	0.25 ± 0.03	0.25 ± 0.04
pH ₂ S (mbar)	0	0.015	0.03	0.08	0.15
Test duration	7 days				

Table 3: Test matrix part B; marginally sour TLC

Investigating	TLC in mixed CO ₂ /H ₂ S environment				
Total pressure (bar)	1				
pCO ₂ (bar)	0.8				
Gas temperature (°C)	60				
Steel Temperature (°C)	43.0 ± 1.3	42.0 ± 0.7	40.2 ± 1.3	41 ± 2.4	40 ± 1.9
Condensation rate (mL/m ² /s)	1.47 ± 0.13	0.45 ± 0.22	1.50 ± 0.32	1.60 ± 0.10	1.65 ± 0.25
pH ₂ S (mbar)	0	0.015	0.03	0.08	0.15
Test Duration	7 days				

Table 4: Test matrix part C; marginally sour TLC

Investigating	Effect of exposure time		
Total pressure (bar)	1		
pCO ₂ (bar)	0.9		
Gas temperature (°C)	40		
pH ₂ S (mbar)	0.03		
Steel Temperature (°C)	31 ± 2	27.4 ± 0.8	28 ± 1
Condensation rate (mL/m ² /s)	0.14 ± 0.04	0.28 ± 0.06	0.25 ± 0.05
Test Duration (days)	0-3	0-7	0-21

4.1.4 *Experimental and Analytical Procedures*

Prior to each experiment, the weight loss coupons (X65 carbon steel) were polished using isopropyl alcohol as coolant, with silicon carbide abrasive papers of up to 600 grit. The coupons were then flush mounted to the glass cell lid using a specially designed holder. The bottom solution consisted only of deionized water deoxygenated for two hours by purging with nitrogen gas. H_2S and CO_2 were then mixed using a rotameter to achieve the desired concentration of H_2S , as shown in Figure 17, and introduced into the glass cell. The gas mixture was continuously sparged into the glass cell throughout the experiments. The concentration of H_2S in the gas phase was measured by using a colorimetric gas detector tube every two days to confirm that it remained constant. Effluent gas was passed through a bed of activated carbon prior to being released to the combustion system (Figure 17).

The water condensation rate was measured every day by collecting and measuring the volume of condensed water over specific durations. Thus, by knowing the volume of condensed water, the duration time, and the surface area of the sample, the water condensation rate can be calculated (values as shown in the test matrices). The ferrous ion concentration in the collected condensed water was measured using spectrophotometry. The principle of this measurement is ferrous ion reacting with o-phenanthroline to form a colored complex ion. The intensity of the colored species is measured using the spectrophotometer. The concentration of the unknown ferrous ion in the condensed water sample is determined using a constructed calibration curve (absorbance as a function of concentration) [51]. The steel temperature was measured

every day by placing a thermocouple at the back side of the steel sample, facing out from the glass cell lid.

Upon removal from the system, coupon surfaces were rinsed with isopropyl alcohol, dried, and stored in desiccators for further surface analysis. ASTM G1 standard [52] was followed to remove the corrosion products and determine the corrosion rate by weight loss. Half of the coupons were generally used for weight loss measurements, the others were preserved for further corrosion product evaluation. Scanning electron microscopy (SEM) was used to study the corrosion product morphology while energy dispersive X-ray spectroscopy (EDS) microanalysis and X-ray diffraction (XRD) were used for chemical analysis and identification of the crystal structure, respectively. Prior to SEM/EDS, samples were sputter coated with palladium. In addition, after removal of the corrosion product layer, a surface profile analysis was conducted using an optical profilometry microscope, in order to identify topographical surface features due to corrosion.

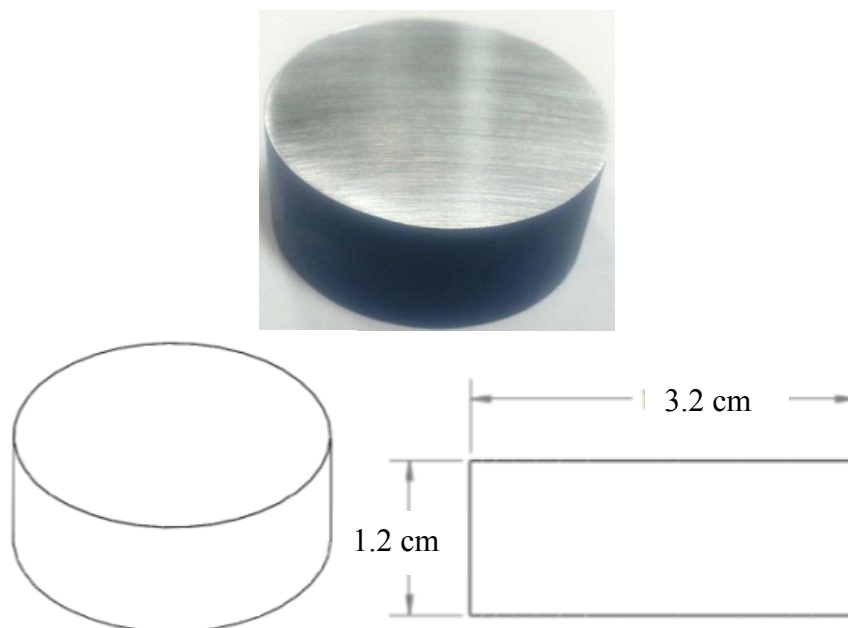


Figure 16: X65 sample coupon for marginally sour TLC experiments

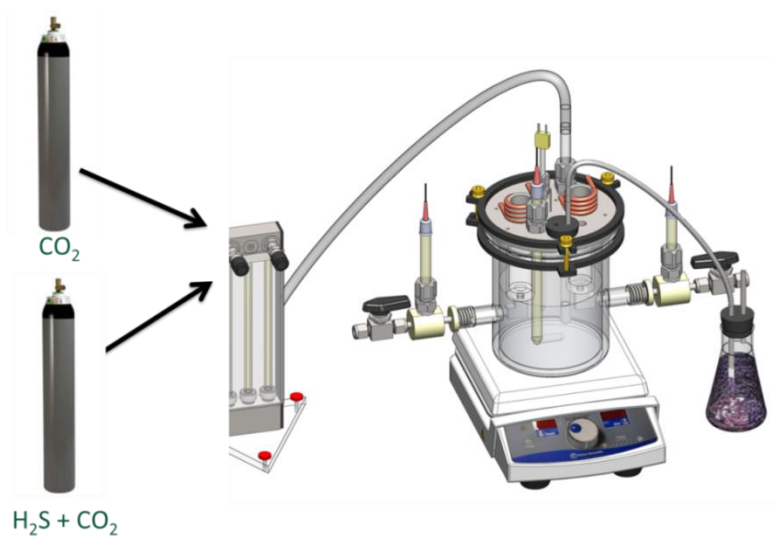


Figure 17: Overall experimental setup for marginally sour TLC experiments. Image courtesy of Cody Shafer, ICMT

4.2 TLC in Highly Sour Environments

This section describes the experimental design used to investigate TLC behavior in highly sour environments, with total pressure up to 30 bars. The concentrations of H₂S in the gas phase were between 0.2 and 5 bars, and the experiments were conducted at various gas/steel temperatures and water condensation rates. The design of the experimental setup, sample characteristics, test matrices, and experimental/analytical procedures are described in the following sections.

4.2.1 Equipment

Experiments were conducted in a 20 Liter autoclave made of UNS⁽¹⁾ N10276 Hastelloy[†], as shown in Figure 19. The autoclave is specially manufactured to enable corrosion measurements under condensing conditions up to a maximum pressure of 1000 psi. The top lid of the autoclave is equipped with an internal cooling system and a sample holder plate, as shown in Figure 18. A total of eight steel samples can be installed for a single test. The design of the sample holder enables study of the effect of two condensation rates corresponding to two steel temperatures in a single test. This was done by “hanging” four of the steel samples in the gas phase at a particular distance away from the cooled plate, which makes the samples less cooled, thus changing the condensation rate thereon. The four steel samples directly attached to the cooling plate will have a

⁽¹⁾ Unified Numbering System for Metals and Alloys (UNS). UNS numbers are listed in Metals & Alloys in the Unified Numbering System, 10th ed. (Warrendale, PA: SAE International and West Conshohocken, PA: ASTM International, 2004).

[†] Trade name

lower temperature, and therefore have a different condensation rate. No samples were immersed in the bulk liquid phase.

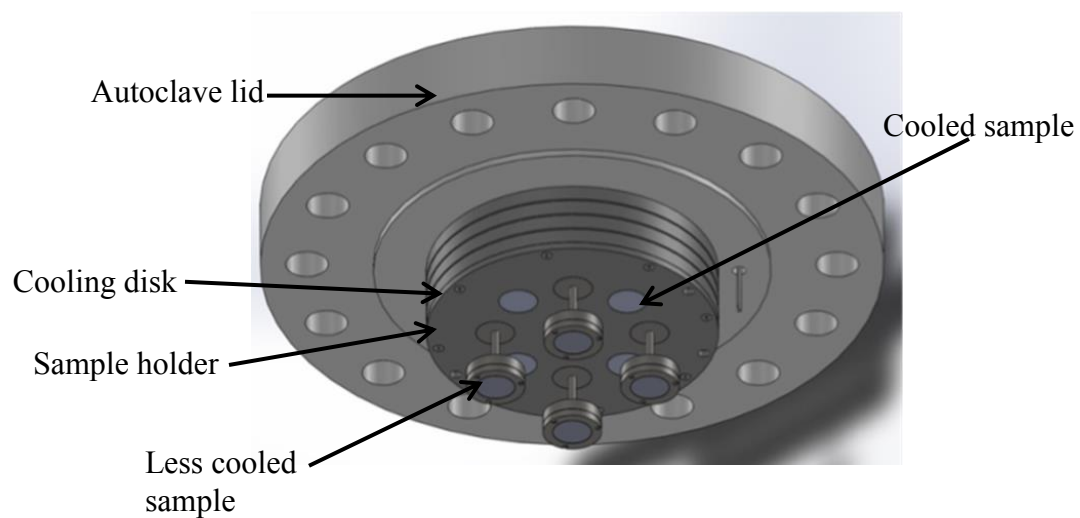


Figure 18: Holder for TLC samples; highly sour TLC experiments

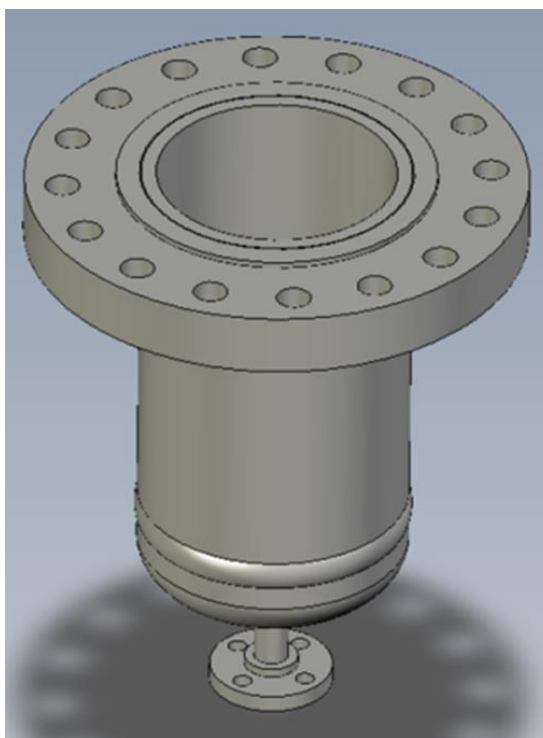


Figure 19: 20L UNS N10276 autoclave; highly sour TLC experiments

4.2.2 Material Tested

The material tested is identical to that used for the tests in marginally sour environments, a quenched & tempered API 5L X65. The composition of the material is shown in Table 1. The steel samples are designed specifically for the sample holder, with a 3.2 cm diameter and 1.3 cm thickness. The samples were coated on the sides and bottom with Teflon™ paint to avoid any galvanic effect with the sample holder, leaving an exposed area of 8 cm² as shown in Figure 20.

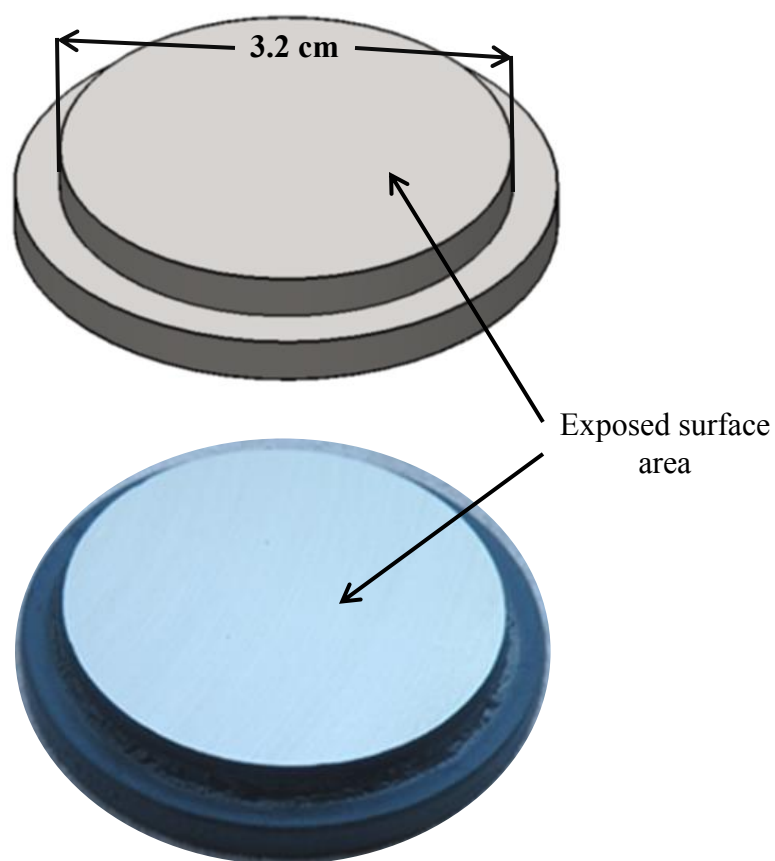


Figure 20: Weight loss sample coupon for TLC in highly sour environments

4.2.3 Test Matrices

In this part of the work, the experiments were also divided into two parts. The first series was designed to study the effect of temperature and water condensation rates in a highly sour environment. This could be achieved by varying the gas and steel temperature and maintaining the partial pressure of H₂S at 2 bars, as shown in the test matrix in Table 5. The second part was to investigate the effect of H₂S concentration in highly sour environments. This was done by varying the H₂S partial pressure at 0.2, 2, and 5 bars and maintaining the gas temperature at 40°C, as shown in the test matrix in Table 6. In each case there was a total pressure of 28 bar with a 10 bar CO₂ partial pressure.

Table 5: Test matrix for the effect of temperature/water condensation rate; highly sour TLC

Investigating	Temperature/water condensation rate							
Test material	API 5L ⁽³⁾ X-65 carbon steel							
Total pressure (bar)	28							
Gas Temperature (°C)	25		40		60		80	
Steel temperature (°C)	20	15	35	22	55	19	75	34
Condensation rate (mL/m ² /s)	0.005	0.012	0.01	0.04	0.02	0.21	0.02	0.51
H ₂ S partial pressure (bar)	2							
CO ₂ partial pressure (bar)	10							
Test duration	21 days							

⁽³⁾ American Petroleum Institute (API), 1220 L St. NW. Washington, DC 20005-4070

Table 6: Test matrix for the effect of H₂S partial pressure; highly sour TLC

Investigating	H ₂ S Partial pressure					
Test material	API 5L ⁽³⁾ X-65 carbon steel					
Total pressure (bar)	28					
Gas Temperature (°C)	40					
Steel temperature (°C)	35	21	35	22	35	18
Condensation rate (mL/m ² /s)	0.01	0.04	0.01	0.04	0.01	0.05
H ₂ S partial pressure (bar)	0.2		2		5	
CO ₂ partial pressure (bar)	10					
Test duration	21 days					

4.2.4 Experimental and Analytical Procedures

Typically, 8 liters of deionized water were added to the autoclave and deoxygenated by purging with nitrogen gas for two hours prior to the beginning of each test. The sample holder was then attached to the top lid and the autoclave was sealed, heated to the required temperature, and pressurized with N₂ to a total pressure of 5 bars. Pure H₂S gas was then bubbled into the fluid until the total pressure reached a stable reading corresponding to an H₂S partial pressure of 2 bars. In the same manner, CO₂ was added until it reached a partial pressure of 10 bars. The total pressure was then increased to 28 bars with N₂. The concentration of H₂S in the gas phase was measured at the end of the test using colorimetric gas detector tubes. The temperature of the steel attached to the cooled sample holder was measured using a thermocouple. The temperature of the steel

⁽³⁾ American Petroleum Institute (API), 1220 L St. NW, Washington, DC 20005-4070

that was suspended away from the cooling plate was not directly measured but was assumed to be close to the gas temperature. A conservative estimate of a 5°C sub-cooling temperature was taken in this study, and the water condensation rate was calculated using an in-house heat/mass transfer model. Consequently, for every gas temperature tested, two steel temperatures and water condensation rates were obtained, as shown in Table 5 and Table 6.

At the end of each test, the gas phase was purged with nitrogen for two hours before the autoclave was opened and the steel samples were removed. The steel samples were rinsed with isopropanol, dried, and weighed. X-ray diffraction (XRD), scanning electron microscopy (SEM), and electron dispersive X-ray spectroscopy (EDS) analyses were performed before the ASTM G1-03 [52] procedure was followed to remove the corrosion products and determine the corrosion rate by weight loss. Surface profile analysis was then performed to investigate the extent of localized corrosion.

CHAPTER 5: RESULTS AND DISCUSSIONS

Parts of this chapter have been published as a paper at the NACE (National Association of Corrosion Engineers) International Conference 2014. The data was also reported in TLC Mitigation Joint Industry Project (JIP) Board Meeting Reports, Ohio University (2011-2014) [53]–[56].

5.1 TLC in Marginally Sour Environments

It was hypothesized that low H₂S concentration could lead to a high localized corrosion rate in marginally sour environments. Thus, in this section, the hypothesis is tested and results analyzed, which includes a comparison of general and localized corrosion rates, condensed water analysis (Fe²⁺ concentration, supersaturation of FeS and FeCO₃), corrosion product analysis, and surface profilometry. Results are reported separately for part A and part B as described above, with gas temperatures of 40°C and 60°C, respectively, with H₂S partial pressures of 0, 0.015, 0.03, 0.08, and 0.15 mbar.

5.1.1. Results and Discussion for 40°C and 60°C Gas Temperatures

The test matrix associated with the experiments for part A was described in the previous chapter and shown in Table 2. The gas temperature was maintained at 40°C, while the steel temperature was cooled to between 25 and 28°C. This would result in a condensation rate of 0.25-0.38 ml/m²/s. For part B, the test matrix that describes the experiments is shown in Table 3. In that case, the gas temperature was maintained at

60°C, while the steel temperature was cooled to between 40 and 43°C. This would result in a condensation rate of 1.50-1.65 ml/m²/s.

5.1.1.1 *Corrosion rate analysis*

Comparisons of general corrosion rate, obtained from weight loss measurement, and pit penetration rate from the depth of the deepest pit which is in accordance with ASTM G 46-94 [57], measured by profilometry analysis (IFM), are plotted for experiments in Part A as shown in Figure 21. Overall, the uniform corrosion rate decreased with increasing H₂S partial pressure, from 0 to 0.15 mbar. The uniform corrosion rate was reduced from 0.38 mm/yr at 0 mbar H₂S to 0.16 mm/yr at 0.15 mbar H₂S. The reduction of TLC rate with increasing H₂S concentration has also been reported and explained by other authors [12]. Interestingly, the presence of 0.015 mbar and 0.03 mbar H₂S resulted in pit penetration rates of 2.3 mm/y and 4.0 mm/y, respectively. At these critical H₂S partial pressure the pitting ratios, which is the ratio between pit penetration rate and general corrosion rate, were calculated at 9 and 16, at 0.00.015 mbar and 0.03 mbar H₂S, respectively. According to an internal procedure developed to evaluate pitting, any ratio above the value of 5 would constitute a clear case of localized corrosion[45]. Thus, from this observation, it is clear that steel samples exposed to the 0.03 mbar H₂S environment suffered the highest localized corrosion rate. However, as the H₂S partial pressure was increased to 0.08 and 0.15 mbar, no localized corrosion was observed, as only the general corrosion rate was measured and plotted. Further

explanations to support this TLC behavior are discussed in the next section of this dissertation, which includes corrosion product and surface profile analyses.

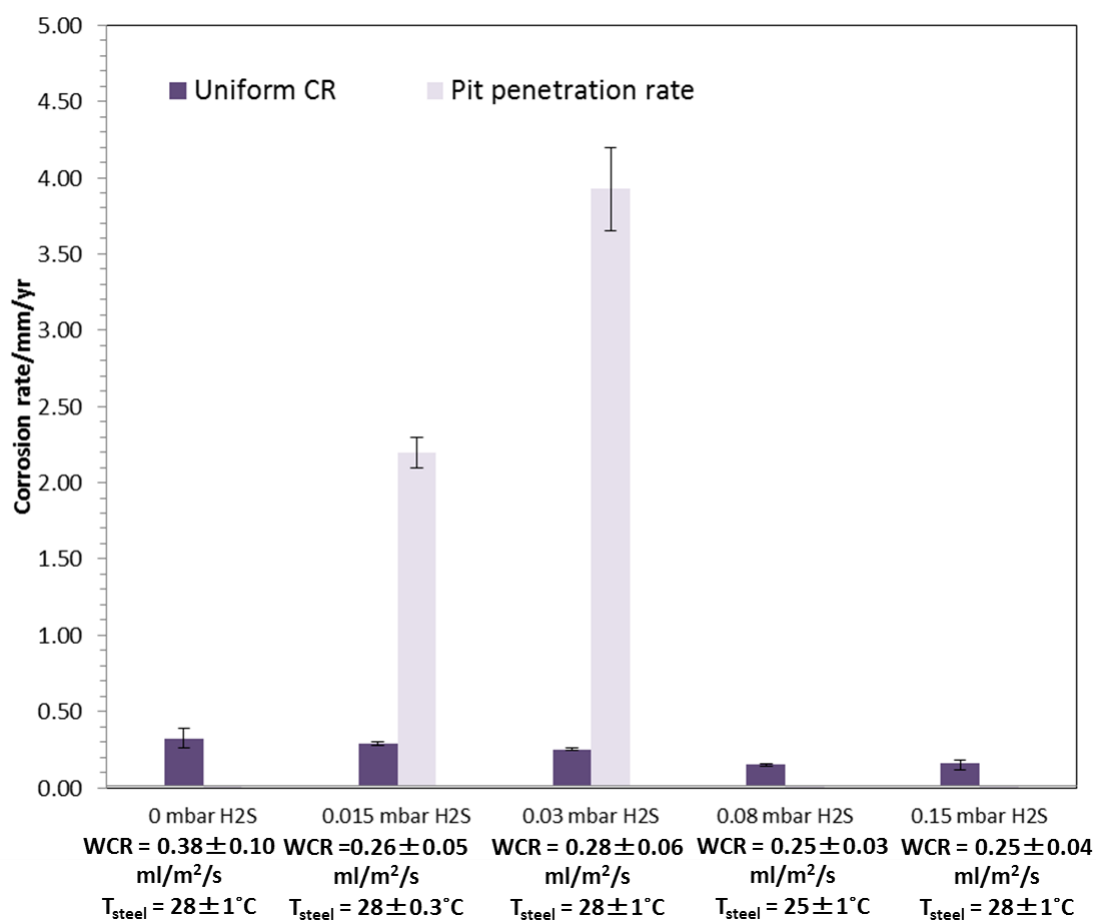


Figure 21: Comparison of corrosion rate from weight loss measurement and pit penetration rate-Part A (gas temperature = 40°C)

In part B, the same method of corrosion rate analysis was performed as in Part A for 0, 0.015, 0.03, 0.08, and 0.15 mbar H₂S, at the gas temperature of 60°C. The highest general corrosion rate was 1.1 mm/yr when no H₂S was present. The general corrosion rate decreased with increasing H₂S partial pressure, as shown in Figure 22. At 0.015 and

0.03 mbar H₂S, no significant difference in general corrosion rate was observed; 0.65 mm/yr in each case. However, the pit penetration rate was not as high as observed in the lower temperature test condition (part A, Figure 21). The pit penetration rates were calculated to be 1.9 and 1.4 mm/y, which result in lower pitting ratios of 2.8 and 2.2, at 0.015 mbar and 0.03 mbar H₂S, respectively. As stated above, according to an internal procedure developed to evaluate pitting, any pitting ratio above the value of 5 would constitute a clear case of localized corrosion. Thus, the results obtained here could not be described as localized attack since the pitting ratio was significantly below 5. This type of attack was described as “localized uniform corrosion”, which is a common scenario in TLC [40]. As the H₂S partial pressure increased to 0.08 mbar and 0.15 mbar, no localized corrosion was observed as only a general corrosion rate of 0.4 mm/yr was determined for both conditions.

Overall, the pit penetration rate in part B was lower when compared to Part A analyses, most significantly at 0.03 mbar H₂S. This can be ascribed to kinetic effects. In Part B the temperature was higher, which increased the rate of formation of the FeS layer inside the pits and protected the steel from further localized attack. However, the general corrosion rate in Part B was higher as compared to Part A. This can be explained by the fact that in Part B a higher water condensation rate was observed. This limits saturation with respect to aqueous species required for formation of both FeCO₃ and FeS, phases that can confer a degree of protection against corrosion. This is similar to TLC behavior in sweet environments; increased water condensation rate (from part A at 0.25 ml/m²/s to part B at 1.5 ml/m²/s) leads to a higher TLC rate.

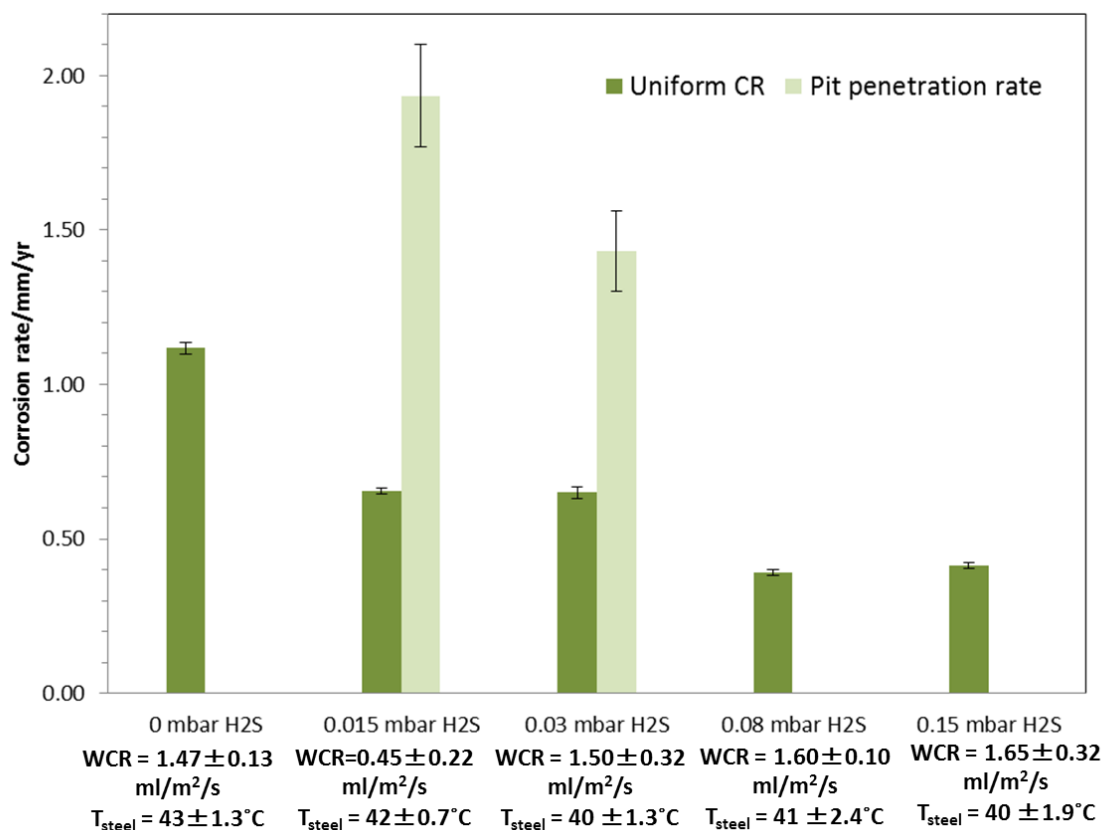


Figure 22: Comparison of corrosion rate from weight loss measurement and pit penetration rate-Part B (gas temperature = 60°C)

5.1.1.2 Comparison of scale formation rate and corrosion rate

In most TLC behavior, the formation of corrosion product layers reduces the corrosion rate as they act as a protective barrier between the steel and the corrosive species in the condensed water. In this case, specifically in the presence of H₂S, the reduction of TLC rate with increasing H₂S partial pressure, as shown in Figure 21 and Figure 22, was due to the formation of a quasi-protective iron sulfide (FeS) layer. Thus, in order to make a direct comparison between the corrosion rates (CR) and scale formation rates (SFR) (amount of corrosion product formed on the steel surface), the

units for both processes were converted into reaction rates expressed in mol/m²/hr. The corrosion rate (CR) value was determined from the general corrosion rate (from the weight loss method), while the scale formation rate (SFR) was calculated from the mass of corrosion product layer in milligrams (mg), which was obtained after the experiments. Equations to calculate the value of CR and SFR are shown in the Appendix B. Based on the reaction rates for both processes, the ratio of scaling formation rate (SFR) to corrosion rate (CR) is determined. This is called the scaling tendency (ST), as shown in equation 35 [58].

$$ST = \frac{SFR}{CR} \quad (35)$$

These three values (CR, SFR and ST) are compared for each H₂S partial pressure, from 0 to 0.15 mbar, and plotted for part A as shown in Figure 23. First, from the comparison of CR and SFR it was observed that for all H₂S partial pressure, there is a much higher CR as compared to SFR, with the difference significantly exceeding an order of magnitude at low H₂S partial pressure. In other words, given the total amount of iron oxidized and dissolved in the corrosion process, only a small amount was incorporated in the corrosion product layer on the steel surface. Note that the scaling tendency increased with H₂S partial pressure, which explained the reduction of the uniform corrosion rate. The highest scaling tendency values, of 0.14 and 0.12, were observed for 0.08 mbar and 0.15 mbar H₂S, respectively. Further explanations relating to the occurrence of high localized corrosion rates at 0.03 mbar H₂S will be discussed in the next section, with supporting data from corrosion product and surface profile analyses.

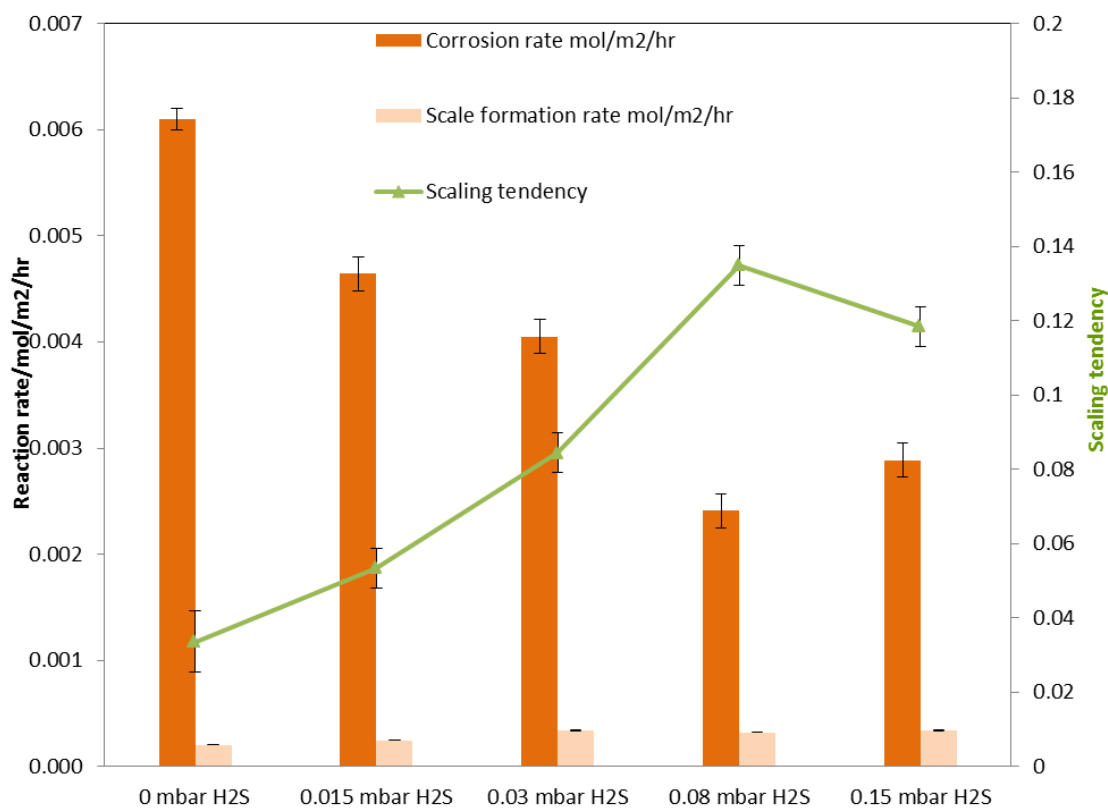


Figure 23: Comparison of reaction rate (CR and SFR) and scaling tendency (ST)-Part A (gas temperature 40°C)

The same comparisons as were done in part A for corrosion rate (CR), scale formation rate (CFR), and scaling tendency (ST) were also done for part B, plotted for each studied H₂S concentration in Figure 24. Again, it was observed that for all conditions there was a higher CR as compared to the SFR, and only a small fraction of dissolved iron ended up in formed corrosion product layers on the steel surface. Nevertheless, the scaling tendency increased, which explained the reduction in uniform corrosion rate with increasing H₂S partial pressure. The scaling tendency is not as high as compared to part A. The highest scaling tendency was calculated to be between 0.06 and 0.07 for H₂S partial pressure from 0.03 to 0.15 mbar. The low scaling tendency was most

likely a result of the high water condensation rate, where the ferrous ion was carried away by the detaching water droplet. Thus, this would lead to low saturation of FeS and/or FeCO₃, and minimal precipitation on the steel surface. This would explain the high TLC rates (general corrosion) observed since the steel was unprotected by a corrosion product layer.

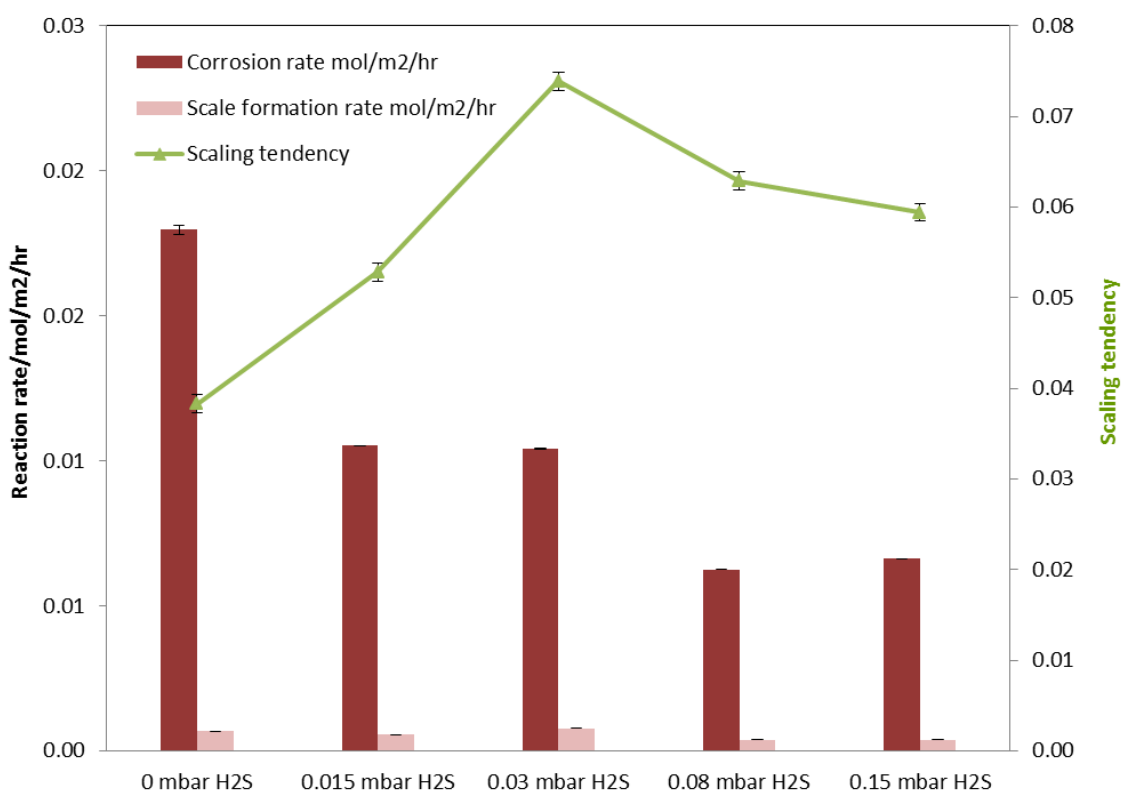


Figure 24: Comparison of reaction rate (CR and SFR) and scaling tendency (ST)-Part B (gas temperature 60°C)

Additional hypothesis testing was done using statistical analysis approach in order to test the hypothesis for TLC in marginally sour environments which focus on the localized corrosion. Based from the calculated value of scaling tendency, the null and the alternative hypotheses were constructed. In this test, only the value of scaling tendency in experiment part A ($T_{\text{gas}} = 40^{\circ}\text{C}$) was done since in part B ($T_{\text{gas}} = 60^{\circ}\text{C}$), lower pitting ratio (pitting ratio < 5) was obtained which was not considered as localized corrosion.

In this statistical analysis, the null hypothesis (H_0) was claimed that localized corrosion will not occur if the mean (μ) value of scaling tendency is more or equal than 0.1. The alternative hypothesis (H_A) would be the localized corrosion will not occur if the mean value of scaling tendency is less than 0.1. Thus, the hypothesis testing using P-value method was done. Detail calculation methods are shown in Appendix C. The test statistic (z) value was calculated to be 0.5. Thus, by using the left-tailed analysis ($H_A < 0.1$), the $P(z < 0.5)$ value of 0.708 was obtained from the table in appendix A[59] at significance level (α) of 0.05. Since the P-value is more than (α), failed to reject the null hypothesis which supported the initial explanation where increase in scaling tendency lead to no localized corrosion.

In order to gain a better understanding of the relationship between iron dissolution resulting from the corrosion process and the corrosion product layer which formed on the steel surface, a mass balance was done by comparing the: total mass of iron loss from the corrosion process, mass of iron in the corrosion product layer, and mass of ferrous ion in condensed water, which were calculated for all experiments, as shown in Figure 25. From these analyses, it could be surmised that most iron loss from corrosion (green line) ended

up in the condensed water (blue bar) rather than in the corrosion product layer (red bar). It can be postulated that minimal FeS formed on the steel surface as there was a limited amount of H₂S present in the system, and most of the ferrous ions were carried away by the detaching water droplets.

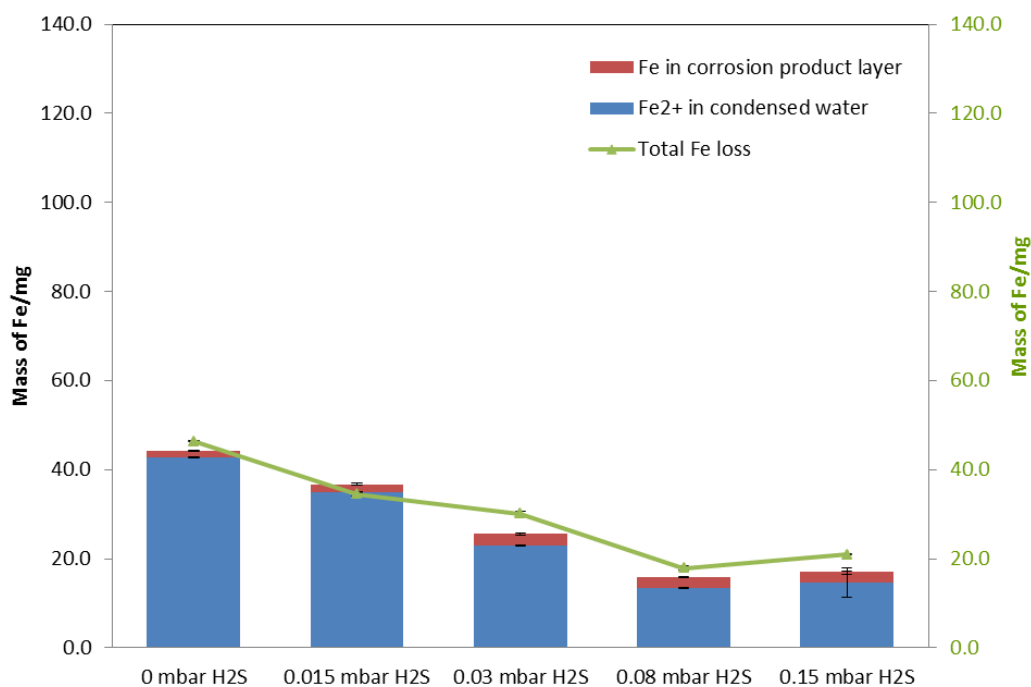


Figure 25: Mass balance between total Fe loss from corrosion, Fe in corrosion product layer and Fe in condensed water-Part A (gas temperature 40°C)

In part B, at gas temperature 60°C, the same corrosion behavior that was noted as in part A, at gas temperature 40°C, was observed, as shown in Figure 26. Again, most of the iron loss from the corrosion process ended up in the condensed water (blue bars), rather than in the corrosion product layer (red bars). The amount of iron in the corrosion product layer was lower as compared to part A. This was due to the higher water

condensation rate, which resulted in lower scaling tendency, which supported the explanation described previously.

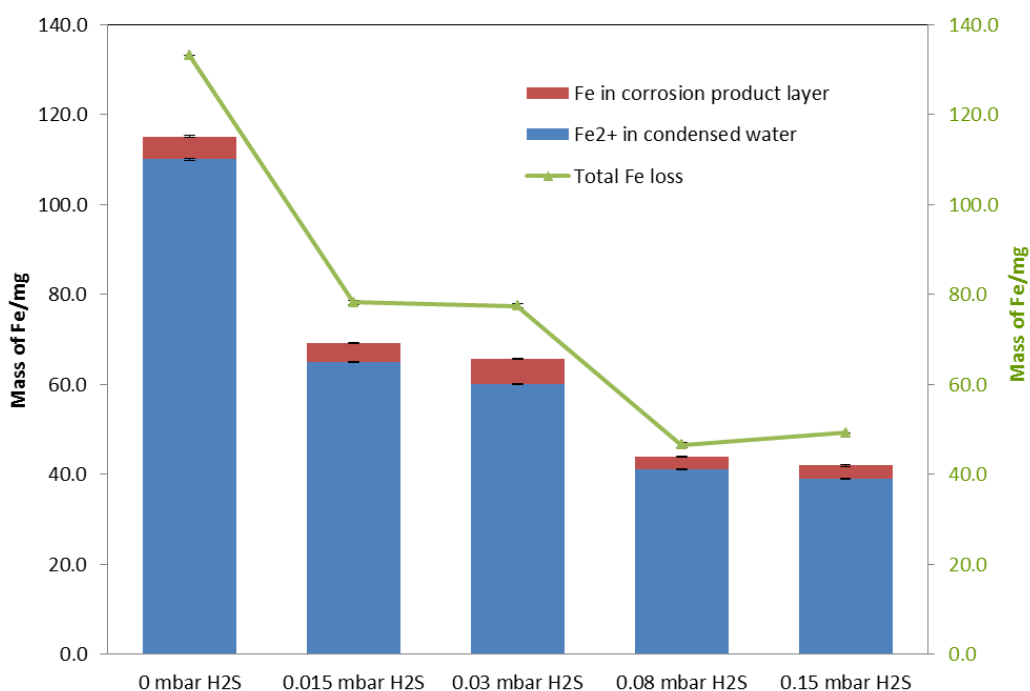


Figure 26: Mass balance between total Fe loss from corrosion, Fe in corrosion product layer and Fe in condensed water-Part B (gas temperature 60°C)

5.1.1.3 Condensed water analysis (Fe^{2+} concentration, pH, and supersaturation of $FeCO_3$ and FeS)

In order to gain better understanding of the corrosion mechanism, the condensed water was collected throughout the experiments and spectrophotometrically analyzed to determine ferrous ion (Fe^{2+}) concentrations, after doing the pH measurements. Saturation values with respect to $FeCO_3$ and FeS were calculated and compared for each H_2S partial pressure. A comparison of ferrous ion concentrations in condensed water with time for

each H₂S partial pressure is shown in Figure 27. Note that the ferrous ion concentration decreased with increasing H₂S pressure, which can be explained by reduction of the general corrosion rate due to the formation of quasi-protective FeS with increasing H₂S partial pressure; formation of FeS is kinetically faster than FeCO₃. Higher concentration of Fe²⁺ in the condensed water implies a higher rate of iron dissolution from the corrosion process, and *vice versa*. Further comparisons of the FeS layers which formed on the steel surface for each H₂S partial pressure are made in the next section.

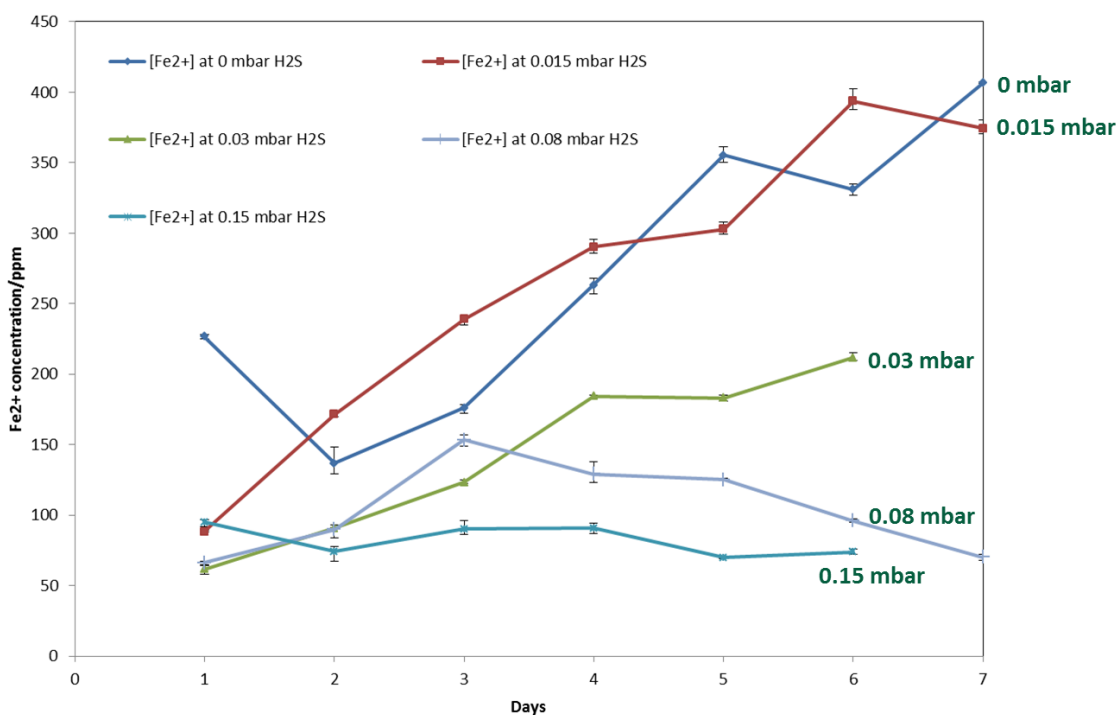


Figure 27: Comparison of Fe²⁺ concentration in condensed water-Part A (gas temperature 40°C)

The same procedure that was completed in part A was conducted for Part B, where the condensed water was collected throughout the experiments and analyzed. The

concentrations of ferrous ion in condensed water are compared for each H₂S partial pressure and plotted as shown in Figure 28. Overall, a similar profile to part A was determined, where the ferrous ion concentration decreased with increasing H₂S concentration. The highest concentration of ferrous ion was observed at 0 mbar H₂S; this represents a higher rate of iron dissolution due to the CO₂ corrosion process. The lowest ferrous ion concentrations were measured at 0.08 mbar and 0.15 mbar H₂S partial pressure. This is in accord with the lowest corrosion rates obtained. At higher H₂S partial pressure - more H₂S is present in the condensed water to consume Fe²⁺ and form a protective FeS layer on the steel surface.

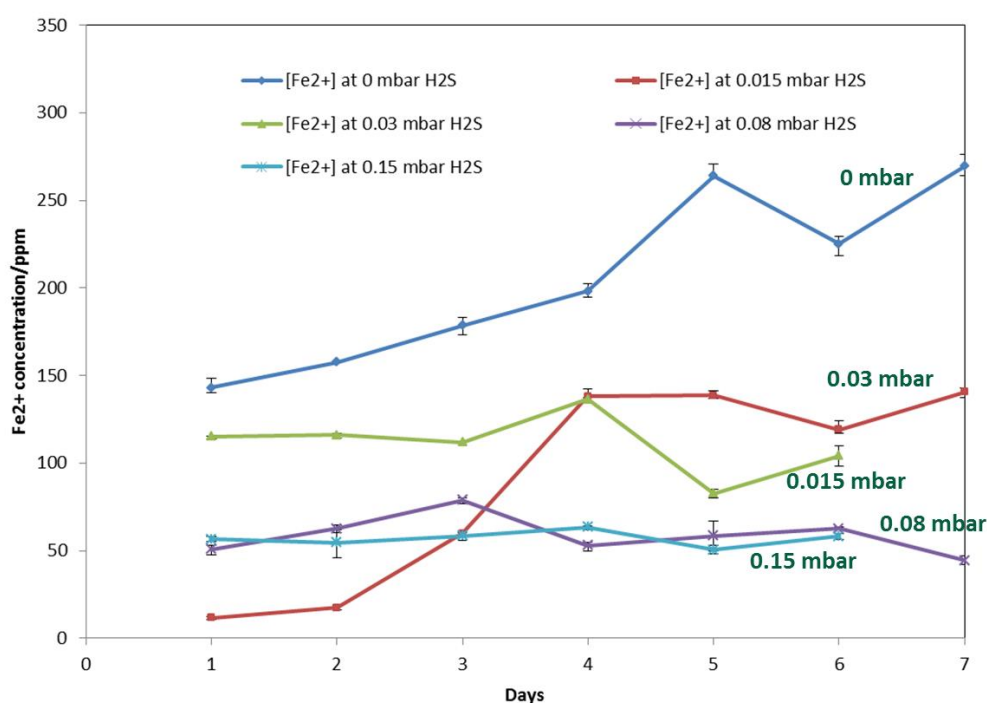


Figure 28: Comparison of Fe²⁺ concentration in condensed water-Part B (gas temperature 60°C)

As mentioned in the previous chapter, the pH of condensed water was measured *in situ* during each experiment. Measured pH was also verified and compared to the calculated pH obtained using back-calculation by solving for electroneutrality (see equation 26). This is done by calculating all species concentrations, cations and anions, and by including the measured ferrous ion concentration. The measured and calculated pH values of condensed water are compared for each H₂S partial pressure and plotted in Figure 29. Typically, the pH value of freshly condensed water with acid gases dissolved therein is between 3 and 4. However, as the corrosion process takes place, with accompanying dissolution of ferrous ions into the condensed water, acidity (H⁺ ions) are consumed and pH increases. As a rule, the higher the concentration of ferrous ions in the condensed water is – the higher pH, and *vice versa*. This effect can be seen clearly when the water condensation rate is low. The condensed water pH is shown in Figure 29; this shows that increases in H₂S partial pressure from 0 to 0.15 mbar reduced the pH. This data supported the ferrous ion concentration measurements in the condensed water as described previously, where the pH was lower at higher H₂S partial pressure due to lower ferrous ion concentrations. Based on the graph, the highest pH (5.7-5.8) was obtained at 0 mbar H₂S while the lowest pH (5.2-5.3) was at 0.15 mbar H₂S. However, this pH value represents the bulk condition of the condensed water. The pH value near the steel surface would be different from the one shown in the graph. Normally, the pH near the steel surface would be roughly one to two units higher than the value in the bulk. This is very important since the formation of a corrosion product layer (FeS) is dependent on the conditions near the steel surface than in the bulk.

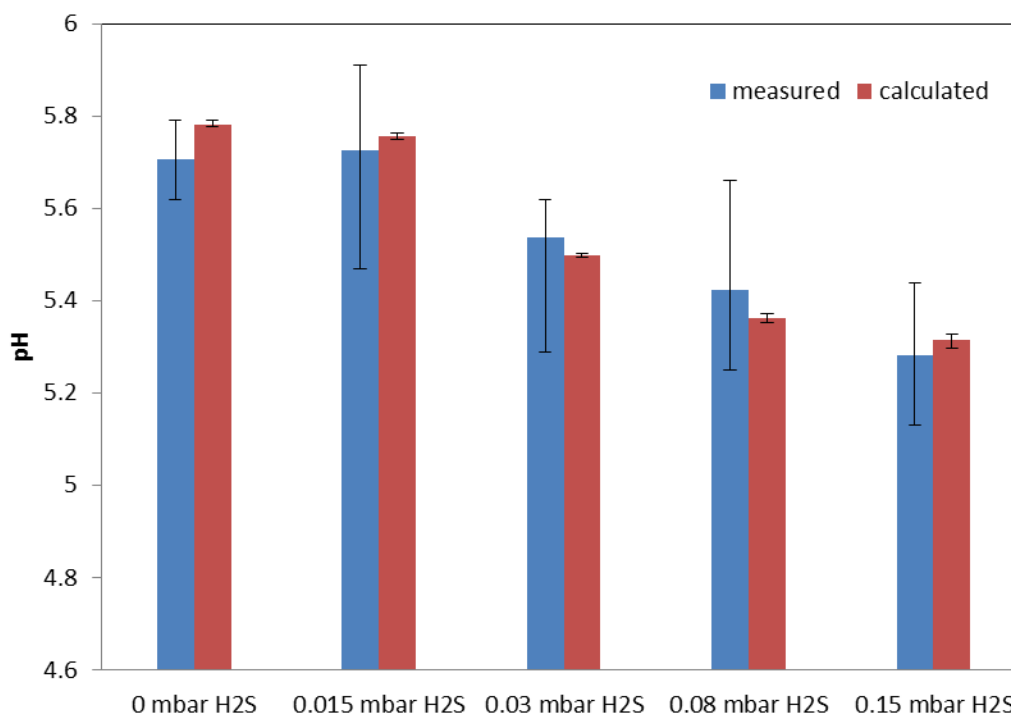


Figure 29: Comparison of measured and calculated condensed water pH-Part A (gas temperature 40°C)

For part B, gas temperature 60°C, the values of measured and calculated pH of condensed water are compared for each H₂S concentration and plotted as shown in Figure 30. The condensed water pH did not show a clear pH reduction with increasing H₂S concentration, as was shown previously in part A (gas temperature 40°C). Only a marginal pH reduction was observed. Based on the graph, the highest pH (5.6-5.8) was obtained at 0 mbar H₂S while the lowest pH (5.3-5.4) was at 0.15 mbar H₂S.

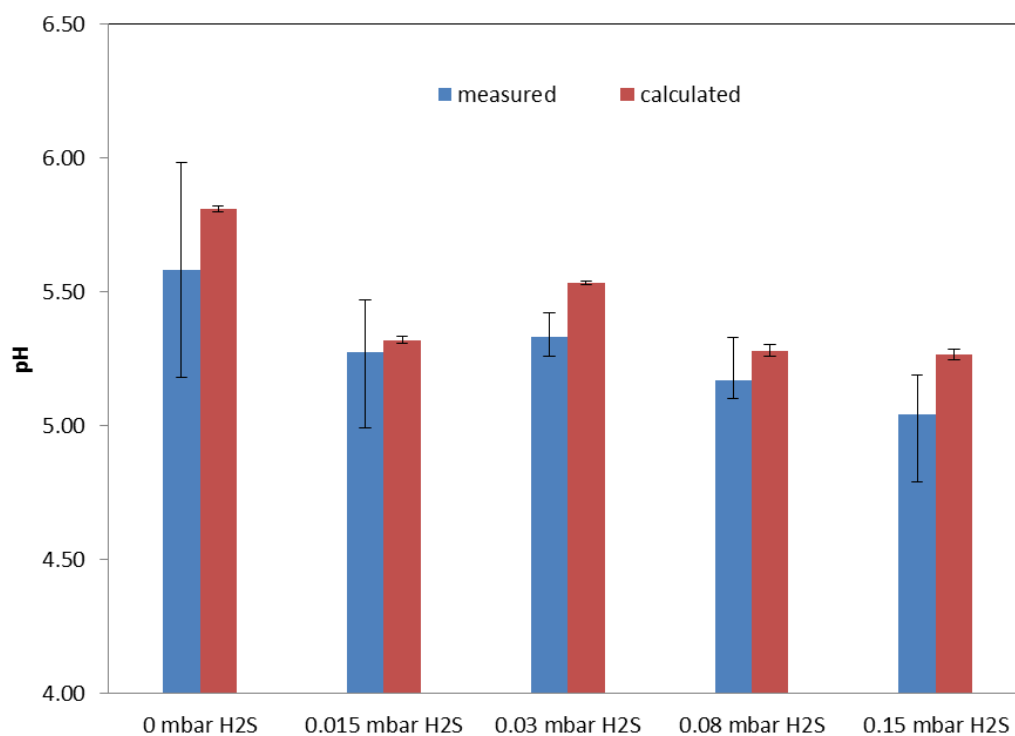


Figure 30: Comparison of measured and calculated condensed water pH-Part B (gas temperature 60°C)

Analysis of the corrosion product layer that formed on the steel surface is very important in order to gain more information on the corrosion mechanism. In determining the identity and the likelihood of formation of a particular compound, analysis is frequently focused on saturation/supersaturation levels with respect to FeS and FeCO₃. The supersaturation values for both corrosion products were calculated based on the measured ferrous ion concentration in the condensed water, as explained in the previous chapter, using equations (28) and (32) for both FeCO₃ and FeS, respectively. As shown in Figure 31, which shows the FeS saturation level at different H₂S partial pressure, the saturation level of FeS decreased to the point of being unsaturated as H₂S partial pressure increased. The highest saturation level of FeS was obtained at 0.015 mbar H₂S, while the

lowest saturation levels of FeS (undersaturation), was obtained at 0.15 mbar H₂S. In other words, the saturation level of FeS at 0.015 mbar and 0.03 mbar H₂S exceeded the value of one and continues increasing until the end of the experiment. For the 0.08 mbar and 0.15 mbar H₂S environments, a different pattern emerged, once saturation values of one were reached, the value then decreased after 3-4 days. Bearing in mind that the calculated value of FeS saturation level in this analysis represented the condition in the bulk, the conditions near the steel surface will be different. However, only the bulk value could be used quantitatively, while only a directional estimate of the conditions near the steel surface is possible.

A possible explanation for this behavior at 0.015 mbar and 0.03 mbar H₂S is that even though the FeS saturation level exceeded one, FeS did not form a precipitate on the steel surface to protect against corrosion as the corrosion at these conditions was high and has undermined any possibility of forming a FeS layer. At higher H₂S partial pressure (0.08 and 0.15 mbar), the saturation level of FeS was reduced after it reached the value of one. This was due to the precipitation of an FeS layer on the steel surface. Further details of this corrosion mechanism are described in the next chapter. This analysis supported the result described in the previous section where, no localized corrosion was observed. In order to support the explanation related to the precipitation of FeS on the steel surface, further discussions of corrosion product layer analysis are made below.

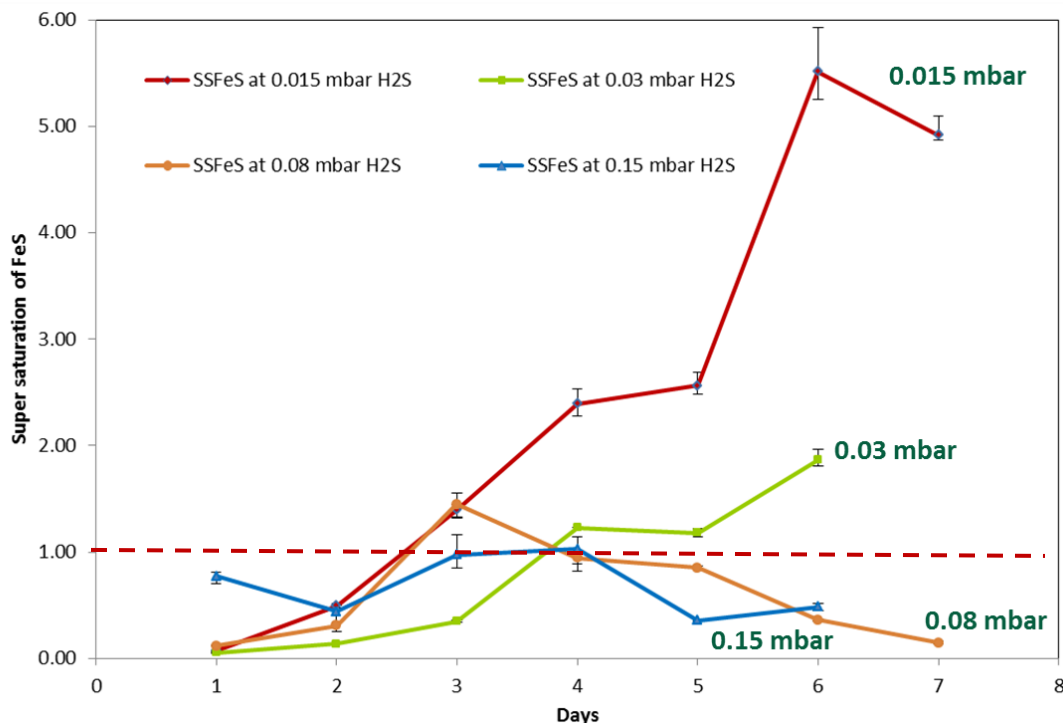


Figure 31: Comparisons of saturation of FeS-Part A (gas temperature 40°C)

Comparisons of saturation of FeS at different H₂S partial pressure for part B, gas temperature 60°C, are shown in Figure 32. Generally, supersaturation was not readily achieved, implying that FeS could have difficulty precipitating on the steel surface. At higher H₂S partial pressure of 0.03-0.15 mbar, saturation of FeS did reach the value of one on day 3-4, and after that decreased. This would imply that precipitation of FeS likely occurred at that point and thereafter, even as the value of FeS bulk saturation decreased (given differences between bulk and surface conditions). The FeS saturation data supported the corrosion rate behavior described above, where the general corrosion rate decreased with increasing H₂S partial pressure due to formation of a protective FeS layer.

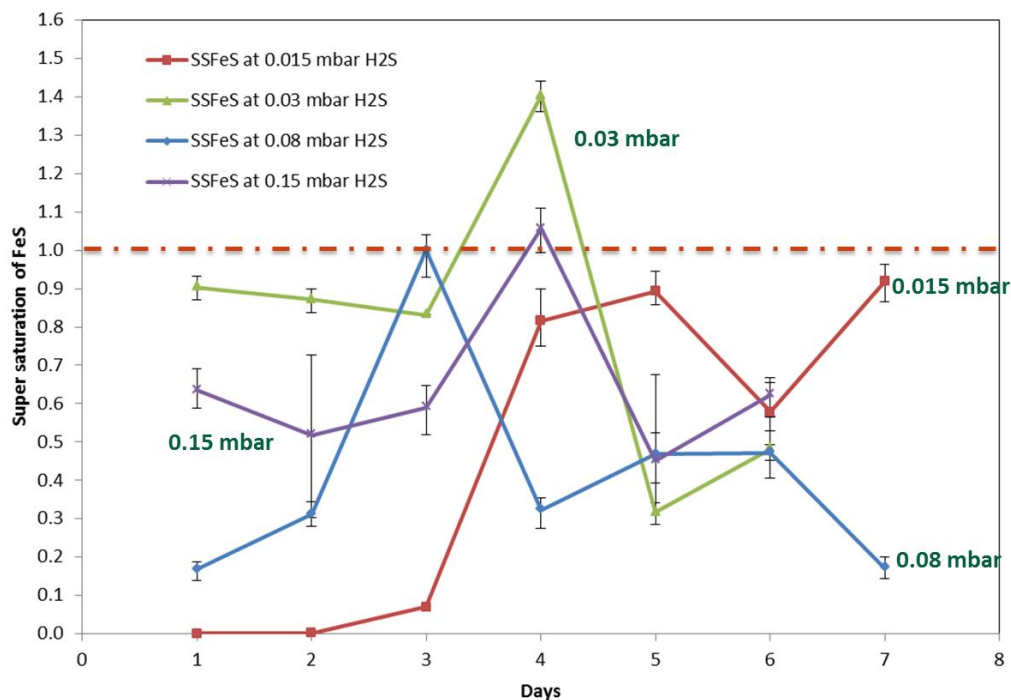


Figure 32: Comparisons of saturation of FeS-Part B (gas temperature 60°C)

Comparison of FeCO_3 saturation for each test at the gas temperature of 40°C is shown in Figure 33. A similar profile was observed as compared to saturation of FeS, where FeCO_3 saturation level decreased with increasing H_2S partial pressure. In these experiments, the partial pressure of CO_2 was constant at 0.9 bars throughout the experiments. Based on the data, it appears that FeCO_3 supersaturation values were readily achieved for all H_2S partial pressure except for the 0.15 mbar case. At this point, the FeCO_3 saturation level did reach the value of one only after 3 to 4 days, then decreased until the end of the test. However, for all tests, one could not observe any formation of FeCO_3 using SEM/EDX. This was probably due to the test temperature being insufficiently high for FeCO_3 formation, as this is preferred at temperatures greater than 50°C [60].

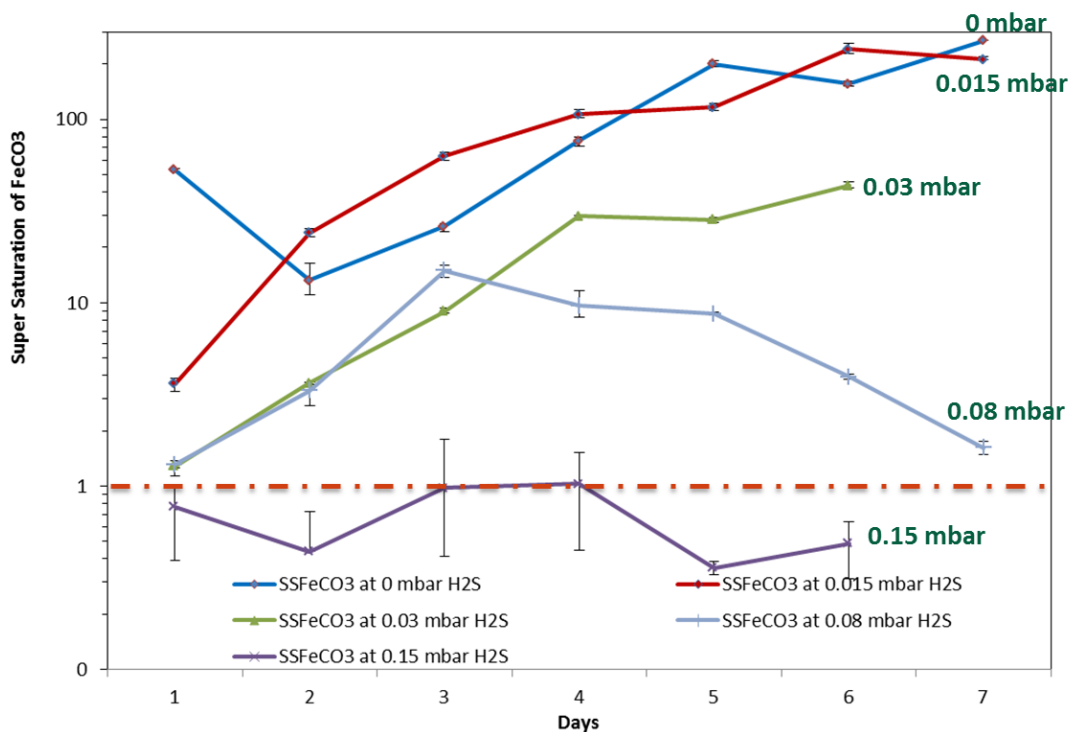


Figure 33: Comparisons of saturation of FeCO_3 -Part A (gas temperature 40°C)

The comparisons of FeCO_3 saturation for each H_2S partial pressure for part B are shown in Figure 34. Similar to the FeCO_3 saturation data presented for part A, supersaturation was readily achieved in tests conducted at 0, 0.015, 0.03, and 0.08 mbar H_2S , but not at 0.15 mbar. At 0.15 mbar H_2S , FeCO_3 saturation level did reach the value of one after 4 days, and then decreased thereafter. Even though supersaturation with respect to FeCO_3 was measured, SEM/EDX only showed the appearance of a product consistent with being FeCO_3 at 0 mbar H_2S . Further analysis, such as that done by XRD, would confirm this.

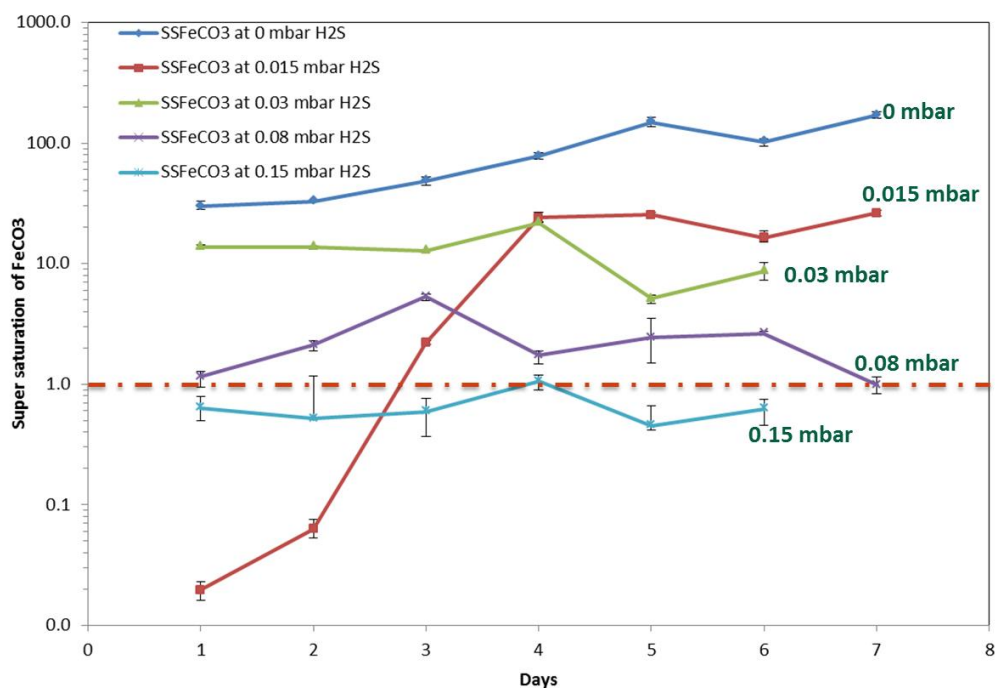


Figure 34: Comparisons of saturation of FeCO_3 -Part B (gas temperature 60°C)

5.1.1.4 Corrosion product analysis (SEM/EDX)

After each experiment, corrosion product layers for each H_2S concentration were analyzed using SEM and compared, as shown from Figure 35 to Figure 39 for part A (gas temperature 40°C). At 0 mbar H_2S , no FeCO_3 crystals were observed and the surface chemical analysis (EDX) showed the presence of residual alloying elements (Cu, Fe, Mo, C & Cr) which suggests the presence of Fe_3C . At 0.015 and 0.03 mbar H_2S , the corrosion product retained polishing marks from the sample preparation process. This could be an indication that this is the first FeS to form by a fast reaction at the original steel surface. It is important to note that some spots where the layer failed to form were found, as shown in Figure 36 and Figure 37. These failed layers are most likely the spots where localized corrosion occurred. In addition to alloying elements, the EDX analysis shows the

presence of sulfur, which suggests the presence of FeS on the steel surface. It could also be seen that the broken FeS layer was most likely a result of undermining corrosion that occurred beneath the FeS layer. At this point, the undermining corrosion rate was very high and the precipitation rate or scale formation rate was low; this indicating an increased the likelihood of localized corrosion.

At higher H₂S partial pressure (0.08-0.15 mbar), distinct FeS layers were observed where the second FeS layer formed on the initial FeS layer (FeS with polishing marks), as shown in Figure 38 and Figure 39. Judging by its appearance, this second layer was most likely formed by a precipitation process. Thus, at higher H₂S partial pressure, the scaling tendency was increased and led to FeS layer precipitation that conferred a degree of protection to the steel from corrosion. No broken FeS layer was observed under these conditions. This corrosion behavior was supported by the calculated scale formation rate and scaling tendency, which was previously shown in Figure 23

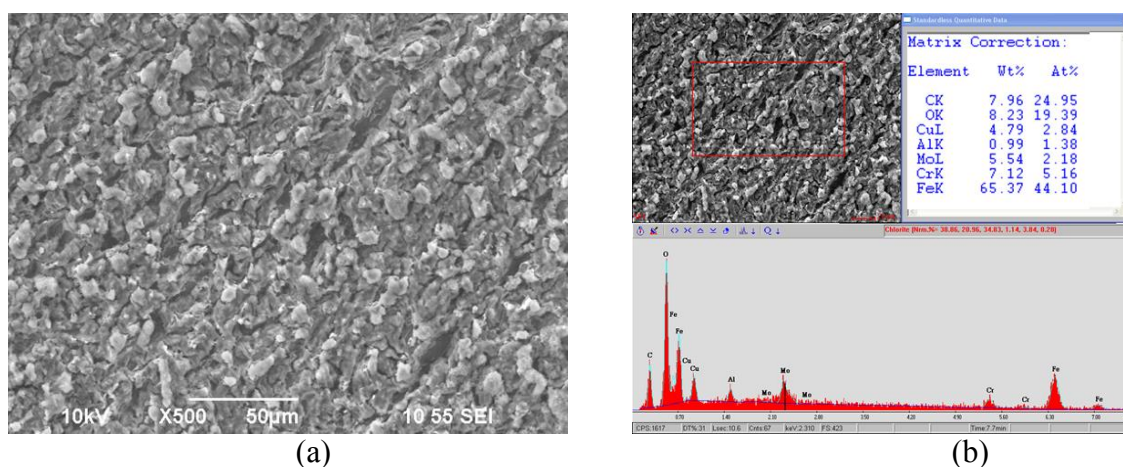


Figure 35: SEM/EDX analysis with corrosion product layer (0 mbar H₂S, T_{gas} = 40°C)

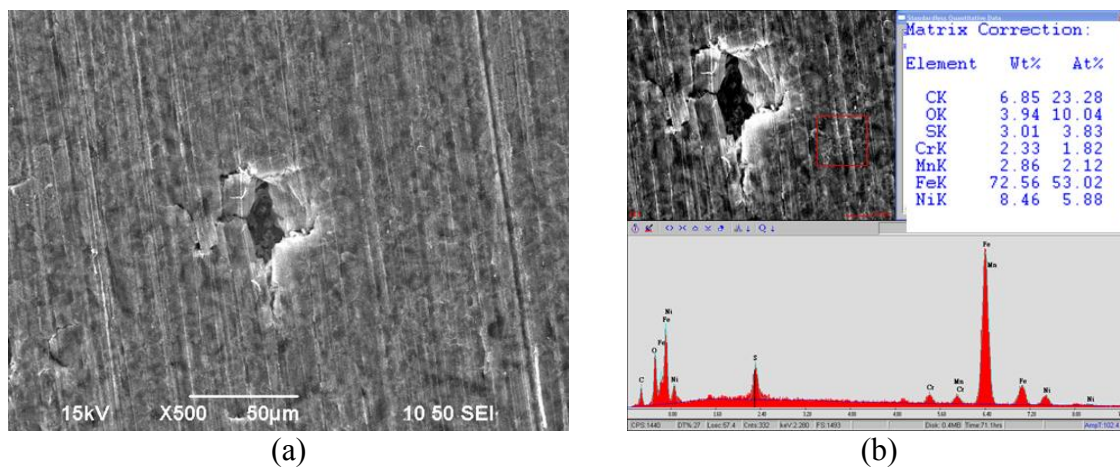


Figure 36: SEM/EDX analysis with corrosion product layer (0.015 mbar H_2S , $T_{\text{gas}} = 40^\circ\text{C}$)

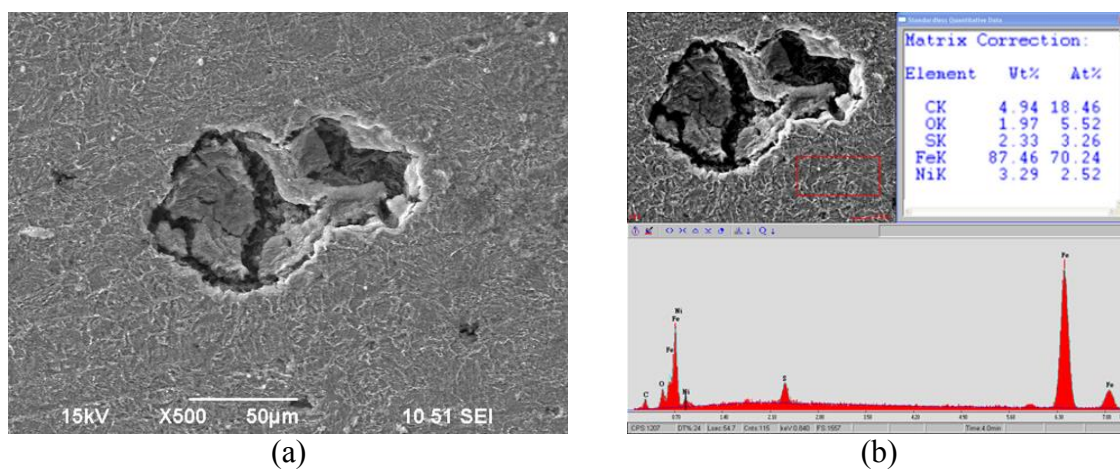


Figure 37: SEM/EDX analysis with corrosion product layer (0.03 mbar H_2S , $T_{\text{gas}} = 40^\circ\text{C}$)

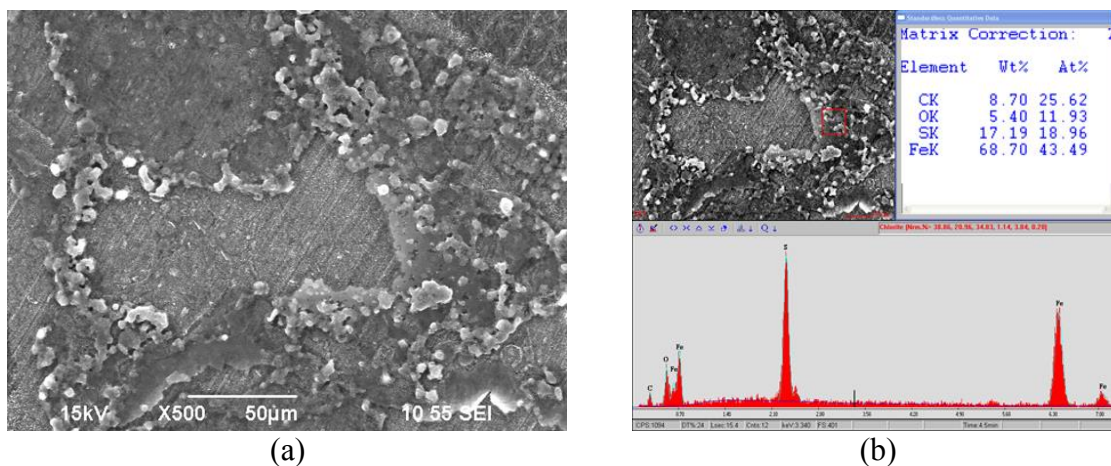


Figure 38: SEM/EDX analysis with corrosion product layer (0.08 mbar H₂S, T_{gas} = 40°C)

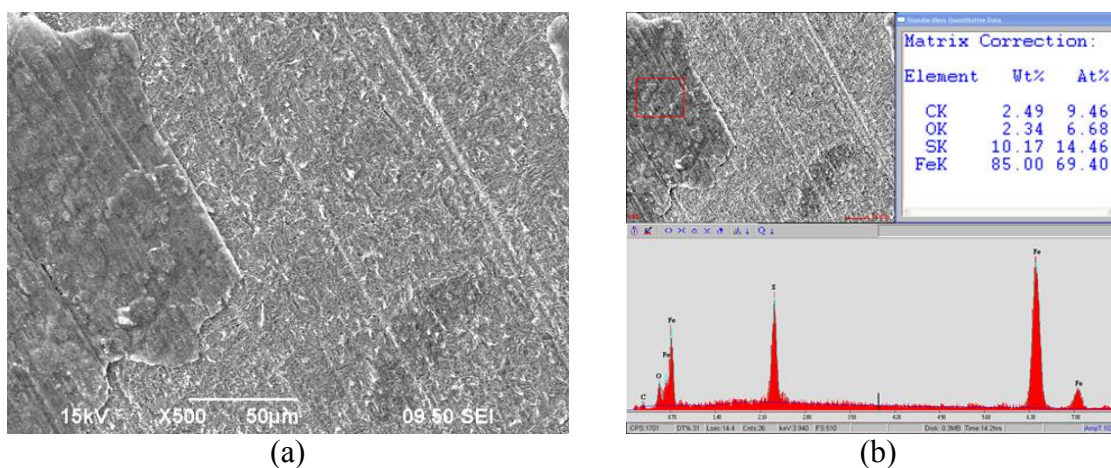


Figure 39: SEM/EDX analysis with corrosion product layer (0.15 mbar H₂S, T_{gas} = 40°C)

For part B, gas temperature 60°C, the surface profile analysis was also done for the corrosion product layer on the steel surface using SEM/EDX. Comparisons at each H₂S partial pressure from 0 mbar to 0.15 mbar H₂S are shown in Figure 40 to Figure 44. At 0 mbar H₂S, observed morphologies and compositional analysis support the presence of FeCO₃. Polishing marks could still be seen between crystals and, from EDX analysis, sulfur was present, indicative of the formation of FeS. This is also an indication that this

is the first FeS layer to form likely by a fast reaction at the original steel surface. At 0.015 and 0.03 mbar H_2S , fewer corrosion product failures, in the form of fractures, were observed as compared to the results in Part A. Furthermore, at higher H_2S partial pressure (0.08-0.15 mbar), different layers of corrosion products were observed on the steel surface (Figure 43 and Figure 44). The second layer of FeS implied it's formed by precipitation processes. This observation supported the explanation given previously on the supersaturation of FeS. Overall analysis by EDX showed the presence of FeS on the steel surface at 0.015, 0.03, 0.08, and 0.15 mbar H_2S .

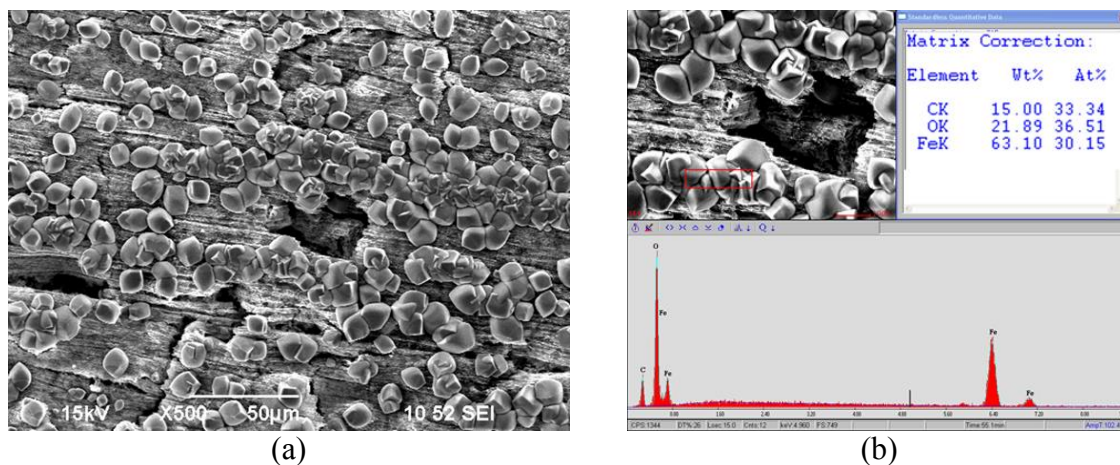


Figure 40: SEM/EDX analysis with corrosion product layer (0 mbar H_2S , $T_{gas} = 60^\circ C$)

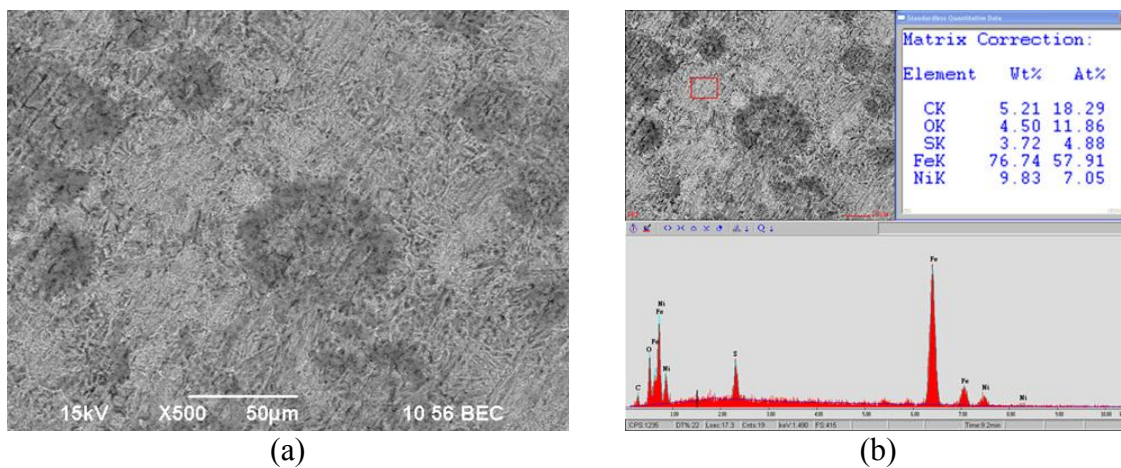


Figure 41: SEM/EDX analysis with corrosion product layer (0.015 mbar H₂S, T_{gas} = 60°C)

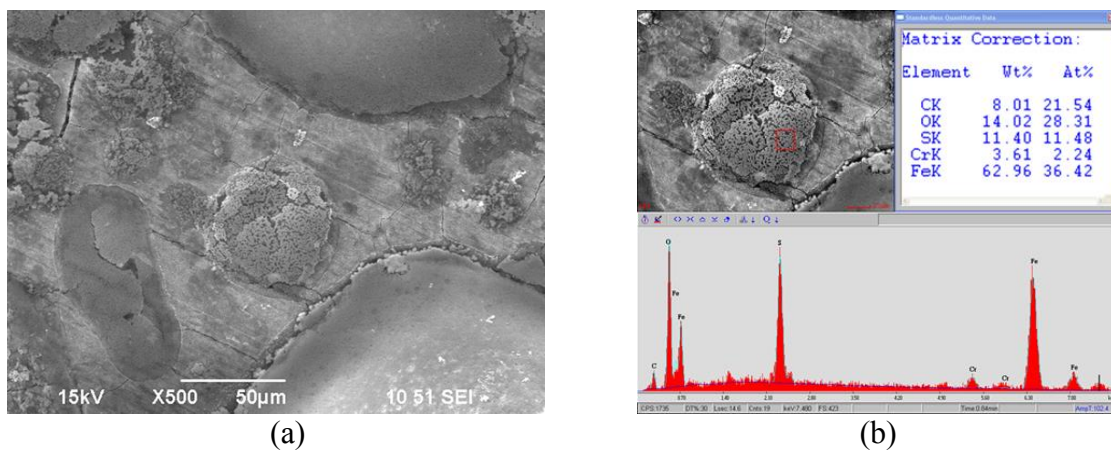


Figure 42: SEM/EDX analysis with corrosion product layer (0.03 mbar H₂S, T_{gas} = 60°C)

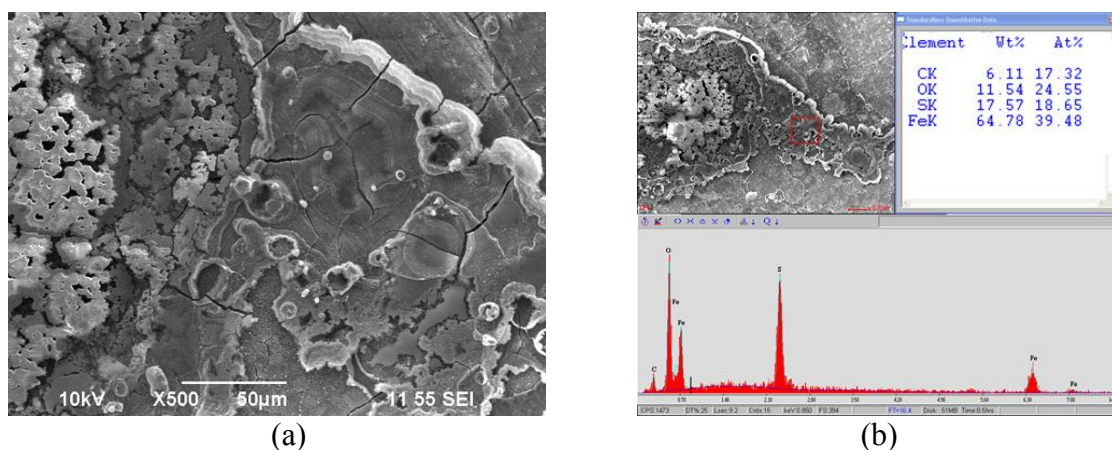


Figure 43: SEM/EDX analysis with corrosion product layer (0.08 mbar H₂S, T_{gas} = 60°C)

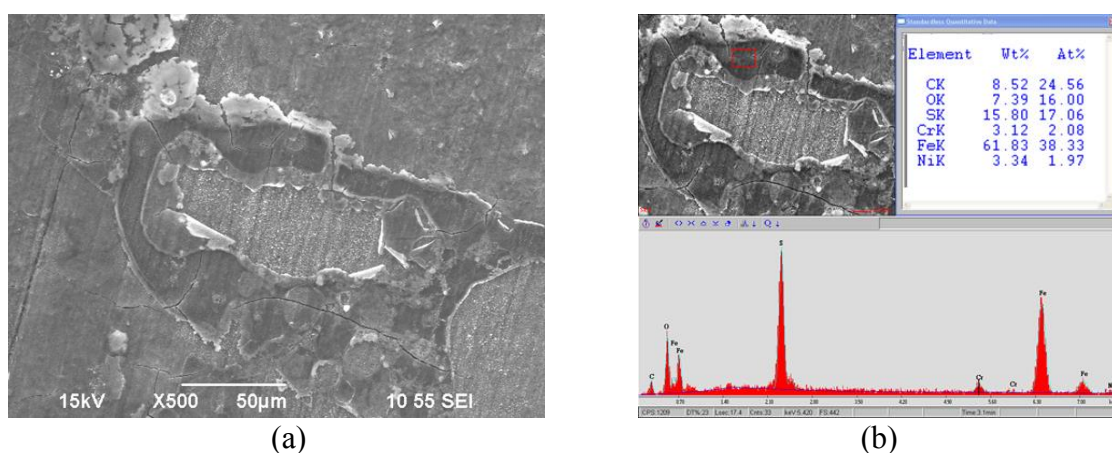


Figure 44: SEM/EDX analysis with corrosion product layer (0.15 mbar H₂S, T_{gas} = 60°C)

5.1.1.5 Cross-section analysis

For cross-sectional analysis, steel samples which were not used for weight loss determination were mounted in epoxy, cross-sectioned, polished and the corrosion product layer analyzed using SEM. The comparisons of the cross-section for samples exposed to various H₂S partial pressure are shown for part A, gas temperature 40°C, from Figure 45 to Figure 49. At 0 mbar H₂S, the corrosion product layer was very thin, only 1-2 µm thick, with no pitting as shown in Figure 45. However, as the H₂S partial pressure

was increased to 0.015 and 0.03 mbar H_2S , pits were observed as deep as $50\mu m$. EDX analysis inside the pits revealed traces of FeS , as shown in Figure 46 and Figure 47. In the image at higher magnification the location of the pit (area A) and protected area (area B) in Figure 47 showed the presence of an FeS layer on area B, which protected the steel from localized corrosion. However, area A suffered localized corrosion since it was not covered with a corrosion product layer. Further explanations regarding the localized corrosion mechanism are discussed in the next chapter.

As previously explained in the corrosion rate analysis, no localized corrosion was observed at higher H_2S partial pressure (0.08-0.15 mbar). These findings are supported by the cross-section images in which the steel was fully covered and protected by a thicker FeS layer, as shown in Figure 48 and Figure 49.

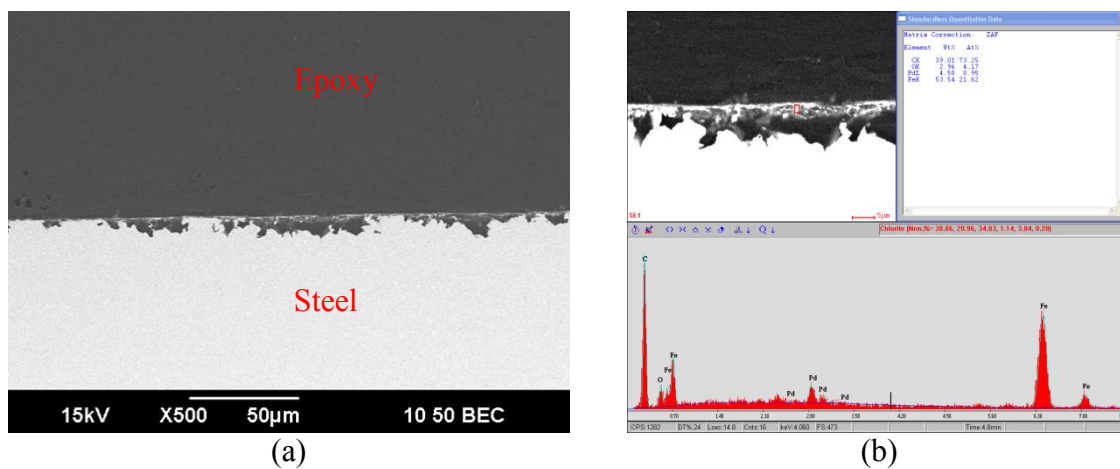


Figure 45: Cross-section analysis with corrosion product layer (0 mbar H_2S , $T_{gas} = 40^\circ C$)

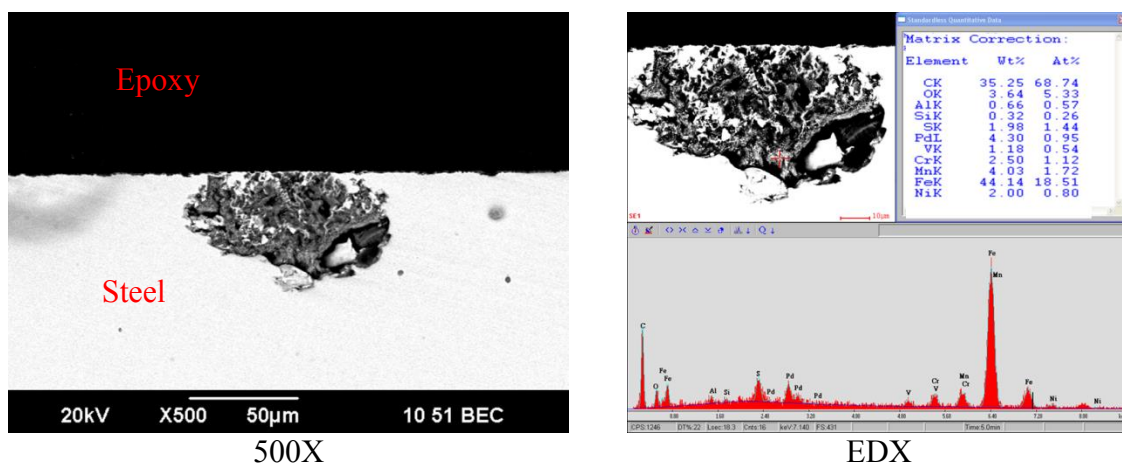


Figure 46: Cross-section analysis with corrosion product layer (0.015 mbar H₂S, T_{gas} = 40°C)

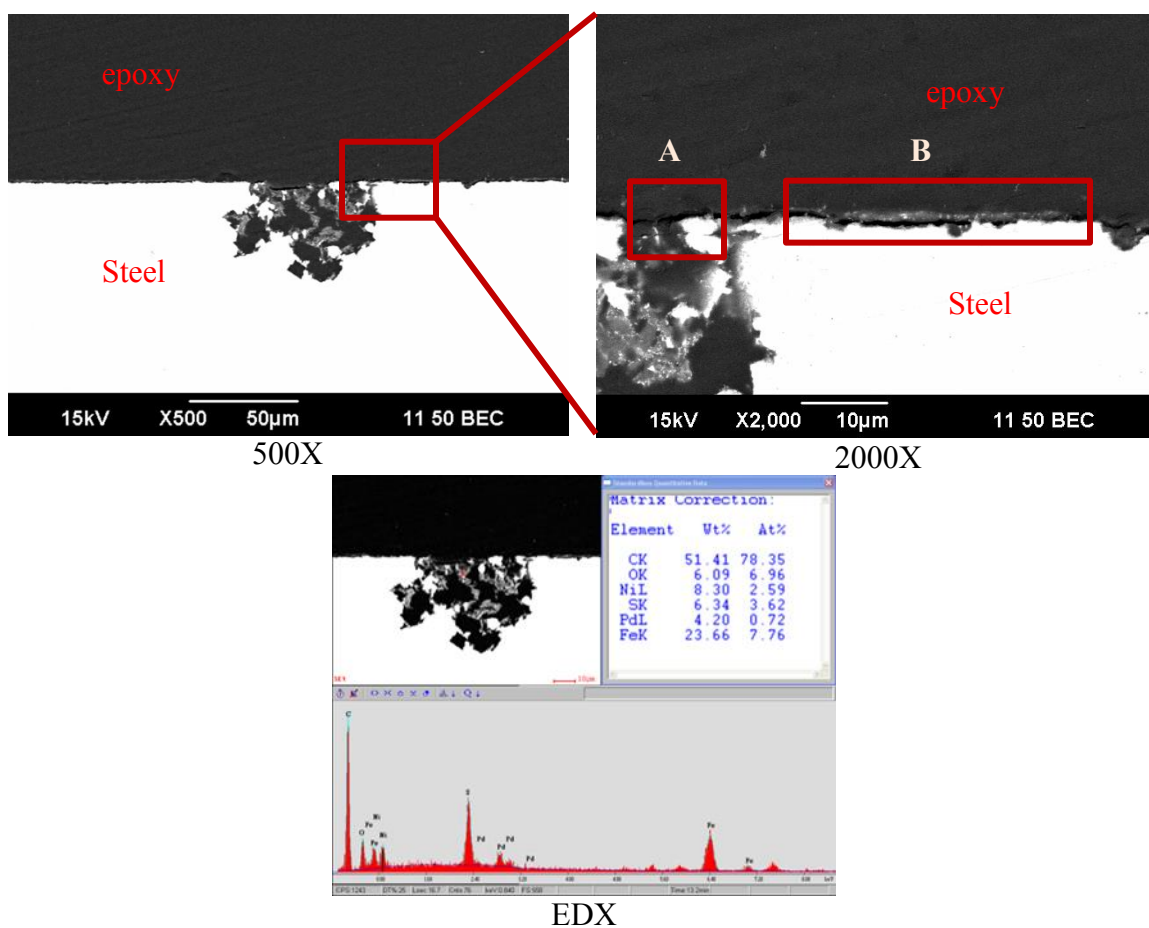
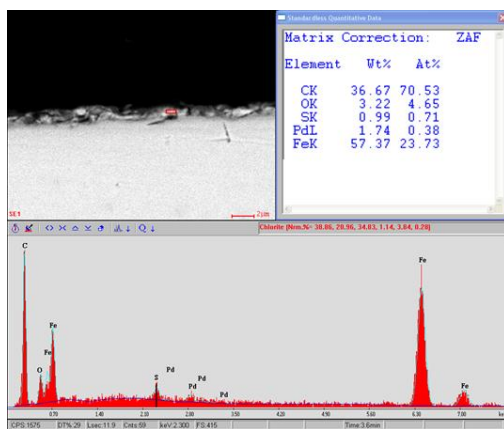
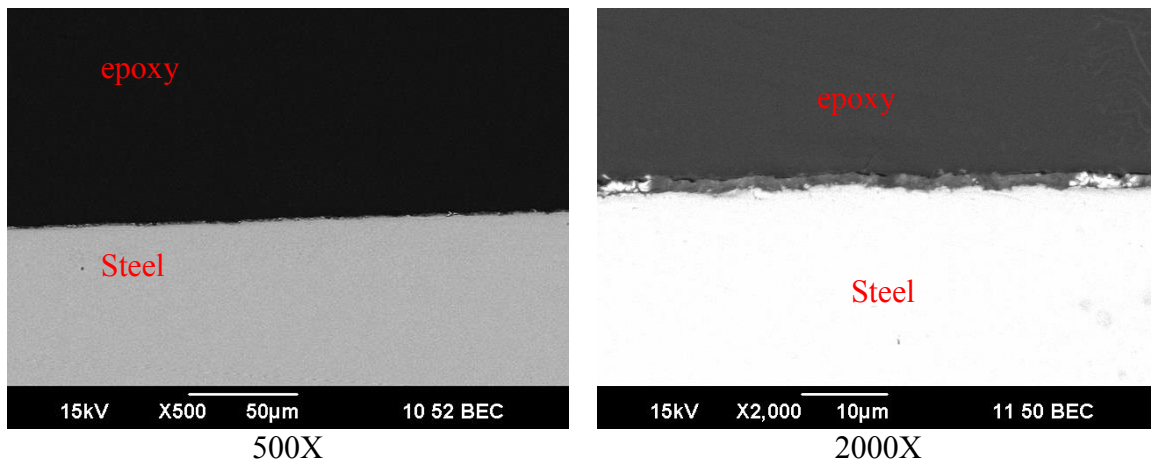


Figure 47: Cross section analysis with corrosion product layer (0.03 mbar H₂S, T_{gas} = 40°C)



EDX

Figure 48: Cross section analysis with corrosion product layer (0.08 mbar H₂S, T_{gas} = 40°C)

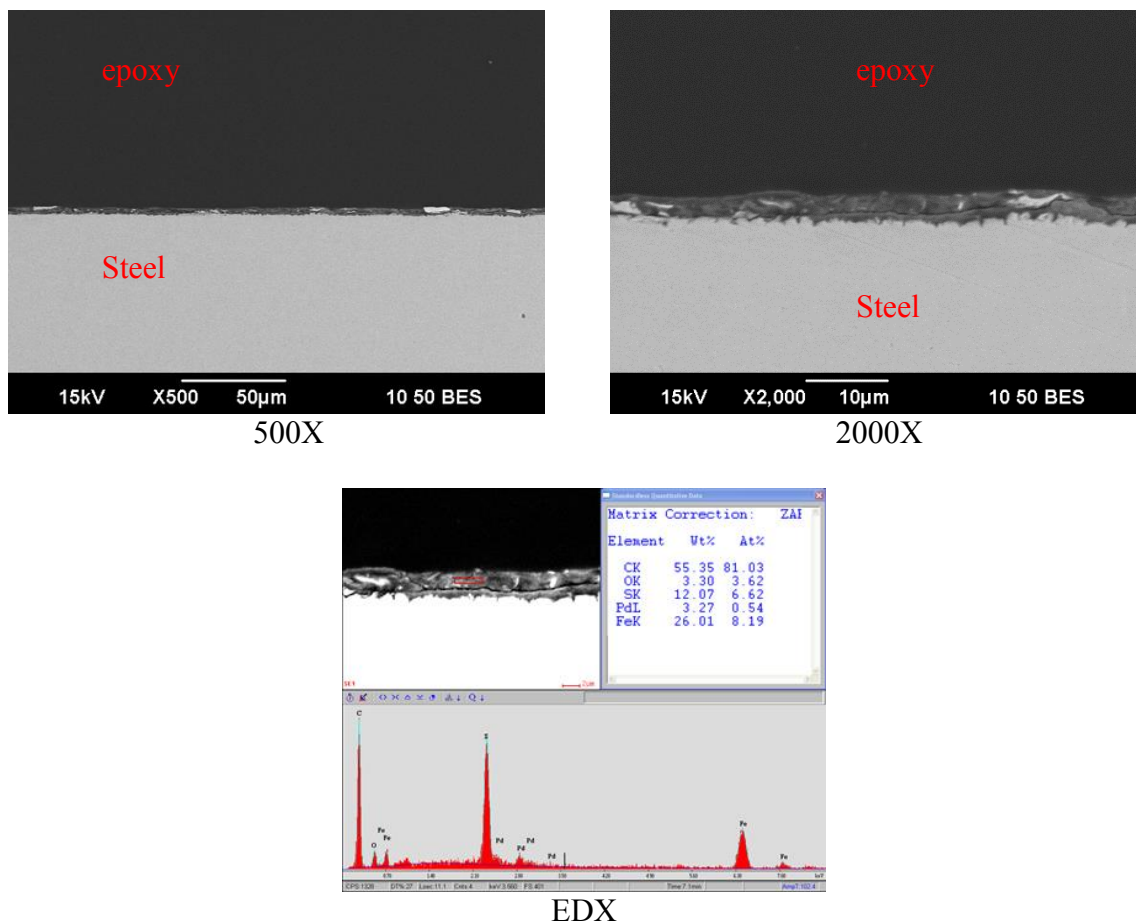


Figure 49: Cross section analysis with corrosion product layer (0.15 mbar H_2S , $T_{gas} = 40^\circ C$)

The same cross-sectional analysis procedure that was done for part A was also completed for part B, gas temperature $60^\circ C$. Samples were mounted in epoxy, cross-sectioned, polished, and the corrosion product layer analyzed using SEM. At 0 mbar H_2S , the corrosion product layer was thicker as compared to that in Part A; 5-6 μm thick with no pitting as shown in Figure 50. However, in part B at a gas temperature of $60^\circ C$, as the H_2S partial pressure increased to 0.015 mbar and then 0.03 mbar, the samples suffered more from general corrosion since, compared with part A, there were no small/deep pits. The pits which formed were wide, as shown in Figure 51 and Figure 52. This finding

supported the corrosion rate analysis because, at this point, the pitting ratio was below 3; this could not be considered as localized corrosion. EDX analysis inside the pits showed traces of FeS. As was also the case in Part A, no pitting was observed at higher H₂S partial pressure (0.08-0.15 mbar). The steel was fully covered with a thin FeS layer, as shown in Figure 53 and Figure 54. It is noteworthy that residual alloying elements were less likely to be present in the corrosion product layer as the tested H₂S partial pressure increased.

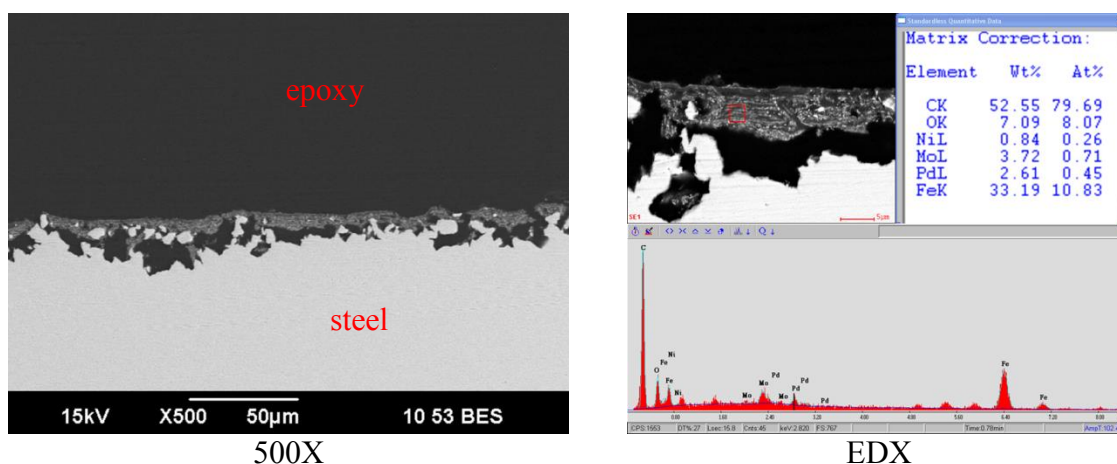
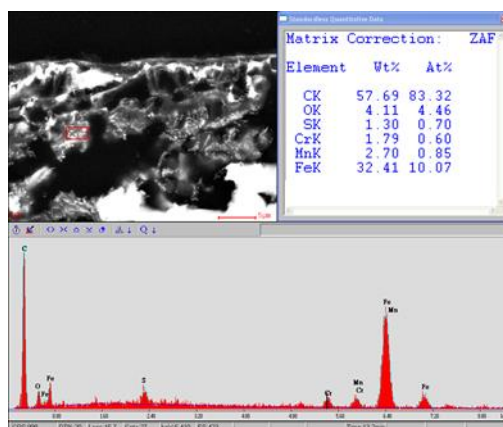
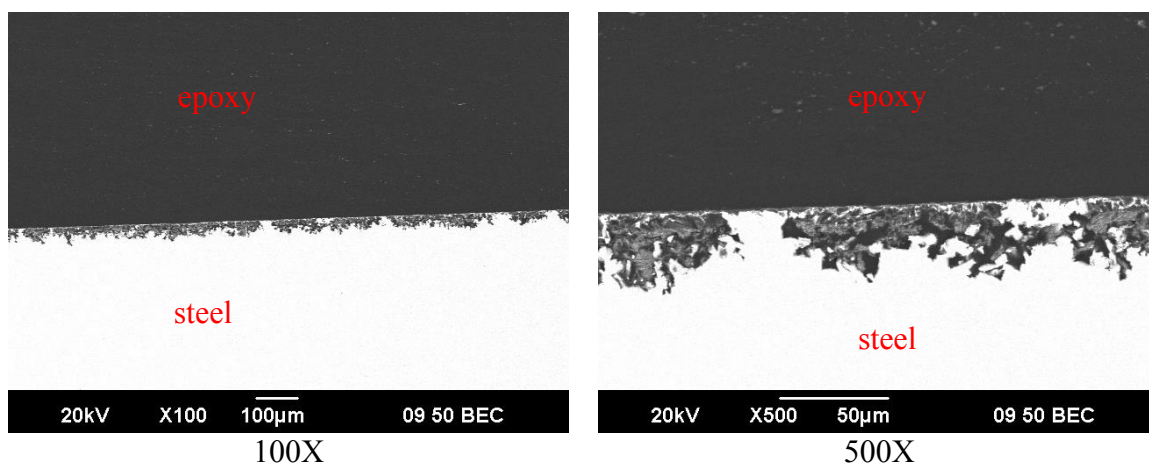


Figure 50: Cross-section analysis with corrosion product layer (0 mbar H₂S, T_{gas} = 60°C)



EDX

Figure 51: Cross-section analysis with corrosion product layer (0.015 mbar H₂S, T_{gas} = 60°C)

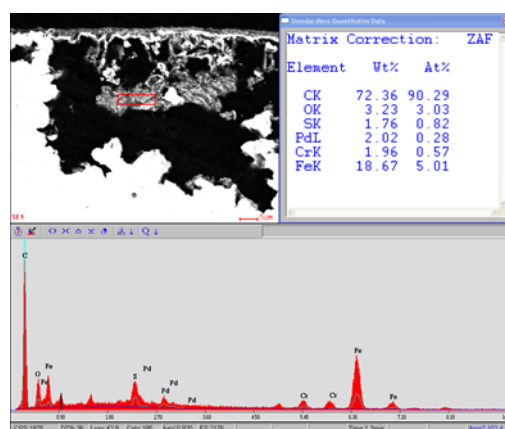
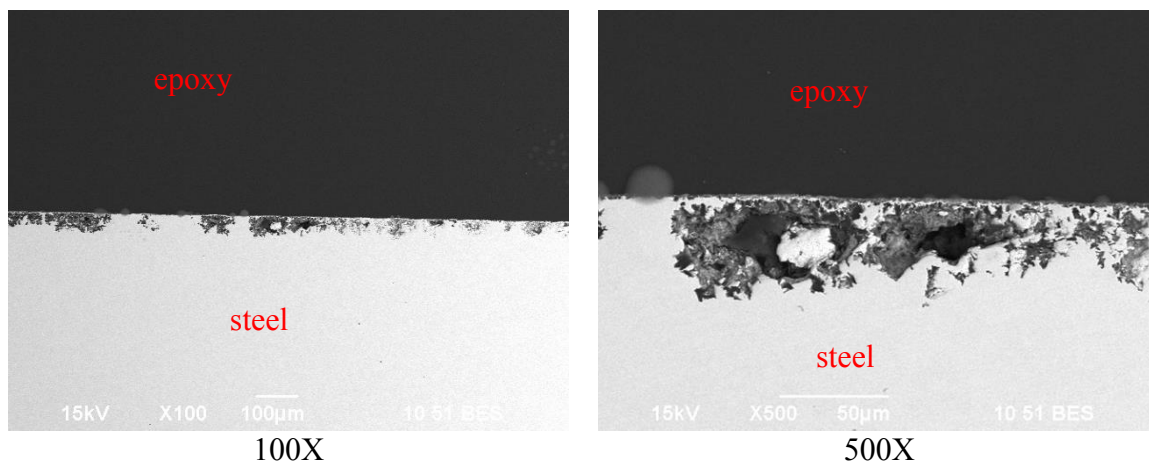


Figure 52: Cross-section analysis with corrosion product layer (0.03 mbar H_2S , $T_{gas} = 60^\circ C$)

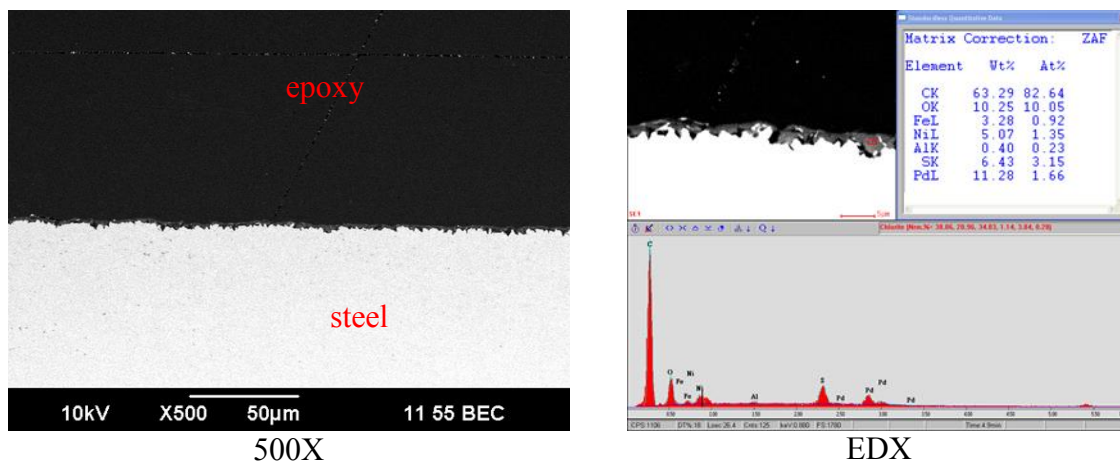


Figure 53: Cross-section analysis with corrosion product layer (0.08 mbar H_2S , $T_{gas} = 60^\circ C$)

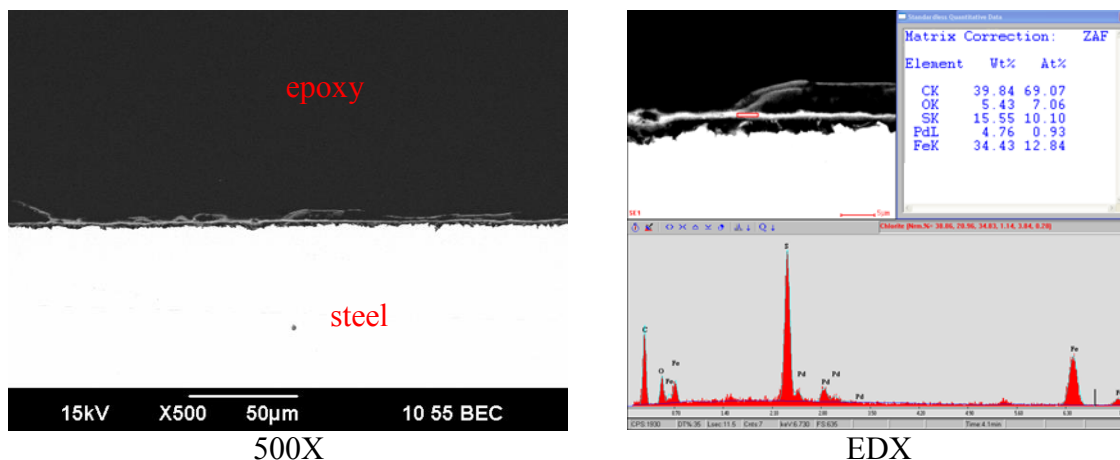


Figure 54: Cross-section analysis with corrosion product layer (0.15 mbar H_2S , $T_{gas} = 60^\circ C$)

5.1.1.6 Surface analysis after removal of corrosion product

Surface analysis of the specimens after removal of the corrosion product layer was done for each H_2S partial pressure using SEM. As shown in Figure 55, initiation of pitting was observed at 0.015 mbar and 0.03 mbar H_2S . The population of pitting was observed to be higher at 0.015 mbar than at 0.03 mbar H_2S . No pitting was observed at

higher H_2S partial pressure (0.08 mbar and 0.15 mbar). Detailed analyses of the depth of the pitting were done using profilometry, as shown in the next section.

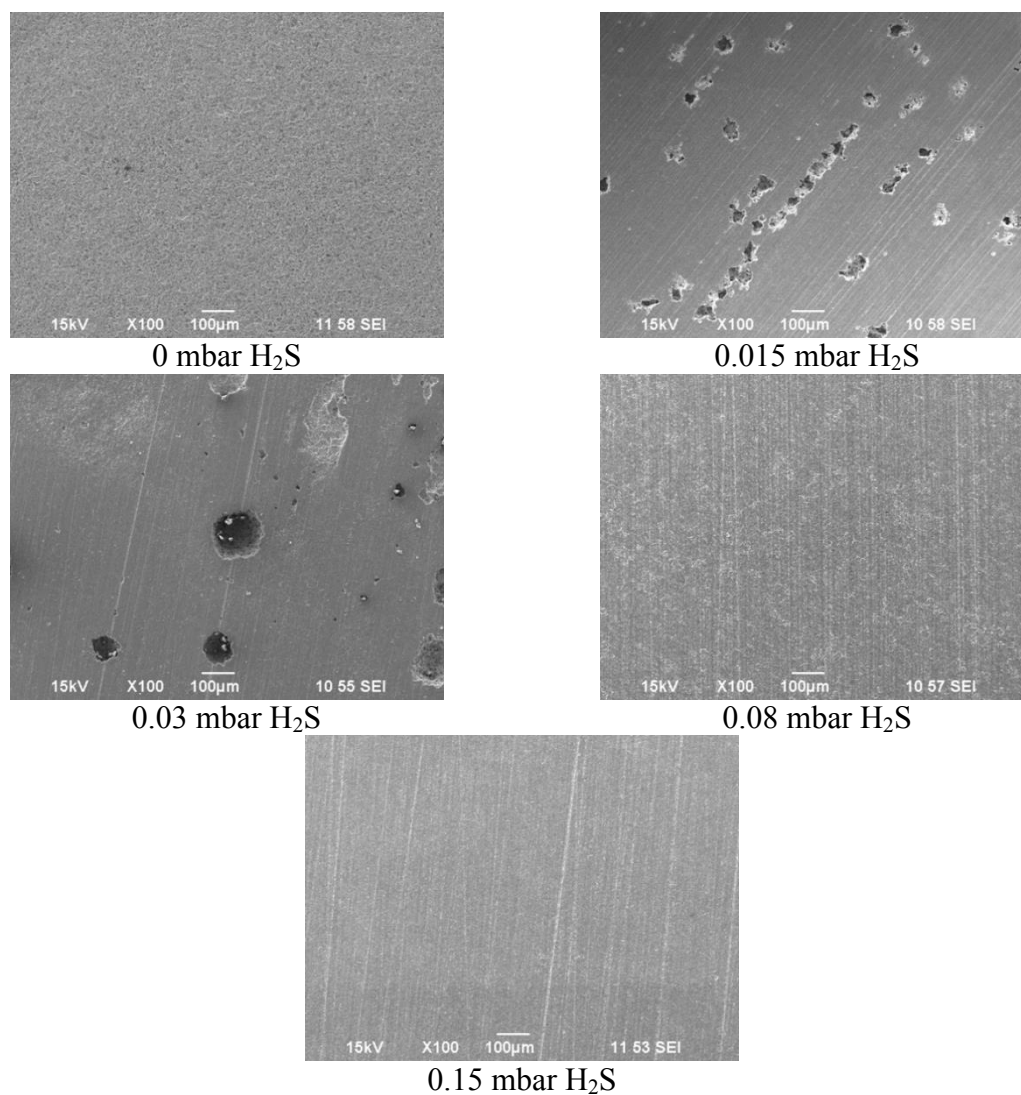


Figure 55: SEM surface analysis after removal of corrosion product layer (0, 0.015, 0.03, 0.08, and 0.15 mbar H_2S . $T_{\text{gas}} = 40^\circ\text{C}$)

In part B, surface analysis of steel after removal of the corrosion product layer was also done for each H_2S concentration using SEM. As shown in Figure 56, and in a

similar fashion to Part A, initiation of pitting was observed at 0.015 mbar and 0.03 mbar H_2S . However, the pitting population was higher as compared to part A. Again, no pitting was found at higher H_2S partial pressure (0.08 mbar – 0.15 mbar). Detailed analyses of the depth of the pitting were performed using profilometry data, as shown in the next section.

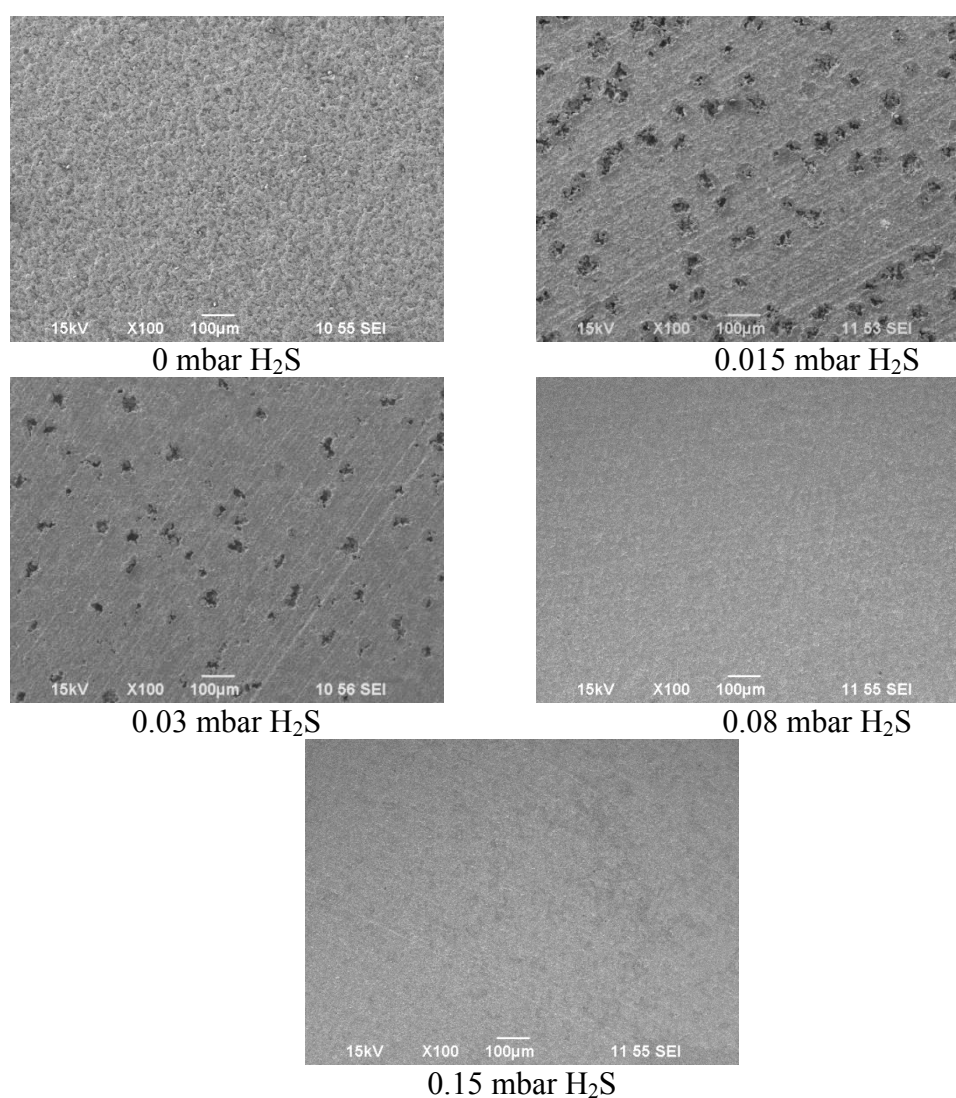


Figure 56: SEM analysis on steel surface after removal of corrosion product layer (0, 0.015, 0.03, 0.08, and 0.15 mbar H_2S , $T_{gas} = 60^{\circ}C$)

5.1.1.7 *Surface profilometry*

Profilometry analysis was performed on the steel surface after removal of the corrosion products in order to assess the occurrence of localized corrosion in more detail. At 0 mbar H₂S, no localized corrosion was observed; only surface roughness from general corrosion was measured (Figure 57). As the partial pressure of H₂S was increased to 0.015 mbar and 0.03 mbar, pitting as deep as 45 and 80 μm, respectively, was observed. The highest pit penetration rate was calculated to be 4.2 mm/y at 0.03 mbar H₂S, as shown in Figure 58 and Figure 59. No localized corrosion was observed at higher H₂S partial pressure (0.08-0.15 mbar), as only surface roughness from general corrosion was measured, as shown in

Figure 60 and Figure 61. This profilometry analysis supported the results obtained in part A; localized corrosion was initiated at 0.015 and 0.03 mbar H₂S, while only general corrosion was observed at higher H₂S partial pressure (0.08-0.15 mbar).

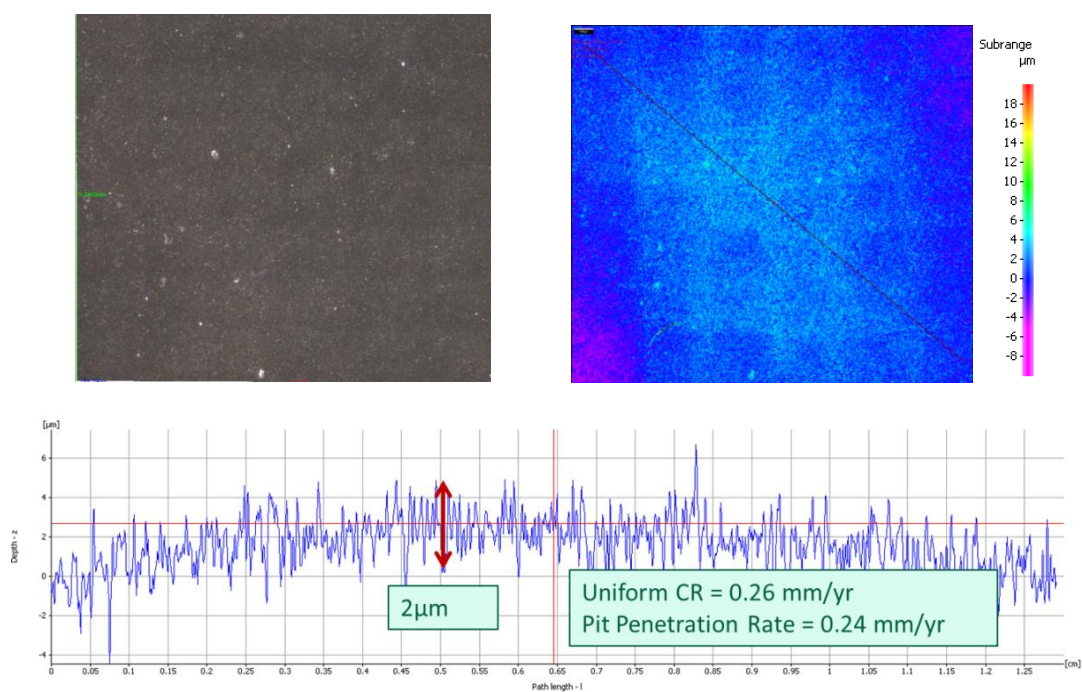


Figure 57: Surface profilometry analysis after removal of corrosion product layer (0 mbar H_2S , $T_{\text{gas}} = 40^\circ\text{C}$)

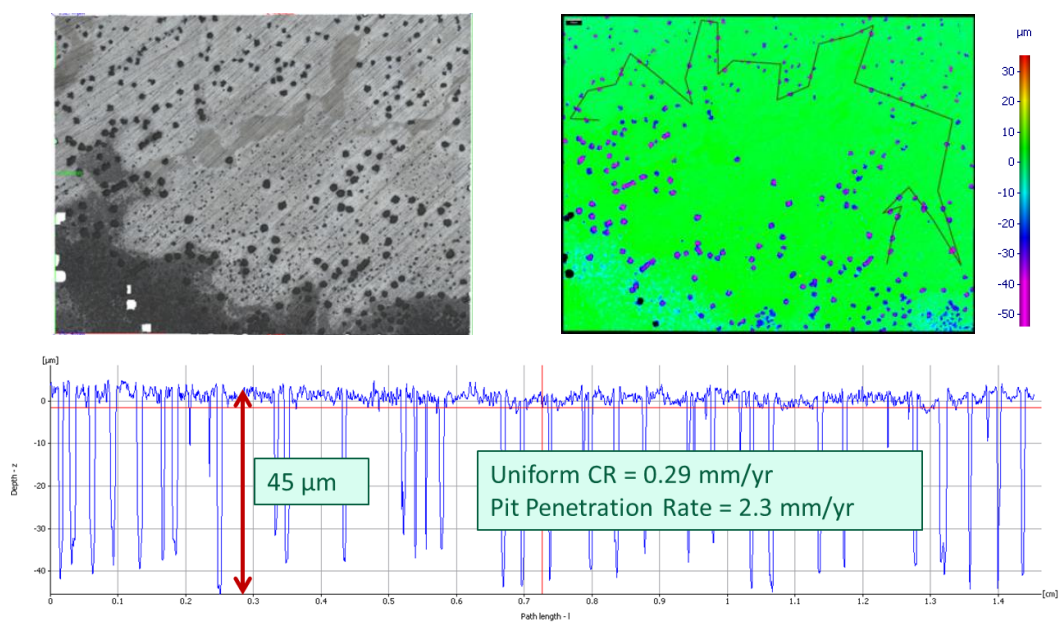


Figure 58: Surface profilometry analysis after removal of corrosion product layer (0.015 mbar H_2S , $T_{\text{gas}} = 40^\circ\text{C}$)

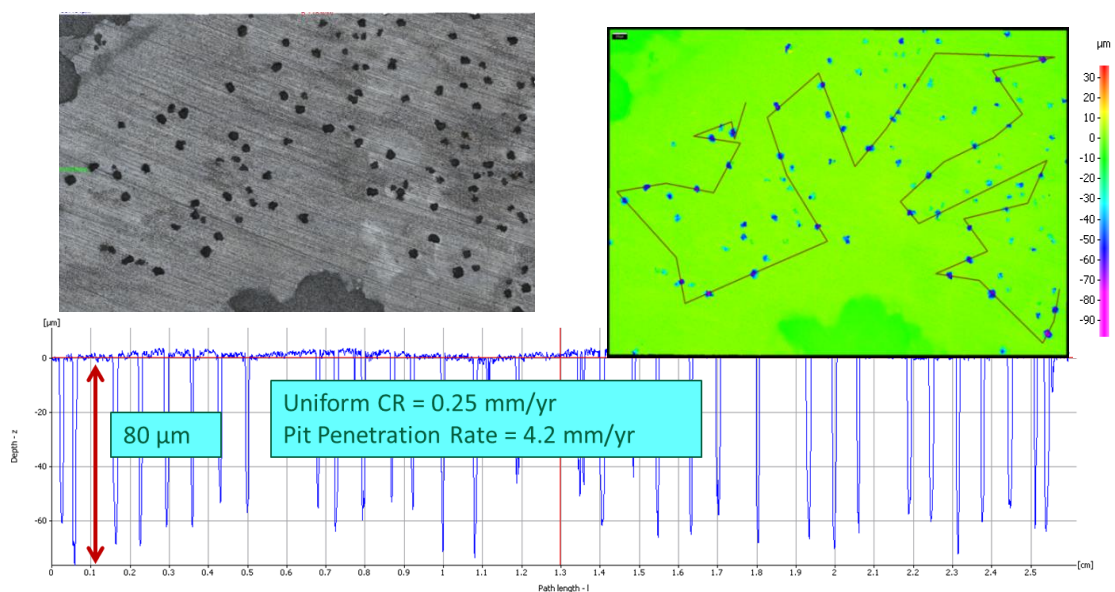


Figure 59: Surface profilometry analysis after removal of corrosion product layer (0.03 mbar H_2S , $T_{\text{gas}} = 40^\circ\text{C}$)

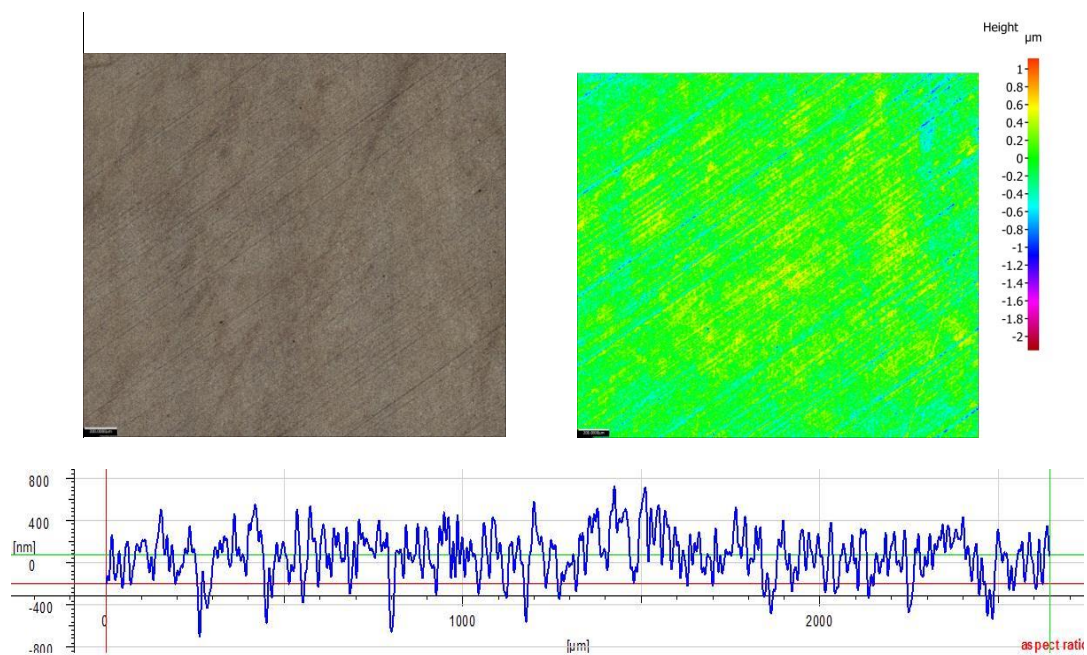


Figure 60: Surface profilometry analysis after removal of corrosion product layer (0.08 mbar H_2S , $T_{\text{gas}} = 40^\circ\text{C}$)

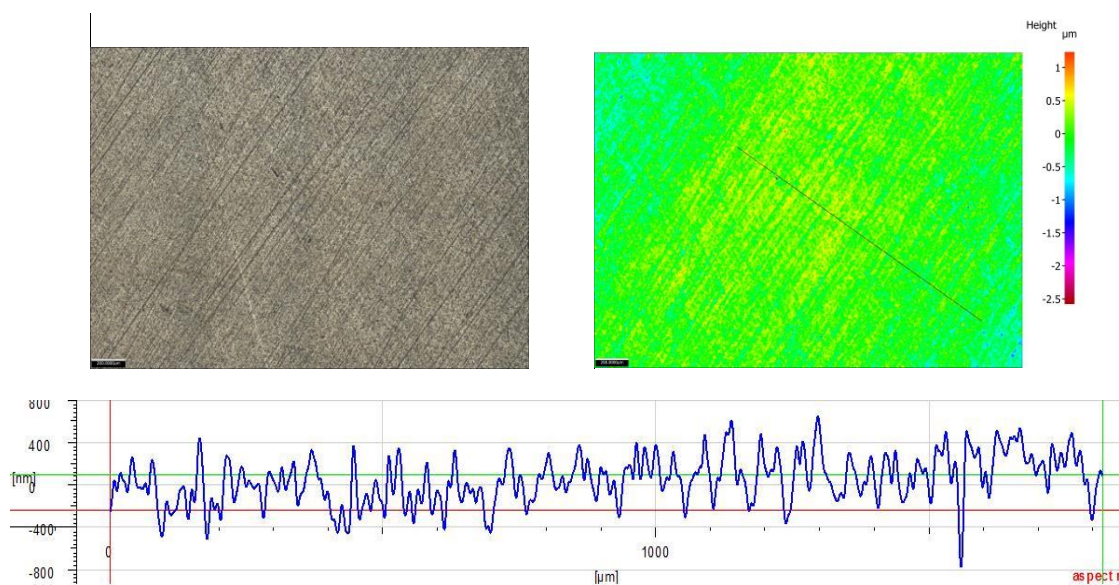


Figure 61: Surface profilometry analysis after removal of corrosion product layer (0.15 mbar H_2S , $T_{\text{gas}} = 40^\circ\text{C}$)

Similarly for part B, profilometry was used for measurement of pit depth on the steel surface after removal of the corrosion product layer. Comparisons for various H_2S partial pressure are shown from Figure 62 to Figure 66. At 0 mbar H_2S there was again no localized corrosion detected, as only surface roughening from general corrosion was observed, as shown in Figure 62. As the H_2S partial pressure was increased to 0.015 mbar and then 0.03 mbar, pitting as deep as 34 and 30 μm , respectively, was observed. As mentioned previously, the pit depth was not as deep as that observed in part A. The highest pit penetration rate was calculated to be 1.8 mm/y and 1.6 mm/y with 0.015 mbar and 0.03 mbar H_2S , respectively, as shown in Figure 63 and Figure 64. Furthermore, the pit population is considered to be high for both 0.015 mbar and 0.03 mbar H_2S in accordance with ASTM G46-94 [57]. Again, similar to part A, no localized corrosion was found at 0.08-0.15 mbar H_2S (Figure 65 and Figure 66).

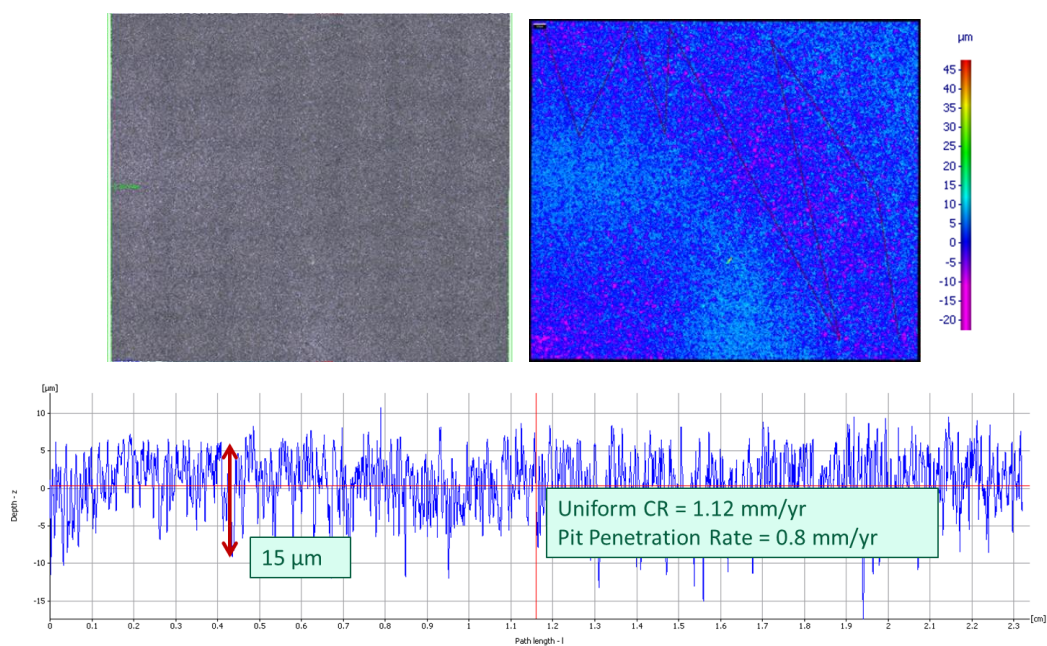


Figure 62: Surface profilometry analysis after removal of corrosion product layer (0 mbar H_2S , $T_{\text{gas}} = 60^\circ\text{C}$)

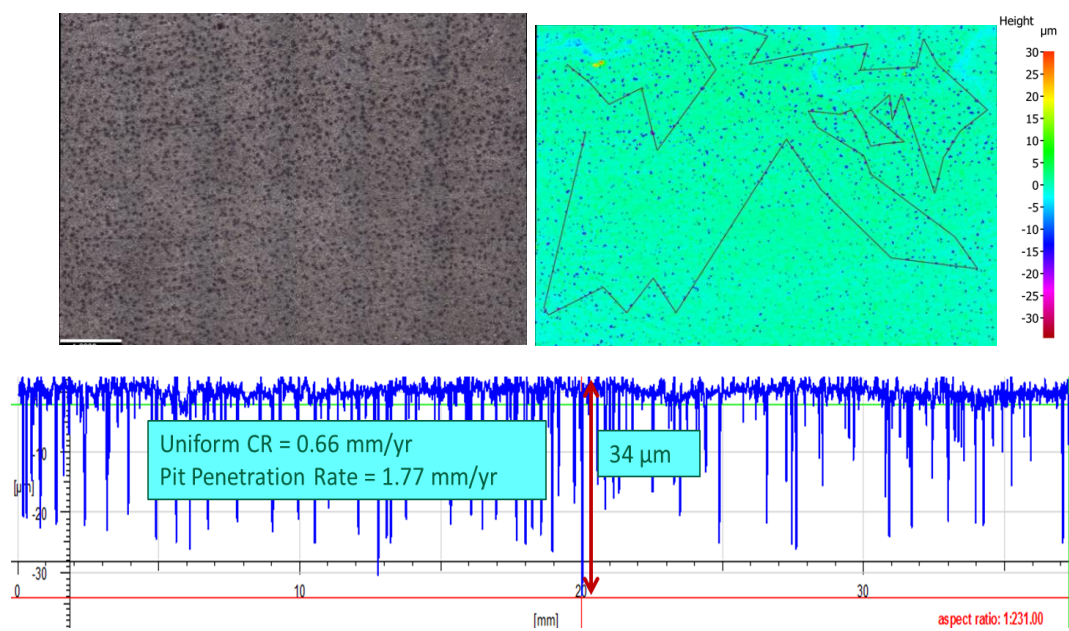


Figure 63: Surface profilometry analysis after removal of corrosion product layer (0.015 mbar H_2S , $T_{\text{gas}} = 60^\circ\text{C}$)

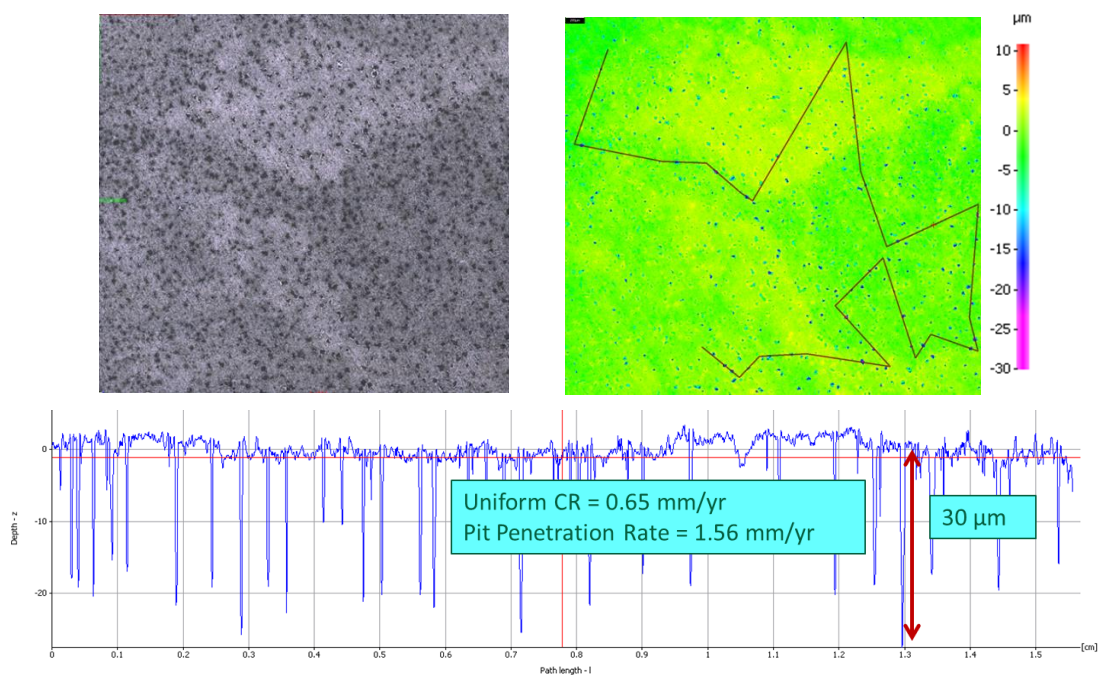


Figure 64: Surface profilometry analysis after removal of corrosion product layer (0.03 mbar H_2S , $T_{\text{gas}} = 60^\circ\text{C}$)

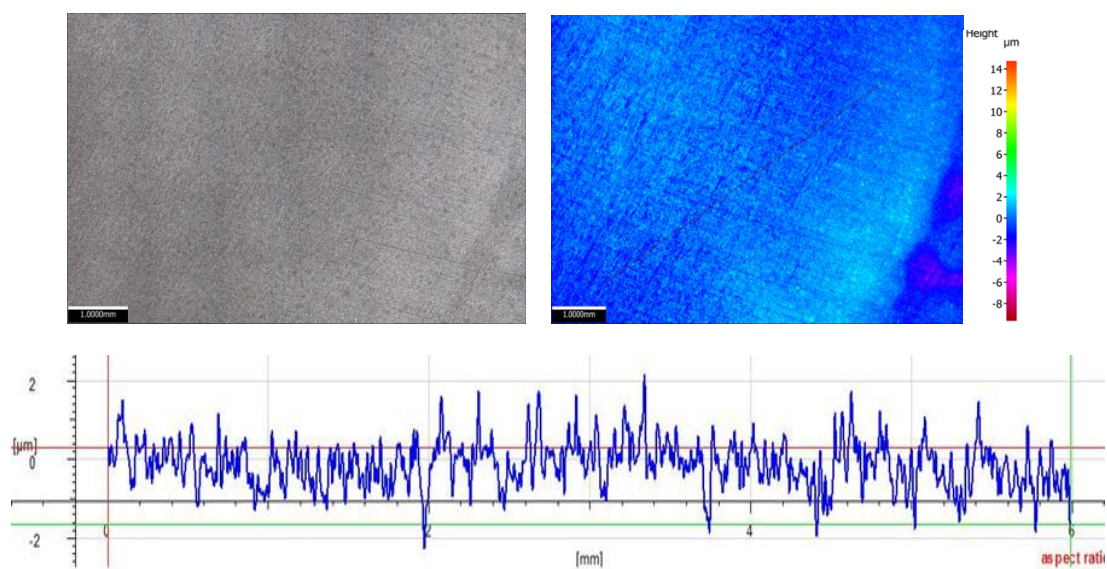


Figure 65: Surface profilometry analysis after removal of corrosion product layer (0.08 mbar H_2S , $T_{\text{gas}} = 60^\circ\text{C}$)

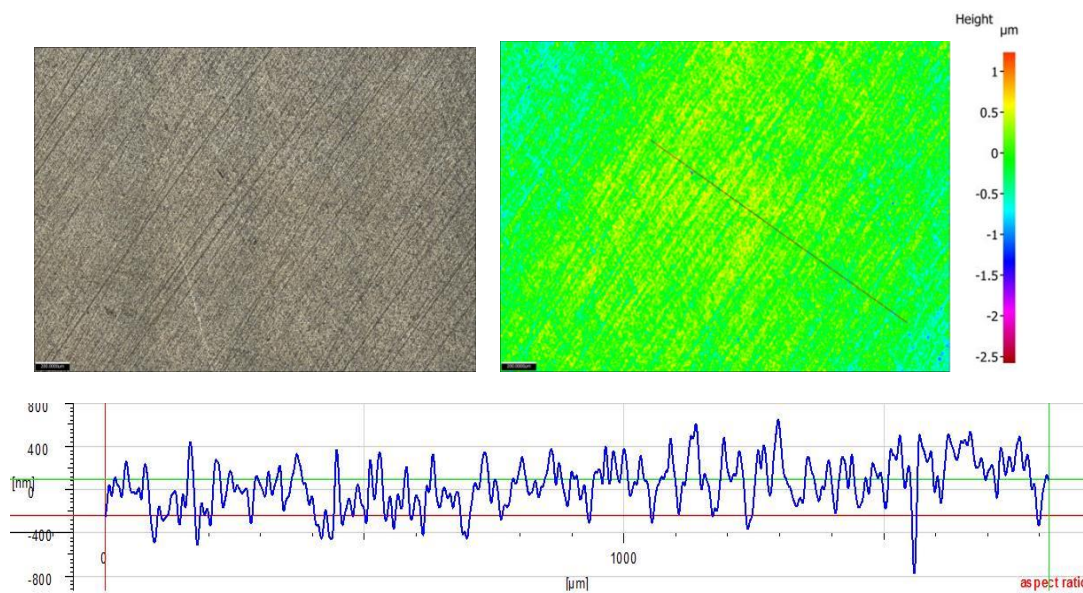


Figure 66: Surface profilometry analysis after removal of corrosion product layer (0.15 mbar H_2S , $T_{\text{gas}} = 60^\circ\text{C}$)

5.1.1.8 Summary for parts A and B

Based on analyses for parts A and B, which include corrosion rate, condensed water characteristics, surface profilometry, and corrosion product layer analysis, a summary can be made.

- 1) The general corrosion rate decreased with an increase in H_2S partial pressure from 0 mbar to 0.15 mbar H_2S for both studied gas temperatures (40°C and 60°C). The reduction in general corrosion rate was due to the formation of a partly protective FeS layer at higher H_2S partial pressure.
- 2) At a gas temperature of 40°C , localized corrosion rates of up to 4.2 mm/yr were measured at 0.015 mbar and 0.03 mbar H_2S . The pitting ratio (PR) was calculated

to be as high as 15, which clearly indicates the occurrence of localized corrosion ($PR > 5$).

- 3) At a gas temperature of 60°C , lower localized corrosion rates of up to 1.8 mm/yr, as compared for 40°C , were obtained at 0.015 mbar and 0.03 mbar H_2S . Corresponding pitting ratios were calculated to be a maximum of 2.8, which does not qualify as localized corrosion ($PR < 5$).
- 4) No pitting was found at 0.08 mbar and 0.15 mbar H_2S at both 40°C and 60°C .
- 5) Scaling tendency increased with increasing H_2S partial pressure, as this facilitated FeS precipitation on the steel surface, which reduced the corrosion rate.
- 6) Increased H_2S partial pressure, from 0 – 0.15 mbar, reduced the pH and lowered the amount of Fe^{2+} in the condensed water (since the H_2S is consumed by Fe^{2+} to form the FeS layer).
- 7) Saturation values with respect to FeCO_3 and FeS were also reduced as the partial pressure of H_2S increased.
- 8) At 0.015-0.15 mbar H_2S the main corrosion product found was FeS replacing Fe_3C and FeCO_3 .
- 9) Pitting initiation was related to partial or faulty coverage of FeS, this can be hypothesized to be the result of localized undermining by corrosion of the FeS layer.

5.1.2. Effect of Exposure Time

In this part of the research program, named part C, the effects of exposure time were studied. These experiments focused on the sustainability of localized corrosion at 0.03 mbar H₂S and 40°C; this concentration was selected as having the highest rate of localized corrosion of all conditions looked at in parts A and B. The three different test durations were used: 0-3 days, 0-7 days, and 0-28 days. The test matrix for part C is shown in Table 4. The analyses cover measurement of corrosion rate, pit penetration rate, corrosion product identification, and surface profilometry, as explained in the next sections.

5.1.2.1 Corrosion rate analysis

Comparisons of uniform corrosion rate, calculated from weight loss, and pit penetration rate, from profilometry, are shown in Figure 67. The pit penetration rate initially increased from 2.5 mm/yr after 3 days to 4.2 mm/yr after 7 days. However, as the experimental duration was increased to 28 days, the pit penetration rate significantly decreased to 0.6 mm/y. Therefore, it can be unequivocally stated that localized corrosion was not sustained over time. However, the uniform corrosion rate doubled from 0.25 mm/y after 7 days to 0.5 mm/y at 28 days.

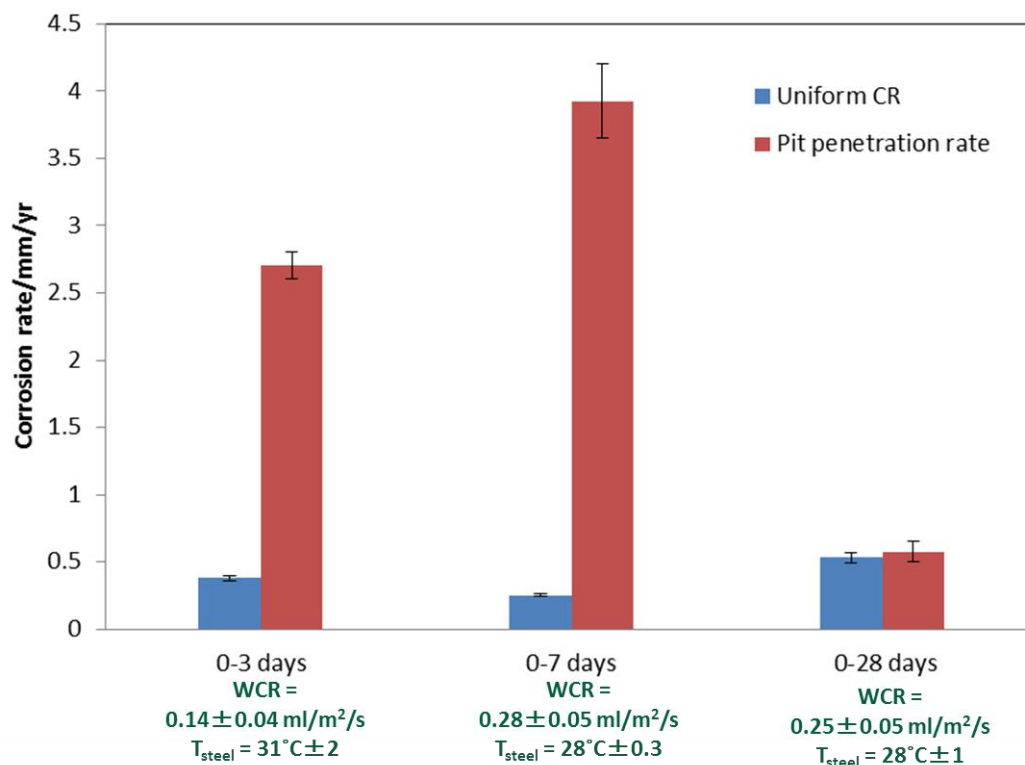


Figure 67: Comparison of corrosion rate from weight loss measurement and pit penetration rate at 3, 7, and 28 days

5.1.2.2 Corrosion product analysis (SEM/EDX)

Comparisons of SEM images with corrosion products were done for various experimental durations. At 3 days and 7 days duration, the corrosion product retained the scratch marks from the sample polishing process. EDX analysis showed the presence of sulfur, which suggests the formation of FeS. It was also observed that there were some spots where the layer failed indicating possible pitting, as shown in Figure 68 and Figure 69. As the experimental duration was increased to 28 days, no defective layer was found (Figure 70). Besides alloying elements, the EDX analysis also shows the presence of sulfur, which suggests the presence of FeS on the steel surface.

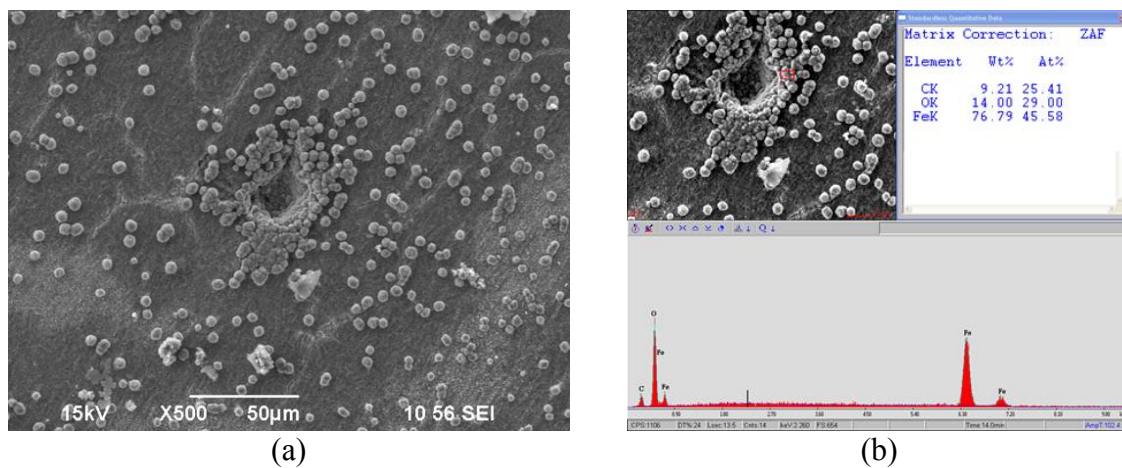


Figure 68: SEM/EDX analysis with corrosion product layer (0.03 mbar H_2S , $T_{\text{gas}} = 40^\circ\text{C}$, 0-3 days)

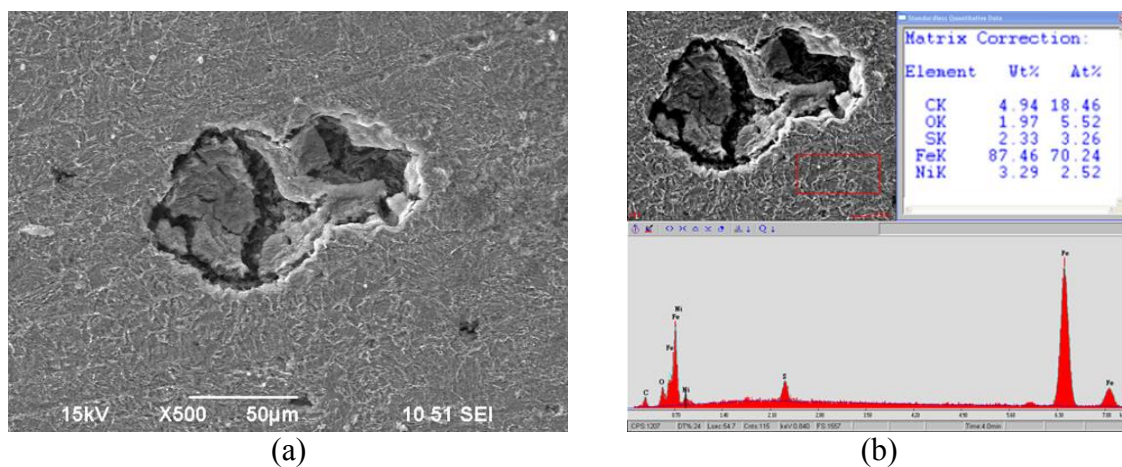


Figure 69: SEM/EDX analysis with corrosion product layer (0.03 mbar H_2S , $T_{\text{gas}} = 40^\circ\text{C}$, 0-7 days)

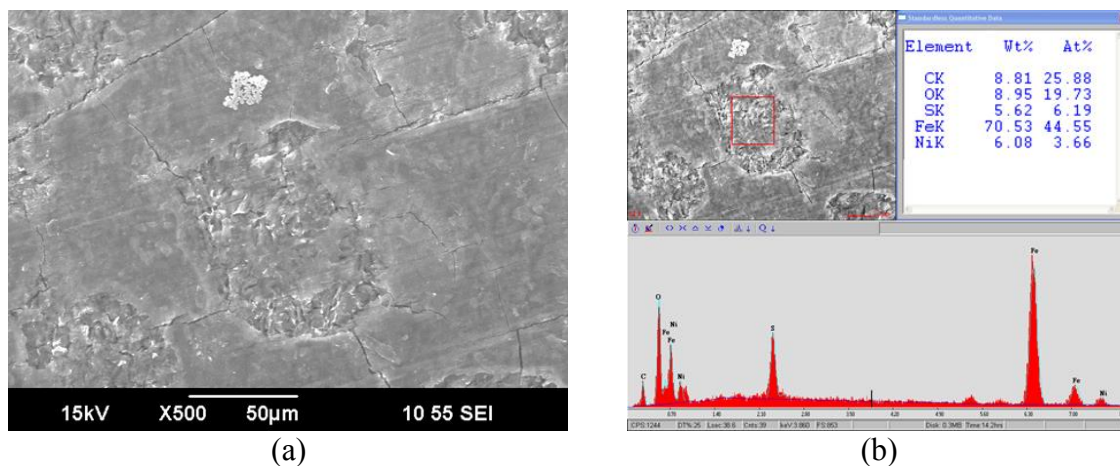


Figure 70: SEM/EDX analysis with corrosion product layer (0.03 mbar H₂S, T_{gas} = 40°C, 0-28 days)

5.1.2.3 Comparison of SEM images without layer

Comparisons of SEM images after removal of the corrosion product layer are shown in Figure 71, for experimental durations of 7 days and 28 days. From the comparison, it can be seen that the density of the pitting seemed to be reduced with increasing experimental duration. Detailed profilometry comparisons are shown in the next section.

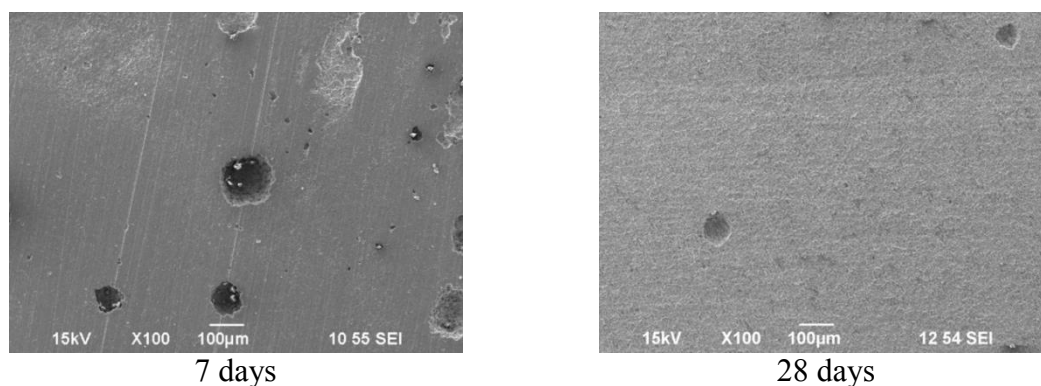


Figure 71: Comparison of SEM images without corrosion product layer at 0-7 and 0-28 days (0.03 mbar H₂S, T_{gas} = 40°C)

5.1.2.4 Comparison of profilometry analysis at 7 and 28 days

Detailed profilometry analyses are shown in Figure 72 and Figure 73. The deepest pit (80 μm) was found in the 0-7 day experiment, as compared to only a 50 μm pit depth at 0-28 days. The density of the pitting was also reduced with increasing experiment duration, such that only a few pits were observed following the 28 day experiment. This supports the above observation that the localized corrosion rate is unsustainable over time. Further data relating to pit disappearance after 28 days are shown and discussed with the cross-section images in the next section.

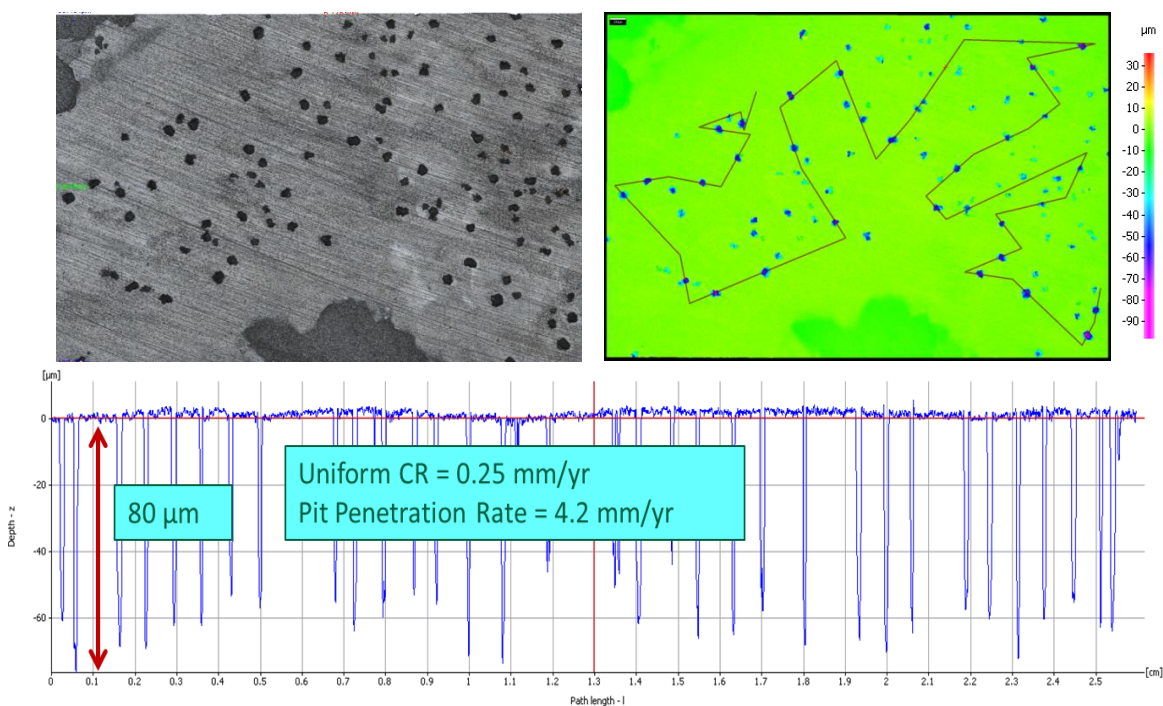


Figure 72: Surface profilometry analysis after removal of corrosion product layer (0.03 mbar H_2S , $T_{\text{gas}} = 40^\circ\text{C}$, 0-7 days)

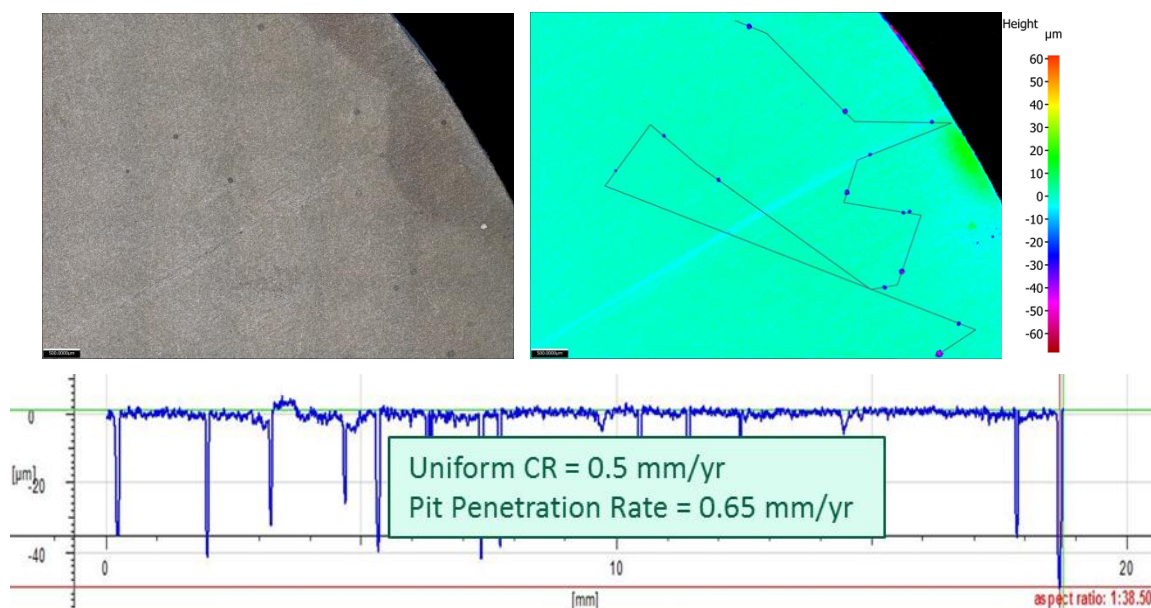


Figure 73: Surface profilometry analysis after removal of corrosion product layer (0.03 mbar H₂S, T_{gas} = 40°C, 0-28 days)

5.1.2.5 Comparison of cross section images at 0-3, 0-7, and 0-28 days

Comparison of the cross-section images for 0-3, 0-7, and 0-28 days are shown in Figure 74. The red and blue lines represent the reference and initial steel surface positions, respectively. It can be seen that the pit started to form as early as 3 days and kept on growing until day 7. From the profilometry analysis, the pit depth reached up to 80 μm. However, as the experimental duration increased, pit growth was not sustained while the uniform corrosion rate appreciably increased. At longer durations, the water chemistry inside the pit could significantly change as more FeS formed inside the pits. Thus, this would decrease the diffusion rate of corrosive species and ferrous ions inside the pits, as the generated FeS layer would create a barrier. Thus, pit growth is impeded. Furthermore, since the general corrosion rate was increased to 0.5 mm/yr, which is equivalent to 78 μm of steel thickness loss, the pits which were formed initially were

"eaten away" due to general corrosion. This resulted in the disappearance of initial pits, with their traces remaining as low depth features after 28 days of experiment. This explains why the localized corrosion rate decreased and the density of the pitting was reduced after 28 days.

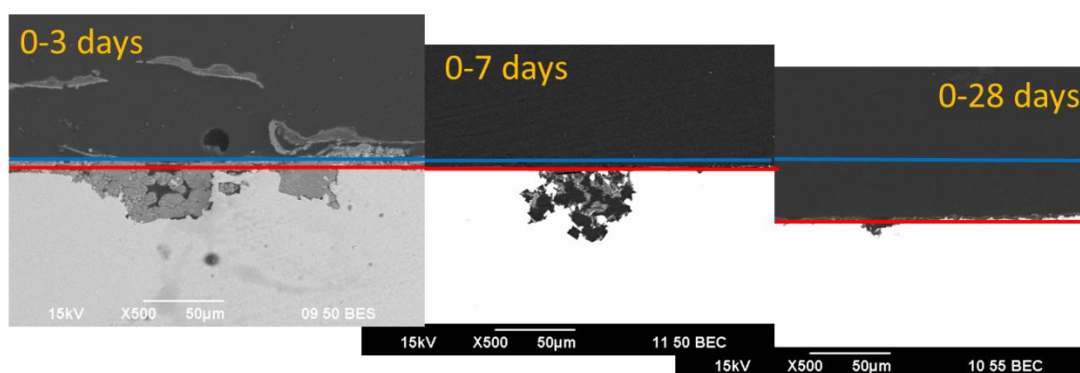


Figure 74: Cross-section images at 0-3, 0-7, and 0-28 days, 0.03 mbar H₂S, T_{gas} = 40°C

5.1.2.6 Summary for part C

Based on the results discussed for the effect of exposure duration, the following summary can be made.

- The localized corrosion rate observed in long term exposure (0-28 days) was not sustained over time.
- At 0.03 mbar H₂S, the localized corrosion rate was reduced from 4.2 mm/yr (0-7 days) to 0.65 mm/yr (0-28 days).
- The pitting density was reduced over time.
- General corrosion rate doubled with time (at 0.25 mm/yr from 0-7 days exposure to 0.5 mm/yr from 0-28 days exposure).

5.2 TLC in Highly Sour Environments

In this part of the work, the main focus was to investigate TLC behavior in highly sour environments. As outlined in the hypothesis, in highly sour environments TLC behavior is primarily dependent on the temperature of the steel, which affects the formation of a partly protective FeS layer, while water condensation rate (WCR) acts as the secondary factor, where a higher WCR leads to lower steel temperature, slower corrosion product layer formation and increase in the TLC rate. Thus, the discussion in this section is divided into parts related to the effects of gas/steel temperature, water condensation rate, and variations in H₂S partial pressure. The test matrices related to these experimental series are shown in Table 5 and Table 6.

5.2.1 *Effect of Gas/Steel Temperature and Water Condensation Rate*

A series of experiments to study the effect of gas temperature at 2 bar H₂S partial pressure were done where gas temperatures were varied between 25°C and 80°C, which resulted in a steel temperature between 15°C and 75°C, and a condensation rate between 0.005 ml/m²/s and 0.52 ml/m²/s (as shown in Table 5). Various analyses for top of the line samples were performed, such as weight loss calculation to determine the general corrosion rate, corrosion product/cross-section analysis by SEM/EDX, surface profilometry, and characterization of encountered FeS polymorphs by XRD. Most of the data in this section were published at a NACE (National Association of Corrosion Engineers) International Conference 2014 [53].

5.2.1.1 Corrosion rate analysis

Results for general TLC rates from weight loss analysis at different steel temperatures are given in Figure 75. The extent of corrosion at the top of the line can be correlated to the steel temperature; a decrease in corrosion rate with increasing steel temperature is observed. If the steel temperature is above 30°C, the TLC rate does not reach more than 0.15 mm/year. It is also noteworthy that if the steel temperature is less than 20°C, a higher TLC rate of up to 0.35 mm/yr is measured. However, there seems to be a combined effect between steel temperature and water condensation rate. In sour systems, the FeS layer is fairly insoluble in water and FeS formation occurs almost instantaneously at the metal surface.

In these conditions, the effect of the condensation rate is minimized, so the influence of condensation is insignificant (Figure 76). Based upon the above observations, water condensation serves as a cooling process for the steel. However, high condensation rates do not lead to greater corrosion if the steel temperature is sufficiently high (greater than 30°C) in the presence of H₂S. Other authors have made similar observations, determining that condensation has a secondary influence and stressing the importance of the formed iron sulfide's characteristics [42]. In addition, the dilution effect from the condensation process on the formation of FeS layer is not significant since the kinetic formation of FeS layer is much faster as compared to that of FeCO₃. However, the corrosion reaction, including layer formation, should be controlled by the temperature at which it occurs, *i.e.*, the steel temperature instead of the gas temperature, which can be quite different.

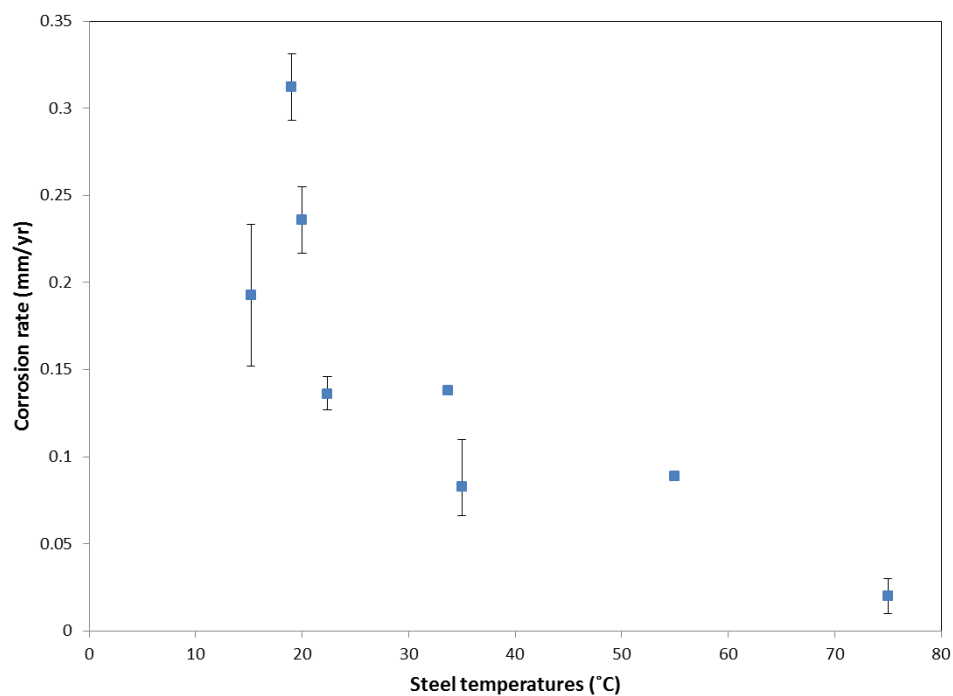


Figure 75: Top of the line general corrosion rate: effect of steel temperature

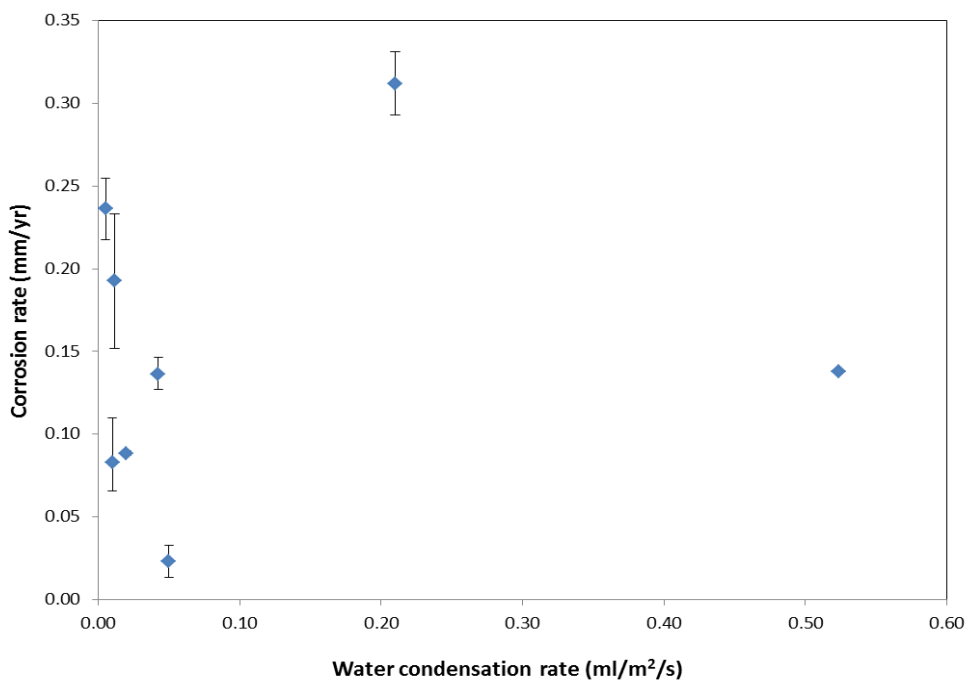


Figure 76: Top of the line general corrosion rate: effect of water condensation rate

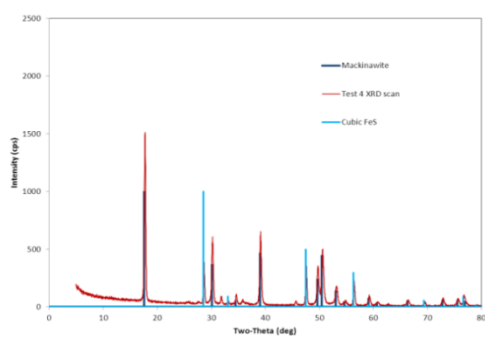
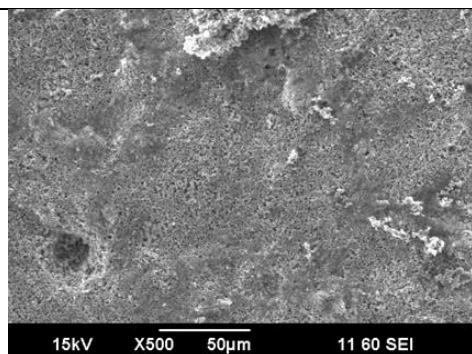
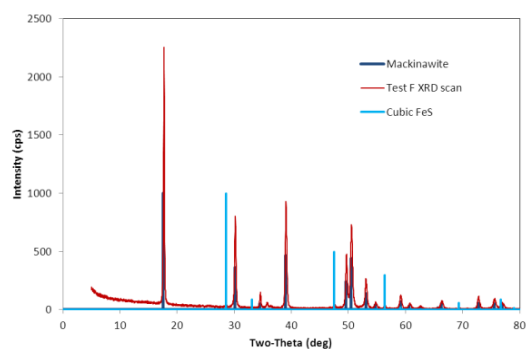
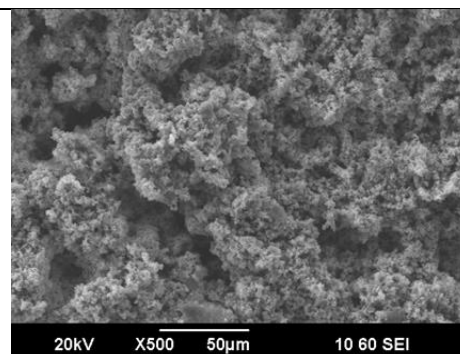
5.2.1.2 Corrosion product analysis

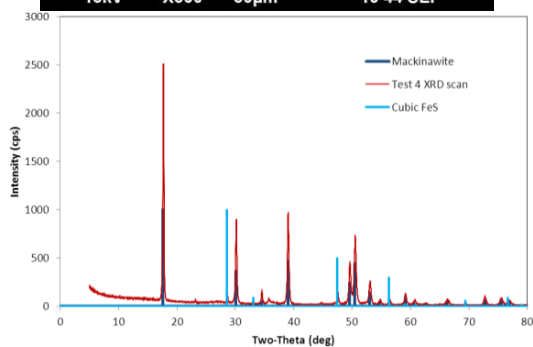
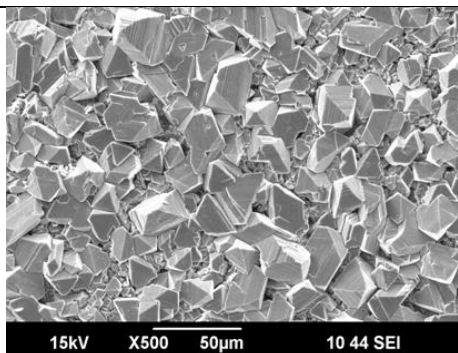
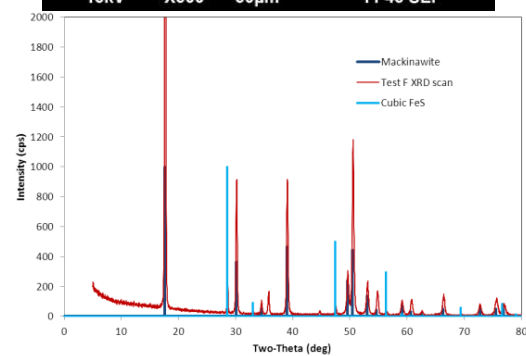
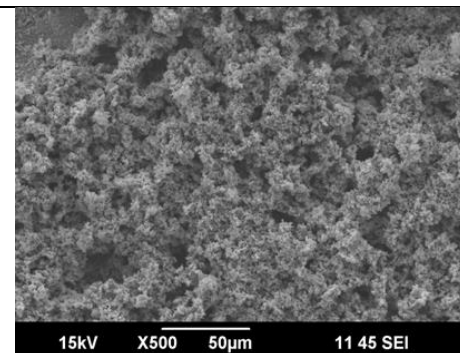
Comparisons of corrosion product layer images from SEM analysis are shown for each gas and steel temperature. Various crystal morphologies were observed that commonly constitute those observed in FeS layers; their variety implies that potentially different polymorphs of FeS formed on the steel surface. The corresponding X-ray diffraction analyses of the corrosion product layer shows the presence, depending on the gas temperature, of troilite, mackinawite, and cubic FeS (all stoichiometric iron sulfides). The results for XRD analysis are also shown along with SEM data showing crystal morphology.

The identity and stability of iron sulfides forming at the metal surface (such as mackinawite and pyrrhotite) is dependent on temperature, H₂S partial pressure, and pH [43]. Various FeS morphologies were observed by SEM in the current work, as shown in Figure 77. The variety of observed morphologies is indicative of the different polymorphs of FeS formed on the steel surface. The steel temperature is also related to which FeS polymorph forms and confers a degree of protection to the metal surface. X-ray diffraction (XRD) analysis showed the presence of mackinawite, cubic FeS, and troilite, depending on the gas/steel temperature. Explanations as to the occurrence of these particular iron sulfide corrosion products have been described by Smith, *et al.* [43]. Mackinawite seems to be a dominant FeS phase as a corrosion product of mild steels, as it is favored over a wide range of temperatures and it possesses rapid formation kinetics; faster than for any other FeS polymorph [24]. The second FeS polymorph observed in the present work is known as cubic FeS. This is rarely observed due to its relative instability

compared to other FeS phases. It is associated with high saturation levels with respect to FeS (*i.e.*, high aqueous concentrations of Fe^{2+} ions) and moderate temperatures (35-50°C). Cubic FeS is hardly ever found at the bottom of the pipeline, since its formation is inhibited by the presence of ions such as Cl^- [61]. Thus, it would be more readily found at the top of the pipeline in a cooler condensed water environment, free from chloride or other anions, which represents an ideal condition for its formation. Due to its relative instability *versus* other FeS polymorphs, cubic FeS can quickly transition into a more stable phase such as pyrrhotite. The third common type of FeS phase found in the studied sour TLC environment is known as troilite. Its formation has been previously described by Singer, *et al.* [45]. Troilite, which is the stoichiometric end-member of the pyrrhotite (Fe_{1-x}S) series, has a characteristic elongated morphology in TLC environments. Due to its solubility behavior, its occurrence is favored in more acidic solutions, but it has slower formation kinetics than mackinawite. Thus, to promote the formation of troilite, a combination of higher temperature, lower pH and higher pH_2S is required [43].

Due to the wide range of steel temperatures tested in this study (15°C to 75°C), mackinawite and cubic FeS were identified to be the most dominant polymorphs. This could be explained by the lower steel temperature, due to high water condensation rate, which does not favor kinetically slow reactions, *i.e.*, troilite formation. However, at a gas temperature of 80°C and steel temperature of 75°C, corresponding to the highest studied temperature and a low condensation rate, the presence of troilite was confirmed by XRD. In this condition, higher gas temperature leads to higher steel temperature, which logically facilitates the formation of troilite.

$T_{\text{gas}} = 25^{\circ}\text{C}$

 $T_{\text{steel}} = 20^{\circ}\text{C}$
 mackinawite, cubic FeS

 $T_{\text{steel}} = 15^{\circ}\text{C}$
 mackinawite, cubic FeS

 $T_{\text{gas}} = 40^{\circ}\text{C}$

 $T_{\text{steel}} = 35^{\circ}\text{C}$
 mackinawite, cubic FeS

 $T_{\text{steel}} = 22^{\circ}\text{C}$
 mackinawite, cubic FeS

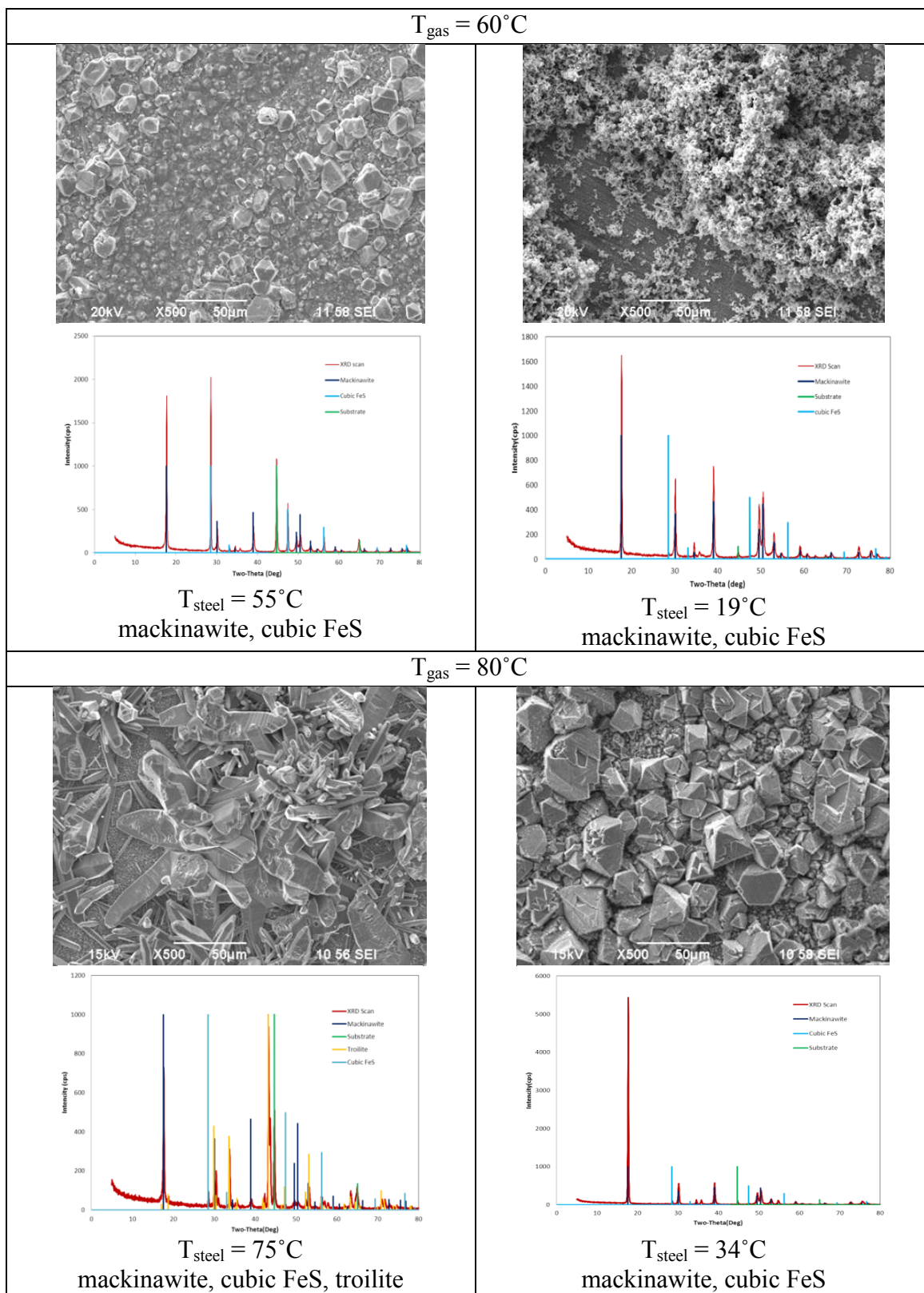


Figure 77: SEM images and XRD patterns of FeS polymorphs at studied conditions

5.2.1.3 *Comparison of cross-section analyses*

Cross-section images which show the morphology of the FeS layer attached to the steel surface at various steel temperatures and water condensation rates are shown in Figure 78. Generally, the FeS layer consists of two distinct layers attached to the steel. A two-step mechanism involving the rapid initial formation of a thin FeS layer, identified as mackinawite, on the metal surface which can then be overlaid by different phases of iron sulfide has been described by Smith [43]. This two-step mechanism seems to be supported by the cross-sectional analyses performed in this study.

The growth rate of the first layer appears to be directly related to the corrosion rate, as its thickness often corresponds to the uniform metal loss. The identity of the second phase depends more on the actual test conditions than on the kinetics of corrosion product formation. Low steel temperatures between 15 and 19°C (linked to higher condensation rate) seem to favor the formation of a very porous outer FeS layer. However, as the steel temperature increased (to greater than 20°C), regardless of the condensation rate value, a more coherent and protective FeS layer was formed as evidenced by reduced TLC rates. Less pitting was also observed. The severity of the localized attack was high at a steel temperature of 19°C but, overall, only a small fraction of the surface was affected by pitting.

Thus, the reduction of general TLC rate with increasing steel temperature as mentioned previously is supported by this cross-section analysis. The TLC behavior was mainly governed by the formation of a more protective and dense FeS layer at higher steel temperatures.

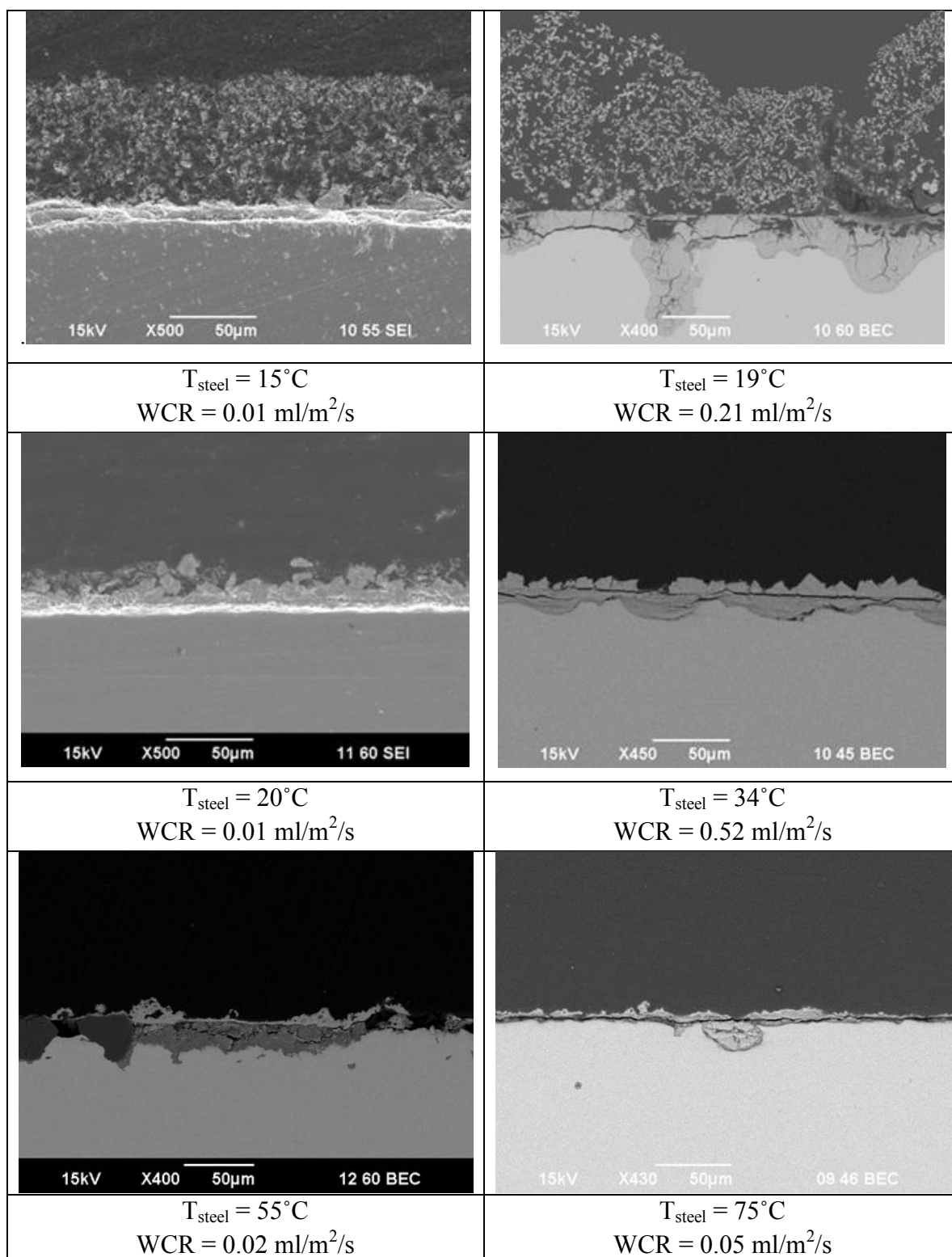


Figure 78: SEM cross-section images at studied steel temperatures and water condensation rates

5.2.1.4 *Comparison of corrosion product thickness*

Influence of the film thickness on the corrosion rate was also quantified, as shown in Figure 79. Greater thickness of the FeS layer does not seem to protect the metal from corrosion. Protectiveness is governed more by adherence to the metal surface and the characteristics (dense or porous) of the layer formed particularly that immediately adjacent to the steel surface. Higher thickness of the FeS layer correlated with higher corrosion rate; more FeS was formed from the steel dissolution due to corrosion.

Thus, it is justified to conclude that TLC behavior in highly sour environments, in this case at 2 bar H₂S partial pressure, is totally different when compared to that in sweet TLC. The TLC rate in highly sour environments is totally dependent on the formation of a protective FeS layer formed at higher steel temperature, in line with its physical characteristic of being either dense or porous. Water condensation rate, which is the main parameter in controlling sweet TLC behavior, only acts as a secondary parameter in highly sour TLC. Higher WCR leads to lower the steel temperature, poorly protective FeS layers and increase the TLC rate.

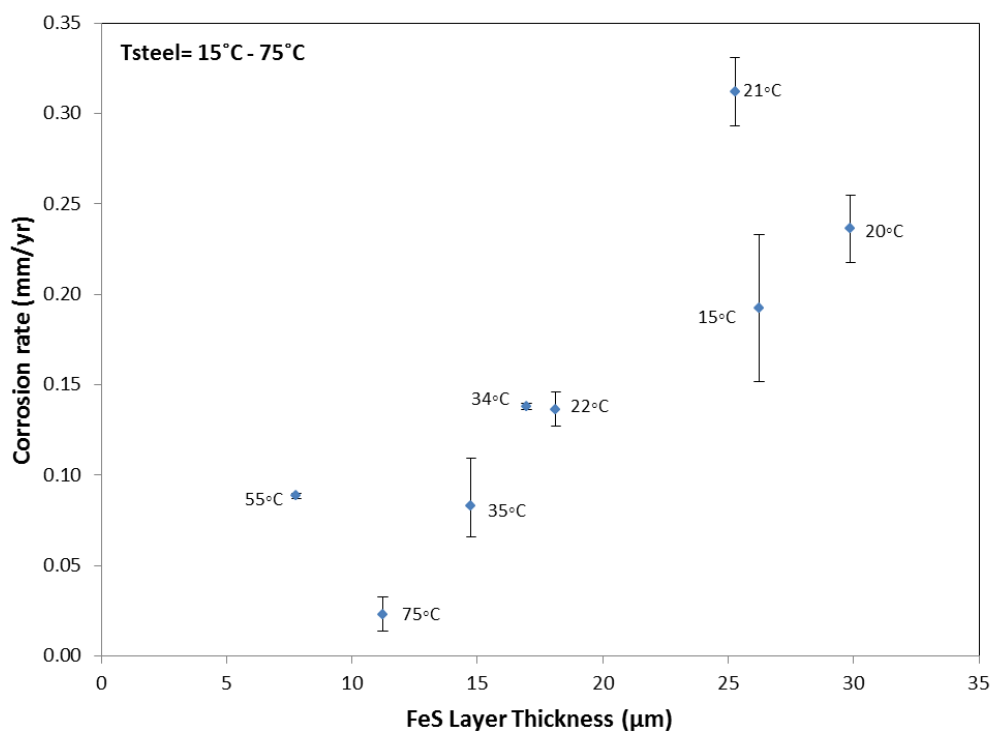


Figure 79: Comparison of FeS layer thickness on highly sour TLC rate

5.2.1.5 Summary relating to the effect of temperature and water condensation rate in highly sour TLC

The gas temperatures tested were 25°C, 40°C, 60°C, and 80°C, with 2 bar H₂S partial pressure, 10 bar of CO₂, and 28 bars of total pressure. The following summary can be made.

- 1) The general trend of corrosion rate decreases with increasing steel temperature. The lowest TLC general corrosion rate (0.02 mm/yr) was obtained at the highest steel temperature (75°C). Higher steel temperature seems to be the main factor governing formation of a protective, dense FeS layer with reduced porosity.

- 2) A very dense and thin layer was always present on the metal surface. In some conditions, such as at a high condensation rate, a second much thicker but more porous outer layer was also observed.
- 3) Higher FeS layer porosity can be correlated with an increase in general TLC. The FeS film thickness by itself does not seem to have a clear correlation with the corrosion rate.
- 4) Mackinawite and cubic FeS were always identified at the top-of-the-line, except at a gas temperature of 80°C (WCR=0.05ml/m²/s, T_{steel}=75°C), where troilite was observed.
- 5) At gas temperatures of 60 and 80°C, localized corrosion was observed on top-of-the-line samples. The severity of the localized attack was higher at 80°C, but overall only a small fraction of the surface was affected by localized attack.

5.2.2 *Effect of H₂S Partial Pressure*

In this section, a series of experiments to study the effect of H₂S partial pressure in highly sour TLC are described. Experimental conditions were a gas temperature 40°C, 10 bar CO₂ partial pressure, 28 bar total pressure, and varying H₂S content at 0.2 bar, 2 bar, and 5 bar of H₂S partial pressure, as shown in Table 6. Similar analyses to those reported for other conditions, such as weight loss calculation to determine the general corrosion rate, corrosion product layer and cross section analyses by SEM/EDX, profilometry, and identification of various FeS polymorphs by XRD analysis were conducted.

5.2.2.1 Corrosion rate analysis

Comparisons of general TLC rate, calculated from weight loss, for experiments conducted with 0.2, 2, and 5 bar of H₂S partial pressure are shown in Figure 80 and Figure 81. As mentioned previously, each test setup is capable of having two water condensation rate values in a single test. Thus, Figure 80 shows the comparison of TLC rates at 0.01 ml/m²/s, while Figure 81 represents a higher WCR of 0.04 ml/m²/s. Generally, the results showed a trend of decreasing corrosion rate with increasing H₂S partial pressure.

In order to explain this corrosion behavior, comparisons between the time-averaged flux of Fe²⁺ leaving the steel and the time-averaged flux of Fe²⁺ consumed for the FeS scale formation, as reaction rate, are plotted and shown in Figure 82 and Figure 83, at WCR 0.01 ml/m²/s and 0.04 ml/m²/s, respectively. Overall, it can be seen that between 0.2 and 5 bars of H₂S partial pressure, the iron dissolution rate was reduced, which increased the scaling formation rate. The scaling tendency (ST) was also increased from 0.3 to 0.99. At higher H₂S partial pressure (2 to 5 bars), almost all ferrous ions from the dissolution process were consumed by H₂S to form the FeS layer. The increase in the scaling tendency would indicate that more FeS film was developed from the steel dissolution, which to a degree protected the metal from corrosion. Almost all of the Fe²⁺ ions released through corrosion was used for the layer formation at 5 bar H₂S partial pressure. This would explain the lowest general corrosion rate obtained under those conditions.

As mentioned previously, steel temperature plays a significant role in controlling sour TLC rate through the formation of a dense and protective FeS layer. Thus, the effects of H₂S partial pressure and steel temperature are compared and plotted as shown in Figure 84. It can be seen from the graph that the corrosion behavior could still be correlated to the steel temperature. First, by comparing the TLC rate at the same steel temperature (35°C), with varying H₂S partial pressure from 0.2, 2, and 5 bars, an increase in H₂S partial pressure would result in reduced TLC rate. The lowest TLC rate was obtained at 5 bars of H₂S partial pressure. This behavior supported the earlier explanation since, at higher H₂S contents, more FeS formed, giving better protection to the steel. Nevertheless, when TLC rates at different H₂S partial pressures and steel temperatures are compared, there seems to be a combined effect between them. The lowest TLC rate was obtained at 2 bars of H₂S partial pressure, at the highest steel temperature (22°C); the next lowest was at 5 bars H₂S partial pressure with a lower steel temperature (17°C). As such, the steel temperature would remain the primary parameter controlling TLC rate, followed by H₂S partial pressure.

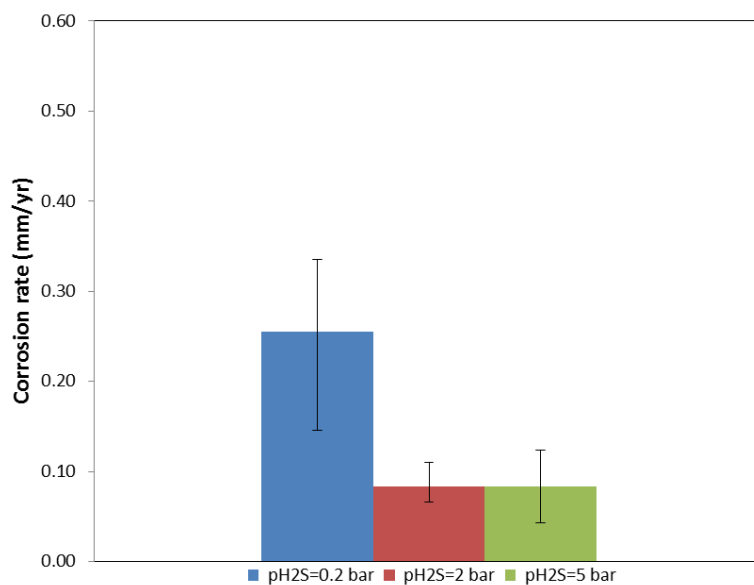


Figure 80: Effect of H₂S partial pressure on sour top of line corrosion rate ($T_{\text{gas}}=40^{\circ}\text{C}$, $p\text{CO}_2=10$ bar, $\text{WCR} = 0.01$ ml/m².s)

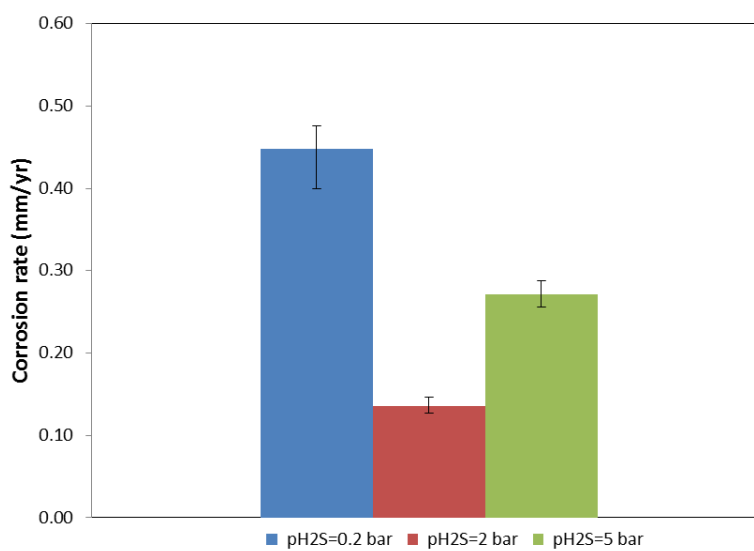


Figure 81: Effect of H₂S partial pressure on sour top of line corrosion rate ($T_{\text{gas}}=40^{\circ}\text{C}$, $p\text{CO}_2=10$ bar, $\text{WCR} = 0.04-0.05$ ml/m²/s)

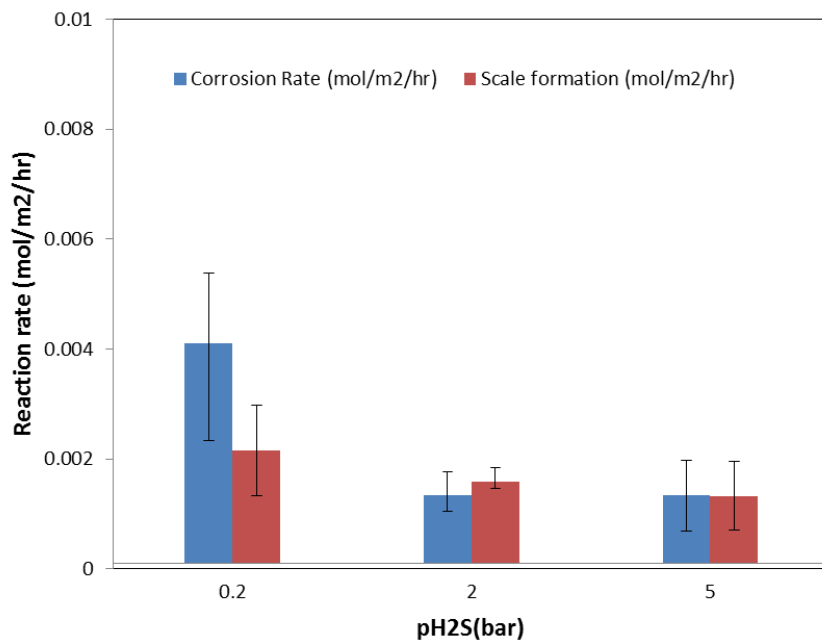


Figure 82: Influence of H₂S partial pressure on sour top of line reaction rate ($T_{\text{gas}}=40^{\circ}\text{C}$, $p\text{CO}_2=10$ bar, $\text{WCR} = 0.01$ ml/m²/s)

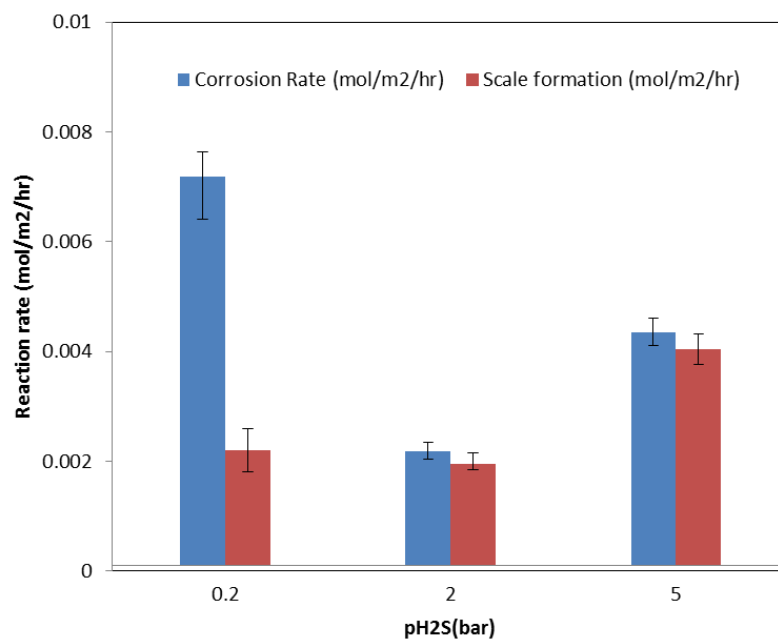


Figure 83: Influence of H₂S partial pressure on sour top of line reaction rate ($T_{\text{gas}}=40^{\circ}\text{C}$, $p\text{CO}_2=10$ bar, $\text{WCR} = 0.04$ ml/m²/s)

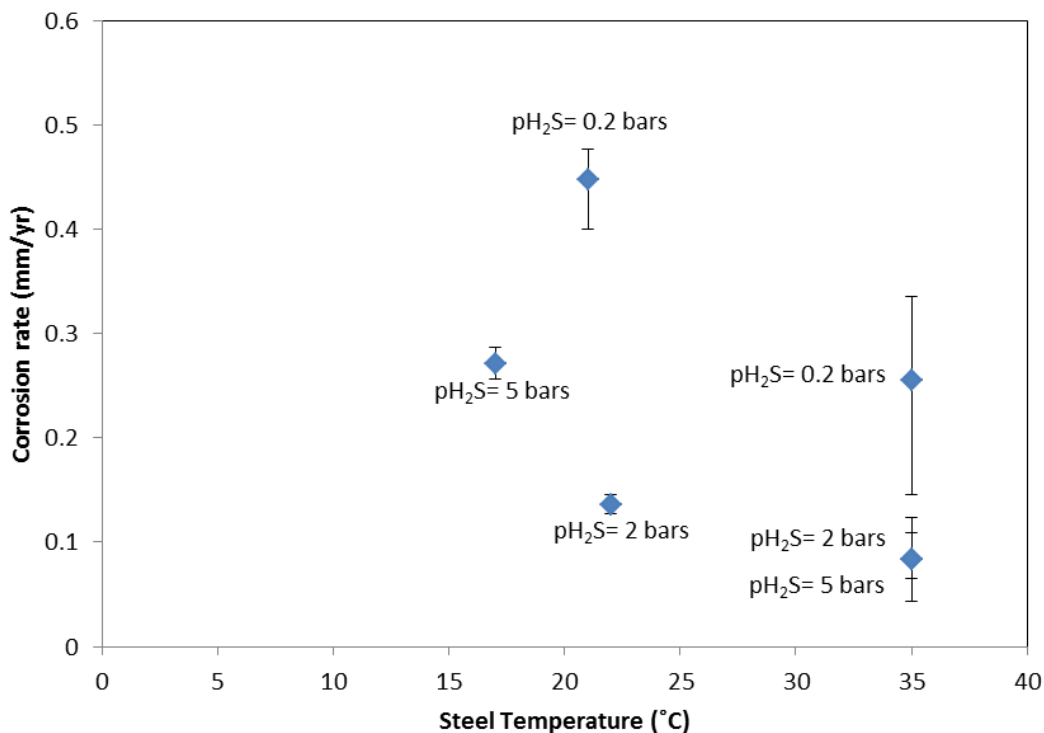
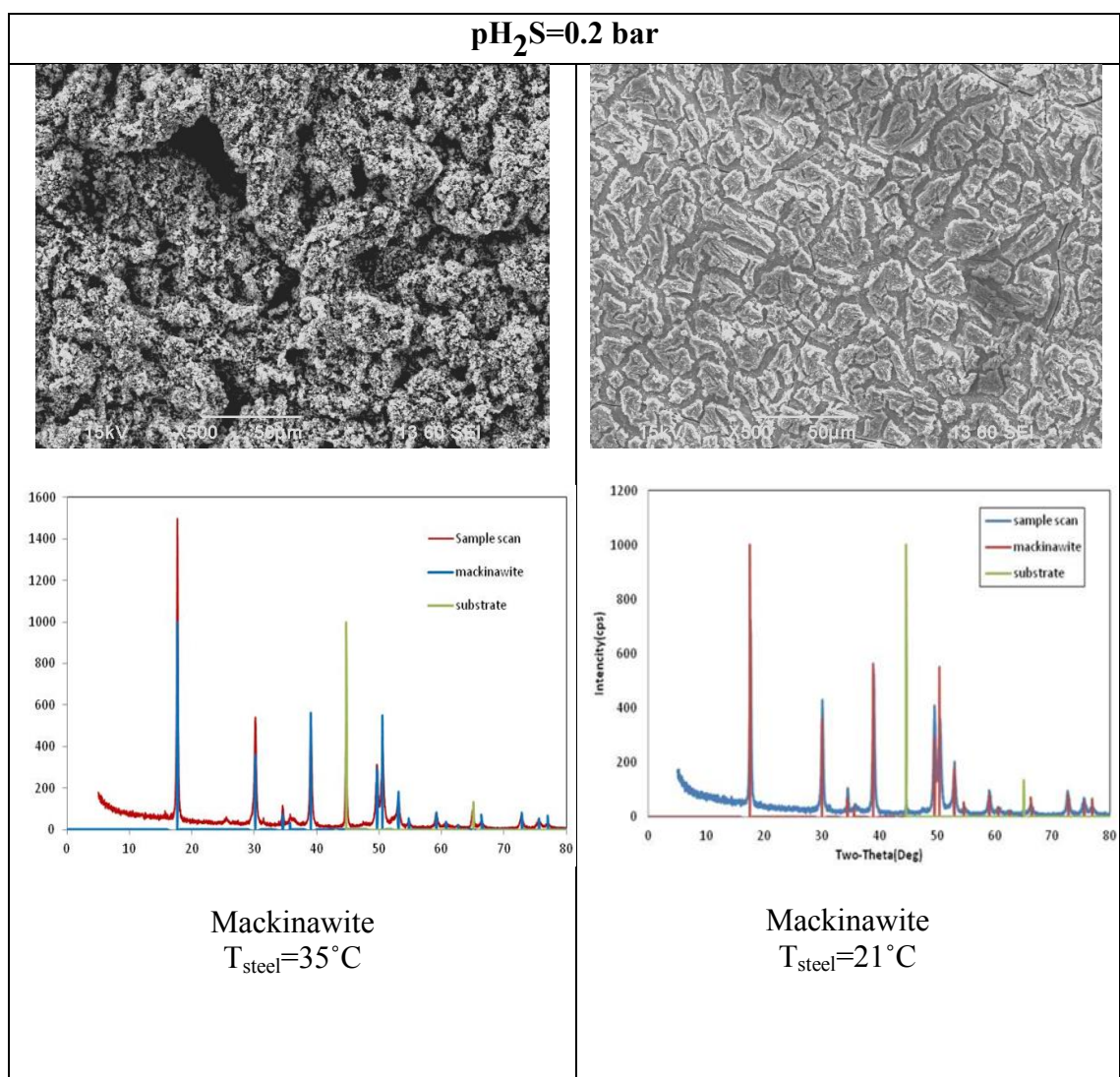


Figure 84: Influence of H₂S partial pressure and steel temperatures on sour TLC rate ($T_{\text{gas}}=40^{\circ}\text{C}$, $p_{\text{CO}_2}=10$ bar, $\text{WCR} = 0.01\text{-}0.05$ ml/m².s)

5.2.2.2 Corrosion product analysis

The comparisons of corrosion product layer images from SEM analysis are shown for each H₂S partial pressure between 0.2 and 5 bars in Figure 85. The corresponding XRD analysis of the corrosion product layer shows the presence, depending on the gas temperature and H₂S partial pressure, mostly of mackinawite and cubic FeS. At a H₂S partial pressure of 0.2 bars, mackinawite is the favored polymorph, since its formation is kinetically the fastest among all possible FeS polymorphs. No other FeS besides mackinawite was formed, especially as the H₂S partial pressure was low at 0.2 bars. From the SEM images at 0.2 bars H₂S partial pressure, a very thin and porous layer of FeS was observed.

As the H_2S partial pressure increased to 2 bar, the presence of mackinawite and cubic FeS was observed from the XRD analysis. Cubic FeS is favored to form since no “foreign ions” such as Cl^- were present at the top which would inhibit the formation of this particular polymorph [61]. At the highest H_2S partial pressure tested (5 bars), mackinawite exclusively was formed as, at this condition, the steel temperature of between 17 and 35°C and H_2S partial pressure of 5 bar favored its formation.



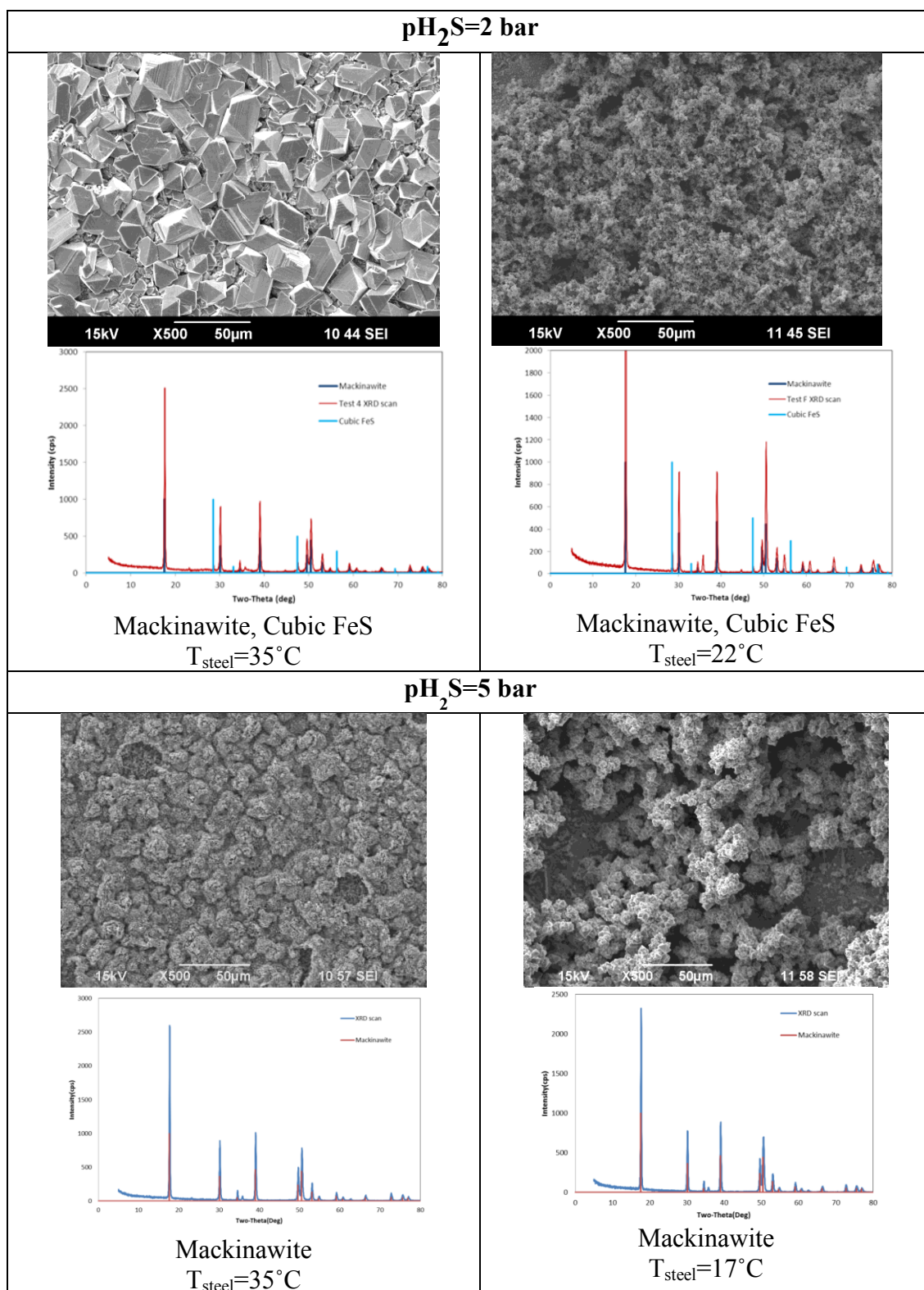


Figure 85: SEM and XRD Image comparison for different H₂S partial pressure (T_{gas}=40°C, pCO₂=10bars, WCR = 0.01-0.05 ml/m².s)

5.2.2.3 Comparison of cross-section analyses

Cross-section images which show the morphology of the FeS layer attached to the steel surface at various H₂S partial pressures, steel temperatures, and water condensation rates are shown in Figure 86. However, the cross-section analysis can only be compared between 0.2 and 5 bars of H₂S partial pressure, as the cross-section at 2 bars of H₂S partial pressure was not available due to sample limitations.

At 0.2 bar of H₂S partial pressure, a very dense and adherent 7 μm thick FeS layer formed on the metal surface. The steel lost an average of 14 μm due to corrosion at the 35°C temperature. Approximately 50% of the dissolved iron was consumed for the formation of the FeS. However, there was a second more porous layer, with a thickness of 20 μm.

The same observation was made at a lower steel temperature (21°C), where the steel lost a wall thickness on average of 26 μm, as compared to only an 11 μm thickness of the dense FeS layer formed. The second FeS layer comprised of a very porous layer as thick as 30 μm. This FeS layer observation would explain the highest general corrosion rate calculated at low H₂S partial pressure (0.2 bars) as the metal was not well protected by the FeS since it was not fully developed. This observation also supports the result from iron dissolution and scale formation rate analyses, as mentioned previously.

As the H₂S concentration was increased (5 bar), the corrosion product layer seems to be comprised of two distinct layers. At higher steel temperature (35°C), the first layer was dense and well attached to the metal surface. The thickness of this layer was calculated at 7 μm and was higher than the wall thickness loss of 5 μm. The thickness of

the second porous layer was calculated at 24 μm . The higher thickness of FeS as compared to wall thickness loss shows that the layer was most likely developed by a precipitation process. At this point, the corrosion rate was calculated at the low value of 0.1 mm/yr, which shows the protectiveness of the FeS layer.

However, at lower steel temperature (17°C), the same layer was also comprised of a dense FeS as thick as 33 μm , while the wall thickness loss was only 15.5 μm . The outer layer was thick and porous, with 88 μm thickness. The porosity of the second outer layer was higher as compared to the one at higher steel temperature. Furthermore, the corrosion rate which was calculated at this point was higher than the previous value at 0.3 mm/yr. No localized corrosion was observed for all the analyses done.

Thus, these analyses showed that both steel temperature and H₂S partial pressure play an important role in controlling the TLC behavior through formation of a protective FeS layer. However, steel temperature seems to be dominant as a controlling factor rather than the H₂S partial pressure.

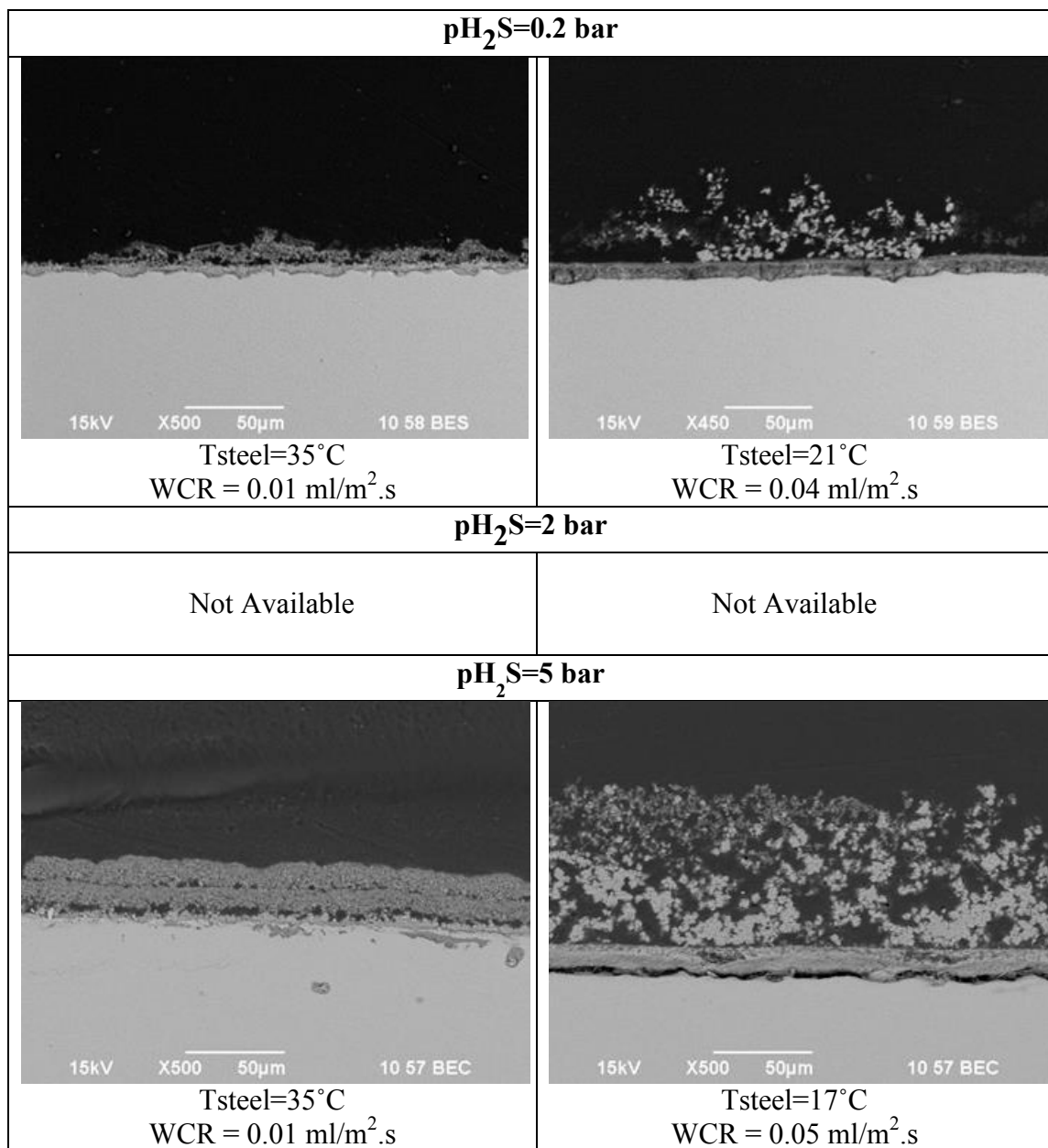


Figure 86: Cross-section analysis comparison for H₂S partial pressure (T_{gas}=40°C, pCO₂=10 bars, WCR = 0.01-0.05 ml/m².s)

5.2.2.4 Summary relating to the effect of H₂S partial pressure on TLC

The H₂S partial pressure was varied between 0.2, 2, and 5 bars at 40°C gas temperature and the resultant postulates are summarized below.

- 1) Overall, the general TLC rate was reduced at higher H₂S partial pressure and steel temperature.
- 2) Higher H₂S partial pressure and steel temperature promote the formation of thicker and denser FeS layers, which confer better protection to the steel.
- 3) Mackinawite was observed to be the dominant phase formed at all H₂S partial pressures tested, while cubic FeS was only observed at 2 bars of H₂S partial pressure (T_{gas}=40°C).
- 4) No localized corrosion was observed at 0.2, 2, or 5 bars H₂S partial pressure.
- 5) Steel temperature seems to be dominant as a controlling factor rather than the H₂S partial pressure.

CHAPTER 6: DESCRIPTIVE MODEL OF TLC CORROSION MECHANISMS

In this chapter, based on the experimental data obtained for TLC in marginally and highly sour environments, a new descriptive model for TLC corrosion behavior is proposed. The starting point is TLC behavior in sweet environments, phenomena observed therein being related to what occurs in sour scenarios.

6.1 TLC Corrosion Mechanism in Sweet Environments

Sweet TLC models have been developed by various researchers [5], [9], [10], [40], as has been discussed elsewhere in Chapter 2. Recently, research reported by Singer [40] explained TLC mechanisms with an emphasis on the initiation and propagation of localized corrosion as follows. Initially, steel undergoes uniform corrosion due to droplets of water condensing on the steel surface. Carbon dioxide dissolves into this water, resulting in its acidification. This results in acid corrosion of the steel, with oxidative dissolution of ferrous ions into the condensed water increasing its pH. In addition to reducing its corrosivity, this can promote formation of a quasi-protective corrosion product layer. If aqueous saturation with respect to FeCO_3 reaches a level of one or higher, FeCO_3 crystals have the potential to nucleate and grow. This precipitation process leads to protection of the steel from further corrosion due to mass transfer limitations governed by the formation of the corrosion product layer.

Formation of the FeCO_3 layer, and observed corrosion phenomena, depend on the water condensation rate. At higher condensation rates, supersaturation with respect to FeCO_3 cannot be reached and the steel suffers from higher corrosion rates, and *vice*

versa. At longer durations, since the uniform corrosion rate is low, the local presence of fresh, acidified droplets of condensed water on the surface will lead to a surface pH of 3.5 to 4.0. This creates an unsaturated condition with respect to FeCO_3 . If this happens adjacent to FeCO_3 the corrosion product layer will dissolve; the pH required to maintain saturation is in the range of 5.5 to 6.0. Thus, dissolution of the FeCO_3 layer would expose the bare steel surface to the acidic condition of condensed water and lead to localized corrosion. This summarizes the TLC mechanism for localized corrosion in sweet environment, as paraphrased by the author of this dissertation. Model descriptions for marginally and highly sour environments, explained in the next sections, have the sweet TLC mechanism as their foundation.

6.2 TLC Corrosion Mechanisms in Marginally Sour Environments

Based on the previously discussed experimental data, see section 5.1, localized corrosion was observed in marginally sour environments with 0.015 to 0.03 mbar H_2S . At higher partial pressure of H_2S , 0.08 and 0.15 mbar, only low general corrosion rates were determined. Thus, in this chapter, a detailed descriptive model which describes the localized corrosion mechanism at low H_2S partial pressure (0.015-0.03 mbar) is proposed.

6.2.1 Basis of Localized Corrosion Mechanism in Marginally Sour Environments

In most descriptions of localized corrosion mechanisms, pitting occurs under a corrosion product layer that confers partial coverage to the steel surface. With no layer or

full coverage on the steel surface, no localized corrosion is observed. Work done by Sun and Nesic [62], which studied different partial pressures of CO_2 and pH in a series of flow loop experiments, verified pitting occurrence under a corrosion product layer that conferred partial coverage. The concept of scaling tendency (ST), mentioned previously in equation (35), was also introduced to evaluate the possibility of occurrence of localized corrosion; scaling tendency is based on the ratio between scaling formation rate (SFR) and corrosion rate (CR), where the SFR values are based on the precipitation rate calculated from FeCO_3 formation. Furthermore, localized corrosion itself is a complicated and potentially stochastic process [63]–[67]. One of the mechanistic steps which leads to localized corrosion is believed to be the breakdown of an initial passive layer that formed on the steel surface [68]. Work done by Pots, *et al.*, [69], proposed a two dimensional (2-D) stochastic algorithm to simulate the morphology of localized corrosion. The basic mechanism for this model is based on the assumption that localized corrosion attack is dependent on the balance of two processes, corrosion which leads to loss of metal and precipitation which confers metal protection. In this model the scaling tendency parameter is also used; if the scaling tendency is high (which means the precipitation rate exceeds the corrosion rate), the steel is protected by a uniform corrosion product layer. This leads to a reduction in the corrosion rate. However, if the corrosion rate is higher than the precipitation rate, which means low scaling tendency, a protective corrosion product could not form due to there being a high corrosion rate underneath the corrosion product layer. This is termed undermining corrosion, where its rate is faster than the precipitation rate to form a protective layer. Based on this initial model of

localized corrosion by Pots, *et al.*, which only used scaling tendency as an input parameter, work done by Xiao and Netic [63][70] incorporated temperature, pH, partial pressure of CO₂, velocity, etc., for the prediction of localized corrosion

This localized corrosion model has been validated only in sweet environments; it was not validated in sour environments where the presence of an FeS layer is possible. However, with regards to the descriptive model proposed for TLC in marginally sour environments, this is underpinned by the scaling tendency as applied as a general parameter for corrosion product layer types (FeS or FeCO₃).

6.2.2 *Descriptive Model for TLC in Marginally Sour Environments*

The following narrative is proposed to explain the TLC mechanism in marginally sour environments, which includes the occurrence of localized corrosion at low H₂S partial pressure (0.015-0.03 mbar) and low general TLC rate without any localized corrosion at higher H₂S partial pressure (0.08-0.15 mbar). Key points are as follows:

- 1) As mentioned previously, in sweet environments, initially, TLC will be uniform and mainly depends on the water condensation rate. The occurrence of localized corrosion could only be seen at longer durations.
- 2) In marginally sour TLC with the presence of small amount of H₂S, in this case 0.015 to 0.03 mbar, the first drop of water condensing on the steel surface would lead to the formation of very thin FeS layer. FeS would form more rapidly as compared to FeCO₃, due to its fast kinetics of formation. This has been observed in many open literature papers. The formation of this thin FeS layer is proposed to

be by a fast reaction, where H_2S directly reacts with the steel surface to form an FeS layer. The assumption is supported by the visibility of the polishing marks on the FeS layer.

- 3) The presence of this thin FeS layer is not fully protective. High corrosion rates underneath the FeS layer (undermining corrosion) could still happen, which leads to FeS layer failure at random locations on the steel surface; this is a stochastic contribution. Thus, the steel surface becomes segregated in accordance with areas which are protected by the FeS layer and areas which are exposed to corrosion. This leads to pitting, as shown in Figure 87 and Figure 88.

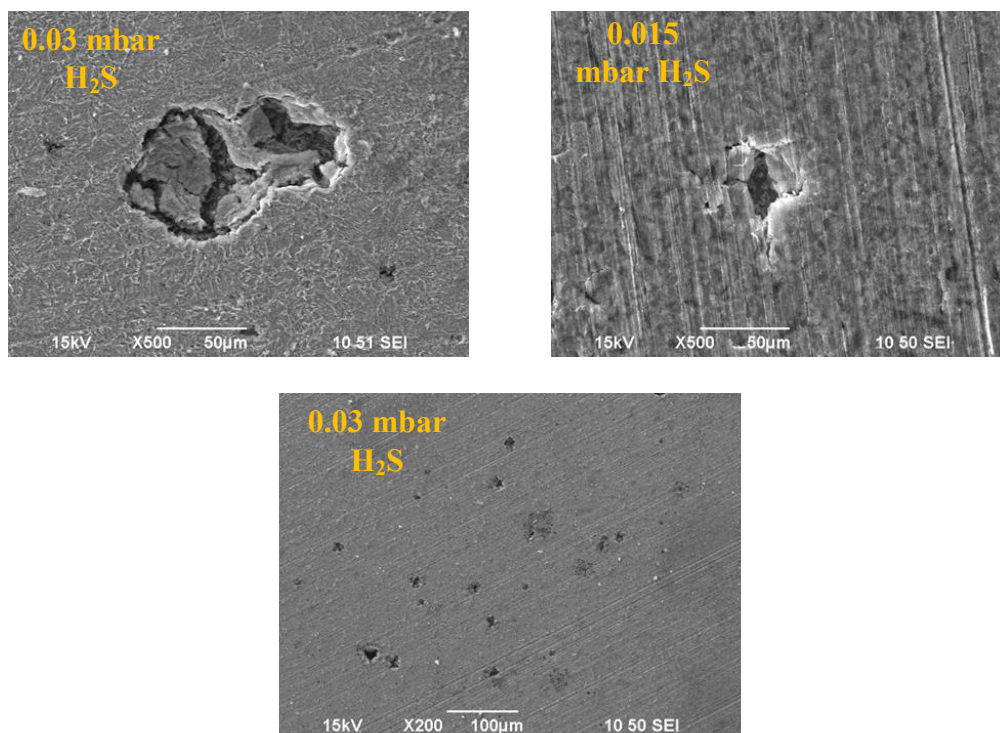


Figure 87: SEM images of the breakdown of the FeS layer due to undermining corrosion at 0.015 and 0.03 mbar H_2S , $T_{\text{gas}} = 40^\circ\text{C}$)

- 4) The undermining corrosion rate is very high as compared to the precipitation rate. This means that at a low scaling tendency, a protective corrosion product layer could not form due to the high corrosion rate underneath the layer. In other words, a protective FeS layer could not form since the FeS layer can only precipitate onto a corroding steel surface at a rate which is much lower than the corrosion rate. The corrosion rate, scale formation rate, and scaling tendency were calculated and explained previously in Figure 23.

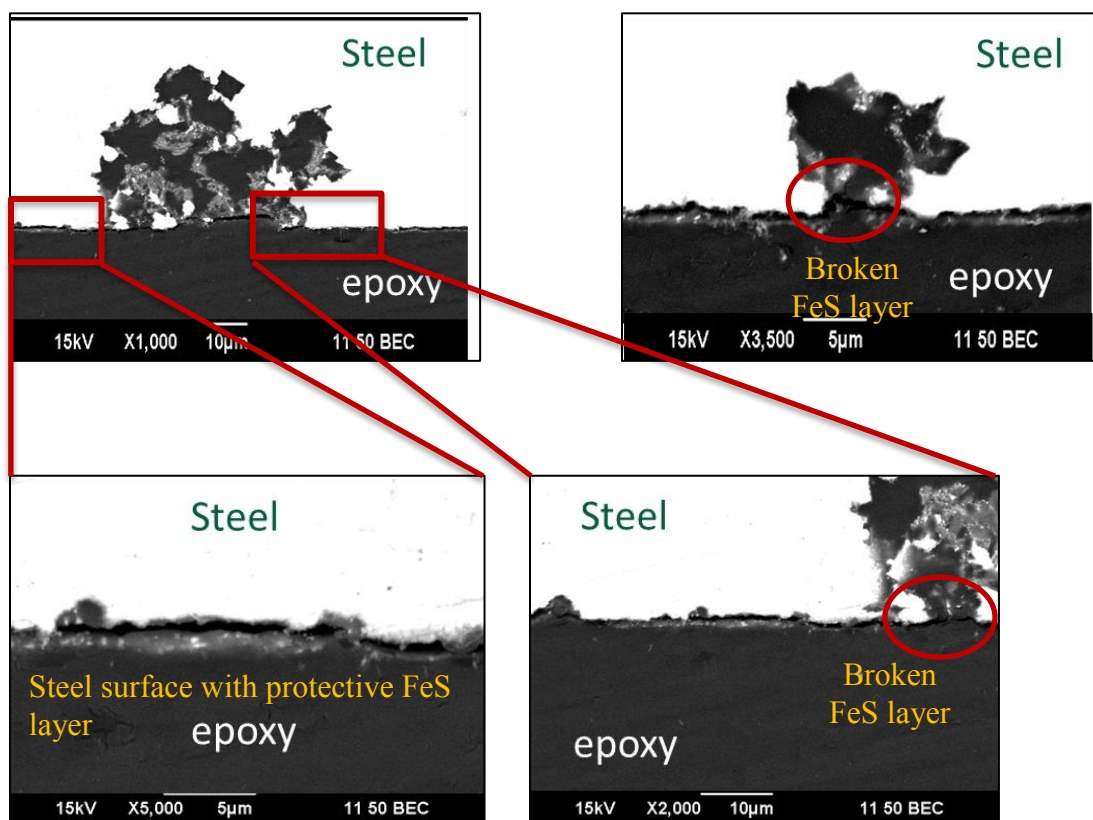


Figure 88: SEM cross-section images of the breakdown of the FeS layer due to undermining corrosion at 0.015 and 0.03 mbar H_2S , $T_{gas} = 40^\circ C$)

- 5) The concentration of H_2S near the steel surface is depleted since most of the available H_2S is consumed in step with the high rate of ferrous ion dissolution from the undermining corrosion. The depletion of H_2S near the steel surface is proposed to be the factor of low scaling tendency to form a protective FeS layer.
- 6) By comparing the measured concentration of ferrous ions in the condensed water and the supersaturation level of FeS as shown in Figure 27 and Figure 31, respectively, at 0.015 and 0.03 mbar H_2S , both the ferrous ion concentration and FeS supersaturation continue increasing until the end of the experimental duration. This is an indication that the condition near the steel surface is always under saturated with respect to FeS , since no significant precipitation of an FeS layer occurred. At this point only a thin FeS layer, which formed by direct H_2S reaction with the steel, is observed. Images from the SEM analysis also support the behavior, as shown in Figure 36 and Figure 37.
- 7) As the H_2S concentration is increased to 0.08 and then 0.15 mbar, the scaling tendency also increased, which showed an increase in precipitation rate of the FeS layer. This is consistent with there being greater availability of H_2S near the steel surface. Increased precipitation (rate) of FeS would provide more protection to the steel from the undermining corrosion, hence retarding the localized corrosion.
- 8) Based on the ferrous ion concentration and FeS supersaturation level as shown in Figure 27 and Figure 31, respectively, the supersaturation level of FeS reached a value of one between day 3 and day 4 and was reduced thereafter. This shows that precipitation occurred on the steel surface at that point. SEM images, as shown in

Figure 89 and Figure 90, support the result where multiple FeS layers are formed on the steel surface.

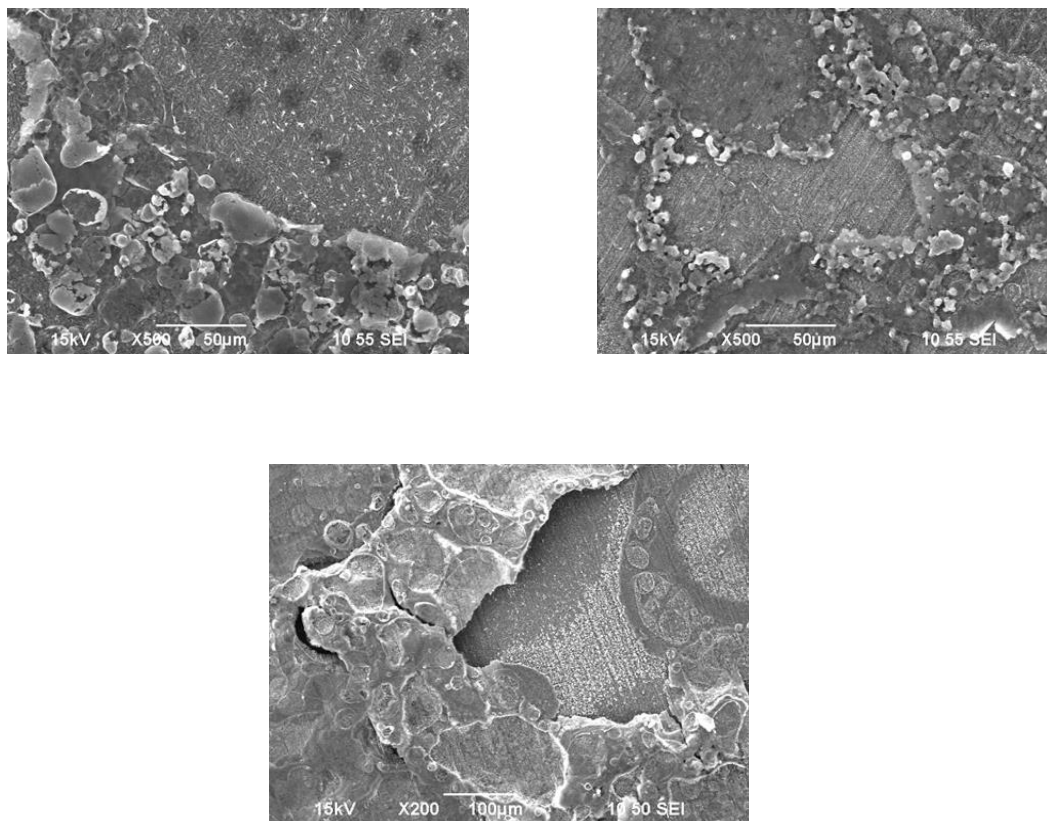


Figure 89: SEM images of multiple layers of FeS by precipitation at 0.08 and 0.15 mbar H_2S , $T_{\text{gas}} = 40^\circ\text{C}$)

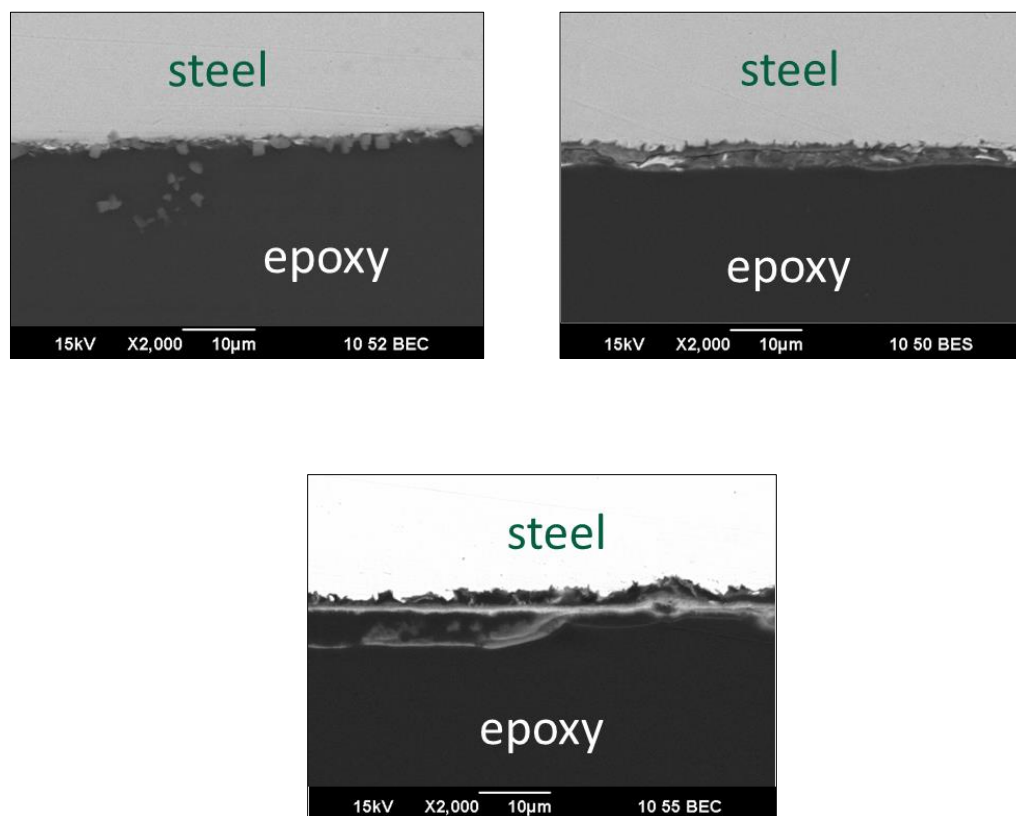


Figure 90: Cross-section SEM images of multiple layer of FeS by precipitation at 0.08 and 0.15 mbar H_2S , $T_{gas} = 40^\circ C$)

- 9) An increase of H_2S concentration would reduce the pH of condensed water, since any ferrous ions which are released from the steel surface into the condensed water will be consumed by H_2S to form an FeS layer. An increase in the concentration of H_2S in condensed water would reduce the localized corrosion rate, since the steel surface is fully covered as enough H_2S is present, especially near the steel surface.

6.2.3 Descriptive Model for the Effect of Exposure Time on Localized Corrosion in Marginally Sour TLC

Based on the experimental results explained previously, the following key points explain the mechanism related to the effect of exposure time on the onset of localized corrosion at low H_2S partial pressure (0.015-0.03 mbar).

- 1) As mentioned before, the formation of an FeS layer on the steel surface occurs *via* a direct reaction that occurs almost instantaneously. The formation of pits can be observed at as early as 3 days due to the high rate of undermining corrosion, which leads to FeS breakdown in random areas on the steel surface, as shown in Figure 91 and Figure 92.

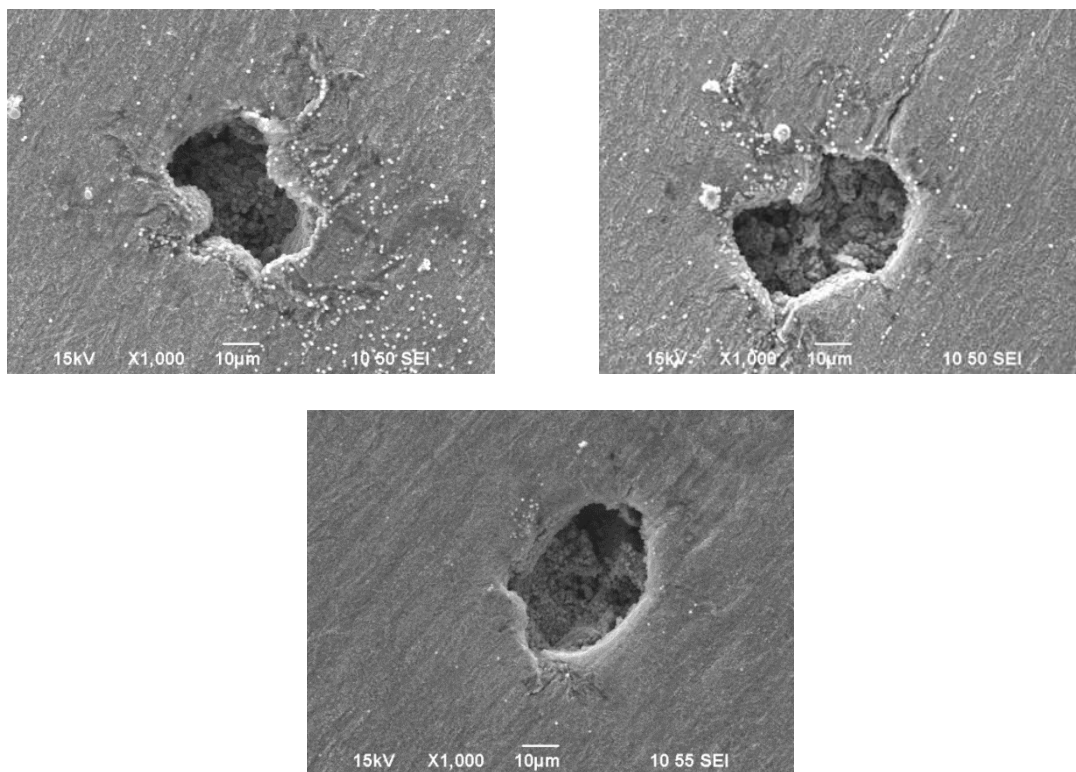


Figure 91: SEM images of FeS failure at 0.03 mbar H_2S , $T_{gas} = 40^\circ C$, 3 days duration

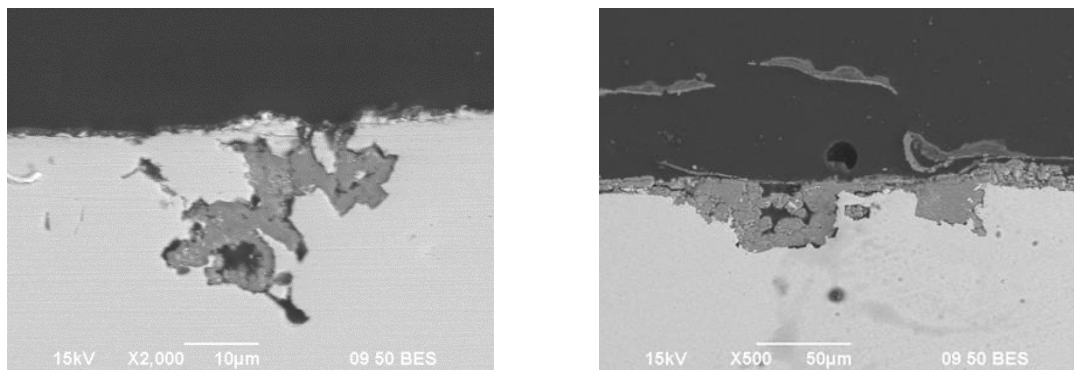


Figure 92: Cross-section SEM images for FeS failure at 0.03 mbar H₂S, T_{gas} = 40°C, 3 days duration

- 2) As the exposure time is increased to 7 days, localized corrosion was still observed but at a higher rate. FeS layer breakdown at random locations due to undermining corrosion was observed, which led to localized corrosion. This mechanism has been explained in detail in the previous section.

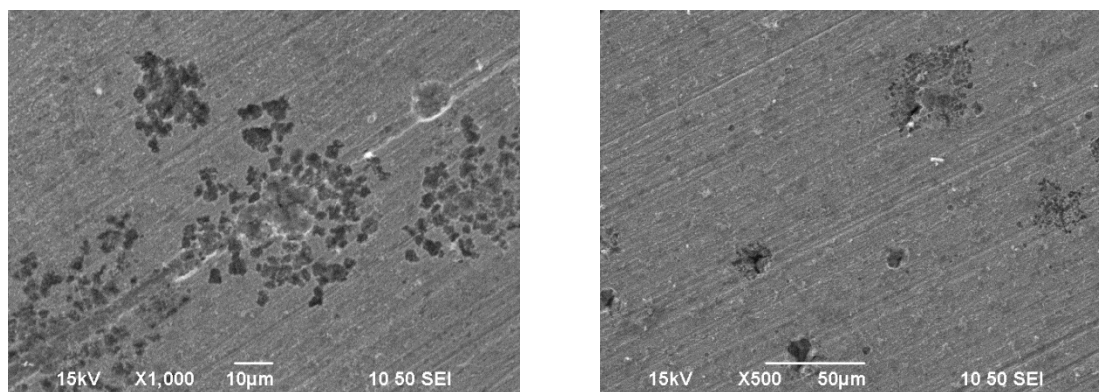


Figure 93: SEM images of FeS failure at 0.03 mbar H₂S, T_{gas} = 40°C, 7 days duration

- 3) However, when the exposure time is increased to 28 days, the existing pits that were formed initially, „disappeared“. This behavior has been previously explained where the pits were not sustained and stopped growing. At longer duration, the water chemistry inside the pits changes with time due to formation of the FeS

layer. This creates a barrier inside the pits which lowers the diffusion rate of corrosive species and ferrous ions. At the same time, since the undermining corrosion rate is high, the uniform corrosion reduces the thickness of the steel and eliminates the existing pits which were initially formed. The initial FeS layer which was formed by direct reaction can still be seen, since the polishing marks were still observed. The initial FeS layer is also shown in the cross-section images (Figure 94), which also shows the corrosion beneath the layer. The comparison of the cross-section images at 3, 7, and 28 days are shown in Figure 74, which explains the elimination of pitting due to undermining corrosion.

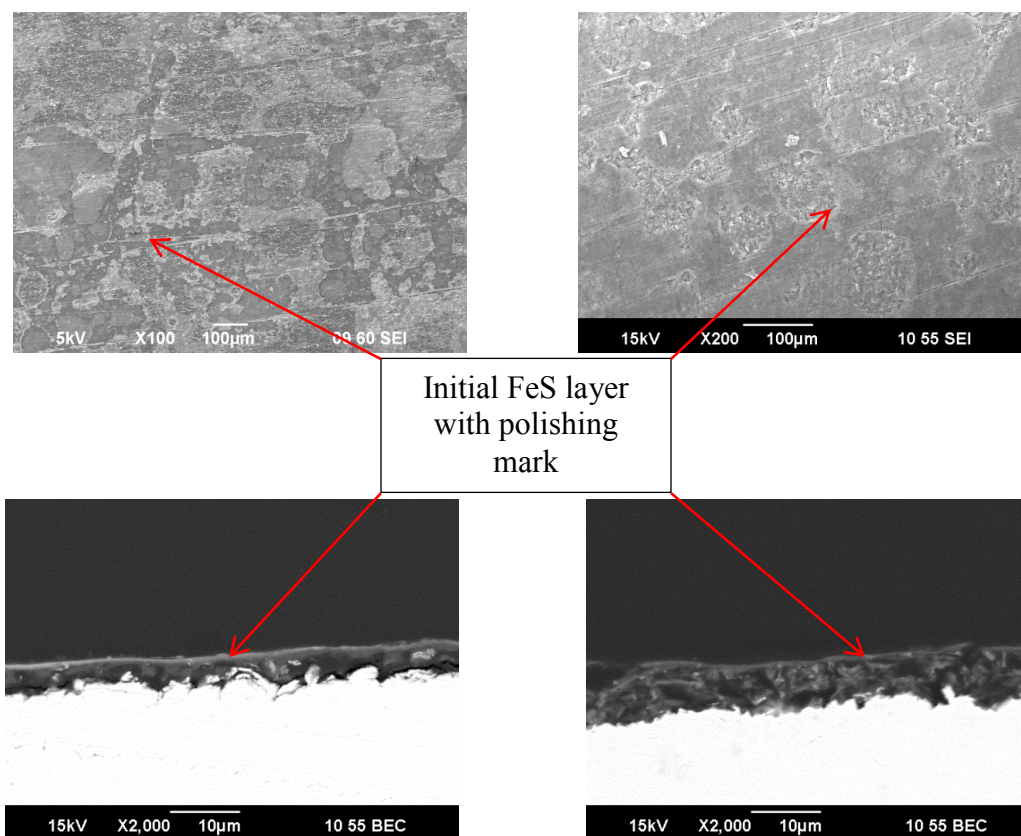


Figure 94: Top view and cross-section images of initial FeS layer by SEM at 0.03 mbar H_2S , $T_{gas} = 40^\circ C$, 28 days duration

6.3 TLC Corrosion Mechanism in Highly Sour Environments

Based on the experimental data previously described in section 5.2, TLC rates in highly sour environments are mainly dependent on the steel temperature through the formation of dense and protective FeS layers, regardless of water condensation rates. Thus, in this chapter, a descriptive model of the highly sour TLC mechanism is proposed.

The following key points are proposed to explain the TLC mechanism in highly sour environments:

- 1) The first drop of water condensing on the steel surface will lead to growth of an FeS layer, due to its faster formation kinetics compared to FeCO_3 .
- 2) The physical properties of the FeS layer formed on the steel surface (dense or porous) are dependent on temperature. If the steel temperature is greater than 30°C , at higher gas temperature, the first and second FeS layers that formed are more coherent (dense); this protects the steel from corrosion as shown in the cross-section images in Figure 95. Fast scale formation rates overwhelm possible undermining corrosion, and significantly reduce the TLC rate.

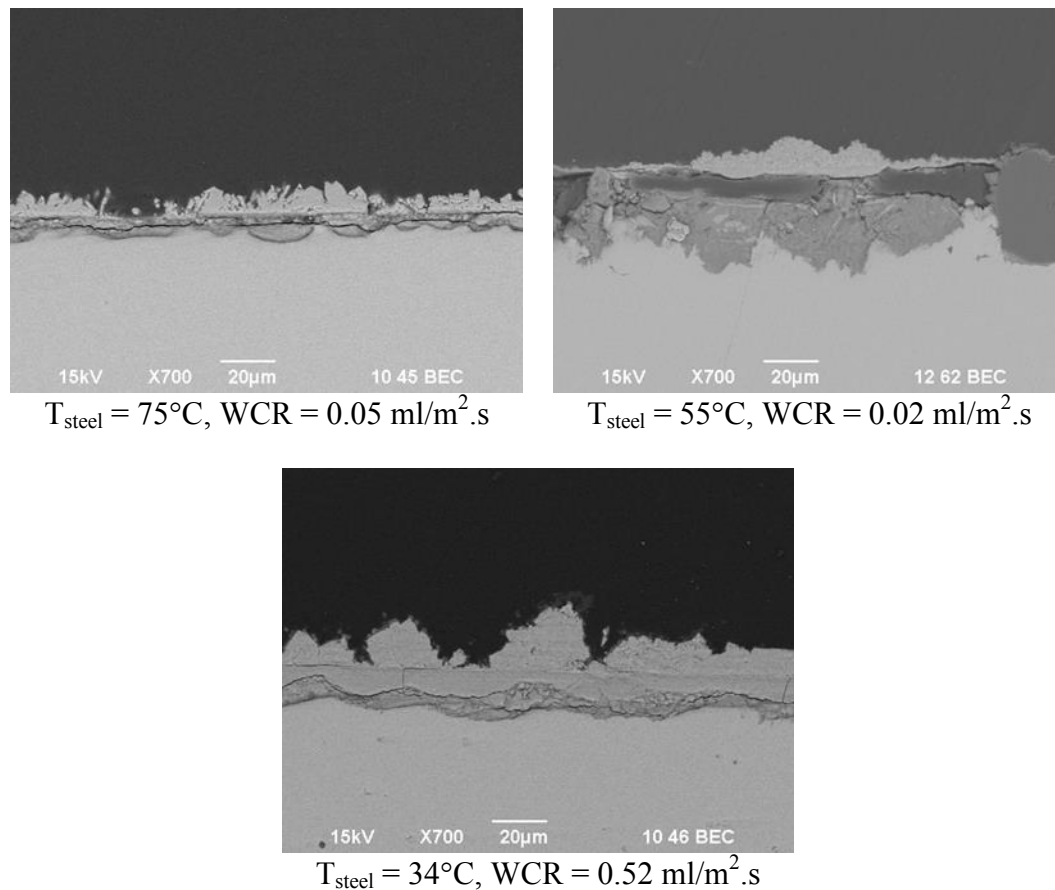


Figure 95: Cross section images of first and second FeS layer by SEM at T_{steel} more than 30°C , $\text{pH}_2\text{S} = 2 \text{ bar}$, $\text{pCO}_2 = 10 \text{ bar}$, 21 days duration

- 3) If the steel temperature is less than 30°C , the FeS layer which forms is porous and not protective (Figure 96). The highly porous second FeS layer, which formed by precipitation, is not protective and does not overcome undermining corrosion; H_2S can diffuse through to the steel surface and accelerate corrosion. This TLC rate with the effect of steel temperature has been explained in detail, as shown in Figure 75.

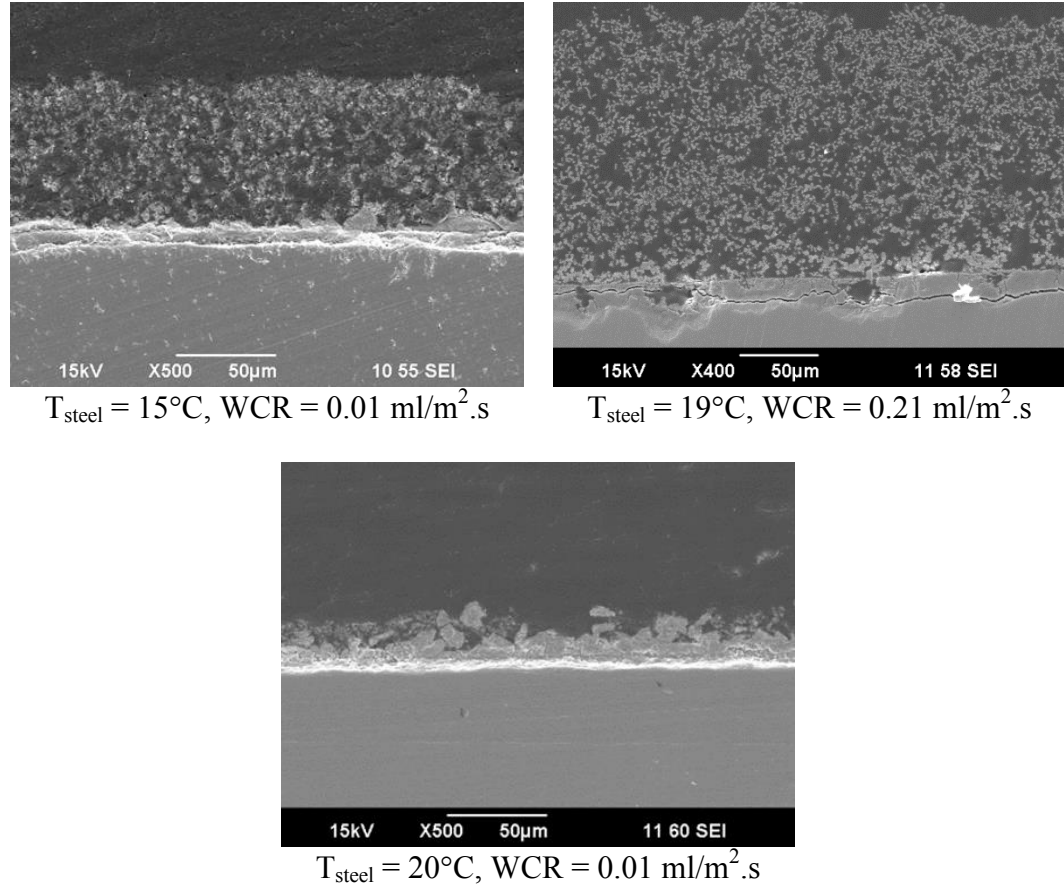
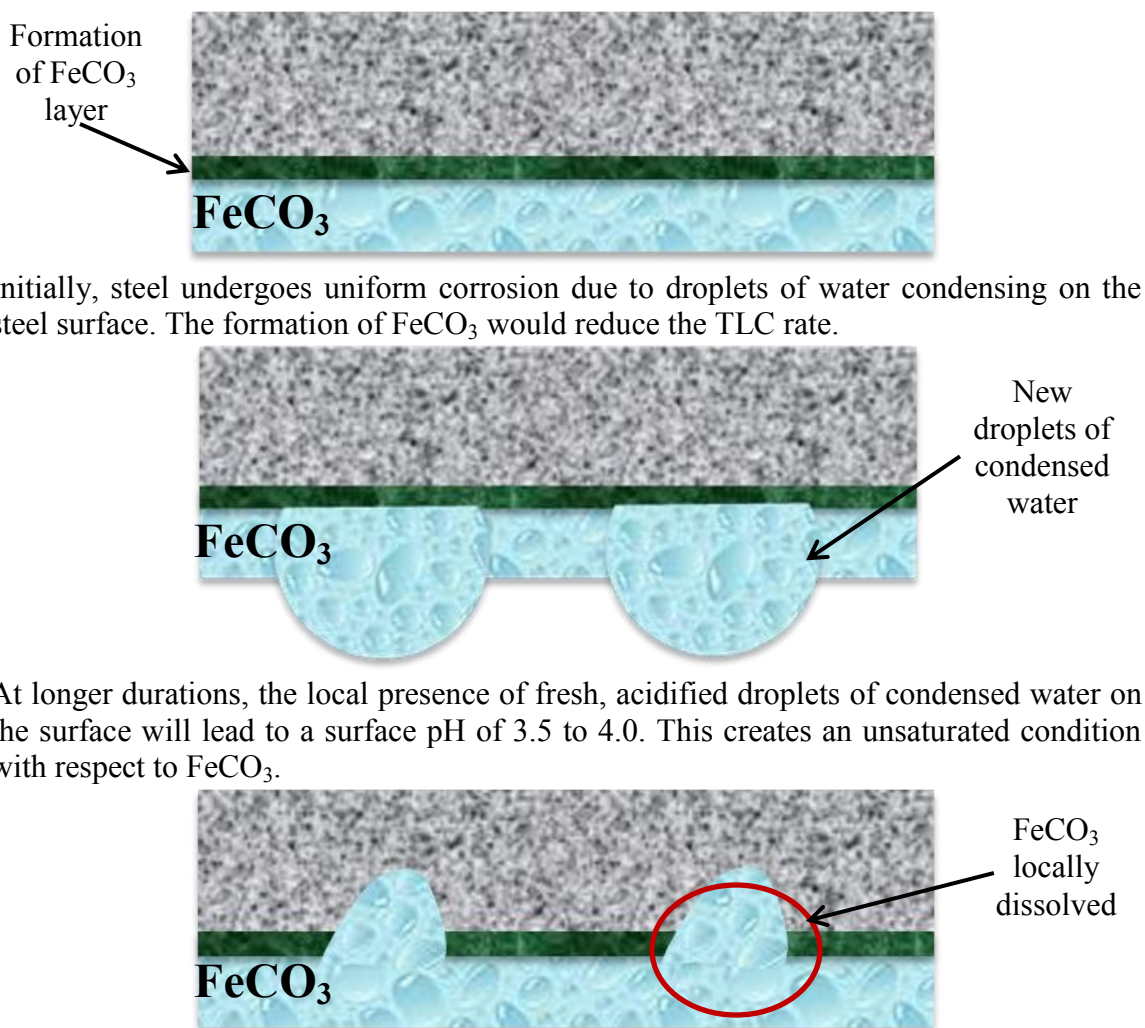


Figure 96: Cross section images of first and second FeS layer by SEM at T_{steel} less than 30°C , $p_{\text{H}_2\text{S}} = 2 \text{ bar}$, $p_{\text{CO}_2} = 10 \text{ bar}$, 21 days duration

- 4) Since the FeS layer is only sparingly soluble in water and FeS formation occurs almost instantaneously at the metal surface, the water condensation rate is not the main parameter which controls the protectiveness of the FeS layer, as it has no clear effect on TLC rate (as shown in Figure 76).
- 5) Thus, it is proposed that the water condensation rate acts as the second parameter which controls the TLC rate, where at higher condensation rates more water droplet formation occurs on the steel surface. This lowers the steel temperature and, paradoxically, leads to higher TLC rates and *vice versa*.

6.4 Overall Schematic of TLC Behavior in CO₂/H₂S Environments

Based on the key points explained previously for the TLC mechanisms, the following schematics are proposed to describe its behavior. The schematics include TLC behavior in sweet, marginally sour, and highly sour environments.

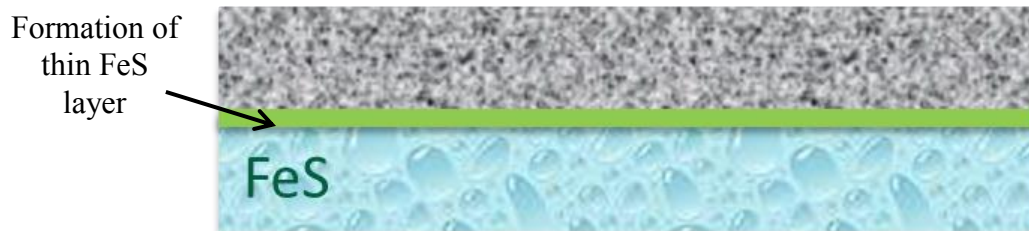


Initially, steel undergoes uniform corrosion due to droplets of water condensing on the steel surface. The formation of FeCO_3 would reduce the TLC rate.

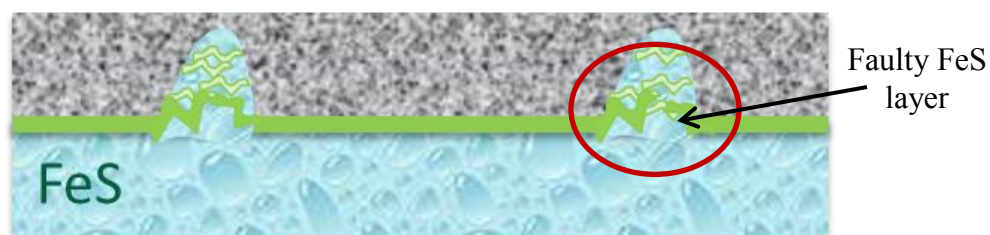
At longer durations, the local presence of fresh, acidified droplets of condensed water on the surface will lead to a surface pH of 3.5 to 4.0. This creates an unsaturated condition with respect to FeCO_3 .

If this happens adjacent to FeCO_3 the corrosion product layer will dissolve; the pH required to maintain FeCO_3 saturation is in the range of 5.5 to 6.0. Dissolution of the FeCO_3 layer would expose the bare steel surface to the acidic conditions of the condensed water and lead to localized corrosion.

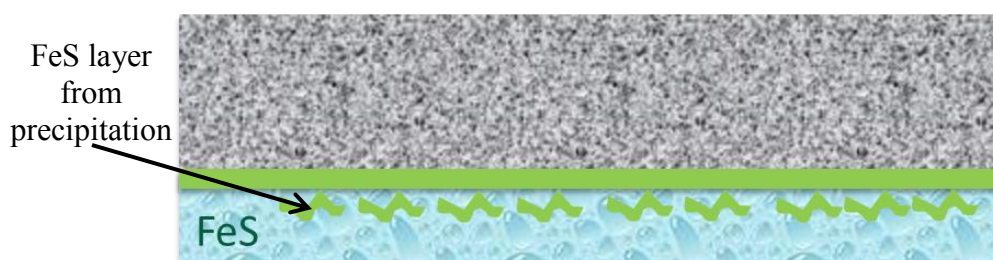
Figure 97: Localized corrosion schematic of TLC mechanism in sweet environments



Initial thin FeS layer formed instantaneously on the steel surface *via* direct H₂S reaction with the steel.

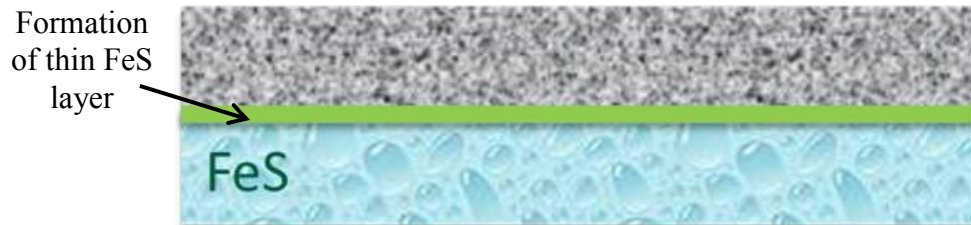


At low H₂S concentration (0.015-0.03 mbar), the thin FeS layer is not protective. Undermining corrosion leads to FeS layer failure at random locations on the steel surface. This results in localized corrosion.

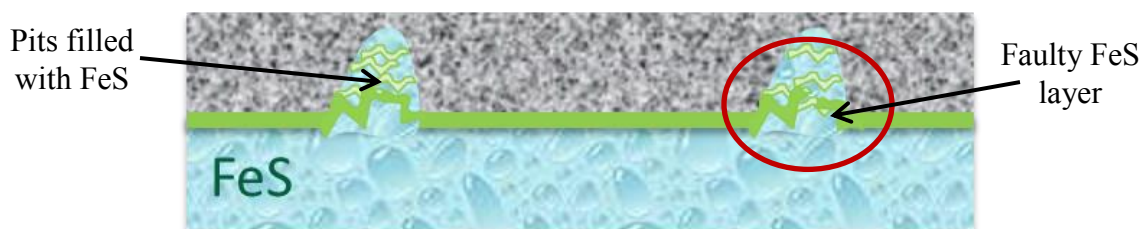


At higher H₂S partial pressure (0.08-0.15 mbar), thicker and more protective FeS layers are formed due to there being more H₂S available near the steel surface. The scaling tendency increases, which overcomes the undermining corrosion rate. There is no FeS failure; FeS precipitates on the steel surface which reduces the TLC rate.

Figure 98: Localized corrosion schematic of TLC mechanism in marginally sour environments



Initially, a thin FeS layer formed instantaneously on the steel surface *via* direct H₂S reaction with the steel

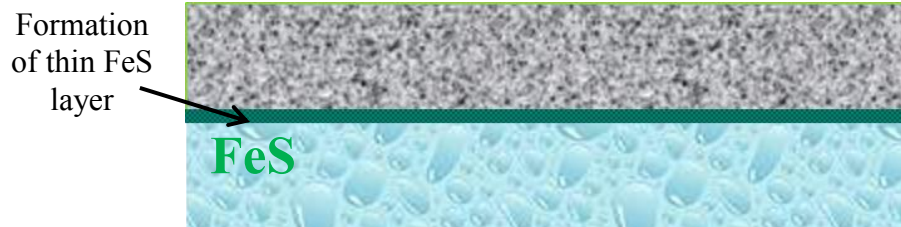


At low H₂S partial pressure (0.015-0.03 mbar), the thin FeS layer is not protective. The undermining corrosion leads to FeS layer failure at random places on the steel surface which results in localized corrosion. As the exposure time increases, the pits are filled with an FeS layer which stops their growth

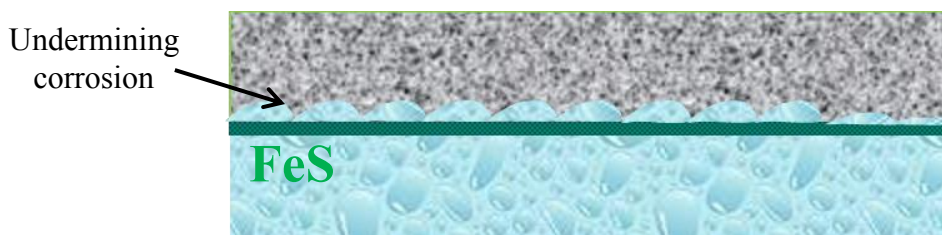


The undermining corrosion reduces the thickness of the steel and eliminates the initial pits which were formed

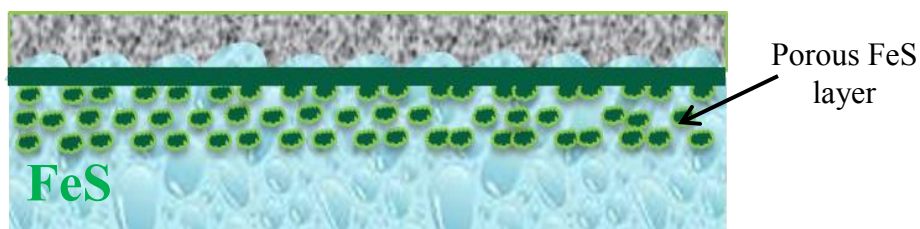
Figure 99: Localized corrosion schematic of TLC mechanism in marginally sour environments; effect of exposure time



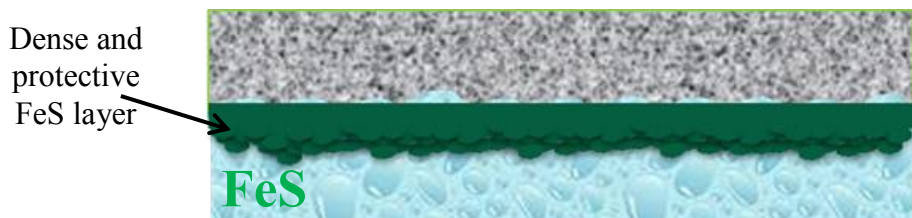
Initially, thin FeS layers are formed instantaneously on the steel surface *via* direct reaction of H_2S with the steel



Generated FeS layers are not protective, which causes undermining corrosion beneath the FeS layer



Due to low steel temperature, the second FeS layer which formed by precipitation is porous and not sufficiently protective to reduce the TLC rate



At higher steel temperature, the second FeS layer formed is dense and protective, which overcomes undermining corrosion and reduces the TLC rate.

Figure 100: Schematics for TLC mechanism in highly sour environments

6.5 Summary of TLC Descriptive Model in CO₂/H₂S Environments

Based on the experimental results and analysis explained previously for the TLC in both marginally and highly sour environments, the following Table 7 and Table 8 summarized the effect of temperature, water condensation rate and H₂S partial pressure in TLC rate for both marginally and highly sour environments, respectively.

Table 7: Summary of TLC key factors in marginally sour environments

Effect of temperature	0.015 mbar \leq pH ₂ S \leq 0.03 mbar	
	Increase in temperature $40^{\circ}\text{C} \leq T_{\text{gas}} \leq 60^{\circ}\text{C}$ $25^{\circ}\text{C} \leq T_{\text{steel}} \leq 40^{\circ}\text{C}$	Decrease in pit penetration rate $2 \text{ mm/yr} \leq \text{pit penetration rate} \leq 4 \text{ mm/yr}$
Effect of WCR	0.015 mbar \leq pH ₂ S \leq 0.15 mbar	
	Increase in WCR $0.3 \text{ ml/m}^2/\text{s} \leq \text{WCR} \leq 1.6 \text{ ml/m}^2/\text{s}$	Increase in uniform TLC rate $0.3 \text{ mm/yr} \leq \text{uniform TLC rate} \leq 0.7 \text{ mm/yr}$
Effect of pH ₂ S	Increase in pH₂S $0 \text{ mbar} \leq \text{pH}_2\text{S} \leq 0.15 \text{ mbar}$	Decrease in uniform TLC rate $0.16 \text{ mm/yr} \leq \text{uniform TLC rate} \leq 0.33 \text{ mm/yr}$ ($T_{\text{gas}} = 40^{\circ}\text{C}$, $T_{\text{steel}} = 25^{\circ}\text{C}$)
		Decrease in uniform TLC rate $0.4 \text{ mm/yr} \leq \text{uniform TLC rate} \leq 1.1 \text{ mm/yr}$ ($T_{\text{gas}} = 60^{\circ}\text{C}$, $T_{\text{steel}} = 40^{\circ}\text{C}$)

Table 8: Summary of TLC key factors in highly sour environments

Effect of temperature	$p_{H_2S} = 2 \text{ bar}$ $p_{CO_2} = 10 \text{ bar}$ $0.01 \text{ ml/m}^2/\text{s} \leq \text{WCR} \leq 0.5 \text{ ml/m}^2/\text{s}$	
	Increase in temperature $T_{\text{steel}} > 30^\circ\text{C}$	Decrease in uniform TLC rate Uniform TLC rate $\leq 0.15 \text{ mm/yr}$
	Decrease in temperature $T_{\text{steel}} < 30^\circ\text{C}$	Increase in uniform TLC rate $0.16 \text{ mm/yr} \leq \text{uniform TLC rate} \leq 0.35 \text{ mm/yr}$
Effect of WCR	No clear effect	
Effect of p_{H_2S}	$0.2 \text{ bar} \leq p_{H_2S} \leq 5 \text{ bar}$ $T_{\text{gas}} = 40^\circ\text{C}$	
	Increase in p_{H_2S} $T_{\text{steel}} > 30^\circ\text{C}$	Decrease in uniform TLC rate $0.08 \text{ mm/yr} \leq \text{uniform TLC rate} \leq 0.25 \text{ mm/yr}$
	$T_{\text{steel}} < 30^\circ\text{C}$	$0.14 \text{ mm/yr} \leq \text{uniform TLC rate} \leq 0.45 \text{ mm/yr}$

CHAPTER 7: CONCLUSIONS AND RECOMMENDATIONS

7.1 Conclusions

7.1.1 TLC Behavior in Marginally Sour Environments

- A non-homogenous FeS surface coverage occurred at low H₂S partial pressure (0.015-0.03 mbar). This led to distinct protected and not protected regions on the steel surface. This resulted in high localized corrosion rates and severe pitting due to undermining corrosion.
- FeS formation could not overcome the undermining corrosion rate (low scaling tendency) since H₂S is depleted near the steel surface as most of the H₂S is consumed by ferrous ions, from the oxidative dissolution process, with subsequent FeS formation inside the pits.
- As the partial pressure of H₂S is increased (0.08-0.15 mbar), no localized corrosion with low TLC rate was observed. This is due to the greater availability of H₂S near the steel surface, which increased the scaling tendency and overcame the undermining corrosion by precipitating more FeS on the steel, protecting the steel from corrosion.
- The onset of localized corrosion at 0.03 mbar H₂S is not sustained, and the pits were eliminated with the increased experimental duration of 28 days. The pits stop growing due to the formation of a protective FeS layer inside the pits. At the same time, the undermining corrosion rate is very high, which reduces the steel thickness and the initial pits which are formed disappear.

7.1.2 *TLC Behavior in Highly Sour Environments*[53]

- The main parameter which controls TLC behavior in highly sour environments is the gas/steel temperature; water condensation rate acts as a secondary effect.
- The TLC rates are reduced with increasing steel temperature through the formation of more coherent FeS layers, which conferred greater protectiveness at higher steel temperature, regardless of the water condensation rate.
- A very dense and thin FeS layer was always present on the metal surface. In some conditions, such as low temperature with a high water condensation rate, a second thicker, but more porous outer layer was observed.
- Mackinawite and cubic FeS were identified in the corrosion product layer at the top of the line in most of the conditions tested, while troilite was only observed at higher temperature (gas temperature of 80°C and steel temperature 75°C).
- Water condensation rate did not have a strong effect on the TLC rate. Consequently, it is believed that the primary effect of water condensate is to lower the steel temperature.

7.1.3 *TLC Descriptive Model in CO₂/H₂S Environments*

- A descriptive model which explained the TLC behavior in CO₂/H₂S environments in marginally and highly sour environments was developed in this work in order to understand the corrosion mechanism under both conditions.

- The TLC descriptive model in marginally sour environments is based on the scaling tendency, which mainly explained the occurrence of localized corrosion at low H₂S partial pressure.
- The TLC descriptive model in highly sour environments is based on the formation of dense and protective FeS layers at higher gas/steel temperature, regardless of the condensation rates.

7.2 Recommendations for Future Research

Suggestions for future research are provided below.

- In marginally sour environments, the present experimental work was done only at two values of water condensation rate (WCR), 0.25 and 1.5 ml/m².s. Thus, the localized corrosion mechanism could be further verified at lower WCR and temperature.
- The verification of corrosion product layer identity in marginally sour TLC should be further analyzed using XRD or transmission electron microscopy (TEM) since, at this condition, both FeCO₃ and FeS could form.
- The localized corrosion mechanism in marginally sour TLC was based on the existing localized corrosion model which was developed using the scaling tendency of FeCO₃ as the main parameter. Thus, in H₂S environments, in the future, the localized corrosion model based on the scaling tendency of the FeS layer should be developed first and used instead.

- The water chemistry for the condensed water in both marginally and highly sour environments should be studied and modeled further, at various condensation rates in terms of species mass transfer, so that conditions near the steel surface could be calculated and predicted, which would more accurately represent the TLC process.

REFERENCES

- [1] R. Heidersbach, *Metallurgy and Corrosion Control in Oil and Gas Production*. New Jersey: John Wiley and Sons, 2011.
- [2] S. D. Kapusta, B. Pots, and R. Connell, “Corrosion Management of Wet Gas Pipelines,” in *Proc. Corrosion*, Houston, TX, 1999, paper no. 99045.
- [3] S. L. Asher, R. Ojifinni, C. Li, S. Ling, W. Sun, J. L. Pacheco, and J. Nelson, “Top of the Line Corrosion Prediction in Wet Gas Pipelines,” in *Proc. Corrosion*, Houston, TX, 2012, paper no. C2012-0001303.
- [4] D. Hinkson, M. Singer, Z. Zhang, and S. Nestic, “A Study of the Chemical Composition and Corrosivity of the Condensate in Top of the Line Corrosion,” in *Proc. Corrosion*, Houston, TX, 2008, paper no. 08466.
- [5] Y. M. Gunaltun and D. Larrey, “Correlation of Cases of Top of Line Corrosion with Calculated Water Condensation Rates,” in *Proc. Corrosion*, Houston, TX, 2000, paper no. 00071.
- [6] S. Olsen and A. Dugstad, “Corrosion Under Dewing Conditions,” in *Proc. Corrosion*, Houston, TX, 1991, paper no. 472.
- [7] B. Pots and E. Hendriksen, “CO₂ Corrosion Under Scaling Conditions-The Special Cases of Top-Of-The-Line-Corrosion in Wet Gas Pipelines,” in *Proc. Corrosion*, Houston, TX, 2000, paper no. 00031.
- [8] Z. Zhang, D. Hinkson, M. Singer, H. Wang, and S. Nestic, “A Mechanistic Model of Top-of-the-Line Corrosion,” vol. 63, no. 11, pp. 1051–1062, 2007.

- [9] F. Vitse, S. Nestic, Y. Gunaltun, D. Larrey, and P. Duchet-Sucaux, "Mechanistic Model for the Prediction of Top-of-the-Line Corrosion Risk," in *Proc. Corrosion*, Houston, TX, 2003, Paper no 3633.
- [10] R. Nyborg and A. Dugstad, "Top of Line Corrosion and water Condensation Rates in Wet Gas Pipelines," in *Proc. Corrosion*, Houston, TX, 2007, paper no. 07555.
- [11] M. Singer, S. Nestic, and J. Al-Khamis, "Corrosion Assessment in Karan Gas Field Development," in *Proc. Corrosion*, Houston, TX, 2012, paper no. C2012-0001411.
- [12] A. Camacho, M. Singer, B. Brown, and S. Nestic, "Top of the Line Corrosion in H₂S/CO₂ Environments," in *Proc. Corrosion*, Houston, TX, 2008, paper no. 08470.
- [13] I. H. Omar, Y. M. Gunaltun, J. Kvarekval, and A. Dugstad, "H₂S Corrosion of Carbon Steel Under Simulated Kashagan Field Conditions," in *Proc. Corrosion*, Houston, TX, 2005, paper no. 05300.
- [14] C. Li, W. Sun, S. Ling, and J. L. Pacheco, "Experimental Study of Top of Line Corrosion in Slightly Sour Environments," in *Proc. Corrosion*, Houston, TX, 2012, paper no. C2012-0001306.
- [15] R. Nyborg, A. Dugstad, and T. G. M. Ret, "Top of Line Corrosion with High CO₂ and Traces of H₂S," in *Proc. Corrosion*, Houston, TX, 2009, paper no. 09283.
- [16] J. Kvarekval, R. Nyborg, and H. Choi, "Formation of Multilayer Iron Sulfide Film During High Temperature CO₂/H₂S Corrosion of Carbon Steel," in *Proc. Corrosion*, Houston, TX, 2003, paper no. 03339.

- [17] S. Netic, J. Postlethwaite, and S. Olsen, "An Electrochemical Model for Prediction of Corrosion of Mild Steel in Aqueous Carbon Dioxide Solutions," *Corros. Sci.*, vol. 52, no. 4, pp. 280–294, 1996.
- [18] Y. Kharaka, W. Gunter, P. Aggarwal, E. Perkins, and J. Dedraal, "SOLMINEQ.88: A Computer Program for Geochemical Modeling of Water-Rock Interactions," Alberta Research Council, Menlo Park, CA, U.S. Geological Survey 88-4227, 1998.
- [19] J. Oddo and M. Tomson, "Simplified Calculation of CaCO_3 Saturation at High Temperatures and Pressures in Brine Solutions," *J. Pet. Technol.*, vol. 34, no. 7, pp. 1583–1590, 1982.
- [20] D. Palmer and R. Van Eldik, "The Chemistry of Metal Carbonate and Carbon Dioxide Complexes," *Chem. Rev.*, vol. 83, no. 6, pp. 651–731, 1983.
- [21] O. Suleimenov and R. Krupp, "Solubility of Hydrogen Sulfide in Pure Water and in NaCl Solutions, from 20 to 320C and at Saturation Pressures," *Geochim. Cosmochim. Acta*, vol. 58, no. 11, pp. 2433–2444, 1994.
- [22] J. Greenberg and M. Tomson, "Precipitation and Dissolution Kinetics and Equilibria of Aqueous Ferrous Carbonate vs. Temperature," *Appl. Geochemistry*, vol. 7, pp. 185–190, 1992.
- [23] C. Silva, X. Liu, and F. Millero, "Solubility of Siderite (FeCO_3) in NaCl Solutions," *J. Solution Chem.*, vol. 31, pp. 97–108, 2002.

- [24] D. W. Shoesmith, P. Taylor, and M. Grant, "The Formation of Ferrous Monosulfide Polymorphs during the Corrosion of Iron by Aqueous Hydrogen Sulfide at 21°C," *J. Electrochem. Soc.*, vol. 127, no. 5, pp. 1007–1015, 1980.
- [25] S. N. Smith and J. L. Pacheco, "Prediction of Corrosion in Slightly Sour Environments," in *Proc. Corrosion*, Houston, TX, 2002, paper no. 02241.
- [26] L. G. Benning, R. T. Wilkin, and H. L. Barnes, "Reaction Pathways in the Fe–S System Below 100°C," *Chem. Geol.*, vol. 167, pp. 25–51, 2000.
- [27] J. Smith and J. Miller, "Nature of Sulfides and Their Corrosive Effect on Ferrous Metals: A Review," *Br. Corros. J.*, vol. 10, no. 3, pp. 136–143, 1975.
- [28] J. Morse, J. Frank, C. Jeffrey, and D. Rickard, "The Chemistry of the Hydrogen Sulfide and Iron Sulfide Systems in Natural Waters," *Earth-Science Rev.*, vol. 24, pp. 1–42, 1987.
- [29] S. N. Smith, "A Proposed Mechanism for Corrosion in Slightly Sour Oil and Gas Production," in *Proc. Intl. Corrosion Congress*, Houston, TX, 2001, paper no. 01304.
- [30] J. Ning, Y. Zheng, D. Young, B. Brown, and S. Nešić, "A Thermodynamic Study of Hydrogen Sulfide Corrosion of Mild Steel," *Proc. Corros.* Houston, TX, 2013, paper. no. 2462.
- [31] W. Sun, S. Nesic, and S. Papavinasam, "Kinetics of Iron Sulfide and Mixed Iron Sulfide/Carbonate Scale Precipitation in CO₂/H₂S Corrosion," in *Proc. Corrosion*, Houston, TX, 2006, paper no. 06644.

- [32] W. Sun and S. Nesic, "A Mechanistic Model of H₂S Corrosion of Mild Steel," in *Proc. Corrosion*, Houston, TX, 2007, paper no. 07655.
- [33] R. Shannon and R. Ross, "Definition of Topotaxy," *Nature*, vol. 202, pp. 1000–1001, 1964.
- [34] F. Lotgering, "Topotactical Reaction with Ferrimagnetic Oxides having Hexagonal Crystal," *J. Org. Nucl. Chem.*, vol. 9, no. 2, pp. 113–123, 1959.
- [35] Y. Zheng, "Electrochemical Mechanism and Model of H₂S Corrosion of Carbon Steel," PhD dissertation, Russ College of Engineering., Dept of Chemical Engineering., Ohio University, May 2015.
- [36] Y. M. Gunaltun and J. Achmad, "Top of Line Corrosion in Multiphase Gas Lines. A Case History," in *Proc. Corrosion*, Houston, TX, 1999, Paper No 36.
- [37] R. Pailassa, M. Dieumegarde, and M. Estavoyer, "Corrosion Control in the Gathering System at Lacq Sour Gas Field," in *Proc. 2nd Intl. Congress of Metallic Corrosion NACE*, New York, 1963, pp. 410-417.
- [38] D. Ho-Chung-Qui, A. Williamson, and P. Eng, "Corrosion Experiences and Inhibition Practices in Wet Sour Gathering Systems," in *Proc. Corrosion*, Houston, TX, 1987, paper no. 46.
- [39] N. Bich and K. Szklarz, "Crossfield Corrosion Experience," in *Proc. Corrosion*, Houston, TX, 1988, paper no. 196.
- [40] M. Singer, "Study and Modeling of the Localized Nature of Top of Line Corrosion," PhD dissertation, Russ College of Engineering., Dept of Chemical Engineering., Ohio University, 2013.

- [41] Y. Gunaltun, R. Piccardino, and D. Vinazza, "Interpretation of MFL and UT Inspection Results in Case of Top of line Corrosion," in *Proc. Corrosion, Houston, TX, 2006*, paper no. 6170.
- [42] D. Pugh, S. Asher, J. Cai, W. Sisak, J. L. Pacheco, F. C. Ibrahim, E. J. Wright, A. Dhokte, S. Venaik, and D. Robson, "Top-of-Line Mechanism for Sour Wet Gas Pipelines," in *Proc. Corrosion, Houston, TX, 2009*, paper no. 09285.
- [43] S. N. Smith, B. Brown, and W. Sun, "Corrosion at Higher H₂S Concentration and Moderate Temperatures," in *Proc. Corrosion, Houston, TX, 2011*, paper no. 11081.
- [44] P. Bai, S. Zheng, H. Zhao, Y. Ding, J. Wu, and C. Chen, "Investigations of the diverse corrosion products on steel in a hydrogen sulfide environment," *Corros. Sci.*, vol. 87, pp. 397–406, Oct. 2014.
- [45] M. Singer, A. Camacho, B. Brown, and S. Netic, "Sour Top of the Line Corrosion in the Presence of Acetic Acid," in *Proc. Corrosion, Houston, TX, 2010*, paper no. 10100.
- [46] A. Dunlop, H. Hassell, and P. Rhodes, "Fundamental Considerations in Sweet Gas Well Corrosion," in *Proc. Corrosion, Houston, TX, 1987*, paper no. 46.
- [47] S. N. Smith, "Discussion of the History and Relevance of the CO₂/H₂S Ratio," in *Proc. Corrosion, Houston, TX, 2011*, paper no. 11065.
- [48] B. Brown and S. Netic, "Aspects of Localized Corrosion in an H₂S/CO₂ Environment," in *Proc. Corrosion, Houston, TX, 2012*, paper no. C2012-0001559.

- [49] S. N. Esmaeely, "CO₂ / H₂S Corrosion at Low Concentration of H₂S," Institute for Corrosion and Multiphase Technology , Ohio Univ., Athens, OH, CCJIP Advisory Board Meeting, Oct. 2013.
- [50] W. Yan, "Effect of Low pH₂S on CO₂ Corrosion of Mild Steel," Institute for Corrosion and Multiphase Technology , Ohio Univ., Athens, OH, CCJIP Advisory Board Meeting, Oct. 2013.
- [51] D. Skoog, D. West, F. Holler, and S. Crouch, *Analytical Chemistry: An Introduction, Chapters 21 and 22*, 7th ed. pp. 547–592.
- [52] ASTM G1-03, "Standard Practice for Preparing, Cleaning and Evaluating Corrosion Test," *ASTM, Philadelphia, PA*, pp. 17–23, 2009.
- [53] N. Yaakob, M. Singer, and D. Young, "Top of the Line Corrosion Behavior in Highly Sour Environments: Effect of the Gas/Steel Temperature," in *Proc. Corrosion*, Houston, TX, 2014, paper no. 3807.
- [54] N. Yaakob, "Study of Top of the Line Corrosion in Marginally Sour Environments," Institute for Corrosion and Multiphase Technology , Ohio Univ., Athens, OH, MTLJIP Advisory Board Meeting, Oct. 2014, Ohio University.
- [55] N. Yaakob, "Experimental Study of Highly Sour Top of the Line Corrosion," Institute for Corrosion and Multiphase Technology , Ohio Univ., Athens, OH, TLJIP Advisory Board Meeting Topical Report, 2012.

- [56] N. Yaakob, "Study of Top of the Line Corrosion in Marginally Sour Environments; (H₂S Concentration 0-30 ppm)," Institute for Corrosion and Multiphase Technology, Ohio Univ., Athens, OH, MTL CJIP Advisory Board Meeting, March. 2014.
- [57] ASTM G46-94, "Standard Guide for Examination and Evaluation of Pitting Corrosion," *ASTM, Philadelphia, PA*, pp. 1–7, 1999.
- [58] W. Sun, "Kinetics of Iron Carbonate and Iron Sulfide Scale Formation in CO₂/H₂S Corrosion," PhD dissertation, Russ College of Engineering., Dept of Chemical Engineering., Ohio University, 2006.
- [59] D. Montgomery, G. Runger, and N. Hubele, *Engineering Statistics*, 4th ed. New Jersey: John Wiley and Sons, 2007.
- [60] S. Netic, "Carbon Dioxide Corrosion of Mild Steel," in *Uhlig's Corrosion Handbook*, 3rd ed., John Wiley and Sons, 2011, pp. 229–246.
- [61] J. Murowchick and H. Barnes, "Formation of Cubic FeS," *Am Mineral.*, vol. 71, pp. 1243–1246, 1986.
- [62] W. Sun and S. Netic, "A Parametric Study and Modelling on Localized CO₂ Corrosion in Horizontal Wet Gas Flow," in *Proc. Corrosion*, Houston, TX, 2000, paper no. 4380.
- [63] S. Netic and Y. Xiao, "A Quasi 2-D Localized Corrosion Model," in *Proc. Corrosion*, Houston, TX, 2004, paper no. 04628.

- [64] D. E. Williams, C. Westcott, and M. Fleischmann, "Stochastic Models of Pitting Corrosion of Stainless Steels: I. Modeling of the Initiation and Growth of Pits at Constant Potential," *J. Electrochem. Soc.*, vol. 132, no. 8, pp. 1796–1804, 1984.
- [65] D. E. Williams, C. Westcott, and M. Fleischmann, "Stochastic Models of Pitting Corrosion of Stainless Steels: II. Measurement and Interpretation of Data at Constant Potential," *J. Electrochem. Soc.*, vol. 132, no. 8, pp. 1804–1811, 1985.
- [66] B. Wu, J. Scully, and J. Hudson, "Cooperative Stochastic Behavior in Localized Corrosion," *J. Electrochem. Soc.*, vol. 144, no. 5, pp. 1614–1620, 1997.
- [67] C. Gabrielli, F. Huet, M. Keddam, and R. Oltra, "A Review of the Probabilistic Aspects of Localized Corrosion," *Corros. Sci.*, vol. 46, no. 4, p. 266, 1990.
- [68] U. Bertocci, M. Koike, S. Leigh, F. Qiu, and G. Yang, "A statistical Analysis of the Fluctuations of the Passive Current," *J. Electrochem. Soc.*, vol. 133, no. 9, pp. 1782–1786, 1986.
- [69] E. Van Hunnik and B. Pots, "The Formation of Protective Fe_3CO_2 Corrosion Product Layers in CO_2 Corrosion," in *Proc. Corrosion*, Houston, TX, 1996, paper no. 6.
- [70] Y. Xiao and S. Netic, "A Stochastic Prediction Model of Localized CO_2 Corrosion," in *Proc. Corrosion*, Houston, TX, 2005, paper no. 05057.

APPENDIX A: WEIGHT LOSS CORROSION RATE CALCULATION METHOD

The corrosion rate measurement by weight loss method is calculated by equation (37):

$$CR = \frac{m_{loss} \times 87.6}{\rho_{Fe} \times A \times t} \quad (37)$$

Where:

CR: calculated corrosion (mm/yr);

M_{loss} : mass loss of steel sample (measured in grams);

ρ_{Fe} : density of iron (equal to 7.85 g/cm³);

A : surface area (in cm²)

t : exposure time (in hours)

**APPENDIX B: REACTION RATE CALCULATION METHOD (SCALING
FORMATION AND CORROSION RATE)**

The reaction rate in mol/m²/hr for corrosion rate (CR) and scale formation rate (SFR) are calculated by equation (38) and (39).

Corrosion rate (mol/m²/hr)

$$CR = \frac{CR_w \times \rho_{Fe}}{1000 \times MW_{Fe} \times 8760 \times 1000} \quad (38)$$

Where:

CR_w = Corrosion rate from weight loss method (mm/yr)

ρ_{Fe} = density of iron (equal to 7850 kg/m³);

MW_{Fe} = molecular weight of iron (equal to 55.85 g/mol)

Scale formation rate (mol/m²/hr)

$$SFR = \frac{M_1}{MW_{FeS} \times A \times t} \quad (39)$$

Where:

M₁ = mass of corrosion product layer (in grams)

MW_{FeS} = molecular weight of FeS (equal to 87.9 g/mol)

A = surface area of the steel (in m²);

t = experimental duration (in hour)

APPENDIX C: HYPOTHESIS TESTING USING P-VALUE METHOD

Null hypothesis: $H_0; \mu \geq 0.1$

Alternative hypothesis; $H_A; \mu < 0.1$

Level of significance (α) = 0.05

Test Statistic (z) = $\frac{\bar{x} - \mu}{\sigma / \sqrt{n}} = 0.8$

$P(z < 0.78) = 0.8023$

Thus, since $P > \alpha$,

Fail to reject null hypothesis.

**APPENDIX D: PERMISSION TO REPRODUCE FIGURES FROM NACE
INTERNATIONAL**



**Permission to Reproduce Figures,
Photos, and Tables from
Copyrighted Works**

Date: 1/2/15
 Name: NAJMI DIN YAKUB Title: PhD candidate
 Company ("Publisher"): Ohio University
 Address: 342 West State Street, Athens, OH, 45701
 Tel: 740 818 6768 Fax: 740 593 9949
 Email: ny371109@ohio.edu

Material to be Reproduced ("Work"): Please provide a complete description of the material involved. Include the following elements where applicable: publication name, issue date, page number, figure/photo/table number, paper number, conference name, etc.

"Experimental Study of Top of Line Corrosion in Slightly Sour Environments,"
C. Li, W. Sun, S. Ling, J. L. Pacheco, NACE conference 2012, Paper No 3807,
Figure 2

Reproduction Method ("Publication Media"): Please provide a complete description of how and where the Work will be used. Include the following elements as applicable: publication name, issue, circulation, print run, web site address, conference name, presentation time and place, etc.

It will be used in my dissertation, Ohio University, May 2015

NACE International ("NACE") hereby grants to "Publisher" the right to publish the Work utilizing the Publication Media described above. The publication right granted herein is limited to the specific Publication Media described above. To the extent the publication of the Work is to occur by an above-specified date, such as in a particular periodical or at a particular conference, the right granted herein shall automatically terminate upon the date of such occurrence, whether or not the Work is actually published. To the extent the Publication Media is a web site, the publication right is limited to publication at the specific web site URL identified above. Any right granted herein is a limited, non-transferable, non-exclusive right. No other rights in the Work are granted herein.

Publisher shall not edit or modify the Work except to meet the style and graphic requirements of the individual media involved.

The Publisher shall include the following notation with any publication of the Work: © NACE International YEAR.

The Publisher shall include full bibliographic citations of or references to the original NACE source, where applicable.

Publisher shall obtain a copy of the original Work directly from NACE International and shall not utilize copies of the Work from other sources, including the author(s).

To the extent the Work is published on a web site as authorized herein, the Work shall be posted in a file format that does not allow the content of the Work to be easily copied from the Web Site or changed.

As between NACE and Publisher, Publisher acknowledges that NACE owns all rights in the Works.

Publisher shall not be entitled to any compensation for its efforts in promoting the Work.

THE WORK IS PROVIDED "AS IS." ALL EXPRESS OR IMPLIED COVENANTS, CONDITIONS, REPRESENTATIONS OR WARRANTIES, INCLUDING ANY IMPLIED WARRANTY OF MERCHANTABILITY OR FITNESS FOR A PARTICULAR PURPOSE OR CONDITIONS OF ACCURACY, COMPLETENESS OR QUALITY AND THOSE ARISING BY STATUTE OR OTHERWISE IN LAW, ARE HEREBY DISCLAIMED.

Permission to Publish NACE Copy

IN NO EVENT WILL NACE BE LIABLE FOR ANY DIRECT, INDIRECT, PUNITIVE, SPECIAL, INCIDENTAL OR CONSEQUENTIAL DAMAGES IN CONNECTION WITH OR RELATED TO THIS AGREEMENT (INCLUDING LOSS OF PROFITS, USE, DATA, OR OTHER ECONOMIC ADVANTAGE), HOWSOEVER ARISING.

This Agreement and the rights granted herein may be terminated immediately by NACE upon breach of this Agreement by Publisher. Unless earlier terminated, this Agreement and the rights granted herein will automatically terminate 6 months from the Date set forth above. If the Work has not been published within that time period, a new Agreement must be obtained.

Publisher may not, directly or indirectly, sell, assign, sublicense, lease, rent, distribute, or otherwise transfer this Agreement or any rights granted herein, without the prior written consent of NACE.

If any provision of this Agreement is found to be unenforceable, then this Agreement shall be deemed to be amended by modifying such provision to the extent necessary to make it legal and enforceable while preserving its intent. The remainder of this Agreement shall not be affected by such modification.

This Agreement does not create, and shall not be construed to create, any employer-employee, joint venture or partnership relationship between the parties. No officer, employee, agent, servant or independent contractor of either party shall at any time be deemed to be an employee, servant, agent or contractor of any other party for any purpose whatsoever.

This Agreement shall be governed by, and construed and enforced in accordance with, the laws of the State of Texas, without regard to the choice of law provisions of that State.

This Agreement shall only be effective if signed by authorized representatives of both parties. This Agreement constitutes the entire Agreement between the parties with respect to the subject matter of this Agreement. Any change, modification or waiver hereto must be in writing and signed by authorized representatives of both parties.

Other Terms & Conditions: _____

Publisher hereby requests permission to publish the Work described above and agrees to comply with all Terms and Conditions listed above.

Request submitted by:

YASMOODIN YAAKUB

Printed Name

PhD candidate

Title

Hyman

Signature

1/2/2015

Date

Request approved by NACE:

D. Freeman

Printed Name

ADM

Title

D. Freeman

Signature

1/7/15

Date

Request agreed to by:

Lead Author Printed Name

Lead Author Title

Lead Author Signature

Date



Permission to Reproduce Figures, Photos, and Tables from Copyrighted Works

Date: 1/2/15
 Name: NAJMIDDIN YAAKUB Title: PhD candidate
 Company ("Publisher"): Ohio University
 Address: 342 west state street, Athens, OH, 45701
 Tel: 740 818 6768 Fax: 740 593 9949
 Email: ny371109@ohio.edu

Material to be Reproduced ("Work"): Please provide a complete description of the material involved. Include the following elements where applicable: publication name, issue date, page number, figure/photo/table number, paper number, conference name, etc.

"Sour Top of the Line Corrosion in the Presence of Acetic Acid"
NACE International 2010, Paper No 10100, M. Singer, A. Comacho, B. Anum,
S. Nesic, Figure 13 and Figure 7

Reproduction Method ("Publication Media"): Please provide a complete description of how and where the Work will be used. Include the following elements as applicable: publication name, issue, circulation, print run, web site address, conference name, presentation time and place, etc.

It will be used in my dissertation, Ohio University, May 2015

NACE International ("NACE") hereby grants to "Publisher" the right to publish the Work utilizing the Publication Media described above. The publication right granted herein is limited to the specific Publication Media described above. To the extent the publication of the Work is to occur by an above-specified date, such as in a particular periodical or at a particular conference, the right granted herein shall automatically terminate upon the date of such occurrence, whether or not the Work is actually published. To the extent the Publication Media is a web site, the publication right is limited to publication at the specific web site URL identified above. Any right granted herein is a limited, non-transferable, non-exclusive right. No other rights in the Work are granted herein.

Publisher shall not edit or modify the Work except to meet the style and graphic requirements of the individual media involved.

The Publisher shall include the following notation with any publication of the Work: © NACE International YEAR.

The Publisher shall include full bibliographic citations of or references to the original NACE source, where applicable.

Publisher shall obtain a copy of the original Work directly from NACE International and shall not utilize copies of the Work from other sources, including the author(s).

To the extent the Work is published on a web site as authorized herein, the Work shall be posted in a file format that does not allow the content of the Work to be easily copied from the Web Site or changed.

As between NACE and Publisher, Publisher acknowledges that NACE owns all rights in the Works.

Publisher shall not be entitled to any compensation for its efforts in promoting the Work.

THE WORK IS PROVIDED "AS IS." ALL EXPRESS OR IMPLIED COVENANTS, CONDITIONS, REPRESENTATIONS OR WARRANTIES, INCLUDING ANY IMPLIED WARRANTY OF MERCHANTABILITY OR FITNESS FOR A PARTICULAR PURPOSE OR CONDITIONS OF ACCURACY, COMPLETENESS OR QUALITY AND THOSE ARISING BY STATUTE OR OTHERWISE IN LAW, ARE HEREBY DISCLAIMED.

Permission to Publish NACE Copy

IN NO EVENT WILL NACE BE LIABLE FOR ANY DIRECT, INDIRECT, PUNITIVE, SPECIAL, INCIDENTAL OR CONSEQUENTIAL DAMAGES IN CONNECTION WITH OR RELATED TO THIS AGREEMENT (INCLUDING LOSS OF PROFITS, USE, DATA, OR OTHER ECONOMIC ADVANTAGE), HOWSOEVER ARISING.

This Agreement and the rights granted herein may be terminated immediately by NACE upon breach of this Agreement by Publisher. Unless earlier terminated, this Agreement and the rights granted herein will automatically terminate 6 months from the Date set forth above. If the Work has not been published within that time period, a new Agreement must be obtained.

Publisher may not, directly or indirectly, sell, assign, sublicense, lease, rent, distribute, or otherwise transfer this Agreement or any rights granted herein, without the prior written consent of NACE.

If any provision of this Agreement is found to be unenforceable, then this Agreement shall be deemed to be amended by modifying such provision to the extent necessary to make it legal and enforceable while preserving its intent. The remainder of this Agreement shall not be affected by such modification.

This Agreement does not create, and shall not be construed to create, any employer-employee, joint venture or partnership relationship between the parties. No officer, employee, agent, servant or independent contractor of either party shall at any time be deemed to be an employee, servant, agent or contractor of any other party for any purpose whatsoever.

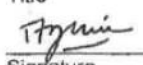
This Agreement shall be governed by, and construed and enforced in accordance with, the laws of the State of Texas, without regard to the choice of law provisions of that State.

This Agreement shall only be effective if signed by authorized representatives of both parties. This Agreement constitutes the entire Agreement between the parties with respect to the subject matter of this Agreement. Any change, modification or waiver hereto must be in writing and signed by authorized representatives of both parties.

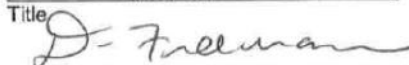
Other Terms & Conditions: _____

Publisher hereby requests permission to publish the Work described above and agrees to comply with all Terms and Conditions listed above.

Request submitted by:

NASIMIDDIN YAKUB
 Printed Name
PhD candidate
 Title

 Signature
1/2/2015
 Date

Request approved by NACE:

D. Freeman
 Printed Name
ADM
 Title

 Signature
1/7/15
 Date

Request agreed to by:

 Lead Author Printed Name

 Lead Author Title

 Lead Author Signature

 Date



Permission to Reproduce Figures, Photos, and Tables from Copyrighted Works

Date: 1/2/15
 Name: NASMOODIN YAAKUB Title: PHD candidate
 Company ("Publisher"): Ohio University
 Address: 342 west state street, Athens, OH, 45701
 Tel: 740 818 6768 Fax: 740 593 9949
 Email: ny371109@ohio.edu

Material to be Reproduced ("Work"): Please provide a complete description of the material involved. Include the following elements where applicable: publication name, issue date, page number, figure/photo/table number, paper number, conference name, etc.

"Top of the Line Corrosion in H₂S/CO₂ Environments", A. Comacho,
 M. Singer, B. Brown, S. Newc, NACE International 2008, Paper No 08470,
 Figure 5

Reproduction Method ("Publication Media"): Please provide a complete description of how and where the Work will be used. Include the following elements as applicable: publication name, issue, circulation, print run, web site address, conference name, presentation time and place, etc.

It will be used in my dissertation, Ohio University, May 2015

NACE International ("NACE") hereby grants to "Publisher" the right to publish the Work utilizing the Publication Media described above. The publication right granted herein is limited to the specific Publication Media described above. To the extent the publication of the Work is to occur by an above-specified date, such as in a particular periodical or at a particular conference, the right granted herein shall automatically terminate upon the date of such occurrence, whether or not the Work is actually published. To the extent the Publication Media is a web site, the publication right is limited to publication at the specific web site URL identified above. Any right granted herein is a limited, non-transferable, non-exclusive right. No other rights in the Work are granted herein.

Publisher shall not edit or modify the Work except to meet the style and graphic requirements of the individual media involved.

The Publisher shall include the following notation with any publication of the Work: © NACE International YEAR.

The Publisher shall include full bibliographic citations of or references to the original NACE source, where applicable.

Publisher shall obtain a copy of the original Work directly from NACE International and shall not utilize copies of the Work from other sources, including the author(s).

To the extent the Work is published on a web site as authorized herein, the Work shall be posted in a file format that does not allow the content of the Work to be easily copied from the Web Site or changed.

As between NACE and Publisher, Publisher acknowledges that NACE owns all rights in the Works.

Publisher shall not be entitled to any compensation for its efforts in promoting the Work.

THE WORK IS PROVIDED "AS IS." ALL EXPRESS OR IMPLIED COVENANTS, CONDITIONS, REPRESENTATIONS OR WARRANTIES, INCLUDING ANY IMPLIED WARRANTY OF MERCHANTABILITY OR FITNESS FOR A PARTICULAR PURPOSE OR CONDITIONS OF ACCURACY, COMPLETENESS OR QUALITY AND THOSE ARISING BY STATUTE OR OTHERWISE IN LAW, ARE HEREBY DISCLAIMED.

Permission to Publish NACE Copy

IN NO EVENT WILL NACE BE LIABLE FOR ANY DIRECT, INDIRECT, PUNITIVE, SPECIAL, INCIDENTAL OR CONSEQUENTIAL DAMAGES IN CONNECTION WITH OR RELATED TO THIS AGREEMENT (INCLUDING LOSS OF PROFITS, USE, DATA, OR OTHER ECONOMIC ADVANTAGE), HOWSOEVER ARISING.

This Agreement and the rights granted herein may be terminated immediately by NACE upon breach of this Agreement by Publisher. Unless earlier terminated, this Agreement and the rights granted herein will automatically terminate 6 months from the Date set forth above. If the Work has not been published within that time period, a new Agreement must be obtained.

Publisher may not, directly or indirectly, sell, assign, sublicense, lease, rent, distribute, or otherwise transfer this Agreement or any rights granted herein, without the prior written consent of NACE.

If any provision of this Agreement is found to be unenforceable, then this Agreement shall be deemed to be amended by modifying such provision to the extent necessary to make it legal and enforceable while preserving its intent. The remainder of this Agreement shall not be affected by such modification.

This Agreement does not create, and shall not be construed to create, any employer-employee, joint venture or partnership relationship between the parties. No officer, employee, agent, servant or independent contractor of either party shall at any time be deemed to be an employee, servant, agent or contractor of any other party for any purpose whatsoever.

This Agreement shall be governed by, and construed and enforced in accordance with, the laws of the State of Texas, without regard to the choice of law provisions of that State.

This Agreement shall only be effective if signed by authorized representatives of both parties. This Agreement constitutes the entire Agreement between the parties with respect to the subject matter of this Agreement. Any change, modification or waiver hereto must be in writing and signed by authorized representatives of both parties.

Other Terms & Conditions: _____

Publisher hereby requests permission to publish the Work described above and agrees to comply with all Terms and Conditions listed above.

Request submitted by:

YASMOODIN YAAKUB

Printed Name

PhD candidate

Title

[Signature]

Signature

1/2/2015

Date

Request approved by NACE:

D. Freeman

Printed Name

ADM

Title

[Signature]

Signature

1/7/15

Date

Request agreed to by:

Lead Author Printed Name

Lead Author Title

Lead Author Signature

Date



Permission to Reproduce Figures, Photos, and Tables from Copyrighted Works

Date: 1/2/15
 Name: NAJMOON YAKUB Title: PhD candidate
 Company ("Publisher"): Ohio University
 Address: 342 West State Street, Athens, OH, 45701
 Tel: 740 818 6268 Fax: 740 593 9949
 Email: ny37109@ohio.edu

Material to be Reproduced ("Work"): Please provide a complete description of the material involved. Include the following elements where applicable: publication name, issue date, page number, figure/photo/table number, paper number, conference name, etc.

Corrosion Assessment in KARAW Karan Gas Field Development,
M. Singer, S. Nesić, J. Al-Khamis, NACE International 2012, paper No C2012-00010
paper No C2012-0001411, Figure 18 and Figure 21

Reproduction Method ("Publication Media"): Please provide a complete description of how and where the Work will be used. Include the following elements as applicable: publication name, issue, circulation, print run, web site address, conference name, presentation time and place, etc.

It will be used in my dissertation, Ohio University, May 2015

NACE International ("NACE") hereby grants to "Publisher" the right to publish the Work utilizing the Publication Media described above. The publication right granted herein is limited to the specific Publication Media described above. To the extent the publication of the Work is to occur by an above-specified date, such as in a particular periodical or at a particular conference, the right granted herein shall automatically terminate upon the date of such occurrence, whether or not the Work is actually published. To the extent the Publication Media is a web site, the publication right is limited to publication at the specific web site URL identified above. Any right granted herein is a limited, non-transferable, non-exclusive right. No other rights in the Work are granted herein.

Publisher shall not edit or modify the Work except to meet the style and graphic requirements of the individual media involved.

The Publisher shall include the following notation with any publication of the Work: © NACE International YEAR.

The Publisher shall include full bibliographic citations of or references to the original NACE source, where applicable.

Publisher shall obtain a copy of the original Work directly from NACE International and shall not utilize copies of the Work from other sources, including the author(s).

To the extent the Work is published on a web site as authorized herein, the Work shall be posted in a file format that does not allow the content of the Work to be easily copied from the Web Site or changed.

As between NACE and Publisher, Publisher acknowledges that NACE owns all rights in the Works.

Publisher shall not be entitled to any compensation for its efforts in promoting the Work.

THE WORK IS PROVIDED "AS IS." ALL EXPRESS OR IMPLIED COVENANTS, CONDITIONS, REPRESENTATIONS OR WARRANTIES, INCLUDING ANY IMPLIED WARRANTY OF MERCHANTABILITY OR FITNESS FOR A PARTICULAR PURPOSE OR CONDITIONS OF ACCURACY, COMPLETENESS OR QUALITY AND THOSE ARISING BY STATUTE OR OTHERWISE IN LAW, ARE HEREBY DISCLAIMED.

Permission to Publish NACE Copy

IN NO EVENT WILL NACE BE LIABLE FOR ANY DIRECT, INDIRECT, PUNITIVE, SPECIAL, INCIDENTAL OR CONSEQUENTIAL DAMAGES IN CONNECTION WITH OR RELATED TO THIS AGREEMENT (INCLUDING LOSS OF PROFITS, USE, DATA, OR OTHER ECONOMIC ADVANTAGE), HOWSOEVER ARISING.

This Agreement and the rights granted herein may be terminated immediately by NACE upon breach of this Agreement by Publisher. Unless earlier terminated, this Agreement and the rights granted herein will automatically terminate 6 months from the Date set forth above. If the Work has not been published within that time period, a new Agreement must be obtained.

Publisher may not, directly or indirectly, sell, assign, sublicense, lease, rent, distribute, or otherwise transfer this Agreement or any rights granted herein, without the prior written consent of NACE.

If any provision of this Agreement is found to be unenforceable, then this Agreement shall be deemed to be amended by modifying such provision to the extent necessary to make it legal and enforceable while preserving its intent. The remainder of this Agreement shall not be affected by such modification.

This Agreement does not create, and shall not be construed to create, any employer-employee, joint venture or partnership relationship between the parties. No officer, employee, agent, servant or independent contractor of either party shall at any time be deemed to be an employee, servant, agent or contractor of any other party for any purpose whatsoever.

This Agreement shall be governed by, and construed and enforced in accordance with, the laws of the State of Texas, without regard to the choice of law provisions of that State.

This Agreement shall only be effective if signed by authorized representatives of both parties. This Agreement constitutes the entire Agreement between the parties with respect to the subject matter of this Agreement. Any change, modification or waiver hereto must be in writing and signed by authorized representatives of both parties.

Other Terms & Conditions: _____

Publisher hereby requests permission to publish the Work described above and agrees to comply with all Terms and Conditions listed above.

Request submitted by:
NASMOODIN YAAKUB
Printed Name
PhD candidate
Title
[Signature]
Signature
1/2/2015
Date

Request approved by NACE:
[Signature]
Printed Name
ADM
Title
[Signature]
Signature
1/7/15
Date

Request agreed to by:

Lead Author Printed Name

Lead Author Title

Lead Author Signature

Date



Permission to Reproduce Figures, Photos, and Tables from Copyrighted Works

Date: 1/2/15
 Name: NAJMOON YAKOB Title: PHD candidate
 Company ("Publisher"): Ohio University
 Address: 342 west state street, Athens, OH, 45701
 Tel: 740 818 6768 Fax: 740 593 9949
 Email: ny371109@ohio.edu

Material to be Reproduced ("Work"): Please provide a complete description of the material involved. Include the following elements where applicable: publication name, issue date, page number, figure/photo/table number, paper number, conference name, etc.

"Top-of-Line Mechanism for sour wet Gas Pipelines," D. Pugh,
 S. Asher, J. Cai, W. Sisak, J. Pacheco, F. C. Ibrahim, E. J. Wright,
 A. Dhokte, S. Venkai, D. Robson, NACE International, paper no 09287, 2009, Figure 1

Reproduction Method ("Publication Media"): Please provide a complete description of how and where the Work will be used. Include the following elements as applicable: publication name, issue, circulation, print run, web site address, conference name, presentation time and place, etc.

It will be used in my dissertation, Ohio University, May 2015

NACE International ("NACE") hereby grants to "Publisher" the right to publish the Work utilizing the Publication Media described above. The publication right granted herein is limited the specific Publication Media described above. To the extent the publication of the Work is to occur by an above-specified date, such as in a particular periodical or at a particular conference, the right granted herein shall automatically terminate upon the date of such occurrence, whether or not the Work is actually published. To the extent the Publication Media is a web site, the publication right is limited to publication at the specific web site URL identified above. Any right granted herein is a limited, non-transferable, non-exclusive right. No other rights in the Work are granted herein.

Publisher shall not edit or modify the Work except to meet the style and graphic requirements of the individual media involved.

The Publisher shall include the following notation with any publication of the Work: © NACE International YEAR.

The Publisher shall include full bibliographic citations of or references to the original NACE source, where applicable.

Publisher shall obtain a copy of the original Work directly from NACE International and shall not utilize copies of the Work from other sources, including the author(s).

To the extent the Work is published on a web site as authorized herein, the Work shall be posted in a file format that does not allow the content of the Work to be easily copied from the Web Site or changed.

As between NACE and Publisher, Publisher acknowledges that NACE owns all rights in the Works.

Publisher shall not be entitled to any compensation for its efforts in promoting the Work.

THE WORK IS PROVIDED "AS IS." ALL EXPRESS OR IMPLIED COVENANTS, CONDITIONS, REPRESENTATIONS OR WARRANTIES, INCLUDING ANY IMPLIED WARRANTY OF MERCHANTABILITY OR FITNESS FOR A PARTICULAR PURPOSE OR CONDITIONS OF ACCURACY, COMPLETENESS OR QUALITY AND THOSE ARISING BY STATUTE OR OTHERWISE IN LAW, ARE HEREBY DISCLAIMED.

Permission to Publish NACE Copy

IN NO EVENT WILL NACE BE LIABLE FOR ANY DIRECT, INDIRECT, PUNITIVE, SPECIAL, INCIDENTAL OR CONSEQUENTIAL DAMAGES IN CONNECTION WITH OR RELATED TO THIS AGREEMENT (INCLUDING LOSS OF PROFITS, USE, DATA, OR OTHER ECONOMIC ADVANTAGE), HOWSOEVER ARISING.

This Agreement and the rights granted herein may be terminated immediately by NACE upon breach of this Agreement by Publisher. Unless earlier terminated, this Agreement and the rights granted herein will automatically terminate 6 months from the Date set forth above. If the Work has not been published within that time period, a new Agreement must be obtained.

Publisher may not, directly or indirectly, sell, assign, sublicense, lease, rent, distribute, or otherwise transfer this Agreement or any rights granted herein, without the prior written consent of NACE.

If any provision of this Agreement is found to be unenforceable, then this Agreement shall be deemed to be amended by modifying such provision to the extent necessary to make it legal and enforceable while preserving its intent. The remainder of this Agreement shall not be affected by such modification.

This Agreement does not create, and shall not be construed to create, any employer-employee, joint venture or partnership relationship between the parties. No officer, employee, agent, servant or independent contractor of either party shall at any time be deemed to be an employee, servant, agent or contractor of any other party for any purpose whatsoever.

This Agreement shall be governed by, and construed and enforced in accordance with, the laws of the State of Texas, without regard to the choice of law provisions of that State.

This Agreement shall only be effective if signed by authorized representatives of both parties. This Agreement constitutes the entire Agreement between the parties with respect to the subject matter of this Agreement. Any change, modification or waiver hereto must be in writing and signed by authorized representatives of both parties.

Other Terms & Conditions: _____

Publisher hereby requests permission to publish the Work described above and agrees to comply with all Terms and Conditions listed above.

Request submitted by:

MAJMOODIN YAAKUB

Printed Name

PhD candidate

Title

[Signature]

Signature

1/2/2015

Date

Request approved by NACE:

[Signature]

Printed Name

ADM

Title

[Signature]

Signature

1/7/15

Date

Request agreed to by:

Lead Author Printed Name

Lead Author Title

Lead Author Signature

Date



Permission to Reproduce Figures, Photos, and Tables from Copyrighted Works

Date: 1/2/15
 Name: NAJMOON YAKOB Title: PhD candidate
 Company ("Publisher"): Ohio University
 Address: 342 west state street, Athens, OH, 45701
 Tel: 740 818 6768 Fax: 740 593 9949
 Email: ny371109@ohio.edu

Material to be Reproduced ("Work"): Please provide a complete description of the material involved. Include the following elements where applicable: publication name, issue date, page number, figure/photo/table number, paper number, conference name, etc.

"Corrosion Experience and Inhibition Practices in wet Sour Gathering Systems", D. Ho - Chung - Qui, A. Williamson and P. Eng, NACE International paper no 46, 1987.

Reproduction Method ("Publication Media"): Please provide a complete description of how and where the Work will be used. Include the following elements as applicable: publication name, issue, circulation, print run, web site address, conference name, presentation time and place, etc.

It will be used in my dissertation, Ohio University, May 2015

NACE International ("NACE") hereby grants to "Publisher" the right to publish the Work utilizing the Publication Media described above. The publication right granted herein is limited to the specific Publication Media described above. To the extent the publication of the Work is to occur by an above-specified date, such as in a particular periodical or at a particular conference, the right granted herein shall automatically terminate upon the date of such occurrence, whether or not the Work is actually published. To the extent the Publication Media is a web site, the publication right is limited to publication at the specific web site URL identified above. Any right granted herein is a limited, non-transferable, non-exclusive right. No other rights in the Work are granted herein.

Publisher shall not edit or modify the Work except to meet the style and graphic requirements of the individual media involved.

The Publisher shall include the following notation with any publication of the Work: © NACE International YEAR.

The Publisher shall include full bibliographic citations of or references to the original NACE source, where applicable.

Publisher shall obtain a copy of the original Work directly from NACE International and shall not utilize copies of the Work from other sources, including the author(s).

To the extent the Work is published on a web site as authorized herein, the Work shall be posted in a file format that does not allow the content of the Work to be easily copied from the Web Site or changed.

As between NACE and Publisher, Publisher acknowledges that NACE owns all rights in the Works.

Publisher shall not be entitled to any compensation for its efforts in promoting the Work.

THE WORK IS PROVIDED "AS IS." ALL EXPRESS OR IMPLIED COVENANTS, CONDITIONS, REPRESENTATIONS OR WARRANTIES, INCLUDING ANY IMPLIED WARRANTY OF MERCHANTABILITY OR FITNESS FOR A PARTICULAR PURPOSE OR CONDITIONS OF ACCURACY, COMPLETENESS OR QUALITY AND THOSE ARISING BY STATUTE OR OTHERWISE IN LAW, ARE HEREBY DISCLAIMED.

Permission to Publish NACE Copy

IN NO EVENT WILL NACE BE LIABLE FOR ANY DIRECT, INDIRECT, PUNITIVE, SPECIAL, INCIDENTAL OR CONSEQUENTIAL DAMAGES IN CONNECTION WITH OR RELATED TO THIS AGREEMENT (INCLUDING LOSS OF PROFITS, USE, DATA, OR OTHER ECONOMIC ADVANTAGE), HOWSOEVER ARISING.

This Agreement and the rights granted herein may be terminated immediately by NACE upon breach of this Agreement by Publisher. Unless earlier terminated, this Agreement and the rights granted herein will automatically terminate 6 months from the Date set forth above. If the Work has not been published within that time period, a new Agreement must be obtained.

Publisher may not, directly or indirectly, sell, assign, sublicense, lease, rent, distribute, or otherwise transfer this Agreement or any rights granted herein, without the prior written consent of NACE.

If any provision of this Agreement is found to be unenforceable, then this Agreement shall be deemed to be amended by modifying such provision to the extent necessary to make it legal and enforceable while preserving its intent. The remainder of this Agreement shall not be affected by such modification.

This Agreement does not create, and shall not be construed to create, any employer-employee, joint venture or partnership relationship between the parties. No officer, employee, agent, servant or independent contractor of either party shall at any time be deemed to be an employee, servant, agent or contractor of any other party for any purpose whatsoever.

This Agreement shall be governed by, and construed and enforced in accordance with, the laws of the State of Texas, without regard to the choice of law provisions of that State.

This Agreement shall only be effective if signed by authorized representatives of both parties. This Agreement constitutes the entire Agreement between the parties with respect to the subject matter of this Agreement. Any change, modification or waiver hereto must be in writing and signed by authorized representatives of both parties.

Other Terms & Conditions: _____

Publisher hereby requests permission to publish the Work described above and agrees to comply with all Terms and Conditions listed above.

Request submitted by:

NASMIODIN YAAKUB

Printed Name

PhD candidate

Title

[Signature]

Signature

1/2/2015

Date

Request approved by NACE:

D. Freeman

Printed Name

ADM

Title

[Signature]

Signature

1/7/15

Date

Request agreed to by:

Lead Author Printed Name

Lead Author Title

Lead Author Signature

Date



Permission to Reproduce Figures, Photos, and Tables from Copyrighted Works

Date: 1/2/15
 Name: NAJMOUDIN YAKUB Title: PhD candidate
 Company ("Publisher"): Ohio University
 Address: 342 west state street, Athens, OH, 45701
 Tel: 740 818 6768 Fax: 740 593 9949
 Email: ny371109@ohio.edu

Material to be Reproduced ("Work"): Please provide a complete description of the material involved. Include the following elements where applicable: publication name, issue date, page number, figure/photo/table number, paper number, conference name, etc.

"Corrosion control in the Gathering System at Lacq Sur Gas Field",
A. Porlass, M. Dieumegarde and M. Estavayer, NACE conference, 1981,
page 860, Figure 2

Reproduction Method ("Publication Media"): Please provide a complete description of how and where the Work will be used. Include the following elements as applicable: publication name, issue, circulation, print run, web site address, conference name, presentation time and place, etc.

It will be used in my dissertation, Ohio University, May 2015

NACE International ("NACE") hereby grants to "Publisher" the right to publish the Work utilizing the Publication Media described above. The publication right granted herein is limited the specific Publication Media described above. To the extent the publication of the Work is to occur by an above-specified date, such as in a particular periodical or at a particular conference, the right granted herein shall automatically terminate upon the date of such occurrence, whether or not the Work is actually published. To the extent the Publication Media is a web site, the publication right is limited to publication at the specific web site URL identified above. Any right granted herein is a limited, non-transferable, non-exclusive right. No other rights in the Work are granted herein.

Publisher shall not edit or modify the Work except to meet the style and graphic requirements of the individual media involved.

The Publisher shall include the following notation with any publication of the Work: © NACE International YEAR.

The Publisher shall include full bibliographic citations of or references to the original NACE source, where applicable.

Publisher shall obtain a copy of the original Work directly from NACE International and shall not utilize copies of the Work from other sources, including the author(s).

To the extent the Work is published on a web site as authorized herein, the Work shall be posted in a file format that does not allow the content of the Work to be easily copied from the Web Site or changed.

As between NACE and Publisher, Publisher acknowledges that NACE owns all rights in the Works.

Publisher shall not be entitled to any compensation for its efforts in promoting the Work.

THE WORK IS PROVIDED "AS IS." ALL EXPRESS OR IMPLIED COVENANTS, CONDITIONS, REPRESENTATIONS OR WARRANTIES, INCLUDING ANY IMPLIED WARRANTY OF MERCHANTABILITY OR FITNESS FOR A PARTICULAR PURPOSE OR CONDITIONS OF ACCURACY, COMPLETENESS OR QUALITY AND THOSE ARISING BY STATUTE OR OTHERWISE IN LAW, ARE HEREBY DISCLAIMED.

Permission to Publish NACE Copy

IN NO EVENT WILL NACE BE LIABLE FOR ANY DIRECT, INDIRECT, PUNITIVE, SPECIAL, INCIDENTAL OR CONSEQUENTIAL DAMAGES IN CONNECTION WITH OR RELATED TO THIS AGREEMENT (INCLUDING LOSS OF PROFITS, USE, DATA, OR OTHER ECONOMIC ADVANTAGE), HOWSOEVER ARISING.

This Agreement and the rights granted herein may be terminated immediately by NACE upon breach of this Agreement by Publisher. Unless earlier terminated, this Agreement and the rights granted herein will automatically terminate 6 months from the Date set forth above. If the Work has not been published within that time period, a new Agreement must be obtained.

Publisher may not, directly or indirectly, sell, assign, sublicense, lease, rent, distribute, or otherwise transfer this Agreement or any rights granted herein, without the prior written consent of NACE.

If any provision of this Agreement is found to be unenforceable, then this Agreement shall be deemed to be amended by modifying such provision to the extent necessary to make it legal and enforceable while preserving its intent. The remainder of this Agreement shall not be affected by such modification.

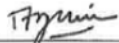
This Agreement does not create, and shall not be construed to create, any employer-employee, joint venture or partnership relationship between the parties. No officer, employee, agent, servant or independent contractor of either party shall at any time be deemed to be an employee, servant, agent or contractor of any other party for any purpose whatsoever.

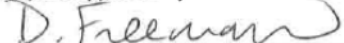
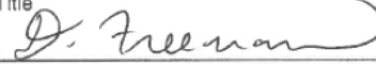
This Agreement shall be governed by, and construed and enforced in accordance with, the laws of the State of Texas, without regard to the choice of law provisions of that State.

This Agreement shall only be effective if signed by authorized representatives of both parties. This Agreement constitutes the entire Agreement between the parties with respect to the subject matter of this Agreement. Any change, modification or waiver hereto must be in writing and signed by authorized representatives of both parties.

Other Terms & Conditions: _____

Publisher hereby requests permission to publish the Work described above and agrees to comply with all Terms and Conditions listed above.

Request submitted by:
NAJMIODIN YAAKUB
 Printed Name
PhD candidate
 Title

 Signature
1/2/2015
 Date

Request approved by NACE:

 Printed Name
ADM
 Title

 Signature
1/7/15
 Date

Request agreed to by:

 Lead Author Printed Name

 Lead Author Title

 Lead Author Signature

 Date



Permission to Reproduce Figures, Photos, and Tables from Copyrighted Works

Date: 1/2/15

Name: NAJMOODIN YAAKUB Title: PhD candidate

Company ("Publisher"): Ohio University

Address: 342 west state street, Athens, OH, 45701

Tel: 740 818 6768 Fax: 740 593 9949

Email: ny371109@ohio.edu

Material to be Reproduced ("Work"): Please provide a complete description of the material involved. Include the following elements where applicable: publication name, issue date, page number, figure/photo/table number, paper number, conference name, etc.

"Top of Line Corrosion in Multiphase Gas Lines: A case History",
Y.M. Gungeltun and J. Achmad, NACE conference, paper No 36, 1999,
Figure 4 and Figure 5

Reproduction Method ("Publication Media"): Please provide a complete description of how and where the Work will be used. Include the following elements as applicable: publication name, issue, circulation, print run, web site address, conference name, presentation time and place, etc.

It will be used in my dissertation, Ohio University, May 2015

NACE International ("NACE") hereby grants to "Publisher" the right to publish the Work utilizing the Publication Media described above. The publication right granted herein is limited to the specific Publication Media described above. To the extent the publication of the Work is to occur by an above-specified date, such as in a particular periodical or at a particular conference, the right granted herein shall automatically terminate upon the date of such occurrence, whether or not the Work is actually published. To the extent the Publication Media is a web site, the publication right is limited to publication at the specific web site URL identified above. Any right granted herein is a limited, non-transferable, non-exclusive right. No other rights in the Work are granted herein.

Publisher shall not edit or modify the Work except to meet the style and graphic requirements of the individual media involved.

The Publisher shall include the following notation with any publication of the Work: © NACE International YEAR.

The Publisher shall include full bibliographic citations of or references to the original NACE source, where applicable.

Publisher shall obtain a copy of the original Work directly from NACE International and shall not utilize copies of the Work from other sources, including the author(s).

To the extent the Work is published on a web site as authorized herein, the Work shall be posted in a file format that does not allow the content of the Work to be easily copied from the Web Site or changed.

As between NACE and Publisher, Publisher acknowledges that NACE owns all rights in the Works.

Publisher shall not be entitled to any compensation for its efforts in promoting the Work.

THE WORK IS PROVIDED "AS IS." ALL EXPRESS OR IMPLIED COVENANTS, CONDITIONS, REPRESENTATIONS OR WARRANTIES, INCLUDING ANY IMPLIED WARRANTY OF MERCHANTABILITY OR FITNESS FOR A PARTICULAR PURPOSE OR CONDITIONS OF ACCURACY, COMPLETENESS OR QUALITY AND THOSE ARISING BY STATUTE OR OTHERWISE IN LAW, ARE HEREBY DISCLAIMED.

Permission to Publish NACE Copy

IN NO EVENT WILL NACE BE LIABLE FOR ANY DIRECT, INDIRECT, PUNITIVE, SPECIAL, INCIDENTAL OR CONSEQUENTIAL DAMAGES IN CONNECTION WITH OR RELATED TO THIS AGREEMENT (INCLUDING LOSS OF PROFITS, USE, DATA, OR OTHER ECONOMIC ADVANTAGE), HOWSOEVER ARISING.

This Agreement and the rights granted herein may be terminated immediately by NACE upon breach of this Agreement by Publisher. Unless earlier terminated, this Agreement and the rights granted herein will automatically terminate 6 months from the Date set forth above. If the Work has not been published within that time period, a new Agreement must be obtained.

Publisher may not, directly or indirectly, sell, assign, sublicense, lease, rent, distribute, or otherwise transfer this Agreement or any rights granted herein, without the prior written consent of NACE.

If any provision of this Agreement is found to be unenforceable, then this Agreement shall be deemed to be amended by modifying such provision to the extent necessary to make it legal and enforceable while preserving its intent. The remainder of this Agreement shall not be affected by such modification.

This Agreement does not create, and shall not be construed to create, any employer-employee, joint venture or partnership relationship between the parties. No officer, employee, agent, servant or independent contractor of either party shall at any time be deemed to be an employee, servant, agent or contractor of any other party for any purpose whatsoever.

This Agreement shall be governed by, and construed and enforced in accordance with, the laws of the State of Texas, without regard to the choice of law provisions of that State.

This Agreement shall only be effective if signed by authorized representatives of both parties. This Agreement constitutes the entire Agreement between the parties with respect to the subject matter of this Agreement. Any change, modification or waiver hereto must be in writing and signed by authorized representatives of both parties.

Other Terms & Conditions: _____

Publisher hereby requests permission to publish the Work described above and agrees to comply with all Terms and Conditions listed above.

Request submitted by:

NASIMODIN YAKUB

Printed Name

phd candidate

Title

[Signature]

Signature

1/2/2015

Date

Request approved by NACE:

D. Freeman

Printed Name

ADM

Title

[Signature]

Signature

1/7/15

Date

Request agreed to by:

Lead Author Printed Name

Lead Author Title

Lead Author Signature

Date



Permission to Reproduce Figures, Photos, and Tables from Copyrighted Works

Date: 1/2/15
 Name: MAJMOON YAKOB Title: PhD candidate
 Company ("Publisher"): Ohio University
 Address: 342 west state street, Athens, OH, 45701
 Tel: 740 818 6768 Fax: 740 593 9949
 Email: ny37109@ohio.edu

Material to be Reproduced ("Work"): Please provide a complete description of the material involved. Include the following elements where applicable: publication name, issue date, page number, figure/photo/table number, paper number, conference name, etc.

"Prediction of Corrosion in Slightly Sour Environment," S.W. Smith, J.L. Pacheco,
 NACE International 2002, Paper no. 02241, Figure 1

Reproduction Method ("Publication Media"): Please provide a complete description of how and where the Work will be used. Include the following elements as applicable: publication name, issue, circulation, print run, web site address, conference name, presentation time and place, etc.

It will be used in my dissertation, Ohio University, May 2015

NACE International ("NACE") hereby grants to "Publisher" the right to publish the Work utilizing the Publication Media described above. The publication right granted herein is limited to the specific Publication Media described above. To the extent the publication of the Work is to occur by an above-specified date, such as in a particular periodical or at a particular conference, the right granted herein shall automatically terminate upon the date of such occurrence, whether or not the Work is actually published. To the extent the Publication Media is a web site, the publication right is limited to publication at the specific web site URL identified above. Any right granted herein is a limited, non-transferable, non-exclusive right. No other rights in the Work are granted herein.

Publisher shall not edit or modify the Work except to meet the style and graphic requirements of the individual media involved.

The Publisher shall include the following notation with any publication of the Work: © NACE International YEAR.

The Publisher shall include full bibliographic citations of or references to the original NACE source, where applicable.

Publisher shall obtain a copy of the original Work directly from NACE International and shall not utilize copies of the Work from other sources, including the author(s).

To the extent the Work is published on a web site as authorized herein, the Work shall be posted in a file format that does not allow the content of the Work to be easily copied from the Web Site or changed.

As between NACE and Publisher, Publisher acknowledges that NACE owns all rights in the Works.

Publisher shall not be entitled to any compensation for its efforts in promoting the Work.

THE WORK IS PROVIDED "AS IS." ALL EXPRESS OR IMPLIED COVENANTS, CONDITIONS, REPRESENTATIONS OR WARRANTIES, INCLUDING ANY IMPLIED WARRANTY OF MERCHANTABILITY OR FITNESS FOR A PARTICULAR PURPOSE OR CONDITIONS OF ACCURACY, COMPLETENESS OR QUALITY AND THOSE ARISING BY STATUTE OR OTHERWISE IN LAW, ARE HEREBY DISCLAIMED.

Permission to Publish NACE Copy

IN NO EVENT WILL NACE BE LIABLE FOR ANY DIRECT, INDIRECT, PUNITIVE, SPECIAL, INCIDENTAL OR CONSEQUENTIAL DAMAGES IN CONNECTION WITH OR RELATED TO THIS AGREEMENT (INCLUDING LOSS OF PROFITS, USE, DATA, OR OTHER ECONOMIC ADVANTAGE), HOWSOEVER ARISING.

This Agreement and the rights granted herein may be terminated immediately by NACE upon breach of this Agreement by Publisher. Unless earlier terminated, this Agreement and the rights granted herein will automatically terminate 6 months from the Date set forth above. If the Work has not been published within that time period, a new Agreement must be obtained.

Publisher may not, directly or indirectly, sell, assign, sublicense, lease, rent, distribute, or otherwise transfer this Agreement or any rights granted herein, without the prior written consent of NACE.

If any provision of this Agreement is found to be unenforceable, then this Agreement shall be deemed to be amended by modifying such provision to the extent necessary to make it legal and enforceable while preserving its intent. The remainder of this Agreement shall not be affected by such modification.

This Agreement does not create, and shall not be construed to create, any employer-employee, joint venture or partnership relationship between the parties. No officer, employee, agent, servant or independent contractor of either party shall at any time be deemed to be an employee, servant, agent or contractor of any other party for any purpose whatsoever.

This Agreement shall be governed by, and construed and enforced in accordance with, the laws of the State of Texas, without regard to the choice of law provisions of that State.

This Agreement shall only be effective if signed by authorized representatives of both parties. This Agreement constitutes the entire Agreement between the parties with respect to the subject matter of this Agreement. Any change, modification or waiver hereto must be in writing and signed by authorized representatives of both parties.

Other Terms & Conditions: _____

Publisher hereby requests permission to publish the Work described above and agrees to comply with all Terms and Conditions listed above.

Request submitted by:
NASMIDDIN YAAKUB
Printed Name
PhD candidate
Title
[Signature]
Signature
1/2/2015
Date

Request approved by NACE:
D. Freeman
Printed Name
ADM
Title
[Signature]
Signature
1/7/15
Date

Request agreed to by:

Lead Author Printed Name

Lead Author Title

Lead Author Signature

Date



OHIO
UNIVERSITY

Thesis and Dissertation Services